SOME ANALYTICAL AND EXPERIMENTAL INVESTIGATIONS TO PREDICT THE BEHAVIOUR OF SOILS UNDER THE RAILWAY TRACKS

A Thesis Submitted
in Partial Fulfilment of the Requirements
for the Degree of
DOCTOR OF PHILOSOPHY

by

JAGDISH T. SHAHU

VOLUME I

Chapter I **INTRODUCTION**
Chapter II **LITERATURE REVIEW**
Chapter III **MATHEMATICAL MODELLING OF RAILWAY TRACK**

DEPARTMENT OF CIVIL ENGINEERING
INDIAN INSTITUTE OF TECHNOLOGY KANPUR
February, 1993

TO

AMMA AND DADA

12/3/93

CERTIFICATE

This is to certify that the thesis entitled, **"SOME ANALYTICAL AND EXPERIMENTAL INVESTIGATIONS TO PREDICT THE BEHAVIOUR OF SOILS UNDER THE RAILWAY TRACKS"**, by Mr. Jagdish T. Shahu, for the award of the Degree of Doctor of Philosophy, of Indian Institute of Technology, Kanpur is a record of bonafide research work carried out by him under our supervision and guidance. The results embodied in this thesis have not been submitted to any other university or institute for the award of any degree or diploma.

(YUDHBIR)
Professor
Department of Civil Engineering
Indian Institute of Technology, Kanpur

5/3/93

(N. S. V. Kameswara Rao)
Professor
Department of Civil Engineering
Indian Institute of Technology, Kanpur

February, 1993

ACKNOWLEDGEMENTS

The author feels immense gratitude and indebtedness to Prof. Yudhbir for his invaluable guidance, numerous suggestions, criticisms and encouragement. In the same breath, author expresses his profound gratitude to Prof. N. S. V. Kameswara Rao for his useful advice and encouragement.

Special thanks are due to Prof. M. R. Madhav for his advice and interest in this work. Thanks are also due to Prof. P. K. Basudhar and Dr. S. Chandra for their kind help.

Author is thankful to Mr. Joyis Thomas for his help in conducting unconfined tests. Sincere thanks are due to Mr. R. P. Trivedi, Mr. A. K. Srivastava, Shri Gulab Chand and Shri Parshuram of Geotechnical engineering laboratory for their day to day help. Careful tracing work of Mr. B. K. Jain is very much appreciated. Help of RDSO is appreciated.

Thanks are due to all friends, especially Miss Pratima Agarwal for her help in time of need.

Special appreciations to his wife, Prabha, for her constant patience and endurance. To his beloved child, Sunny, whose lovely smile has always been a source of strength after a long spell of hard work.

Finally, it were his parents who made many sacrifices due to author's involvement in the present work, but are no more to share the joy of this moment. It is to his parents, Amma and Dada, that this piece of work is gratefully dedicated.

CONTENT

		Page
TITLE PAGE		i
DEDICATION		ii
CERTIFICATE		iii
ACKNOWLEDGEMENTS		iv
CONTENT		v
LIST OF TABLES		xii
lIST OF FIGURES		xv
NOTATION		xxx
SYNOPSIS		xxxx
CHAPTER 1	INTRODUCTION	1
	1.1 General	1
	1.2 Present problem	2
	1.3 Scope of the present investigation	6
CHAPTER 2	LITERATURE REVIEW	8
	2.1 Introduction	8
	2.2 Literature related to analytical studies for stress determination	9
	2.2.1 Empirical approaches	9
	2.2.2 Finite element and other computer oriented approaches	16
	2.3 Literature related to geotechnical testing for evaluation of strength, stress - strain - pore pressure behaviour	21
	2.3.1 Total stress/fatigue studies	21
	2.3.2 Effective stress studies	24
	2.3.2.1 Saturated soils	25
	2.3.2.2 Non-saturated soils	34

2.4 Literature related to track formation design 38

2.5 Literature related to other important aspects 50

2.5.1 Effect of train speed on stresses 50
2.5.2 Characterization of track foundation 51
2.5.3 Soil improvement methods 57
2.5.4 Field measurements and model testing 58

2.6 Summary 61

CHAPTER 3 MATHEMATICAL MODELLING OF RAILWAY TRACK 64

3.1 Introduction 64

3.2 Rigorous elastic method (ELASTIC.F model) 65

3.2.1 Introduction 65
3.2.2 Theoretical background 65
3.2.3 Description of rigorous elastic method (ELASTIC.F model) 67
3.2.4 Limitations 72
3.2.5 Comparison of results 73
3.2.6 Results and discussion 73

3.3 Two dimensional finite element analysis 90

3.3.1 Introduction 90
3.3.2 Description of two dimensional finite element routines 90
3.3.3 Two dimensional finite element model for railway track (2D8N model) 93
3.3.4 Selection of finite element mesh 102
3.3.5 Limitations 119
3.3.6 Comparison of results 122
3.3.7 Results and discussion 122

3.4 Three dimensional finite element analysis 136

3.4.1 Introduction 136
3.4.2 Description of three dimensional finite element routines 136
3.4.3 Track modelling 140

3.4.3.1 Track outline 140
3.4.3.2 Boundary conditions 142
3.4.3.3 Rail element 142
3.4.3.4 Sleepers 146

3.4.4 Selection of finite element mesh 147
3.4.5 Limitations 152
3.4.6 Evaluation of parameters used in constitutive relationship 153
3.4.7 Comparison of results 159
3.4.8 Parametric studies 159
3.4.9 Results and discussion 160

3.5 Comparison of results 183

3.5.1 FAST track 183
3.5.2 So (1978) track 186
3.5.3 Vienna arsenal single sleeper and Derby panel full Scale model tests 189
3.5.4 Field measurements by RDSO on Indian railways 200

3.5.4.1 Tests conducted on section No. 2 on Ambala-Ludhiana section (1964-67) 200
3.5.4.2 Tests conducted on section No. 6 on Ambala-Ludhiana section (1964-67) 202
3.5.4.3 Tests conducted on a dead-end siding near canal bed site at RDSO, Lucknow 202
3.5.4.4 Field measurement of formation pressure due to long haul train trials at Mandah road station, Allahabad division. 202

3.5.5 Empirical formulae available in literature 202

3.6 Comparison of the three models 206

CHAPTER 4 GEOTECHNICAL TESTING FOR EVALUATION OF STRENGTH, STRESS-STRAIN-PORE PRESSURE BEHAVIOUR 210

4.1 Introduction 210

4.2 Explanation of selected terms 211

4.3 Geotechnical nature of Campus silt 212

4.3.1 General 212
4.3.2 Particle size distribution and Atterberg limits 212
4.3.3 Compaction characteristics 216

4.4 Tests performed 216

4.5 Relevance of tests performed with present problem 216

4.6 Technique of testing 221

4.6.1 Equipment used 221
4.6.2 Sample preparation 221
4.6.3 Total stress tests 222

4.6.3.1 Series A1 - Unconsolidated undrained tests without pore pressure measurement 222
4.6.3.2 Series A2 - Unconfined cyclic tests 223
4.6.3.3 Series A3 - Unconfined cyclic softened tests 234

4.6.4 Effective stress tests 225

4.6.4.1 Pore pressure measurement in partially saturated soils 225
4.6.4.2 Series B1 - Unconsolidated undrained tests with pore water pressure measurement 225
4.6.4.3 Series B2 - Unconsolidated undrained cyclic tests with pore water pressure measurement 226
4.6.4.4 Series B3 - Undrained static and cyclic tests with pore water pressure measurement on samples with back pressure saturation 228

4.7 Presentation of test results 230

4.7.1 Total stress tests 230

4.7.1.1 Series A1 - Unconsolidated undrained tests without pore pressure measurement 230
4.7.1.2 Series A2 - Unconfined cyclic tests 230
4.7.1.3 Series A3 - Unconfined cyclic softened tests 244

4.7.2 Effective stress tests 252

4.7.2.1 Series B1 - Unconsolidated undrained tests with pore water pressure measurement 252

4.7.2.2 Series B2 - Unconsolidated undrained cyclic tests with pore water pressure measurement 270
4.7.2.3 Series B3 - Undrained static and cyclic tests with pore water pressure measurement on samples with back pressure saturation 271

4.8 Interpretation and Discussion 292

4.8.1 Introduction 292
4.8.2 Total stress behaviour (static and cyclic) 292

4.8.2.1 Unconfined tests 292
4.8.2.2 Confined tests 305

4.8.3 Effective stress behaviour for static tests 309

4.8.3.1 Quasi saturated behaviour 309
4.8.3.2 Samples exhibiting quasi saturated response 314
4.8.3.3 Stress - strain, pore pressure - strain response with varying confining stress 325
4.8.3.4 Failure envelope 328
4.8.3.5 Comparison of other results 332

4.8.3.5.1 Comparison with Cruz et al. (1985) 332
4.8.3.5.2 Comparison with data for Canyon dam clay 334
4.8.3.5.3 Comparison in terms of total stress behaviour of compacted soils 349

4.8.4 Effective stress behaviour of Campus silt under cyclic load condition and evaluation of threshold stress 354

4.8.4.1 Plastic strain development 354
4.8.4.2 Pore pressure response during cyclic loading 369

4.8.4.3 Evaluation of threshold stress and threshold stress ratio 375

4.8.4.3.1 Plastic strain criterion 376

4.8.4.3.2 Pore pressure during cyclic loading criterion 379

4.8.4.4 Guidelines for evaluation of threshold stress ratio 382

CHAPTER 5 DESIGN METHODOLOGY 391

5.1 Introduction 391

5.2 Broad outline of design methodology 393

5.2.1 Estimation of induced stresses on the subgrade 393
5.2.2 Evaluation of threshold stress 397
5.2.3 Design of depth of formation 398

5.3 Rigorous design 398

5.4 Simplified design 404

5.5 Design example for Campus silt 406

5.5.1 Rigorous design 408
5.5.2 Simplified design 409

CHAPTER 6 CONCLUSIONS AND RECOMMENDATIONS 414

6.1 General 414

6.2 Mathematical modelling 414

6.3 Geotechnical testing 418

6.3.1 Unconfined tests 419
6.3.2 Effective stress static tests 420
6.3.3 Effective stress cyclic tests 424

6.4 Recommendations for further studies 428

REFERENCES 430

Appendices 439

A1 Details of TRACK 1 439

A2 Details of TRACK 2 [Same as FAST TRACK, Selig et al. (1979)] 441

A3 So (1978) TRACK and the range of parameters used 443

A4 Details of Derby and Vienna TRACKS 445

A5 Details of TRACKS tested in India 448

B1 Testing of 2D8N finite element routine 452

B2 Testing of 3D20N finite element routine 458

LIST OF TABLES

Table No.	Name of Table	Page
1.1	Status of formation treatment methods	4
2.1	Track equipment standards by SNCF	48
2.2	Track formation quality by SNCF	48
3.1	Range of Young's modulus for different soils [(Bowles (1984)]	74
3.2	Empirical correlation between formation coefficient 'C' and Young's modulus of subgrade, 'E'	74
3.3	Results of parametric studies (ELASTIC.F model)	76
3.4(a)	Meshes used in trials for rectangular mesh selection	104
3.4(b)	Compartment dimensions of meshes used in trials for rectangular mesh selection	105
3.4(c)	Results of trials for rectangular mesh selection	113
3.5	Results of parametric studies (2D8N model)	124
3.6	Beam problem -- 2D8N vis - a - vis 3D20N	138
3.7(a)	Meshes used in trials for 3-D mesh selection	148
3.7(b)	Compartment dimensions for meshes used in trials for 3-D mesh selection	149

3.7(c)	Result of trials for 3-D mesh selection	150
3.8	Summary of cyclic plate load test results (tests carried out on Sandilla-Rahimabad section near Lucknow)	156
3.9	Results of parametric studies (3D20N model)	170
3.10	Comparison of results for section no. 2, Ambala-Ludhiana section	201
3.11	Comparison of results for section no. 6, Ambala - Ludhiana section	203
3.12	Track properties for canal bed site, Lucknow	203
3.13	Comparison of results for canal bed site, Lucknow	204
3.14	Comparison of results for Mandah road station, Allahabad division	204
3.15	Comparison of results with empirical formulae	205
3.16	Comparison of 3 models in terms of results predicted	207
3.17	Comparison of CPU time on Convex 220	209
4.1	Index properties for Campus silt	215
4.2	Summary of total tests conducted	218
4.3	Details of total stress UU tests (tests with cell pressure > 0)	232
4.4	Details of series A2 tests	233
4.5	Details of series A3 tests	251

4.6	Details of effective stress tests on Campus silt (static tests)	267
4.7	Details of effective stress tests on Campus silt (cyclic and static tests)	268
4.8	Calculation of ultimate stress from Eq. (28.1) from Lambe and Whitman (1978) for Campus silt	323
4.9	Calculation of ultimate stress from Eq. (28.1) from Lambe and Whitman (1978) for Canyon dam clay	324
4.10	Critical state data for Campus silt (static tests)	336
4.11	Critical state data for Campus silt (cyclic and static tests)	337
4.12	Calculation for Roscoe surface	346
4.13	Additional data related to cyclic tests on Campus silt	358
4.14	Value of coefficients in plastic strain model	364

LIST OF FIGURES

		Page
1.1	Track structure	5
2.1	Method of Odemark	12
2.2	Comparison of stress - strain curves of single loading	26
2.3	Peak strength after ten cycles of loading for series I	27
2.4	Comparison of stress-strain curves of single loading and repeated loading	28
2.5	Mohr envelope for compacted soil	37
2.6	Design charts [Rubin et al. (1970)]	39
2.7	Decision diagram for road bed depth	42
2.8(a)	Relationship between tie spacing and road bed pressure	43
2.8(b)	Relationship between ballast depth, the kind of tie and road bed pressure	43
2.9(a)	Relationship between roadbed pressure, liquid limit and mud pumping. (Applied rail pressure is 5 t and ordinary wooden tie is used)	44
2.9(b)	Relationship between roadbed pressure, CBR and mudpumping. Applied rail pressure is 5 t and standard wooden tie is used)	44
2.10	Maximum dynamic vertical stresses exerted on the subgrade	46

2.11	Track depression vs. Load relationship for different tracks	54
2.12	Bearing area of sleeper	56
3.1	Measurement of X in Equation 3.7	68
3.2	Sleeper and load configuration for double wheel load case	68
3.3	Assumed load distribution below the sleeper	70
3.4	Assumed load distribution below the sleeper	70
3.5	Variation of σ_{vt} with E_s for TRACK 1 (ELASTIC.F model)	79
3.6	Variation of σ_{vt} with total depth of construction for TRACK 1 (ELASTIC.F model)	80
3.7	Variation of σ_v inside the subgrade for E_s = 10 MPa for different d_t (ELASTIC.F model)	81
3.8	Variation of σ_v with depth for different d_t (ELASTIC.F model)	82
3.9	Variation of σ_v with depth for different E_s (ELASTIC.F model)	84
3.10	Variation of σ_v inside the subgrade for d_t = 1.0 m for different E_s (ELASTIC.F model)	85
3.11	Variation of σ_{vt} for different proportioning of ballast and subballast depth for d_t = 1.0 m (ELASTIC.F model)	86
3.12	Variation of σ_{vt} with formation coefficient 'C' for d_t = 0.4 m (ELASTIC.F model)	86

3.13	Variation of σ_{vt} with tie spacing for different track conditions (ELASTIC.F model)	88
3.14	Variation of σ_{vt} with moment of inertia of rail, I_r (ELASTIC.F model)	88
3.15	Variation of σ_{vt} with Young's modulus of ballast (ELASTIC.F model)	89
3.16	Variation of σ_{vt} with Young's modulus of subballast (ELASTIC.F model)	89
3.17	Notations used (2D8N model)	94
3.18	Track structure and the referred directions	94
3.19	Track sections	96
3.20	Sleeper section	98
3.21	Wheel configuration	98
3.22	Load distribution - when load is between the sleepers	100
3.23	Load distribution - when load is on the sleeper	100
3.24	Load distribution - Present problem	100
3.25	Track formation originally used for calculations	103
3.26	Discretization for mesh A (2D8N model)	106
3.27	Discretization for mesh B (2D8N model)	107
3.28	Discretization for mesh C (2D8N model)	108
3.29	Variation of σ_1 with depth for TRACK 2 (2D8N model)	110

3.30 Variation of σ_3 with depth for TRACK 2 (2D8N model) 111

3.31 Variation of δ with depth for TRACK 2 (2D8N model) 112

3.32 Scheme for rectangular mesh discretization 114

3.33 Variation of δ with depth for TRACK 2 by different rectangular mesh discretizations (2D8N model) 116

3.34 Variation of σ_1 with depth computed by using different rectangular mesh discretizations for TRACK 2 (2D8N model) 117

3.35 Variation of σ_3 with depth computed by using different rectangular mesh discretizations for TRACK 2 (2D8N model) 118

3.36 Proposed modification to 2D8N model 121

3.37 Variation of displacement with depth for TRACK 1 (2D8N model) 126

3.38(a) Variation of σ_1 with depth for TRACK 1 (2D8N and modified 2D8N model) 127

3.38(b) Variation of σ_3 with depth for TRACK 1 (2D8N model) 128

3.38(c) Variation of τ_{max} with depth for TRACK 1 (2D8N model) 129

3.39 Variation of major and minor principal stress along the sleeper on top of subgrade for TRACK 1 (2D8N model) 131

3.40 Variation of σ_{1t} and σ_{3t} with E_s for different depths of subballast (2D8N model) 132

3.41 Variation of displacement on top of sleeper with E_s for different depths of subballast (2D8N model) 133

3.42 Variation of σ_{1t} with d_b/d_t (2D8N model) 135

3.43 Notations used (3D20N model) 141

3.44 Displacement under the rail seat versus depth for different rail conditions for TRACK 2 144

3.45 σ_1 versus depth for different rail conditions for TRACK 2 145

3.46 Mesh C' discretization 151

3.47 E_s versus depth below formation level - wave propagation test results on Sandilla - Rahimabad section 155

3.48 Variation of displacement under the rail seat with depth for TRACK 1 (3D20N model) 162

3.49(a) Variation of σ_1 with depth for TRACK 1 (3D20N model) 163

3.49(b) Variation of σ_3 with depth for TRACK 1 (3D20N model) 164

3.50 Variation of major principal stress along the sleeper at different depths for TRACK 1 (3D20N model) 165

3.51 Variation of rail deflection along the rail direction for TRACK 1 (3D20N model) 166

3.52 Stresses on top of subgrade along the sleeper for single wheel load with joint element (3D20N model) 167

3.53	Stress distribution in actual track system	173
3.54	Assumed stress distribution in equivalent track system	173
3.55	Elastic plates	175
3.56	Variation of σ_{1t} with Young's modulus of subballast, E_{sb} for reference track (3D20N model)	177
3.57	Variation of σ_{1t} with Young's modulus of ballast, E_b for reference track (3D20N model)	177
3.58	Variation of σ_{1t} with I_r for TRACK 1 (3D20N model)	178
3.59	Variation of σ_{1t} with tie spacing for TRACK 1 (3D20N model)	179
3.60	Variation of σ_{1t} with m	180
3.61	Comparison of results - Vertical displacement with depth for FAST track	184
3.62	Comparison of results for vertical stress with depth for FAST track	185
3.63	Comparison of results for vertical stress along the sleeper at 18 cm depth for FAST track	187
3.64	Comparison of results for rail displacement along rail direction for FAST track	188
3.65	Comparison of results with So (1978)	190
3.66	Comparison of results with So (1978)	190

3.67	Comparison of results with So (1978)	190
3.68	Structures tested at Vienna and Derby [Janin et al. (1983b)]	192
3.69	Comparison of results for total resilient displacement for Derby panel tests	193
3.70	Comparison of results for major principal stress for Derby panel tests	194
3.71	Comparison of results in terms of vertical stresses for Vienna and Derby tests	196
3.72	Comparison of results for horizontal stresses for vienna structure No. 2	197
3.73	Comparison of results for transverse stresses for Derby structures	198
3.74	Comparison of results with Rosalie elasto plastic model	199
4.1	Particle size distribution	213
4.2	Index properties	214
4.3	Water content - dry density relationship	217
4.4	Stress - strain relationship for static unconfined test	231
4.5	Stress - strain relationship for cyclic test (R_f = 6.6 %)	234
4.6	Stress - strain relationship for cyclic test (R_f = 18.7 %)	235
4.7	Stress - strain relationship for cyclic test (R_f = 29.7 %)	236

4.8 Stress - strain relationship for cyclic test (R_f = 36.5 %) 237

4.9 Stress - strain relationship for cyclic test (R_f = 46.0 %) 238

4.10 Stress - strain relationship for cyclic test (R_f = 54.2 %) 239

4.11 Stress - strain relationship for cyclic test (R_f = 64.0 %) 240

4.12 Stress - strain relationship for cyclic test (R_f = 71.3 %) 241

4.13 Stress - strain relationship for cyclic test (R_f = 73.7 %) 242

4.14 Stress - strain relationship for cyclic test (R_f = 76.6 %) 243

4.15 Stress - strain relationship for static softened test 245

4.16 Stress - strain relationship for cyclic softened test (R_f = 18.9 %) 246

4.17 Stress - strain relationship for cyclic softened test (R_f = 37.1 %) 247

4.18 Stress - strain relationship for cyclic softened test (R_f = 54.4 %) 248

4.19 Stress - strain relationship for cyclic softened test (R_f = 70.7 %) 249

4.20 Stress - strain relationship for cyclic softened test (R_f = 82.2 %) 250

4.21	Dry density versus water content relationship for effective stress tests	253
4.22	Cell pressure versus initial pore water pressure	254
4.23	Stress - strain relation for S = (86.5 - 87.2) %	255
4.24	Pore pressure - strain relation for S = (86.5 - 87.2) %	256
4.25	Effective stress ratio - strain relation for S = (86.5 - 87.2) %	257
4.26	Effective stress path for S = (86.5 - 87.2)%	258
4.27	Stress - strain relation for S = (92.0 - 94.6) %	259
4.28	Pore pressure - strain relation for S = (92.0 - 94.6) %	260
4.29	Effective stress ratio - strain relation for S = (92.0 - 94.6) %	261
4.30	Effective stress path for S = (92.0 - 94.6)%	262
4.31	Stress - strain relation for S = (95.1 - 96.1) %	263
4.32	Pore pressure - strain relation for S = 95.1 - 96.1) %	264
4.33	Effective stress ratio - strain relation for S = (95.1 - 96.1) %	265
4.34	Effective stress path for S = (95.1 - 96.1)%	266

4.35 Stress - strain , pore pressure strain relationship for test with R_f = 18.52 % 272

4.36 Stress - strain , pore pressure strain relationship for test with R_f = 31.82 % 273

4.37 Stress - strain , pore pressure strain relationship for test with R_f = 37.68 % 274

4.38 Stress - strain , pore pressure strain relationship for test with R_f = 31.37 % 275

4.39 Effective stress path for test with R_f = 18.52 % 276

4.40 Effective stress path for test with R_f = 31.82 % 277

4.41 Effective stress path for test with R_f = 37.68 % 278

4.42 Effective stress path for test with R_f = 31.37 % 279

4.43 Stress - strain relation for tests with back saturation 280

4.44 Pore - pressure - strain relation for tests with back saturation 281

4.45 Effective stress ratio - strain relation for tests with back saturation 282

4.46 Effective stress path for tests with back saturation 283

4.47 Stress - strain relation for tests with back saturation 285

4.48	Pore - pressure - strain relation for tests with back saturation	286
4.49	Effective stress ratio - strain relation for tests with back saturation	287
4.50	Effective stress path for tests with back saturation	288
4.51	Stress - strain relation for tests with back saturation for (a) R_f = 20.05 % (b) R_f = 14.53 %	290
4.52	Stress - strain relation for tests with back saturation for (a) R_f = 27.78 % (b) R_f = 15.83 % (c) R_f = 28.38 %	291
4.53	Increase in water content from initial state with R_f	294
4.54	Increase in water content due to cyclic loading with R_f	295
4.55	Variation of s_u with δ_w	296
4.56	Variation of s_u with R_f	297
4.57	Variation of plastic strain with δ_w	298
4.58	Stress - strain relation for all unconfined cyclic tests	300
4.59	Variation of E_u/E_i and E_{us}/E_i with R_f	301
4.60	Stress - strain relation for all unconfined softened tests	302
4.61	Variation of Young's modulus with water content	303

4.62	Variation of log (E) with water content	304
4.63	Variation of s_u with water content	306
4.64	Effect of confining pressure on stress - strain behaviour	307
4.65	Total stress failure envelopes	308
4.66	Variation of B with S for (a) Campus silt (b) Canyon dam clay (c) Chiew larn clay	310
4.67	Comparison of stress-strain and pore pressure - strain behaviour (a) dry of optimum (b) wet of optimum	312
4.68	Comparison of peak failure envelope	313
4.69	Variation of $\Delta u_{max}/\sigma_c'$ with σ_c'	316
4.70	Variation of $\Delta u_{max}/(\sigma_1-\sigma_3)$ with σ_c'	317
4.71	Normalized stress paths for Campus silt	318
4.71(a)	Explanation for Figure 4.71	319
4.72	Normalized stress paths for Canyon dam clay [Casagrande and Poulos (1964)]	320
4.73	Variation of $(\sigma_1-\sigma_3)/2$ at failure with σ_c'	321
4.74	Effect of confining pressure on (a) pore pressure - strain behaviour (b) Stress - strain behaviour	326
4.75	Effect of confining pressure on stress strain behaviour	327
4.76	Effective stress failure envelope	329

4.77	Effective stress failure envelope (enlarged view)	330
4.78	Typical stress - strain, pore pressure - strain and stress path for group IV soil [Cruz et al. (1985)]	333
4.79	Variation of P_i' with w_f	335
4.80	Variation of P_f' with w_f	339
4.80(a)	Variation of P' with w	340
4.81	Variation of P_f' with q_f	341
4.82	q/P_e' versus P'/P_e' relationship for Campus silt	343
4.83	q/P_e' versus P'/P_e' relationship for Canyon dam clay	344
4.84	q_f/P_e' versus P_f'/P_e' relationship	345
4.85	Pore pressure parameter A_f versus OCR	348
4.86	Water content versus strength relationship at failure	351
4.87	Variation of s_u with $(w-w_{opt})/I_p$	353
4.88	Increase in plastic strain with cyclic loading (σ_c' = 20-22 kPa)	356
4.89	Increase in plastic strain with cyclic loading (σ_c' = 40 kPa)	357
4.90	Increase in plastic strain with cyclic loading (high confining pressure)	359
4.91	Plastic strain versus R_f for unconfined cyclic tests	360

4.92	Cyclic load triaxial tests - permanent strain versus No. of cycles [Janin et al. (1983a)]	362
4.93	Development of permanent axial strain in cyclic triaxial undrained compression tests on lacustrine clay from Hamilton, Ontario [after Wilson and Greenwood (1974)]	363
4.94	C_p versus R_f	366
4.95	Pore pressure rise with number of cycles	370
4.96	Normalized effective stress path for cyclic tests with high confining pressure	371
4.97	Normalized pore pressure rise with axial strain	373
4.98	q/P_e' versus P'/P_e' relationship for cyclic tests	374
4.99	Rise in plastic strain during 100 cycles versus R_f	377
4.100	$(\sigma_1-\sigma_3)_{At\Delta umax}$ / $(\sigma_1-\sigma_3)_{max}$ and R_{TS} versus σ_c'	381
4.101	Threshold stress ratio versus I_p relationship	384
4.102	Threshold stress versus σ_c' relationship for compacted saturated Campus silt	386
4.103	Threshold stress versus σ_c' relationship for compacted Angul clay [Yudhbir et al. (1992)]	387
4.104	Threshold stress versus σ_c' relationship for NC marine clay [Rehman (1977)]	388

4.105	Threshold stress versus σ_c' relationship	389
5.1	Induced stress $(\sigma_1-\sigma_3)$ versus m	394
5.2	Induced stress (σ_1) versus m	395
5.3	Threshold stress versus total depth of formation	399
5.4	Flow chart	401
5.5	Design chart	402
5.6	Flow chart for simplified design	407
5.7	Cross-section of a typical formation	412
B1.1	Comparison of exact and FE solutions - stress profiles under the load - 2-D case	453
B1.2	Comparison of exact and FE solutions for vertical stress distribution - 2-D case	454
B1.3	Comparison of exact and FE solutions for Lateral pressure distribution - 2-D case	455
B1.4	Comparison of exact and FE solutions for shear stress distribution - 2-D case	456
B1.5	Finite element mesh for 2-D analysis	457
B2.1	Comparison of exact and FE solutions for Vertical stress profile - 3-D case	459
B2.2	Comparison of exact and FE solutions for vertical pressure distribution - 3-D case	460

NOTATION

a, b = intercept and slope of line (used with subscript)

a_1 = angle of distribution of pressure in ballast

A, B = Skempton's pore pressure parameters

b = width of sleeper

$\bar{b}$ = bearing factor = F / 2 S

c_v = coefficient of consolidation

c' = cohesion in terms of effective stresses

C = formation coefficient

c_p = value of $\log(\varepsilon_p)$ at N = 1

CBR = California bearing ratio

CSL = critical state line

CLRS = critical level of repeated stress

d_b = actual depth of ballast

d_{sb} = actual depth of subballast

d_b^* = modified depth of ballast

d_{sb}^* = modified depth of subballast

d_t = total depth of formation ($d_b + d_{sb}$)

D_p = value of first gradient of bilinear log-log plot between ε_p and N

e = maximum horizontal tensile strain at the base of stabilized layers

e_e = elastic strain

e_f = vertical strain at failure

e_0 = initial void ratio

E = tangent Young's modulus

E_b = Young's modulus of elasticity of ballast

E_{equ} = Young's modulus of equivalent system

E_f = Young's modulus of filling material

E_i = tangent Young's modulus of shear failure (before repeated loading)

E_p = value of second gradient of bilinear log-log plot between ε_p and N

E_r = Young's modulus of elasticity of rail

E_s = Young's modulus of elasticity of subgrade

E_{sb} = Young's modulus of elasticity of subballast

E_t = Young's modulus of elasticity of tie (sleeper)

E_{t1}, E_{t2} = Young's modulus of elasticity for discrete sleeper system and continuous sleeper system

E_u = tangent young's modulus of shear failure (after repeated loading but no softening)

E_{us} = tangent Young's modulus of shear failure (after repeated loading and softening)

EI = flexural stiffness

F = bearing area per sleeper

G = track gauge

GDS = Geotechnical Digital System

i = speed impact factor to be multiplied by σ_t to obtain σ_{speed}

I = moment of inertia

I_p = plasticity index

I = moment of inertia per rail

I_{t1}, I_{t2} = moment of inertia of discrete sleeper and continuous sleeper respectively

K_f'line = line in effective stress plot joining maximum failure shear stress points

k_n = normal joint stiffness

k_s = shear joint stiffness (for 2-D case)

k_{s1} = shear joint stiffness (in x-direction in 3-D case)

k_{s2} = shear joint stiffness (in y-direction in 3-D case)

K = ratio of pulsating load causing failure to the static failure strength

K_n = Newmark's influence factor

K_0 = coefficient of earth pressure at rest

l = length of sleeper

L = effective bearing length of sleeper

L_b = base length of ballast track

L1-L10 = load areas

L1'-L10' = load areas

m = modular ratio as a measure of ballast, subballast and subgrade

M = slope of critical state line

$\bar{M}$ = moment force on rail

$\bar{m}$, $\bar{n}$ = parameters used in Newmark's equations

N = number of load cycle

N_f = total number of repetitions required for track for failure

N_r = total number of repetitions in the track life

N_s = value of N where change in gradient from D_p to E_p occurs

OCR = overconsolidation ratio

OMC, w_{opt} = optimum moisture content

ORE = Office for Research and Experiments, International union of railways, Utrecht

p_s = stress below the sleeper where y_r is calculated

P' = $(\sigma_1' + 2\sigma_3')/3$

P_e' = Hvorslev's equivalent consolidation pressure

P_s = load on individual sleeper

q = $(\sigma_1' - \sigma_3')$

$q(x)$ = externally applied load

q_1 = intensity of pressure on rectangular load area

Q = vertical wheel load

$\bar{Q}_1$ = initial range load

Q_1 = load number one under which stresses are needed

Q_2 = load number two -- far side load of axle

R = reaction of sleeper

R_f = cyclic stress ratio

R_{TH} = threshold stress ratio

RDSO = Research, Design and Specifications Organization, Ministry of Indian Railways

s = a factor which depends on track quality

s_u = undrained shear strength

$\bar{S}$ = spacing between the sleepers

S = degree of saturation

SNCF = French railway organization

t = thickness of sleeper

$\bar{t}$ = statistical safety factor

u , k = modulus of railroad reaction or Modulus of elasticity of rail support

u_a = pore air pressure

u_e = track modulus in the elastic range

u_i = track modulus in the initial range

Δu = pore water pressure change

$(\Delta u)_{cyc}$ = cumulative pore water pressure built up in total 100 cycles

Δu_0 = equilibrium pore water pressure when cell pressure was applied. Also called as initial pore water pressure

UU = unconsolidated undrained

v_o = specific volume of sample

V = train speed

w = water content

w_l = liquid limit

w_1 = final water content after softening

Δw = change in water content during series A2 tests

δw = difference between water content after 100 cycles and softening, and water content at equilibrium state (i.e. water content after softening of as compacted sample)

W_1 = moment of resistance of rail foot

W_2 = moment of resistance of rail head

x = horizontal distance of point from the load position on the rail where deflection is needed

X = a parameter that varies with the degree of saturation of sample

X_1 = horizontal distance of point from the load position on the rail where zero bending moment occurs

y_f = distance between the neutral axis of rail and rail flange

y_r = deflection of rail

y_s = deflection of sleeper under total load Q

y_{s1} = deflection of sleeper under initial load $\bar{Q}_1$

y_t = vertical deflection of sleeper due to reaction force 'R' of sleeper

z = rail deflection

z_d = depth of point from surface at which stresses are required

ZLV = Zimmermann's Wheel load

α, β = coefficients in pore pressure rate vs. time relationship

δ = displacement

$\delta\varepsilon_p$ = cumulative plastic strain due to 100 cycles only

$\dot{\varepsilon}_p$ = strain rate per unit time

ε_p = plastic strain

ε_y = strain in y-direction

ϕ' = angle of shearing resistance in terms of effective stresses

ϕ^b = term relating the contribution of matrix suction to the shearing resistance

γ_d = dry density

$\eta(\xi), \mu(\xi)$ = coefficients as a function of ξ

κ = slope of swelling line in consolidation test

λ = slope of virgin consolidation line in volume change plot

ν = Poisson's ratio

θ = stress dispersion angle in equivalent system

θ_1 = stress dispersion angle in ballast

θ_2 = stress dispersion angle in subballast

ρ_s = static rigidity of track

σ = total mean stress

σ_c' = initial effective stress ; Initial consolidation pressure

σ_{dyn} = dynamic stress level in terms of deviator stress during repeated / cyclic loading

σ_{min} = minimum stress level maintained in terms of deviator stress during repeated / cyclic loading

σ_{r1} = stresses in rail foot

σ_{r2} = stresses in rail head

σ_s = maximum pressure at the bottom of sleeper

σ_t = static stress at any point in the track

σ_{ult} = ultimate failure stress in terms of deviator stress

σ_{vmean} = average pressure on top of subgrade

σ_{vt} = vertical pressure on top of subgrade under the rail seat

σ_z = maximum pressure at any point in subgrade after applying increment for given speed

$(\sigma_z)_c$ = vertical stress at corner of any rectangular area due to uniformly distributed load on that area

σ_1 = major principal stress

σ_2 = minor principal stress

σ_3 = cell pressure, minor principal stress

σ_{1t} = maximum major principal stress on top of subgrade

σ_{3t} = maximum minor principal stress on top of subgrade

(σ_1'/σ_3') = effective stress ratio

τ = undrained shear strength of partially saturated soil

τ_{max} = maximum shear stress on top of subgrade

ξ = x / L_b

Subscript

f = failure

TS = at threshold stress level

cyc = cyclic

sr = stress ratio

v = vertical

p	=	plastic
cal	=	calculated
exp	=	experimental
i	=	initial
cs	=	critical state
max	=	maximum
dyn	=	dynamic
sta	=	static
bm	=	beam
sb	=	subballast
b	=	ballast

Name of Student : Jagdish Telangrao Thahu Roll No : 8720363
Degree for which submitted : Ph.D Department : Civil Engg.

Thesis title : Some Analytical and Experimental Investigations to predict the Behaviour of Soils under the Railway Tracks.

Names of thesis supervisors :
1. Dr Yudhbir
2 Dr N S V Kameswara Rao
Month and year of thesis submission : February, 1993

SYNOPSIS

Railway is the most important mode of transportation of both men and materials in India. To increase the transportation efficiency, heavier, longer and faster trains are needed. The track-foundation-soil system is one of the key factors in bringing about these changes. The present method of design of railway formation is based on empirical basis which gives uneconomical design. Moreover, this method does not help decision making in respect of suitability of existing tracks for heavier and faster trains.

When trains pass over the track, subgrade gets subjected to cyclic stress. If this stress is greater than a certain level of stress called threshold stress for soil, cumulative permanent deformations are produced leading to ballast penetration into the subgrade progressively causing the subgrade failure. In some instances, ballast penetration up to 1 m depth into the subgrade has been observed in the field.

The present study to predict the behaviour of soils under the railway formations subjected to cyclic loading has been carried out in three steps viz. (i) mathematical modelling for determination of induced stresses in the subgrade based on

elastic method, 2-D finite element method and 3-D finite element method, (ii) geotechnical testing to evolve a suitable laboratory testing procedure for formation design and to evaluate threshold stress, and (iii) formulation of formation design methodology.

The work contained in the thesis has been organized into six chapters. In Chapter One, the topic has been introduced and the scope of the present study has been outlined. The available literature related to analytical studies for stress determination (empirical, finite element and other computer oriented approaches) ; geotechnical testing for total stress and effective stress studies on both saturated and non saturated soils ; track formation design ; and other important aspects such as effect of train speed on stresses, characterization of track foundation, soil improvement methods, field measurements and model testing has been reviewed in Chapter Two.

Mathematical modelling carried out in this study, is described in detail in Chapter Three. Three models with increasing sophistication viz. ELASTIC.F , 2D8N and 3D20N model have been developed for calculating major and minor principal stresses in the track structure.

ELASTIC.F model consists of determining the stresses at sleeper-ballast interface by considering the rail as a beam on elastic foundation and then using Odemark's method and Newmark's solution for calculating stresses in the subgrade. 2D8N model is a two-dimensional linear, elastic finite element

model which uses 8-noded rectangular elements. Also, a semi-analytical modification to this model is suggested which invokes two trials of 2D8N model. 3D20N model is a three-dimensional linear, elastic finite element model which uses 20-noded brick element and models rail as one-dimensional beam element. Performance of this model is very similar to 'MULTA' model [Selig et al. (1979)] which is like a closed form solution.

Parametric studies using all the three models have been carried out to evaluate the relative importance of each track component. It is observed that depth of formation and type of subgrade are the most important factors.

Results predicted by all the three models have been compared with predicted results by other models ; measured results in the field by ORE (Office of Research and Experiments, International Union of Railways) and Indian Railways ; and full scale model test results by ORE . It has been observed that all the three models predict quite satisfactory results. Comparisons have been also made with values predicted by semi-empirical methods and it is shown that these methods overpredict by as much as 2 to 4 times the measured results.

It is shown that vertical and horizontal stresses predicted by elastic analysis compare well with those obtained by elasto-plastic analysis which takes into consideration 'no tension' condition in granular media. A non-dimensional parameter 'm' has been introduced as a measure of ballast,

subballast and subgrade characteristics (i.e the formation quality).

Chapter four deals with the geotechnical testing carried out on alluvial silt for evaluation of strength, stress-strain-pore pressure behaviour during static and cyclic loading. Total six series of tests viz. total stress static shear tests, unconfined cyclic tests, unconfined cyclic softened tests, effective stress static shear tests, cyclic undrained tests on quasi saturated samples with pore pressure measurement at high confining pressure and cyclic undrained tests on back saturated samples with pore pressure measurement at low cell pressure simulating the track loading conditions, have been carried out.

Relationship between incremental plastic strain, $\delta\varepsilon_p$ after 100 cycles on unconfined compacted samples and corresponding increase in incremental water content on softening has been indicated. The explanation of mudpumping problems encountered by Indian railways under the tracks in alluvial soil deposits has been well brought out by observing the significant degradations in both stiffness and strength following the transient loading and softening.

A simple procedure to ensure quasi saturated response for partially saturated sample is given. It has been shown that stress - strain, pore pressure - strain response and effective stress paths for compacted samples follow non-normalized behaviour with respect to consolidation stress. It is observed that evaluation of failure envelope by Marsal's procedure gives

satisfactory results.

Stress - strain, pore pressure - strain , stress path and other results for IITK Campus silt show remarkable similarities with group IV soils [Cruz et al. (1985)] and with Canyon dam clay [Casagrande and Hirschfeld (1960) ; Casagrande and Poulos (1964)] in all aspects of behaviour of compacted samples. Effective stress data available for Campus silt and Canyon dam clay on compacted samples has been examined in the general framework of critical state model. It has been brought out that compacted soil samples behave like overconsolidated soils with different values of past maximum pressure (produced due to compaction, depending upon moulding water content and dry density for a given compaction energy). It has been observed that compacted soils, when tested at a degree of saturation above a certain value which ensures quasi-saturation, behave like over consolidated soils up to effective confining stresses below that needed for complete saturation and like normally consolidated when tested at effective confining stresses greater than that needed for full saturation.

Guidelines given by Yudhbir and Wood (1989) have been followed in drawing Virgin consolidation line, Critical state line, Recompression lines, Tension cut off etc. It has been observed that these lines show reasonable fit with actual experimental data.

The generalized relationship, initially proposed by Leroueil et al. (1992) between $(\omega-\omega_{opt})/I_p$ and s_u has been modified. This relationship may be used for estimating

undrained strength of compacted clays at OMC or wet of OMC.

A generalized relationship to relate cumulative plastic strain during cyclic loading with number of cycles has been proposed and the values of coefficients required in this relationship for different types of soils have been evaluated. It is observed that end points of cyclic load tests on compacted samples would lie on Hvorslev surface as observed by Hyde and Ward (1984) for normally and overconsolidated soils.

Procedure to evaluate threshold stress on the basis of cumulative plastic strain data is suggested. Rubin et al. (1970) also suggested a similar procedure on the basis of drained cyclic tests. Threshold stress has also been evaluated from the equilibrium line concept suggested by Sangrey (1968).

A generalized relationship between threshold stress ratio, R_{TS} and plasticity index, I_p has been developed for a variety of soils (compacted, stiff, normally consolidated etc.) at low and relatively high effective confining stresses. Relationship of the form $(\sigma_1-\sigma_3)_{TS} = a + b\ \sigma_c'$ has also been given for a variety of soil types at low effective stress ranges.

In Chapter Five, a rational design methodology based on stresses induced and threshold stress evaluated from above study has been proposed. A detailed step by step procedure (flow chart) has been outlined and a simplified method for routine design of formation depth has been recommended.

The conclusions arrived at on the basis of present study and the recommendations for the further studies are given in Chapter Six.

CHAPTER 1

INTRODUCTION

1.1 GENERAL

Railway is the most important mode of transport of both men and materials in India. With the economic development and growth of industries, need to increase the transportation throughput is being increasingly felt. Transportation throughput can be increased by running longer, heavier and faster trains besides other measures. The capacity of track-foundation-soil system is one of the key factors in bringing about these changes.

At present, formation thickness under the railway track is decided on empirical basis. This method on one hand, overpredicts the thickness where subsoil condition is good and is, thus, uneconomical while on the other hand, underpredicts the formation thickness where subsoil condition is poor requiring frequent and expensive maintenance measures and obstruction to the flow of traffic. Moreover, this method does not help decision making for heavy axle loads and high speeds. Thus, in order to increase the speed and the load carrying capacity of trains, it is imperative that a new design criterion based on a rational approach be formulated. This study would also help to establish the suitability of the

existing formations with respect to their capacity to carry heavy and high speed traffic.

1.2 PRESENT PROBLEM

Railway formations in India were constructed till very recently on procedures based on the experience of the engineers involved. A slope of 2:1 for banks and steeper slopes for cuttings were considered to be safe. The ballast depth and sleepers provided for the track foundation were generally sufficient because of the lighter axle loads and less frequency and speed of trains.

However, as the traffic developed, heavier axle loads, longer and faster trains and increased frequency created problems of track maintenance. This necessitated the development of better track structure viz. rails, sleepers, sleeper density and ballast cushion. However, despite these attempts several large stretches of the track could be distinguished where the subgrade soil was responsible for instability of track structure / foundation. Moreover, development of better track structure was not based on any rational design.

On Indian railways, the need for treating such locations having subgrade failure was felt when high speed Rajdhani express trains were planned to be introduced. Simultaneously, on heavily worked routes of Eastern railways, selected remedial measures were tried. Many of these remedial measures were

picked up from procedures and practices evolved for the new Tokaido line in Japan. In the following years, behaviour of treated locations indicated the intricacy of the subject and many of the formation treatment methods which seemed to be very promising in the beginning, did not solve the problem (Table 1.1).

In general, causes of the subgrade failure mentioned above can be attributed to the following causes :

a. Poor construction methods (especially lack of proper compaction control).

b. Lack of proper drainage of track formation.

c. Empirical nature of design methodology without any systematic regard for the effect of cyclic loading on the behaviour of track-foundation-soil system.

Figure 1.1 illustrates the broad outline of subgrade failure mechanism. When trains pass over the track, subgrade is subjected to a certain cyclic stress. If this stress is greater than a particular stress level called threshold stress for the soil, ballast penetrates into the foundation soil progressively causing the subgrade failure. Penetrated ballast tends to store water percolating through the track surface. Under the train loads, mud pumping phenomenon is observed. Mud pumping of track is a phenomenon caused when roadbed soil is softened by the rainfall or groundwater; the mud climbs up through the void inside the ballast and pumped out on the ballast surface by a passing train load. This displaces the clay and fines present in subgrade soil and completely disrupts the drainage system

Table 1.1 Status of formation Treatment Methods

No.	Methods of formation Treatment	Status
1	Lime Piles	IE*
2	Vinyl Drains	IE
3	Sand Drains	IE
4	Blanket Moorum	PE
5	Polythene sheet	IE
6	Cationic Bitumen Emulsion	IE
7	Cement Pressure Grouting	PE (Limited Life)
8	Maxphalt - Crete	IE
9	Ballast Piles	UT
10	Partial Blanket	UT
11	Lime slurry pressure Injection	PE
12	Geotextile	IE
13	Pouring Sand on Ballast (Protzeller's Method)	PE
14	Blanket - Coarse grained	FE
15	Laterite Blocks	UT
	Method of Execution	
1	Blanketing under traffic	PE
2	Relieving Girder	UT

* IE = Ineffective
FE = Fully Effective
PE = Partly Effective
UT = Under Trial

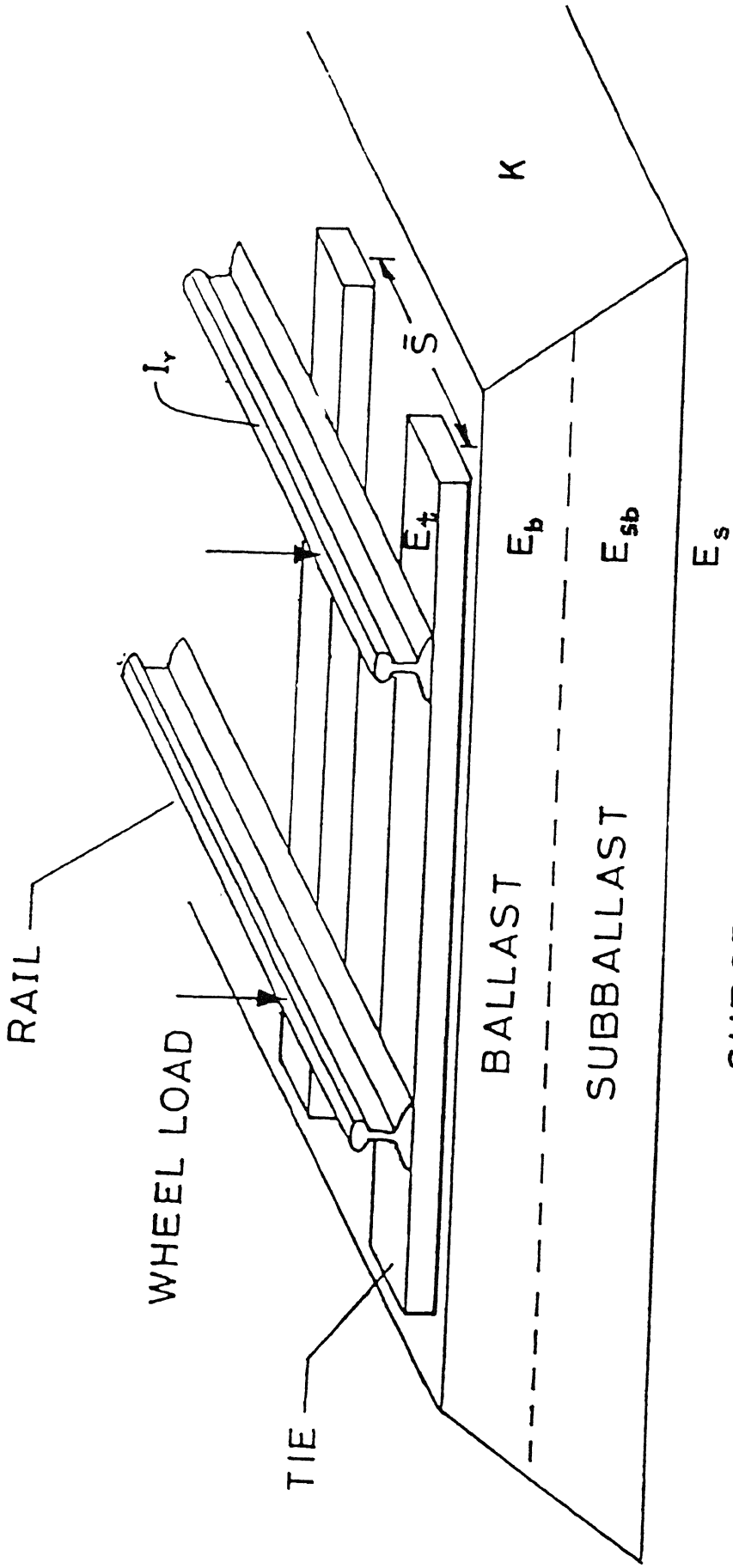

Fig. 1.1 Track structure.

causing further track deterioration. This results in increase in costly and difficult maintenance cycles, making track operation uneconomical. If proper and timely maintenance is not carried out, it may also lead to serious accidents.

The present study aims to evolve a rational criterion for design and construction of railway formations by studying the effect of cyclic loading on subgrade soil.

1.3 SCOPE OF THE PRESENT INVESTIGATION

The proposed study has been carried out in the following steps.

1. Mathematical modelling of railway track to determine the stresses

These studies are carried out in order to estimate the pressure on top of formation due to the faster and heavier train loads using Finite Element method. Parametric studies are carried out to evaluate the relative importance of each component of the track. Design charts for determination of induced stresses in the subgrade have been prepared.

2. Geotechnical testing for evaluation of strength, stress - strain - pore pressure behaviour

This is done in order to evolve a suitable laboratory testing program to simulate track loading conditions in the subgrade soil and to develop procedures for estimation of

threshold stress. General guidelines for evaluation of threshold stress for a variety of soils are suggested.

3. Formulation of design methodology

Based on the analytical and experimental studies, a design methodology for track formation has been recommended.

The details of the present investigation have been presented in Six chapters as outlined below.

Chapter I presents the introduction of present problem indicating the need of present study and broad outline of investigations carried out.

Available literature on the analytical studies for stress determination, geotechnical testing related to track loading conditions, track formation design and other important aspects related to present problem has been reviewed in Chapter II.

Chapter III deals with mathematical modelling of the track structure and the results obtained have been analysed.

Details related to geotechnical testing program, test results and interpretation under both static and cyclic loading conditions have been discussed in Chapter IV.

In chapter V , formulation of design methodology has been presented.

The conclusions arrived at and the recommendations for the future studies are given in Chapter VI.

CHAPTER 2

LITERATURE REVIEW

2.1 INTRODUCTION

In order to predict the behaviour of soils under the railway formations, it is imperative that the stresses inside the track structure should be estimated by proper mathematical modelling and the loading condition should be simulated in laboratory to obtain the threshold stress.

The trends observed in literature related to mathematical modelling can be broadly divided into models which incorporate the exact solution for multilayer elastic system given by Burmister (1945) and models based on finite element analysis (elastic and elasto-plastic). However, all models give the stresses assuming equivalent static load on top of rail. This equivalent static load is obtained by augmenting the wheel load by suitable speed factor.

The simulation of track loading condition in laboratory to determine the threshold stress for soil has been done by Rubin et al. (1970) for London clay and following this approach, Janin et al. (1983a) have also determined the threshold stress for Keuper marl and Boulder clay.

The literature review in this chapter has been carried out under the following heads :

a. Literature related to analytical studies for stress determination.

b. Literature related to geotechnical testing for evaluation of strength, stress - strain - pore pressure behaviour.

c. Literature related to track formation design.

d. Literature related to other important aspects such as speed effect, characterization of elastic foundation, soil improvement methods, and field measurements and model testing.

2.2 LITERATURE RELATED TO ANALYTICAL STUDIES FOR STRESS DETERMINATION

Stresses inside the track structure were earlier determined by empirical and semi empirical approaches. Finite element method and other computer oriented approaches based on closed form solution of multilayer system given by Burmister (1945) were increasingly used for stress determination after 1978. This section has been classified under empirical approaches and finite element and other computer oriented approaches.

2.2.1 EMPIRICAL APPROACHES

1. Zimmermann's Method for Stresses in Rails

Based on assumption of rail supported on infinite number of elastic bearings, Zimmermann gave expressions for deflection, moment and stresses on rail as given below :

$$y_r = Q\eta(\xi)/2\ \bar{b}\ C\ L_b \tag{2.1}$$

$$\bar{M} = Q\ L_b\mu(\xi)/4 \tag{2.2}$$

$$\sigma_{r1} = \bar{M}/W_1 \tag{2.3}$$

$$\sigma_{r2} = \bar{M}/W_2 \tag{2.4}$$

where $$\bar{b} = F\ /\ (2\ \bar{S})\ , \tag{2.5}$$

$$L_b = \sqrt[4]{\frac{4\ E_r I_r}{\bar{b}\ C}}\ , \tag{2.6}$$

y_r = deflection of rail ,

Q = wheel load ,

$\bar{M}$ = total moment on rail ,

x = co-ordinate of point where deflection is needed,

C = formation coefficient, kg/cm^3 ,

$\xi = x/L_b$,

$\bar{b}$ = bearing factor ,

$\bar{S}$ = spacing between sleepers ,

F = bearing area per sleeper ,

L_b = base length of track ,

E_r = Young's modulus of elasticity of rail ,

I_r = moment of inertia per rail ,

W_1 = moment of resistance of rail foot ,

W_2 = moment of resistance of rail head ,

σ_{r1} = stresses on rail foot , and

σ_{r2} = stresses on rail head.

Charts to pick coefficients $\eta(\xi)$ and $\mu(\xi)$ are given in RDSO(B).

2. Method of Odemark for Vertical Stress Calculation in Multilayer Systems

Effect of layering is to reduce the stresses at a given depth. In this method, effect of layering is taken into consideration by increasing the depth based on elastic modulus of different layers and then, calculating the stresses by Boussinesq's method at this new depth [RDSO (B)].

Referring to Fig. 2.1 , the expressions for modified depths are given below :

$$d_b^* = 0.9\, d_b \sqrt[3]{E_b/E_s} \qquad (2.7)$$

$$d_{sb}^* = 0.9\, d_{sb} \sqrt[3]{E_{sb}/E_s} \qquad (2.8)$$

where

d_b^*, d_{sb}^* = modified depths of ballast and subballast respectively,

d_b, d_{sb} = original depths of ballast and subballast respectively, and

E_b, E_{sb}, E_s = Young's modulii of elasticity of ballast, subballast and subgrade respectively.

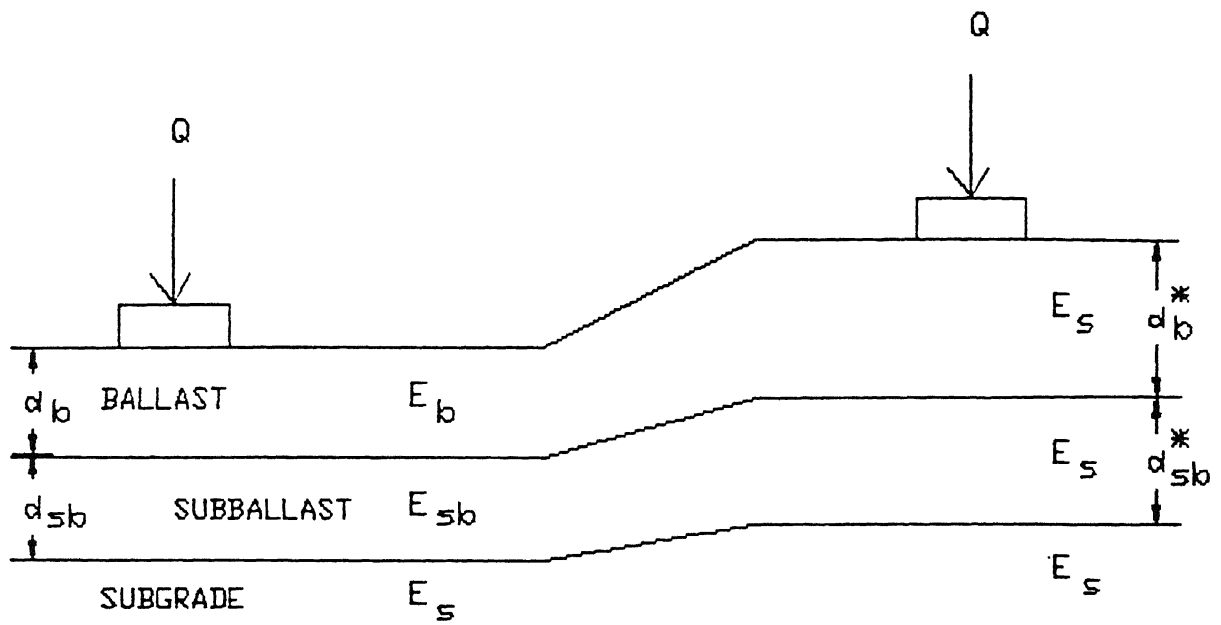

Fig. 2.1 METHOD OF ODEMARK

3. Burmister's Multilayer Approach

Selig et al. (1979) have developed an approach that uses Burmister's multilayer theory [Burmister (1945)] for calculating stresses on ballast and subgrade and a structural model for rail-tie interaction. Contact between tie and ballast is represented by a series of circular areas with uniform pressure.

4. Japanese Approach

Based on elastically supported beam model, pressure, bending moment and deflection in the rail are worked out [RDSO (1987)].

Empirical stress distribution over the ballast layer has been proposed from which average subgrade pressure can be worked out. Maximum subgrade pressure can be found out as :

$$\frac{\sigma_{vt}}{\sigma_{vmean}} = \frac{58}{10 + d_b^{1.35}} \frac{b\ l}{\left(b + 2(d_b - 15)\right)\left(l + 2(d_b - 15)\right)} \qquad (2.9)$$

where b, l = width and length of sleeper respectively,

d_b = ballast depth,

σ_{vt} = maximum subgrade pressure, and

σ_{vmean} = average subgrade pressure.

5. Formation Pressure based on Technical Paper No. 245

On Indian railways,the maximum intensity of pressure on subgrade is calculated as given below [Kapoor et al. (1967a)].

$$P_s = Q \sqrt[4]{\frac{k}{64\ E_r I_r}}\ \bar{S} \tag{2.10}$$

$$\sigma_{vt} = \frac{2}{\pi\ d_b\ L}\ P_s \tag{2.11}$$

where P_s = load on individual sleeper,

L = effective bearing length of sleeper, and

k = modulus of rail road reaction.

6. Formation Pressure Intensity by C.W.Clarke (Technical monograph number 12)

Both average and maximum pressure intensity can be obtained by the following relationship given by C. W. Clarke [Kapoor et al. (1967a)].

$$\sigma_{vmean} = \frac{0.39\ \ ZLV\ \ \bar{S}}{X_1\ \ 0.58\ \ b\ L\ d_b} \tag{2.12}$$

$$\sigma_{vt} = \frac{10}{d_b}\ \ \frac{P_s}{\text{Area of sleeper}} \tag{2.13}$$

where ZLV = Zimmermann Wheel load,

X_1 = distance from load on rail to point of zero bending moment on rail, and

P_s = to be found from Eq. (2.10).

7. Talbot's method for American Standard Gauge Track

A. N. Talbot has proposed following expression for pressure intensity [Kapoor et al. (1967a)].

$$\frac{\sigma_{vt}}{\sigma_s} = \frac{16.8}{d_b^{1.25}} \qquad (2.14)$$

where σ_s = maximum pressure at the bottom of sleeper.

8. Pressure Intensities Calculated by German Railways

Kapoor et al. (1967a) have reported the following expression for maximum subgrade pressure given by German railways :

$$\sigma_v = \frac{1.5\ P_s}{\left(3(1-G)+b\right)\ d_b\ \tan(a_1)} \qquad (2.15)$$

where G = track gauge, and

a_1 = angle of distribution of pressure in formation.

However, it has been observed that the modern trend for determination of formation stresses is based on the use of finite element and other computer oriented approaches.

2.2.2 Finite element and other computer oriented approaches

The various mathematical models that have been used for investigation of track design parameters are given below.

1. So model

It consists of following four different routines [So (1978)].

a. Finite element vertical track model

It is a two dimensional (2-D) finite element model which uses 1-D members to simulate rails and tie foundation stiffness. It predicts vertical rail-tie reactions from given vertical wheel - rail loading.

b. Finite element lateral track model

It is similar to the above model but it simulates track structure behaviour under lateral loading and predicts lateral tie loads.

c. Finite element tie model

It is a 2-D model with similar formulation and capabilities as above models but it generates vertical and

lateral tie-ballast loading from vertical and lateral rail-tie loading output from the above models.

d. Multilayer elastic model

Tie-ballast loading from above is used as input. This model is based on Burmister's solution [Burmister (1945)] for multilayer elastic system.

When all the above four models are used in combination, they give stresses at any point in the track structure, provided compatibility of displacements and forces is satisfied at boundary interfaces.

2. MULTA model

The multi-layer track analysis (MULTA) model is a combination of two routines - Burmister and LAC [Selig et al. (1979)].

Loads and Combination (LAC) routine is a matrix structural analysis model which solves for the tie-ballast reactions using the method of consistent deformations. Rails are assumed to be supported by certain number of ties and each with certain number of divisions. The tie-ballast contact pressures are assumed to be transmitted through these divisions. Reactions between rails and ties and displacements at intersection of rails and ties are also assumed as unknowns.

Burmister routine is based on Burmister's multilayer elastic theory [Burmister (1945)] and above tie-ballast

reactions are taken as input and stresses at required points are found out.

3. PSA model

It consists of two separate algorithms viz. PSA (Prismatic Solid Analysis) code and Wheels code [Selig et al. (1979)].

Wheels code is a matrix structural algorithm and is similar to LAC routine.

PSA code generates the foundation stresses and displacement coefficients. It performs the analysis of a class of 3-dimensional (3-D) problems whose solutions can be approximated by analysis of periodically loaded prismatic solids. The 3-D solution is approximated as Fourier series along the track direction. The coefficients in the series are obtained from 2-D finite element analysis. Summation of this series yields the final solution. The output consists of displacements, strains and stresses at any desired point in the track structure.

4. ILLITRACK model

It simulates the track system with two pseudo plane strain 2-D finite element analysis [Selig et al. (1979)]. The longitudinal 2-D analysis is followed by transverse 2-D analysis using the results from the previous longitudinal analysis as input. It employs following two types of finite elements.

a. Rectangular plane strain elements for ballast, subballast and subgrade.

b. Beam-Spring elements to represent rail tie sub-system.

5. GEOTRACK model

GEOTRACK [Chang et al. (1980)] is a 3-D, multilayer model for the elastic response of railroad track and it considers stress-dependent material properties and separation of tie and ballast. The computer program 'GEOTRACK' was developed starting with the program MULTA and deficiencies noted in 'MULTA' were removed. The changes pertain to the following aspects.

a. Excessively high stresses previously calculated beneath the center of each tie were corrected.

b. Vertical tensile stresses between ties and ballast were avoided.

c. Effects of two axles could be superimposed.

6. Finite element studies by Desai and Siriwardane (1982)

Desai and Siriwardane (1982) have presented 3 finite element formulations based on one-, two-, and three-dimensional idealization for analysis of rail road track support structures. 3-D formulation incorporates nonlinear constitutive behaviour by using four different elasto-plastic laws viz. Variable modulii, Drucker-Prager model, Cap model and Critical state model. It uses thin interface elements for simulation of behaviour at junctions.

a. 1-D model : It assumes rail supported by equivalent springs as a beam on nonlinear foundation. Rail is modelled as 1-D beam with six degrees of freedom system.

b. 2-D model : It involves plane strain idealization and uses 8-noded isoparametric elements for ties, ballast, subballast and soil.

c. 3-D model : Hexahedral elements were used for various track components. Bottom boundary was assumed to be rough and lateral boundaries as smooth. Boundary distance was fixed by parametric studies. A comparison of results was presented using PSA, MULTA, ILLITRACK and three dimensional finite element model with different boundary distances. However, it is observed that results obtained by 3-D finite element are lesser than results obtained from MULTA model.

CPU time comparison has also been given which shows CPU time of 1 min. and 44 sec. for linear 3-D analysis and 15 min. and 36 sec. for nonlinear analysis on IBM 3032 computer system for the mesh adopted therein.

7. Studies by ORE (Office for Research and Experiments, International Union of Railways, Utrecht)

Janin et al. (1983b) have carried out track analysis by two computer programs as given below.

a. BISTRO model : It is an elastic model and is based on Burmister's multilayer theory.

b. ROSALIE model : Both elastic and elasto-plastic, 3-D finite element models were developed. They employ hexahedral elements with 20 nodes.

Track analysis using both programs was carried out for single sleeper box at Vienna and Derby and for the complete panel of track at Derby. Results were compared with field tests and single sleeper box tests.

2.3 LITERATURE RELATED TO GEOTECHNICAL TESTING FOR EVALUATION OF STRENGTH, STRESS-STRAIN-PORE PRESSURE BEHAVIOUR

In order to predict the behaviour of soils under the railway formations and to evaluate a rational design procedure for railway formations, it is important to study the effect of cyclic loading on samples in laboratory simulating the track loading conditions.

This section has been classified into total stress /fatigue studies and effective stress studies.

2.3.1 TOTAL STRESS/FATIGUE STUDIES

1. Bishop and Henkel (1953) observed the effects of applying the stress pulses to undrained samples of Weald clay. They observed that residual pore pressures were left after the removal of load and that the magnitude and sign of these pore

pressures were dependent on the consolidation history of the clay and on the magnitude of the transient stress.

For a normally consolidated clay which develops +ve pore pressures in shear, they have observed that upon removal of the shear stress, a +ve residual pore pressure persists. The reapplication of the shearing stress causes the soil to develop additional +ve pore pressures, apparently increasing the pore pressure to a greater magnitude than would have developed had the first cycle of load been carried to failure.

When a heavily overconsolidated sample was subjected to a shear stress increasingly negative pore pressures were developed after the development of a small positive pore pressure at very low levels of stress and strain. A substantial negative pore pressure remained after unloading.

2. Sangrey (1968) reviewed the existing literature and noted that up to 100,000 cycles, the specimen deformation depended only on total number of cycles and was independent of frequency of cycles (tested for 1 to 20 cycles/min. frequency range). For thixotropic clays, frequency affected the deformation.

3. Janin et al. (1980) performed cyclic triaxial tests of 3 soils namely silt, silty sand and uniform fine sand. They made the following observations :

a. For tests conducted on 10 cm diameter and 20 cm high

samples in frequency range of 1 to 40 hz, no resonance phenomenon was observed. Hence they carried out all other tests with 5 Hz frequency.

b. In fatigue tests, the failure criterion adopted was plastic deformation exceeding the failure deformation values determined in the static triaxial tests. The K-value was defined as pulsating load causing failure to the static failure strength. All tests were carried out with drained conditions.

c. It was found that K-value varied with soil type as given below.

$K = 0.60$ for silt,

$= 0.28$ for silty sand, and

$= 0.30$ for uniform fine sand.

for $\sigma_3 = 15$ kPa.

d. Results of fatigue tests at different lateral stresses showed a distinct increase of plastic deformation with decreasing lateral stress.

e. More the initial density, lesser the plastic deformation in fatigue tests.

f. Water content affected K-value and deformation to a considerable extent in silt as compared to silty sand and uniform sand.

4. Janin et al. (1983a) carried out laboratory tests to determine the properties of sandy silt and silty clay used in

full scale model laboratory tests at Vienna arsenal (Sec. 2.5.3.) and from these tests, they made the following observations.

a. A difference in water content has more pronounced effect on engineering properties of silt than of the clay due to low plasticity.

b. Smooth stress strain curves were obtained for silty clay. But sandy silt showed brittle behaviour at low water content and showed behaviour of strain hardening materials at high water content.

c. Sandy silt showed extremely high friction angle (45 degrees) for undisturbed samples due to pronounced dilatancy at low confining stresses (σ_3 = 35 kPa). However, a lower value of 34 degrees was obtained for compacted samples.

d. The stress-strain relationships of the samples loaded monotonically to failure after cyclic loading (5×10^5 load cycles at different cyclic stress levels) were similar for both soils. A more brittle behaviour and a lower failure strain were observed.

e. Secant modulus decreases with increasing confining stress level.

2.3.2 EFFECTIVE STRESS STUDIES

The literature related to effective stress studies has been reviewed under the following sections :

a. Saturated soils

b. Non saturated soils

2.3.2.1 Saturated soils

1. Sangrey (1968) conducted the series of experiments on saturated clays and made the following observations :

a. For normally consolidated samples, there exists a critical level of repeated stress (CLRS) such that when cycled stress level is below CLRS, plastic deformation is terminating (i.e. equilibrium condition is reached) and when cycled stress level is above CLRS, plastic deformation is non-terminating.

b. Figure 2.2 shows the typical comparison of stress-strain curves of single loading and repeated loading for normally consolidated Newfield clay. Repeated loading curve has been defined by tests conducted at different cyclic stress levels.

c. Figure 2.3 shows peak strength relation with level of cyclic stress.

d. Tests were conducted on normally consolidated samples, anisotropically consolidated samples and overconsolidated samples with overconsolidation ratio, OCR = 2, 4, 6. Behaviour for these samples remains similar to normally consolidated clay in general except that as OCR increases, clay exhibits lesser residual pore pressure development at a given stress level. Typical curve for OCR = 6 is given in Fig. 2.4.

e. Procedure to evaluate critical level of repeated stress

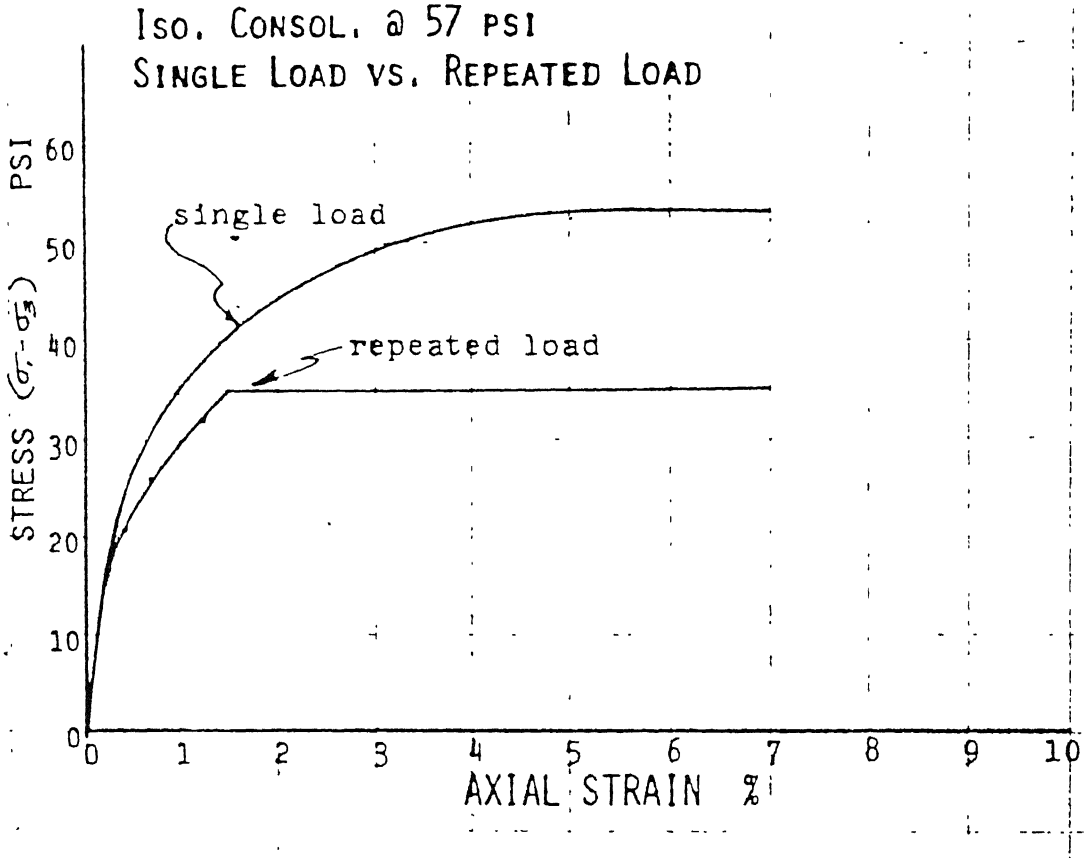

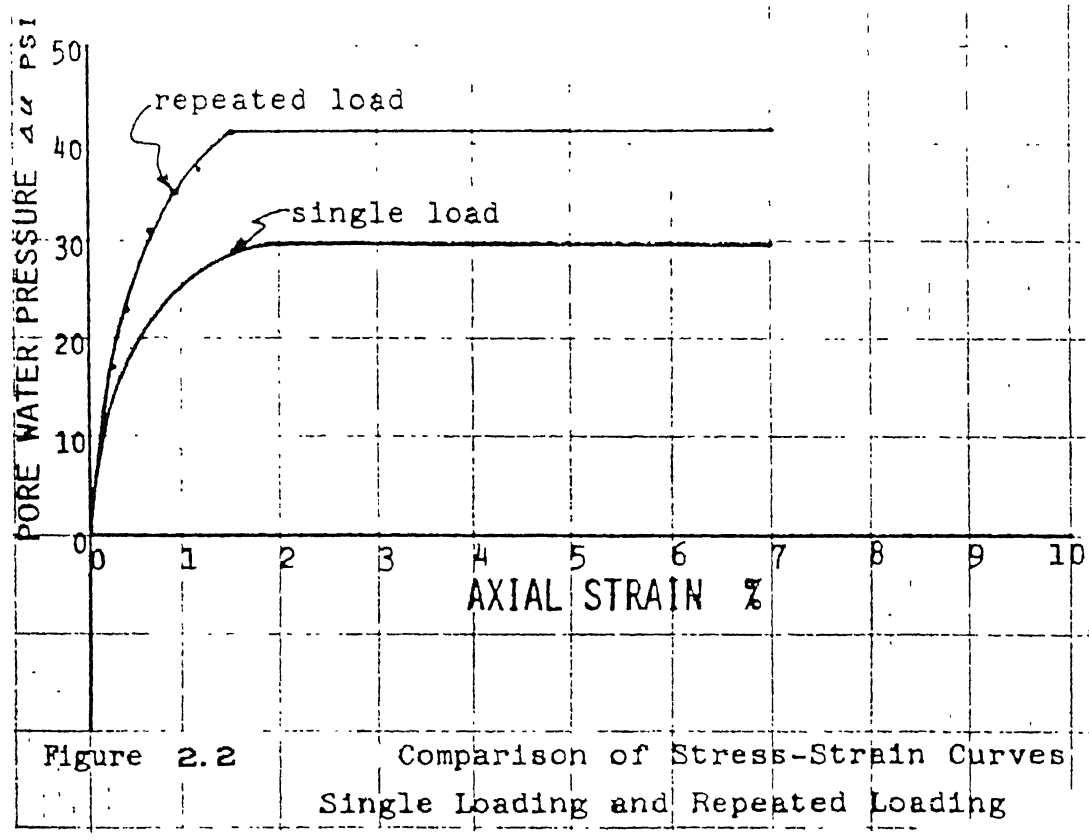

Figure 2.2 Comparison of Stress-Strain Curves of Single Loading and Repeated Loading

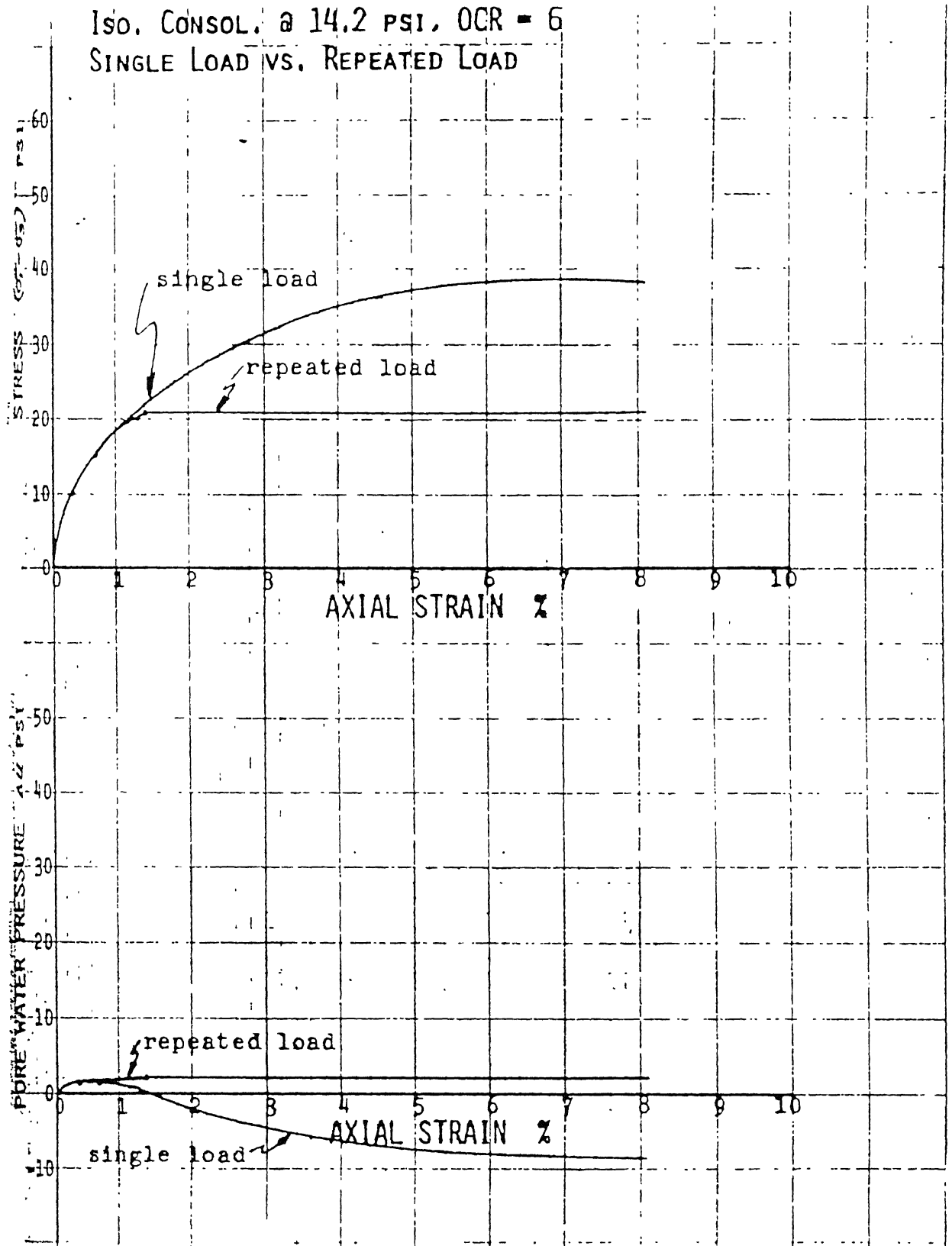

Figure 2.4 Comparison of Stress-Strain Curves of Single Loading and Repeated Loading

(or threshold stress) based on movement of effective stress path due to development of pore pressure during cyclic loading was suggested.

2. Rubin et al. (1970) investigated clay behaviour under dynamic and repeated triaxial loading. Standard repeated triaxial load test is defined as a test at a constant ambient pressure of 35 KPa with cyclic frequency of 30 cycles per minute. Failure criterion was assumed as 10 percent cumulative deformation produced in less than 1000 load cycles. Threshold stress is defined as a maximum stress that can be applied to the sample that does not cause cumulative strain greater than 10 percent in 1000 cycles.

Based on studies related to development of plastic strain with number of cycles at different cyclic stress ratio, a relationship between cumulative plastic strain and number of cycles has been proposed.

It has been observed that as cyclic stress increases, the nature of relationship between plastic strain development and number of load cycles changes from terminating to the non-terminating one. Based on this observation and the above mentioned failure criterion, Rubin et al. (1970) have calculated the threshold stress in drained tests.

No relationship is apparent between the water content changes and the applied stress.

Threshold stress value is not a basic material parameter

but is dependent on mean effective stress, wave shape, frequency and previous loading history.

3. Gupta (1973) carried out static and repeated triaxial tests on saturated normally consolidated Campus silt. Confining pressure was found to have dominant effect on nature of stress-strain curve. For repeated load tests, it is found that for 25 percent and 55 percent stress level, pore pressure increases during loading and decreases with unloading. For 75 percent stress level, the response is reverse. It is observed that for the silty soil on which tests were carried out, equilibrium line exists.

4. Wilson and Greenwood (1974) carried out cyclic tests with pore pressure measurements on lacustrine clay at Hamilton, Ontario. They presented the data for plastic strain development and pore pressure increment with number of load cycles.

5. Schjetne (1976) has carried out stress controlled triaxial tests and simple shear tests on clay with different OCR and concluded that c' and ϕ' remain unaffected by cyclic loading where c' and ϕ' are the effective cohesion and angle of friction of clay. The undrained shear strength after cyclic loading is a function of cyclic shear strain reached and the number of cycles.

6. Based on undrained triaxial tests on remoulded clay, Hyde and Brown (1976) proposed the following relationship .

$$\log \dot{\varepsilon} = C - D \log T \qquad (2.16)$$

where $\dot{\varepsilon}$ = strain rate per unit time,

C = log of strain rate at unit time,

D = strain rate decay constant, and

T = time in secs.

D was found to be constant for samples with the same stress history.

7. Based on results from laboratory testing of Drummen clay under cyclic loading, Andersen et al. (1976) have concluded that for normally consolidated clays, drainage will reduce cyclic displacements and improve stability while for overconsolidated clays, drainage will increase cyclic displacements and will reduce the stability.

8. Based on undrained static and cyclic triaxial tests on normally consolidated plastic clays, Yudhbir and Rehman (1977) made the following observations.

a. Clay with lower plasticity index (I_p) has a lower value of critical stress level than clays with higher I_p.

b. τ_{cyc} / s_u (applied cyclic stress, τ_{cyc} as a fraction

of undrained shear strength, s_u) increases with the increase in confining stresses.

c. Pore pressure set up at equilibrium state increases with cycled stress level and is higher for low I_p clay than for high I_p clay.

9. Sangrey et al. (1978) have presented the relationship between threshold stress ratio and κ/v_0 where κ is the slope of swelling line in triaxial consolidation test and v_0 is the specific volume of sample. The term κ/v_0 is the measure of soil compressibility. From this relation, threshold stress ratio for variety of soils can be evaluated. However, it must be noted that evaluation of κ poses certain problems.

10. Andersen et al. (1980) carried out cyclic triaxial and simple shear tests on Drummen clay for OCR from 1 to 50 and concluded that the behaviour of clay during undrained cyclic loading could be explained in terms of effective stresses. Some of the observations made by them are as follows.

a. A normally consolidated clay is more resistant to undrained cyclic loading than an overconsolidated clay.

b. Results from strain controlled cyclic loading do not coincide with the stress controlled cyclic loading except when interpreted in terms of accumulated cyclic shear strain.

of undrained shear strength, s_u) increases with the increase in confining stresses.

c. Pore pressure set up at equilibrium state increases with cycled stress level and is higher for low I_p clay than for high I_p clay.

9. Sangrey et al. (1978) have presented the relationship between threshold stress ratio and κ/v_0 where κ is the slope of swelling line in triaxial consolidation test and v_0 is the specific volume of sample. The term κ/v_0 is the measure of soil compressibility. From this relation, threshold stress ratio for variety of soils can be evaluated. However, it must be noted that evaluation of κ poses certain problems.

10. Andersen et al. (1980) carried out cyclic triaxial and simple shear tests on Drummen clay for OCR from 1 to 50 and concluded that the behaviour of clay during undrained cyclic loading could be explained in terms of effective stresses. Some of the observations made by them are as follows.

a. A normally consolidated clay is more resistant to undrained cyclic loading than an overconsolidated clay.

b. Results from strain controlled cyclic loading do not coincide with the stress controlled cyclic loading except when interpreted in terms of accumulated cyclic shear strain.

11. Wood (1982) has carried out review on laboratory investigations of the behaviour of soils under cyclic loading and following are some of his findings.

Effective stresses and pore pressures provide the key controlling the behaviour of soils under cyclic loading.

Test procedures need to be such that pore pressures can be reliably monitored. This leads to prefer slow cyclic tests to fast ones on the grounds that pore pressure measurements in the former are more likely to reflect the actual intentions of the soil.

Only first few cycles of cyclic loading are important to make observations on both changes in pore pressure and the stiffness.

12. Hyde and Ward (1985) have shown that permanent pressures built up during cyclic loading of normally consolidated Keuper marl can be expressed by the following relation.

$$\log (\dot{u}/P_e') = \log \alpha - \beta \log N \qquad (2.17)$$

where α = pore pressure rate at n = 1,

β = gradient of log (u/P_e) vs. log N plot,

$\dot{u}$ = rate of change of pore pressure with N, and

P_e' = Hvorslev's equivalent consolidation pressure.

They also describe that though this relation is similar to

Eq. (2.16) but there is no simple relationship between strain and pore pressure development.

They have observed that Hvorslev surface forms the upper boundary for cyclic effective stress tests for failure.

13. Shew et al. (1987) have conducted a series of cyclic triaxial tests on Kaoline clay under 3 triaxial stress paths viz. cyclic compression, cyclic extension and cyclic compression extension and concluded that critical stress level for repeated loading for cyclic compression test is larger than the cyclic extension tests and is much larger than cyclic extension compression tests.

14. Based on undrained triaxial and direct simple shear tests on Drummen clay, Andersen et al. (1988) concluded that cyclic properties of clay depended upon both average shear stress and type of test (e.g. triaxial or direct simple shear).

2.3.2.2 NON SATURATED SOILS

1. Bishop et al. (1960) gave the following equation for shear strength evaluation of partially saturated clay.

$$\tau = c' + (\sigma - u_a)\tan\phi' + X\,(u_a - u_w)\tan\phi' \qquad (2.18)$$

where τ = Undrained shear strength of partially saturated soil.

X = a parameter that varies with the degree of saturation of sample,

u_a = the pore air pressure, and

u_w = the pore water pressure.

2. Lambe (1960) gave mechanistic picture of shear strength of clay and proposed alternative relationship for shear strength prediction of partially saturated clay based on internal attraction and repulsion of clay particles. However, this relationship remained mostly academic in nature due to difficulty in measuring the internal attraction and repulsion.

3. Casagrande and Hirschfeld (1960) and Casagrande and Poulos (1964) have done extensive studies on stress - deformation, strength and pore pressure characteristics of compacted silty soil. They have carried out 3 types of tests :

a. $\bar{Q}$ tests : During these type of tests, compacted partially saturated soil samples are subjected to undrained triaxial shear with constant cell pressure.

b. $\bar{R}$ tests : In these tests, compacted samples are placed in triaxial cell and are back saturated . Then, on these samples, undrained tests are carried out.

c. S tests : These are slow drained tests on compacted back saturated soil.

It may be noted that this silty soil has similar engineering characteristics as the present alluvium silt on which experiments have been carried out.

4. Fredlund et al. (1978) have given the following equation :

$$\tau = c' + (\sigma - u_a)\tan \phi' + (u_a - u_w) \tan \phi^b \qquad (2.19)$$

where ϕ^b relates contribution of matrix suction to the shearing resistance. It may be noted that suction consists of two components -- osmotic suction and matrix suction. $(u_a - u_w)$ is the capillary tension. Suction would be equal to the capillary tension (i.e. matrix suction) only when components of osmotic forces were zero. This puts the limitation on degree of saturation range for which Eq. (2.18) is valid.

5. Marsal (1979) suggested an approximate procedure for deriving the shear strength envelope for the partially saturated soil samples from UU test results.

6. A more detailed analysis has shown that u_a would be very close to zero for high degrees of saturation (in general above 85% and in some soils above 90 %) and that under these conditions the air would be occluded and the soil would be in a state called 'quasi-saturated' [Cruz et al. (1985)].

It is shown that effective stress envelope for partially saturated clay is not a straight line but consists of three straight line sections as shown in Fig. 2.5 depending upon the stress level. For first two sections, values of c'and ϕ' would

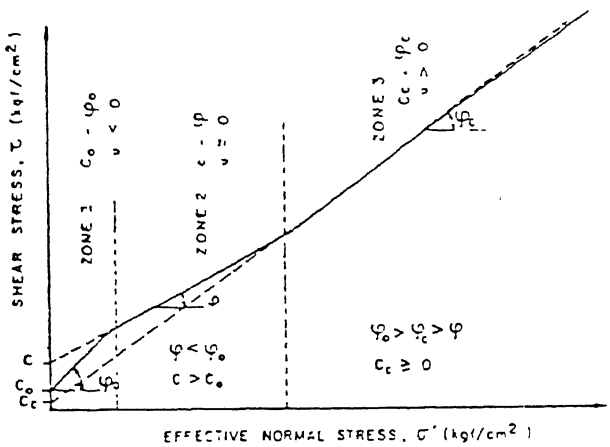

Fig. 2.5 - *MOHR ENVELOPE FOR COMPACTED SOILS*

be different for saturated and partially saturated soil while for third section, saturated and partially saturated test results would be aligned along the same straight line [Cruz et al. (1985)].

7. Yudhbir and Korchoke (1987) have shown that within the narrow range of degree of saturation where air and water void continuity assumption needed for both Bishop et al. (1960) and Fredlund et al. (1978) approaches (Eqs. 2.18 and 2.19) is satisfied (for S range = 75 % to 85 %), both approaches are similar. They have also shown that Marsal's procedure to estimate ϕ' from UU test results gives good results over wide range of degrees of saturation (even below 75 % degree of saturation where most of the field problems are encountered in residual soils).

2.4 LITERATURE RELATED TO TRACK FORMATION DESIGN

1. Rubin et al. (1970) determined the threshold stress-depth relationship for London clay by extrapolation from limited amount of data and superimposed it on maximum shear stress versus depth relationship as shown in Fig. 2.6 and the design criterion suggested was that for a subgrade of given threshold stress, the depth to the subgrade must be greater than that indicated by appropriate nominal axle load.

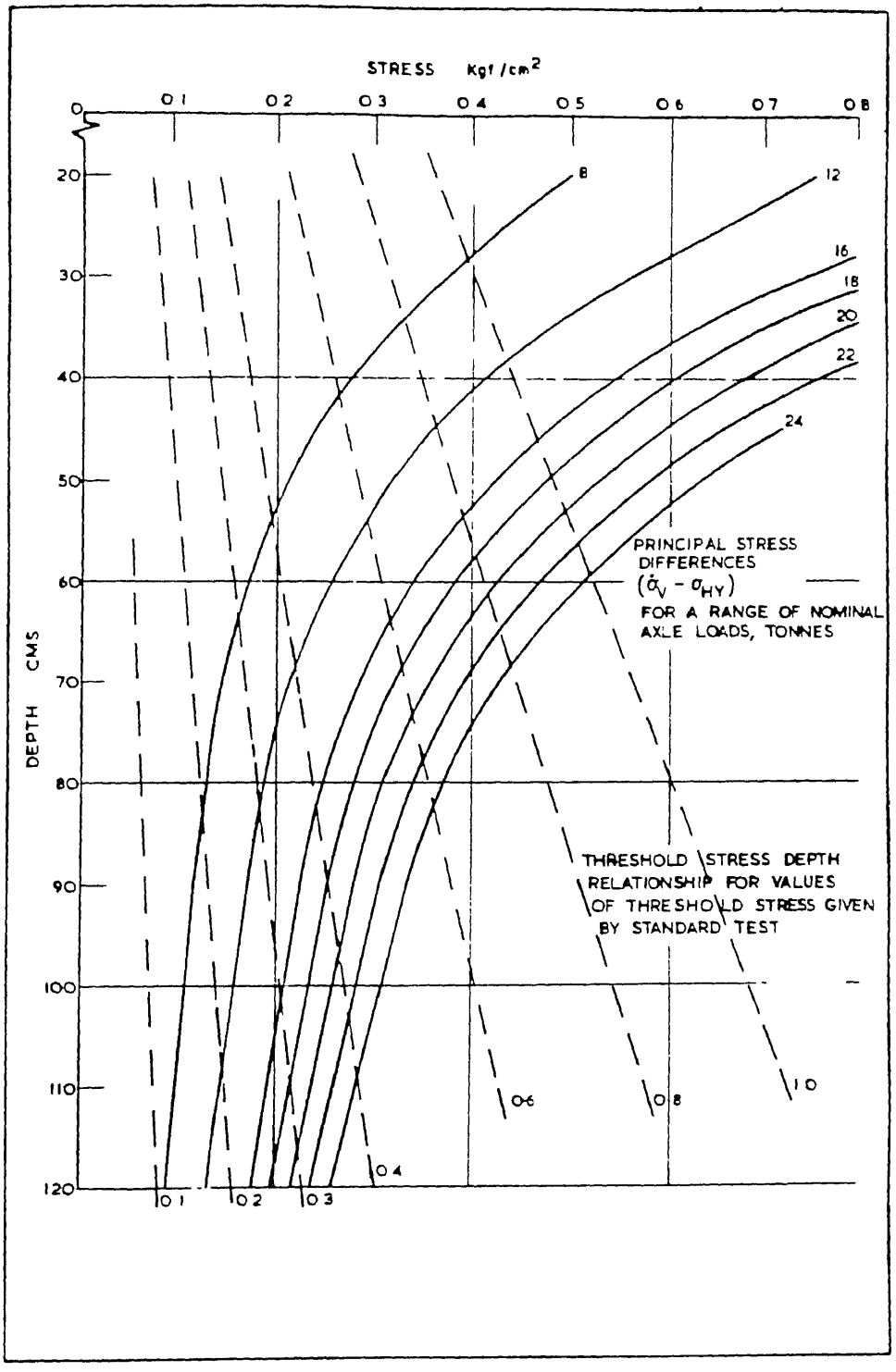

Fig. 2.6 Design Charts (Rubin et al., 1970)

2. Agarwal and Yog (1975) proposed a new approach for design of substructure thickness based on effective stress analysis. Information about net state of stress was found out by adding up the stresses due to the live load and superimposed load (determined by Boussinesq's theory) and plot of total stress path of existing stress condition was developed. Assuming A = 0 (for compacted clay) and B = 1 for different k_0 values, plots of effective stress paths of net state of stress were derived. For any soil, knowing shear strength parameter, k_f' line can be drawn. Intersection of k_f' line with effective stress path (for net state of stress) would give the thickness of ballast and subballast layers. For cohesive subgrades, for different values of c', charts have been proposed between ϕ' and thickness of ballast and subballast layer.

3. So (1978) carried out numerical analysis of track (Sec. 2.2.2) and gave the family of charts. One family of charts for predicting maximum stress level induced in one component of track structure due to change in different track components of reference track was given. Thus, a series of families of charts was given for predicting the maximum stress level induced in different components of track structure.

The family of design charts for subgrade stresses due to the vertical loading has been proposed (Figs. 3.65 to 3.67). Changes due to the tie-spacing, ballast depth and subgrade modulus of elasticity have been considered. Rail size and tie support condition have insignificant effects on subgrade

stresses. The design criterion being the induced stresses calculated from above design charts should not exceed the stress level required for fatigue failure determined by experiment.

4. Tadatoshi et al. (A) have presented charts (Fig 2.7) from which depth of ballast and subballast can be determined in order to avoid the mud pumping.

Mud pumping of roadbed is a phenomenon caused when roadbed soil is softened by the rainfall or groundwater ; the mud climbs up through the voids inside the ballast and pumped out on the ballast surface by a passing train load. Occurrence of mud pumping causes not only reduction of elasticity of ballast but also increases track subsidence, and as a result maintenance overburden is required. Occurrence of mud pumping is caused primarily by softening of roadbed soil by water, by use of unqualified soil, and by overloading to roadbed, according to field investigations and laboratory tests carried out by Japanese national railways [Tadatoshi et al. (A)].

From the empirical formula used by Japanese national railways (Sec. 2.2.1) , they presented the reduction of roadbed pressure achieved by change of track structure viz. narrowing the tie spacing [Fig. 2.8(a)], increase of ballast thickness [Fig. 2.8(b)]. They have also related upper roadbed pressure and mud pumping with liquid limit [Fig. 2.9(a)] and with CBR [Fig. 2.9(b)].

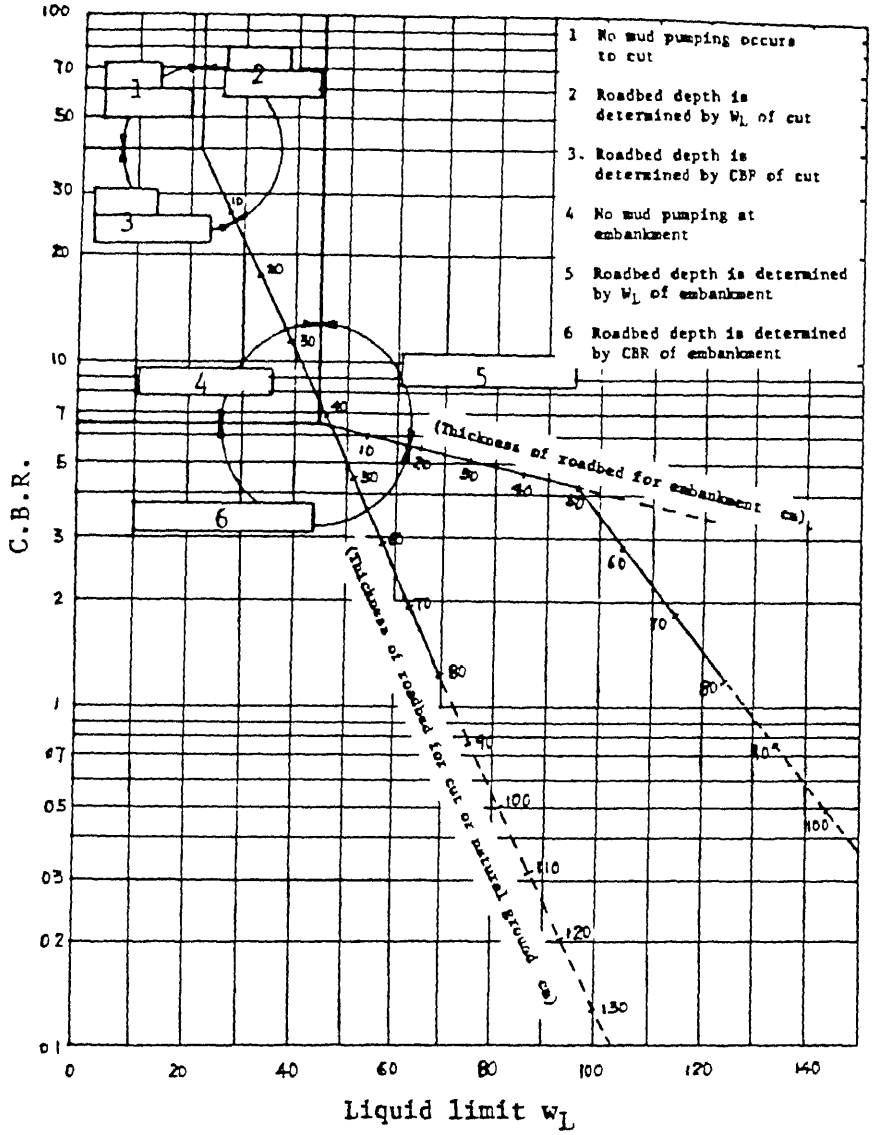

Fig. 2.7 Decision diagram for roadbed depth

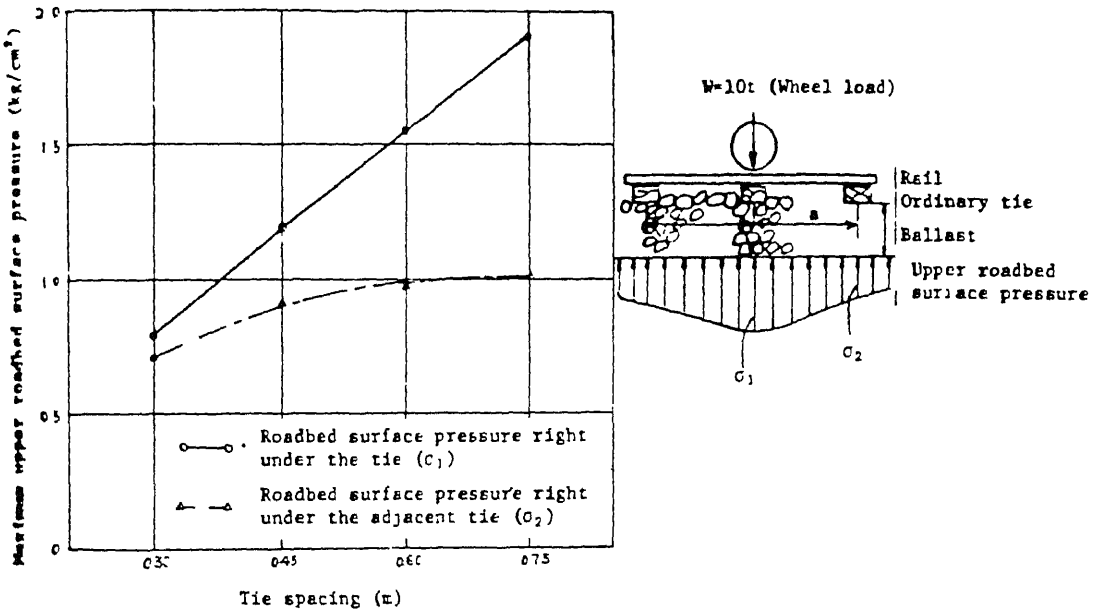

Fig. 2.8A Relationship between tie spacing and roadbed pressure

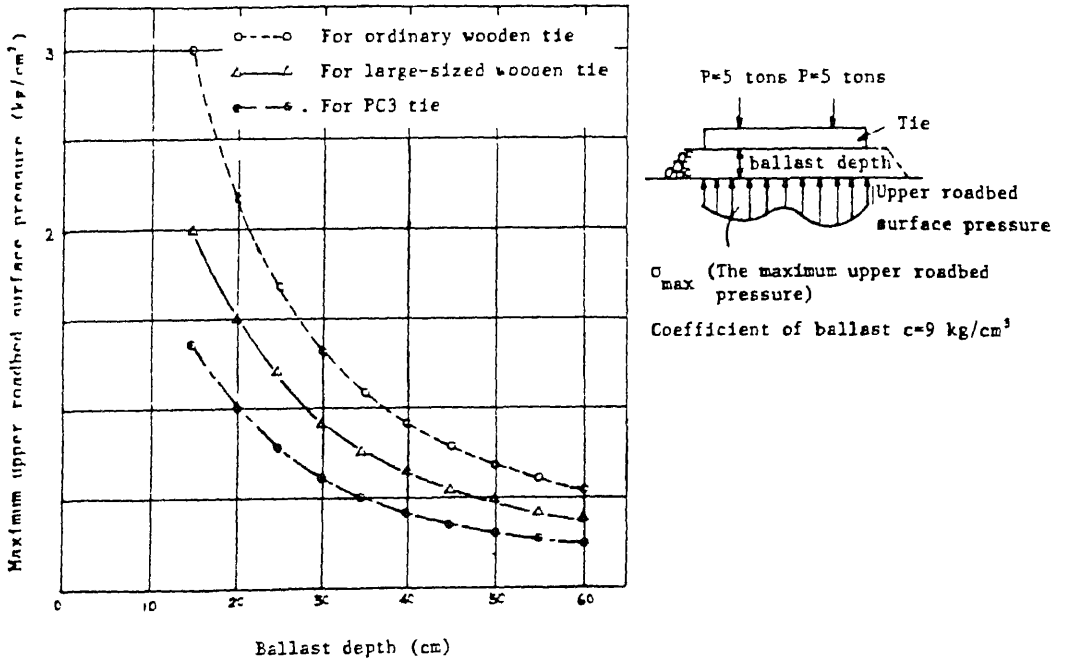

Fig. 2.8B Relationship between ballast depth, the kind of tie, and roadbed pressure

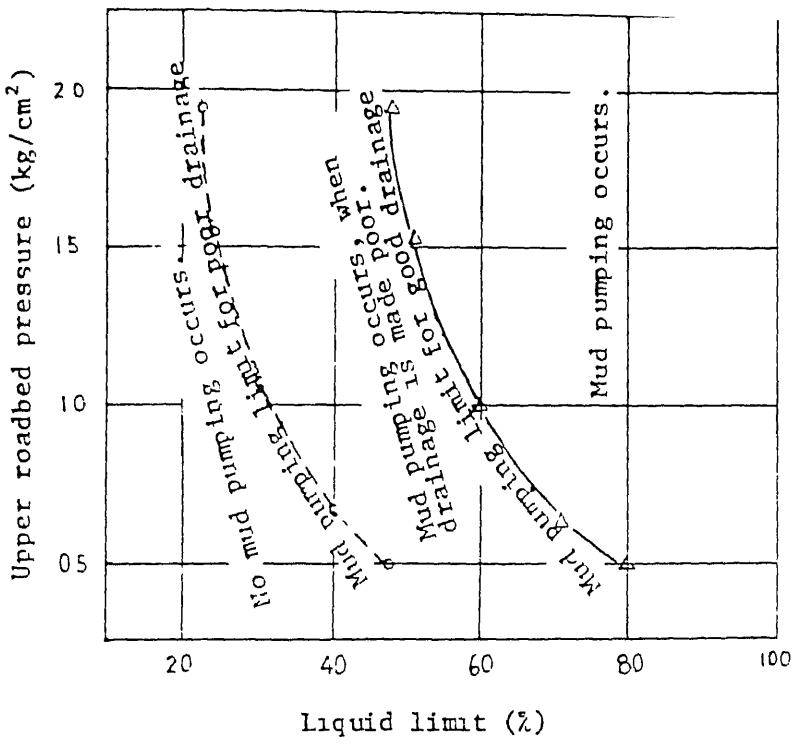

Fig. 2.8A Relationship between roadbed pressure, liquid limit, and mud pumping (Applied rail pressure is 5 t, and ordinary wooden tie is used.)

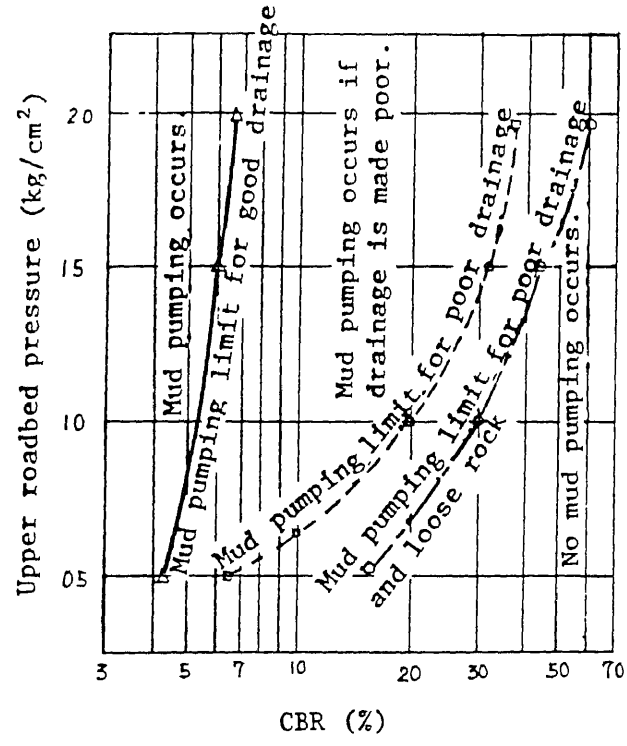

Fig. 2.8B Relationship between roadbed pressure, CBR, and mud pumping (Applied rail pressure is 5 tons and standard wooden tie is used.)

5. Janin et al. (1983c) have argued that deflection of rail (z_{sta}) calculated numerically will be lesser than the actual dynamic deflection because of presence of voids in actual dynamic condition. Now, as the vertical stiffness of rail remains same, i.e.

$$\left(\frac{Q}{z}\right)_{sta} \simeq \left(\frac{Q}{z}\right)_{dyn} \tag{2.20}$$

Therefore, Q_{dyn} will be more than Q_{sta}. A procedure to calculate max Q_{dyn} has been given from which max σ_{dyn} can be found out by multiplying σ_{sta} (obtained numerically) by

$$\left(\frac{\max Q_{dyn}}{Q_{sta}}\right) .$$

where subscript 'dyn' indicates dynamic, and
subscript 'sta' indicates static.

In this way, curves in Fig. 2.10 have been generated. Then, an elaborate design procedure has been given which uses Fig. 2.10 and some other empirical relationships. The design criterion being the compatibility between dynamic stress on subgrade (Fig. 2.10) and the bearing capacity of the subgrade soil.

This study observes that threshold stress ($\sigma_1 - \sigma_3$) design approach by Rubin et al. (1970) is based on fatigue behaviour

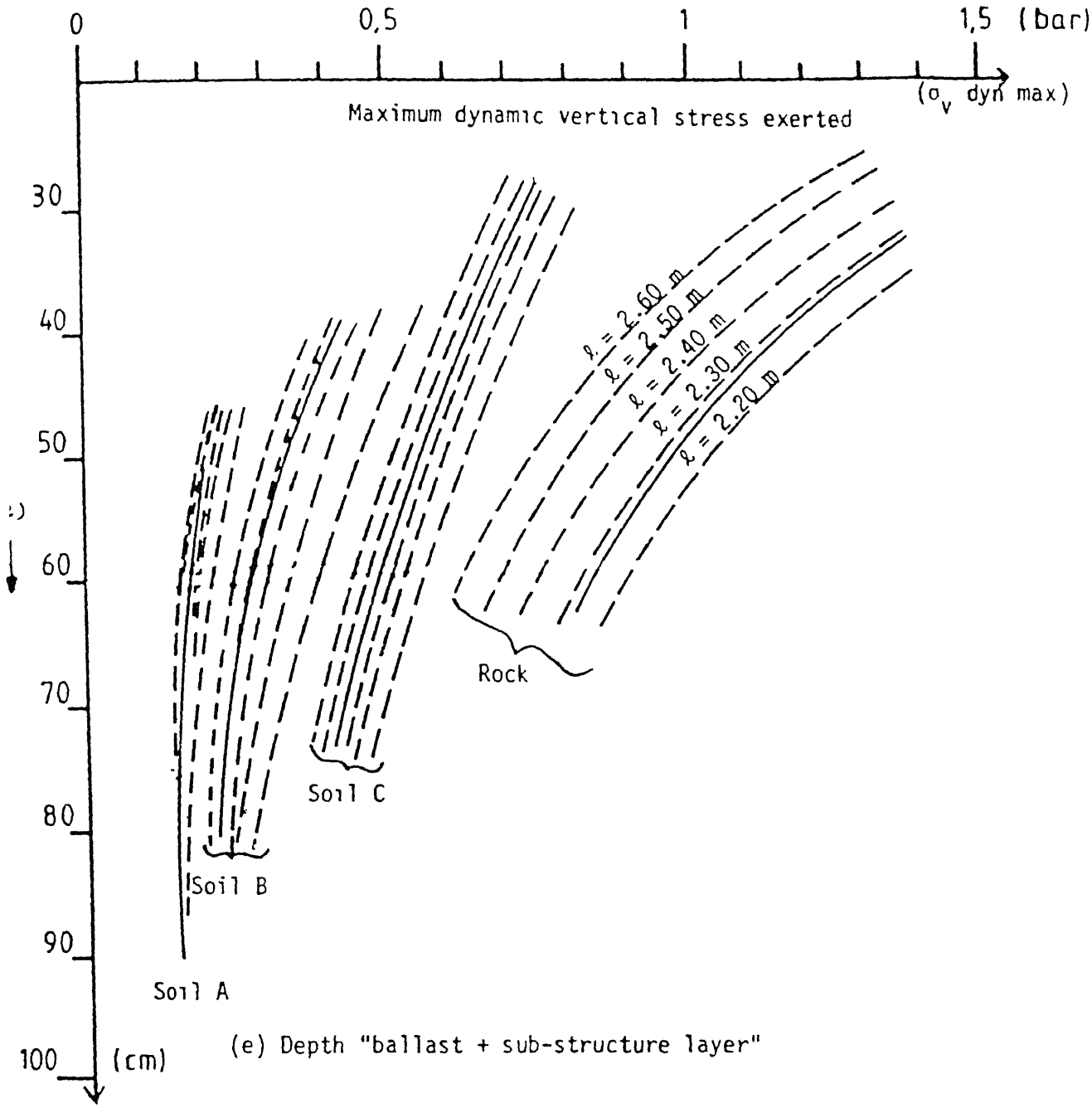

(e) Depth "ballast + sub-structure layer"

———————— Timber sleepers (length 2.60 m)

– – – – – – – – – – Concrete sleepers (various lengths from 2.20 m to 2.60 m)

FIG 2.10 Maximum dynamic vertical stresses exerted on the subgrade

and guards against failure of subgrade but in practice, it is necessary that the foundation be stressed well below the limits of failure to prevent excessive track maintenance.

6. Senac (1984) recognizes two important aspects in way of track design to resist vertical forces viz. track equipment and ballast formation considerations.

Track equipment is defined as $(I_r/y_f) / \bar{S}$ where y_f is the distance between the neutral axis of rail and rail flange. Table 2.1 gives the track equipment standards adopted by SNCF (French Railways) for a formation of normal bearing capacity. The quality of formation has been classified based upon static rigidity, ρ_s (Table 2.2) and formation coefficient, C. Furthermore, SNCF specifies the following minimum substructure depth.

30-55 cm under wooden sleepers.

40-50 cm under concrete sleepers.

depending upon soil characteristics, for tracks handling 50000 t/day with high speed traffic and a minimum depth of 25 - 35 cm on slower , less heavily trafficked line, subjected to favorable hydrogeological and substructure conditions.

7. Hall (A) has described the studies conducted for design of upgraded Richards bay coal export line in South Africa. Track structure parameters (rails, sleeper type and spacing)

Table 2.1 Track Equipment standards (BY SNCF)

Category	Track equipment $(I_r/y_f)/\bar{S}$ (m^2)	Maximum axle load (t)	Maximum Train speed (km/h)
1	100/140	18	70
2	141/179	18	85
3	180/235	20	95
4	236/350	21 to 23	115 to 160
5	> 350	22	200

Table 2.2 Track formation quality (by SNCF)

Formation Quality	Static Rigidity (ρ in t/mm)	Formation Coefficient (C in N/cm^3)
Bad	---	20
Poor	0.6	30
Average or Acceptable	1.7	90 - 100
Good	atleast 3.5	at least 180

were specified beforehand. Hence, only formation design was required. Initially, a theoretical design based on mechanistic type analysis (often used for roadways) was evaluated. Simultaneously, a detailed study was carried out over a similar operating track. The theoretical design was then altered to give more practical final design based on the experience gained from the study of similar operating track.

Failure criterion adopted for theoretical design was based on limiting the vertical strain. Depending upon track life required and traffic to be dealt, total number of repetitions in the track life (N_r) can be calculated.

Then, a design track was assumed for analysis. Mechanistic model for traffic-induced fatigue cracking for stabilized formation was used as :

$$N_f = 10^{9.1(1-e/e_b)} \qquad (2.21)$$

where N_f = number of repetitions required for failure,

e_b = vertical strain at failure, and

e = maximum horizontal tensile strain at the base of stabilized layers (to be calculated from elastic or empirical models).

Thus, N_f was calculated. For satisfactory design, $N_f > N_r$.

Important findings of this study on existing track were as follows :

a. Track defects show marked increase with the rainfall in the surrounding area.

b. Mean moisture content vs. depth relationship remained same for all the tracks whether they were built in cutting or embankment provided water table is not intersecting the formation. This shows that moisture penetrates from top of track structure. The source of moisture being the rainfall.

c. Mud pumping is independent of shear strength of formation and depends upon gradation of subgrade. Mud pumping occurs mostly on tracks built on clays and silts.

2.5 LITERATURE RELATED TO OTHER IMPORTANT ASPECTS

2.5.1 EFFECT OF TRAIN SPEED ON STRESSES

During track analysis, speed effect is normally taken into consideration by a load augmentation factor based upon experiments.

1. Austrian Method

Austrian railways account for speed by a chart giving relation between load-increasing factor vs. speed [RDSO (B)].

2. German Method

German Railways give the following formula [RDSO (B)].

$$\sigma_{speed} = \sigma_t(1 + s\,\bar{t}\,) \qquad (2.22)$$

where s depends on track and varies between 0.1 y to 0.3 y,

$y = 1$ for speed 'V' $\leq$ 60 kmph,

$= 1 + \frac{(V - 60)}{140}$ for V > 60 kmph, and

$\bar{t} = 3$ for a statistical safety of 99.7 %.

3. Japanese Method

According to Japanese practice, speed impact factor can be found out from empirical relation [RDSO (1987)] given below :

$$i = 1 + 0.5\ V / 100 \quad \text{(with joint rail)} \qquad (2.23)$$

$$i = 1 + 0.3\ V / 100$$

'i' should not exceed 1.8

2.5.2 CHARACTERIZATION OF TRACK FOUNDATION

There are several ways in which elastic foundation can be characterized as given below.

1. Formation coefficient 'C' (kg/cm^3) [RDSO (B) and Senac (1984)].

2. Modulus of elasticity of rail support or modulus of rail-road reaction 'k' (kg/cm^2) [Talbot et al. (1923)].

3. Static Rigidity 'ρ' (kg/cm) [Senac (1984)].

The modulus of elasticity of rail support 'k' had been introduced as a measure of vertical stiffness of rail support [Talbot et al. (1923)]. It may be defined as the pressure per

unit length of each rail required to deflect the track per unit.

$$k = \frac{\text{equivalent load / tie}}{\text{Average depression} \times \text{spacing}}$$

It represents the stiffness and yieldability of tie, ballast and roadway but does not involve the stiffness of rail. It is related to tie-spacing, tie-dimensions, depth of ballast, quality of tie, solidity of roadway, character of tamping and surface and other conditions of the track and its maintenance. Naturally, this value must be determined by tests at different locations and over a wide range of conditions. It is denoted by 'u' or 'k'.

In Zimmermann's method, either 'C' or 'k' is used and it is assumed that this 'C' or 'k' characterizes the continuous foundation [RDSO (B)]. This assumption does not have much effect and Zimmermann's method is good to use because although the cross-ties constitute a discontinuous support, their width forms a considerable part of the rail length, and , as the distance from a single wheel load to the point where the track depression is zero covers from 4 to 6 tie spacings, the assumption of continuous support may not be expected to be generally much in error for usual conditions of good track, especially as the method used for determining the value of modulus of elasticity of rail support 'k' will carry into this

value some of the conditions attending the discontinuous support.

Accuracy of analysis using 'k' may be affected because 'k' may not be a constant because initially, some load will cause readjustment of pores and gaps in the track structure. Conditions of track may be classified into following 3 groups as shown in Fig. 2.11 [Yudhbir et al. (1991)].

a. Condition 'A' represents 'Well tamped' track. Load-settlement curve for this track can be represented by straight line passing through the origin.

b. Condition 'B' represents 'track condition where bending of tie is necessary before full bearing is obtained'. Load-settlement curve for this track can be represented by straight line which does not pass through the origin.

c. Condition 'C' represents 'poor' track. Load-settlement curve is not a straight line.

Concept of u_e and u_i :

The load method for the calculation of track modulus [Kapoor et al. (1967a)] is given below

$$\text{Initial range } u_i = \frac{(10.7\ Q_1)^{4/3}}{(I_r^{1/4} \times y_{s1})^{4/3}} \text{ lbs/in/in} \qquad (2.24)$$

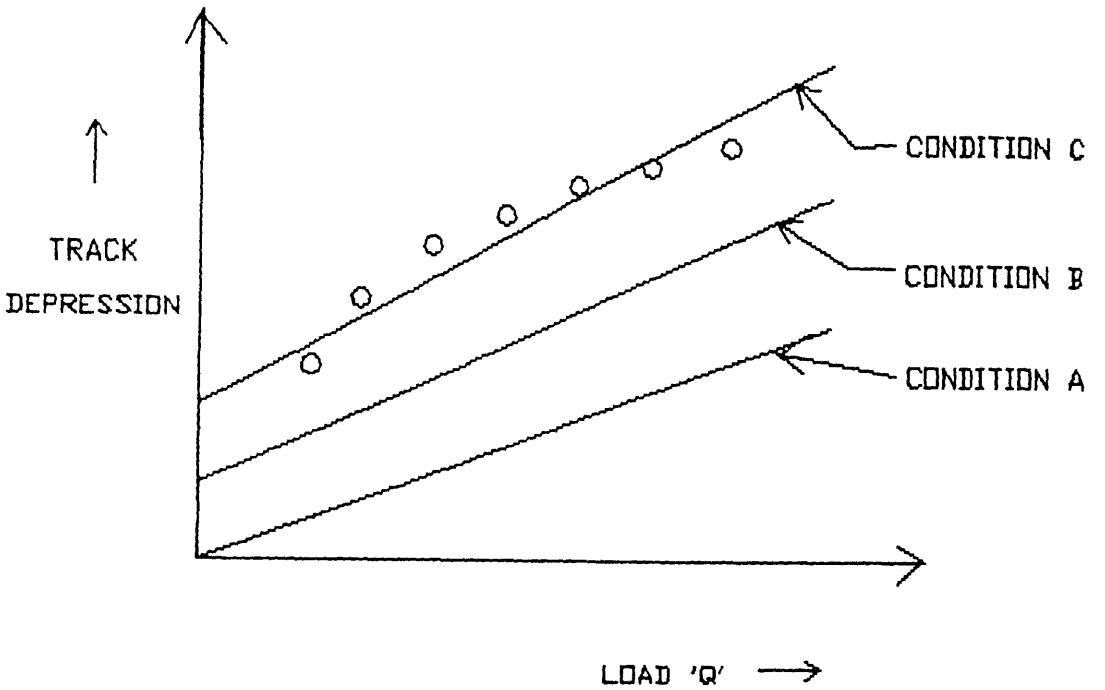

Fig. 2.11 TRACK DEPRESSION VS. LOAD RELATIONSHIP FOR DIFFERENT TRACKS.

where Q = total vertical load

Q_1 = initial load required to bring the track in elastic range.

y_{s1} = deflection of sleeper under load Q.

u_i = modulus of railroad reaction in initial range.

$$\text{elastic range } u_e = \frac{(10.7)^{4/3}\ (Q - Q_1)^{4/3}}{[I_r^{1/4} \times (Y_s - Y_{s1})]^{4/3}} \text{ lbs/in/in} \qquad (2.25)$$

Note 1 kg/cm^2 = 6.89 psi

where u_e = modulus of railroad reaction in elastic range.

Bearing area of sleeper [Mundrey (1988)] :

On empirical basis, the bearing area below sleeper which takes the load is as shown in Fig. 2.12. It is assumed that stresses are uniformly distributed on bearing area.

Bearing length / sleeper as given by Mundrey (1988) = 131.42 cm (as shown in Fig. 2.12).

Bearing length / sleeper as given by Saxena and Arora (1987) = 180 cm.

Bearing length / sleeper as calculated from data given by Senac (1984) = 166.2 cm (adopted here).

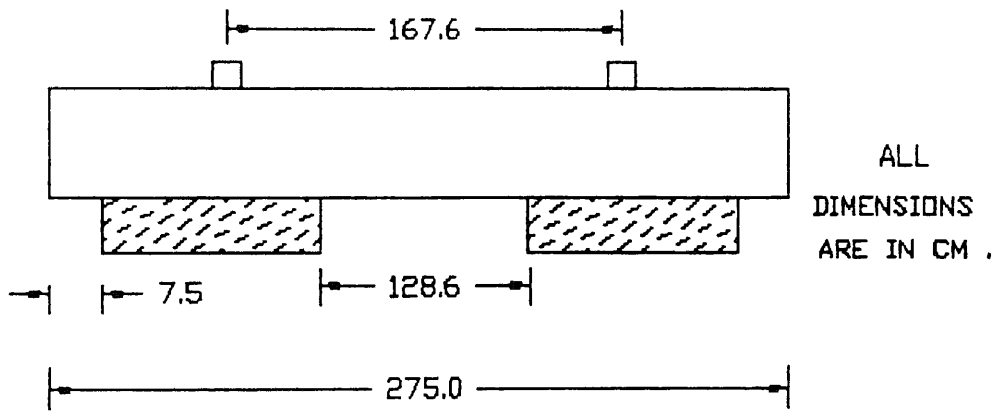

Fig. 2.12 BEARING AREA OF SLEEPER

Relation between 'C', 'ρ' and 'k' [see Yudhbir et al. (1991)] :

$$k = \bar{b}\, C \tag{2.26}$$

where $$\bar{b} = \frac{\text{Bearing Area per sleeper 'F'}}{(2 \times \text{spacing '}\bar{S}\text{'})}$$

$$C = \rho \,/\, F \text{ , and} \tag{2.28}$$

$$\rho = R \,/\, y_t \tag{2.29}$$

with R = Reaction of sleeper, and
y_t = Vertical deflection of sleeper due to force 'R'

$$\rho = 2\, k\, \bar{S} \tag{2.30}$$

2.5.3 SOIL IMPROVEMENT METHODS

This can be achieved by methods given below [RDSO (C) and Tadatoshi et al. (A)].

1. Soil stabilization : A list of usual methods for roadbed stabilization has been given in Table 1.1.

2. Soil drainage : Proper drainage plays very important role in controlling the mud pumping.

3. Soil compaction : Proper compaction increases the threshold stress for soil.

4. Soil reinforcement : Japanese railways have suggested that for high speeds, heavy axle load and increased traffic

density, soil reinforcement may be used in addition to the usual thickness of ballast as obtained from theory of elasticity [RDSO (C)].

2.5.4 FIELD MEASUREMENTS AND MODEL TESTING

1. Field measurements by Indian railways [RDSO (A)].

Empirical formulae need the information on track modulus and hence to find this out for Indian tracks, field studies were carried out in 1960's at Ambala - Ludhiana section which resulted in civil engg. report no. C 47, Nov 1966. Later, track modulus (initial and elastic) values had been recommended as given in civil engg. report no. C-67, Sept. 1968 of RDSO (Research, Design and Specifications Organization, Indian railways).

Track with wooden sleepers : u_i = 50 kg/cm/cm

u_e = 250 kg/cm/cm

Track with metal sleepers : u_i = 75 kg/cm/cm

u_e = 300 kg/cm/cm

Till 1960, no field tests were conducted to check whether empirical formulae apply to Indian track conditions. Hence in 1962-66, dynamic field tests were conducted to measure the maximum pressure on top of formation which resulted into civil engg. report no. C-47, C-48, C-55 and C-56.

Since dynamic field tests were conducted only on tracks with N+3 sleeper density and the track structure later

consisted mainly of N+6 sleeper density, and dynamic tests posed problems due to line capacity, static tests were conducted by RDSO in 1970-74 to find out pressure distribution along the depth. The results were presented in civil engg. report no. C-114, and C-131 of RDSO.

Long haul trains having 4500 t and 9000 t trailing loads were introduced in 1980's on Indian railway tracks. To ascertain the effect of heavy haul trains on the stress coming on the formation, dynamic tests were carried out by RDSO. Finite element analysis requires elastic modulus of formation soil as one of the input parameters. Hence, RDSO in consultation with IIT Kanpur conducted cyclic plate load test and wave propagation test at Moradabad division, northern railway [Kumar et al. (1990), Kumar et al. (1991a) and Kumar et al. (1991b)]. For these tests, in general, test procedure described in IS 1888-1982 and IS 5249-1977 were followed.

2. MODEL TESTING BY ORE

Janin et al. (1982) undertook full scale laboratory testing at Vienna arsenal to determine the settlements and stresses in the track structure under static and dynamic loading. These tests were conducted in a large rectangular reinforced concrete box having a section of the track foundation structure. This substructure was loaded using a single sleeper with 90 kN load. Displacements and stresses were measured at the interface of all layers.

Tests were conducted over four model track beds having varying thickness of substructure layers. Subgrade was made up of clay of low compressibility. Each test was carried out for 6 million cycles with application of approximately sinusoidal loading waveform from 0 to 90 kN at 10 Hz frequency. Simultaneously, computer program 'ROSALIE' was used to calculate displacements and stresses for these tracks. Measured displacements and stresses at first loading for track beds have been compared with calculated results from 'ROSALIE' .

At Vienna Arsenal, Janin et al. (1983a) further carried out similar box tests on a different track bed (having no gravel layer below ballast). Subgrade was made up of sandy silt of low compressibility.

However, most detailed testing programme was carried out at Derby [Janin et al. (1983a)]. An area of 20 m × 4.5 m containing track panel was selected for test site. One half of this site was filled with soft boulder clay and other half with stiff keuper marl clay as subgrade material. Instrumentation of this site consisted of isolating the area from surrounding by a polythene membrane, pressure cells, accelerometers, potentiometers and LVDT recordings of displacement response at the interface of different layers and hydraulic piezometers just below the clay surface for pore water pressure measurement. Dynamic and static tests consisted of loading rail head and single sleeper by servo controlled hydraulic vibrator. Rolling tests were carried out by propelling a two axle vehicle (16t axle load) across the test site.

Four different depths of formation were investigated at Derby. Measurements were taken during rolling, static and dynamic loading to evaluate the effect of depth of formation on the following parameters.

1. Elastic and permanent settlement of ballast, subballast, blanket and subgrade.

2. Vertical, longitudinal and transverse pressures at the subgrade surface.

3. Pore water pressures in the subgrade.

2.6 SUMMARY

The present study to predict the behaviour of soils under the railway formations subjected to cyclic loading requires determination of induced stresses on the subgrade by appropriate mathematical model and the evaluation of threshold stress of subgrade soil by geotechnical testing.

It has been observed that before 1980, induced stresses were determined by empirical formulae. With high speed traffic, sophisticated mathematical computer oriented models were increasingly used. These models can be broadly classified under the finite element models and models which use Burmister's solution for multilayer system [Burmister (1945)]. These all models give the solution by assuming equivalent static load which is obtained by augmenting actual wheel load by speed factor.

It is observed that there are very few simple and yet accurate models available to predict induced stresses. Also, it is seen that most of the two dimensional models predict higher stresses as compared to the measured stresses. In the present study, a simple model 'ELASTIC.F' has been developed and it is shown that this model gives quite accurate results. Also, two dimensional finite element model '2D8N' has been presented along with a modification which enables this model to predict quite reliable vertical stresses. In addition to this, a three dimensional linear elastic model '3D20N' has been developed which predicts result quite similar to 'MULTA' model which is like a closed form solution.

In this literature review, it is found that , in general, there are two different approaches to evaluate the threshold stress for soils subjected to cyclic loading. Following Sangrey (1968), critical level of repeated stress (similar to threshold stress) has been evaluated from stress path movement during undrained cyclic loading and is taken as stress level corresponding to end of equilibrium line. Also, Rubin et al. (1970) have observed that plastic strain development with cyclic loading shows terminating and non-terminating behaviour for undisturbed samples depending upon cyclic stress and based on this, threshold stress can be evaluated. Guidelines given by Sangrey et al. (1978) to evaluate the threshold stress requires determination of κ and hence not easy to use. In the present study, it has been shown that threshold stress for compacted quasi saturated soils during undrained triaxial tests can be

determined by both above mentioned approaches and they yield same results. Also, a generalized relationship between I_p and threshold stress ratio has been proposed.

Literature review also reveals that relationship between cumulative plastic strain and number of loading cycles is available for undisturbed London clay [Rubin et al. (1970)]. However, this model requires determination of elastic strain, e_e (measure of cyclic stress ratio) and hence cannot be used directly. In the present study, a generalized model for plastic strain development with number of loading cycles has been proposed.

In addition, it may be noted that data available on compacted samples subjected to cyclic loading is rather scarce. The present study presents and analyzes the data (both static and cyclic) on compacted samples. Also, an attempt has been made to explain the static data on compacted samples in the critical state framework.

Literature review also reveals several design methodology used by different railways in the world. However, they cannot be directly used in Indian conditions. In the present study, a methodology for design of railway formation has been proposed.

results obtained by other models and field studies is given in Sec. 3.5. Section 3.6 compares behaviour of these three models in terms of accuracy, results obtained and CPU time.

3.2 RIGOROUS ELASTIC METHOD (ELASTIC.F MODEL)

3.2.1 INTRODUCTION

This model consists of determining the stresses at the sleeper ballast interface by considering the rail as a beam on elastic foundation. The stresses inside the track structure are then determined by converting layered system into equivalent homogeneous system by Odemark method and using Newmark's charts. This method has been described below in detail. The parametric studies have been carried out using this method.

3.2.2 THEORETICAL BACKGROUND

The governing equation for beam on an elastic foundation is given as

$$E_{bm}\, I_{bm}\, \frac{d^4y}{dx^4} = -k\, y + q\,(x) \qquad (3.1)$$

where E_{bm} , I_{bm} = Young's modulus and moment of inertia of beam,

x = distance of point where deflection is required from point where load is acting,

y = deflection of beam, and

$q(x)$ = externally applied load.

For the simplest case of single concentrated load 'Q' acting in the vertical plane of symmetry on an infinitely long rail, Timoshenko and Langer (1932) have given following solution :

$$y_r = Q\eta(\xi)/2\ k\ L_b \tag{3.2}$$

where

$$L_b = \sqrt[4]{\frac{4\ E_r I_r}{k}} \tag{3.3}$$

$$y_r = Q \times [\eta(\xi_1) + \eta(\xi_2)] \ / \ 2\ k\ L_b \tag{3.4}$$

$$p_s = y_r \frac{k}{\bar{b}} \tag{3.5}$$

p_s is the stress below the sleeper where 'y_r' has been calculated. p_s is assumed to be uniformly distributed over the bearing area per rail seat (Sec. 2.5.2) of sleeper referred here as Load area.

and $$\eta(\xi) = e^{-\xi}[\cos(\xi) + \sin(\xi)] \tag{3.6}$$

[Hetenyi (1961)]

In Eq. (3.6),

$$\xi = x \ / \ L_b \tag{3.7}$$

Referring to Fig. 3.1, for ξ_1, x in Eq. (3.7) will be the distance from load Q_1 and for ξ_2, x will the distance from load Q_2.

This method to determine stress at sleeper ballast interface is also known as Zimmermann's method [RDSO (B)].

Track structure is generally made up of 3 layers viz. ballast, subballast and subgrade soil (Fig. 1.1). Odemark method is extensively used for vertical stress calculation in multi-layered systems [RDSO (B)]. By Odemark method, layered system can be converted into homogeneous one (Sec. 2.2.1). Odemark method gives good results only when soft layer is underlain by stiff layer.

Referring to Fig. 2.1, the homogeneous equivalent depths for ballast and subballast layers are given as

$$d_b^* = 0.9\, d_b \sqrt[3]{E_b/E_s} \qquad (3.8)$$

$$d_{sb}^* = 0.9\, d_{sb} \sqrt[3]{E_{sb}/E_s} \qquad (3.9)$$

Newmark's charts [Jumikis (1966)] can now be applied to find out the stresses induced at this new equivalent depth ($d_b^* + d_{sb}^*$) from the stresses at sleeper ballast interface.

3.2.3 DESCRIPTION OF RIGOROUS ELASTIC METHOD (ELASTIC.F)

Sleeper and Load configuration for double wheel load case are shown in Fig. 3.2. Load tie is a tie directly above which,

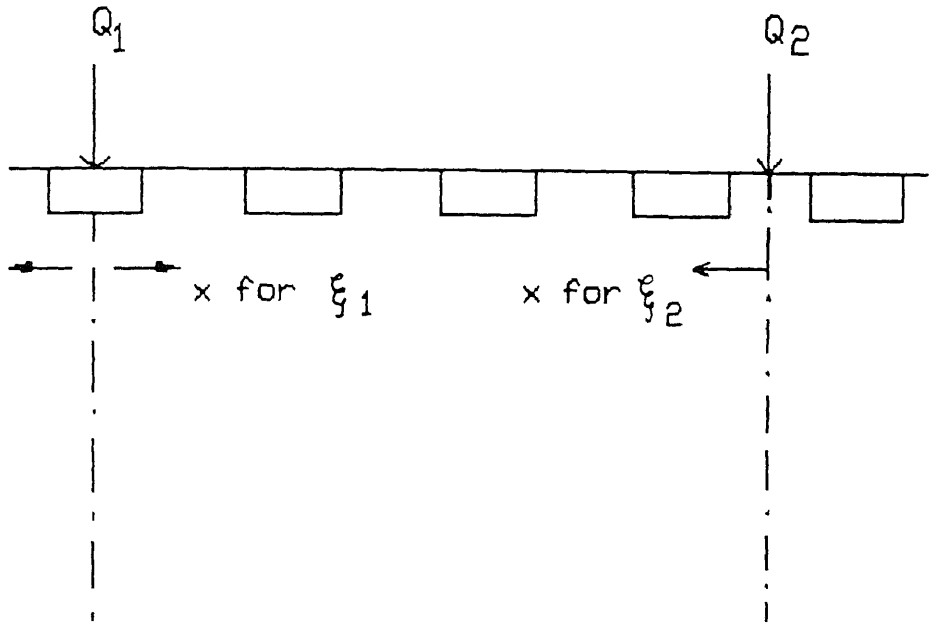

Fig. 3.1 MEASUREMENT OF X IN EQUATION 3.7

PLAN VIEW

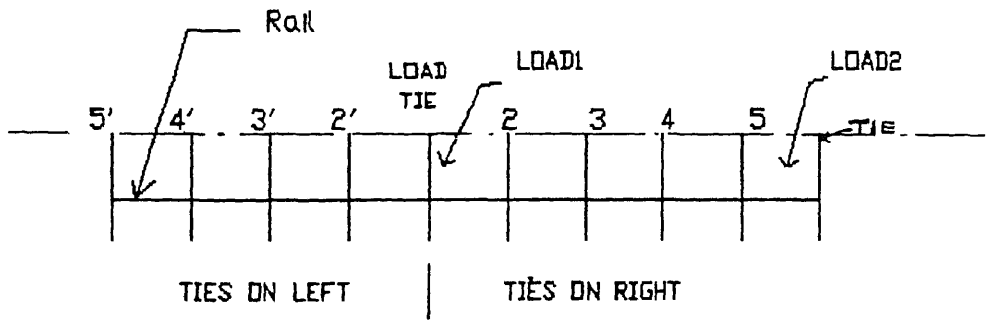

Fig. 3.2 SLEEPER AND LOAD CONFIGURATION FOR DOUBLE WHEEL LOAD CASE

the wheel load is acting. In this method, load tie and 4 ties on either side of it, are considered for stress calculation.

Step 1 - Calculate the stresses at sleeper-ballast interface as given below :

If track characterization is given in terms of formation coefficient, C or static rigidity, 'ρ', convert it into 'k' as given below (Sec. 2.5.2) :

$$k = \frac{\rho}{2\ \bar{S}} \tag{3.10}$$

and $$k = \bar{b}\ .C \tag{3.11}$$

Uniform stress on bearing area per rail seat of sleeper (load area) can be obtained by Eqs. (3.4) and (3.5).

Thus, stress in any load area due to load at any place can be obtained.

In this analysis, interaction of four sleepers on either side of load sleeper has been considered (Fig. 3.3). Due to symmetry, only one quarter of track need to be analyzed (Fig. 3.4). The stresses on load areas L1 to L5 are taken equal to summation of stresses due to loads Q_1 and Q_2 while stresses on load areas L2' and L5' are taken equal to stresses due to load Q_1 only. This is because it has been observed [(Talbot et al. (1923)] that effect of load Q2 need to be taken only on four sleepers on left (i.e. on L1 to L4) and on sleeper L5 for calculating stresses below point A (Fig. 3.4). Stresses on load

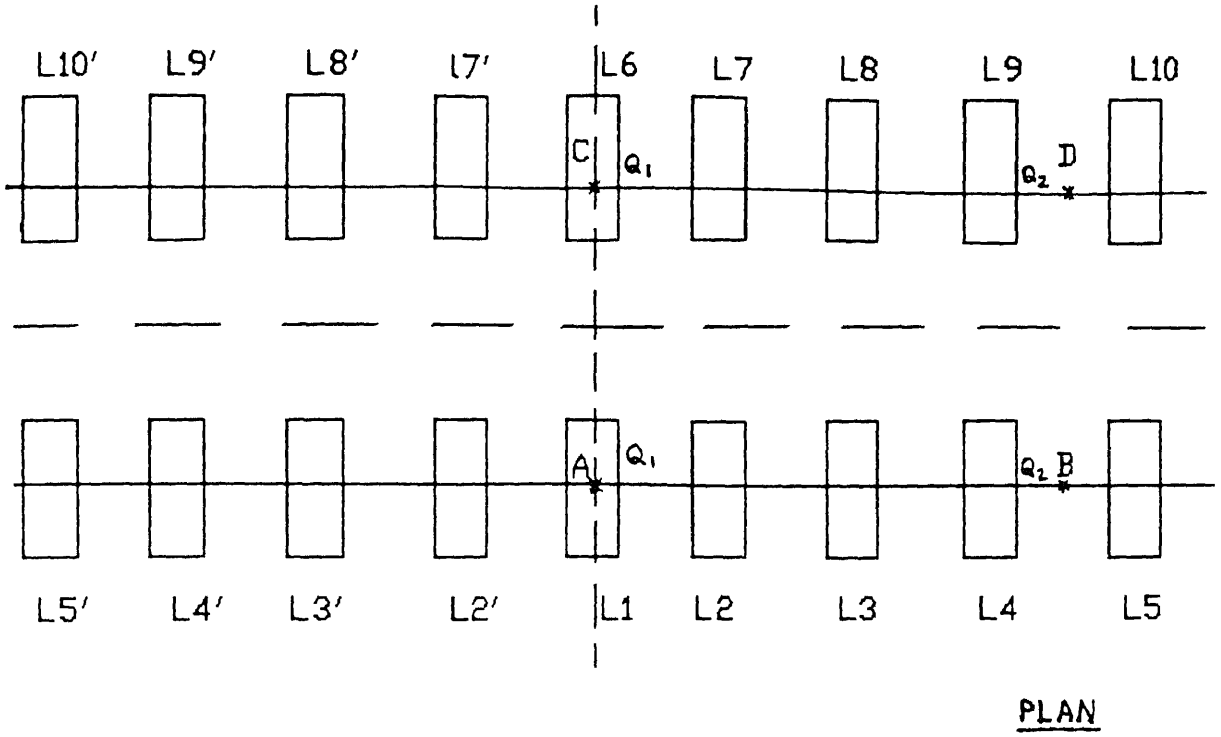

Fig. 3.3 Assumed load distribution below the sleeper

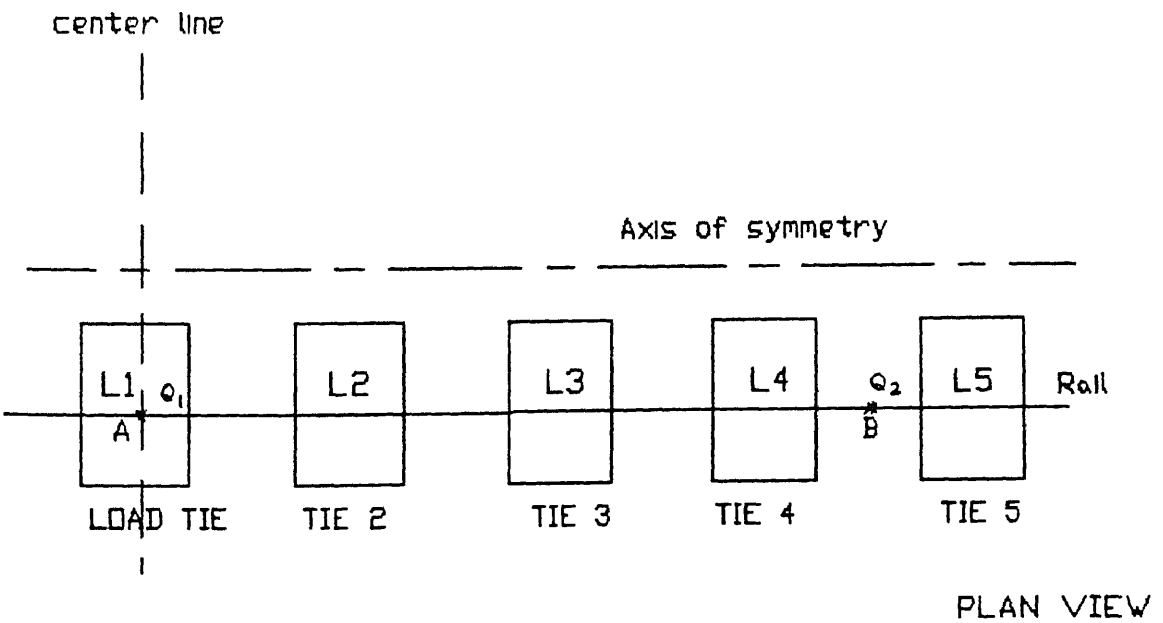

Fig. 3.4 Assumed load distribution below the sleeper

areas L6 to L10 and L7′ to L10′ can be obtained by symmetry.

Step 2 - Conversion of layered track structure into homogeneous system by Odemark method (Fig. 2.1) :

Equivalent heights d_b^* and d_{sb}^* are calculated from Eqs. (3.8) and (3.9).

Step 3 - Calculation of stresses in track structure :

Referring to Fig. 3.3, stresses at any point in the track structure can be found by superimposing the effect due to load areas L1 to L10 and L2′ to L10′.

Stresses due to any rectangular load area (length a, width b) at any point in the track structure can be found by Newmark's solution [Jumikis (1966)] as given below :

Vertical stress at corner of any rectangular area due to uniformly distributed load on total area is given by

$$(\sigma_z)_c = \frac{q}{4\pi}\left\{\frac{2\bar{m}\bar{n}(\bar{m}^2+\bar{n}^2+1)^{1/2}}{\bar{m}^2+\bar{n}^2+\bar{m}^2\bar{n}^2+1}\times\frac{\bar{m}^2+\bar{n}^2+2}{\bar{m}^2+\bar{n}^2+1} + \tan^{-1}\frac{2\bar{m}\bar{n}(\bar{m}^2+\bar{n}^2+1)^{1/2}}{\bar{m}^2+\bar{n}^2-\bar{m}^2\bar{n}^2+1}\right\} \quad (3.12)$$

where

$$\bar{m} = a / z_d \tag{3.13}$$

$$\bar{n} = b / z_d \tag{3.14}$$

with

z_d = depth of point from surface at which stresses are required.

or,

$$(\sigma_z)_c = k_n \, q_1 \tag{3.15}$$

where

q_1 = intensity of pressure on rectangular load area.

k_n = influence factor to be taken from charts given by Newmark.

Eqs. (3.12) or (3.15) can be used for calculation of vertical stress at a point situated either inside or outside the rectangular area by the method of superposition [Jumikis (1962)].

A computer program based on this method has been written [Yudhbir, Kameswara Rao and Shahu (1991)].

3.2.4 LIMITATIONS

1. This model requires experimental determination of modulus of railroad reaction, k or formation coefficient, C in addition to E_r, E_b, E_{sb} and E_s.

Although, no relationship between E_s and the value of

modulus of railroad reaction (k) or formation coefficient 'C' is available in literature, modulus of subgrade soil does have bearing upon the value of modulus of railroad reaction (Sec. 2.5.2). For a rough estimate, the following procedure may be adopted :

Senac (1984) gives the track formation quality in terms of ρ and C (Table 2.2). Bowles (1984) suggests a range of Young's modulus for different soil types (Table 3.1). Table 3.2 shows approximate correlation between C and E_s based on the assumption that formation quality of track is determined by the type of subgrade on which it is laid.

2. Odemark method should not be used for systems where stiff layer is underlain by soft layer. This limitation also applies to this model.

3. This model can not simulate factors such as tie characteristics, outer track geometry, boundary conditions etc.

3.2.5 COMPARISON OF RESULTS

Comparison of results has been given in Sec. 3.5.

3.2.6 RESULTS AND DISCUSSION

TRACK 1 has been considered as reference track. TRACK 1 is the representation of typical Indian track. Details of this track are given in Appendix A1. Parametric studies have been

Table 3.1 Range of Young's modulus values for different soils [Bowles (1984)]

Soil type	E_s (MPa)
Very soft	2 - 15
Soft	5 - 25
Medium	15 - 25
Hard	50 - 100

Table 3.2 Empirical Correlation between formation coefficient, C and Young's modulus of subgrade, E_s

Formation quality	C	Adopted for parametric studies	
		C	E_s
	(N/cm^3)	(N/cm^3)	(MPa)
Bad	> 20 - 30	25	10
Poor	> 30 - 90	75	20
Average	> 90 - 180	125	30
Good	> 180	180	50

carried out by varying range of parameters with reference to this track. Range of parameters used are as follows :

Depth of subballast = 0.15, 0.35, 0.55, 0.75 m

Young's modulus of subgrade soil = 10, 20, 30, 50 MPa

Moment of inertia of rail = 1600, 2158, 3055 cm^4

Tie spacing = 0.50, 0.65, 0.76 m

The results of parametric studies are given in Table 3.3

Figure 3.5 shows the variation of vertical pressure on top of subgrade under the rail seat (σ_{vt}) with Young's modulus of subgrade (E_s). It will be shown later (Sec. 3.3.7 and Fig. 3.39) that the maximum vertical pressure on top of subgrade occurs below the rail seat and thus, σ_{vt} represents maximum vertical pressure on top of subgrade.

From Fig. 3.5, it may be seen that as the soil becomes stiff, σ_{vt} increases. Also, as the total depth of formation (d_t) decreases, σ_{vt} increases. It can be seen that effect of soil stiffness on σ_{vt} is more when total depth of ballast and subballast is less as expected. Figure 3.6 shows the variation of σ_{vt} with total depth of formation for four soil types. The trend in Figs. 3.5 and 3.6 is same as obtained by So (1978).

Figures 3.7 and 3.8 show the variation of vertical stress, σ_v under the wheel load inside the subgrade soil up to 1 meter depth for varying total depth of formation for soft soil (E_s= 10 MPa) and stiff soil (E_s = 50 MPa) respectively. σ_v decreases by only 30 % (Fig. 3.7) for d_t = 1.0 m while for d_t = 0.4 m,

Table 3.3 Results of parametric studies (ELASTIC.F model)

File Name	E_b (MPa)	E_{sb} (MPa)	E_s (MPa)	d_b (cm)	d_{sb} (cm)	I_r (cm^4)	Tie spacing (cm)	σ_v on top of subgrade (kPa)
A1	150	80	10	25	15	2158	65	55 48
A2					35			41 62
A3					55			33.65
A4					75			28 29
B1			20	25	15	2158	65	73 77
B2					35			54 37
B3					55			43 53
B4					75			36 52
C1			30	25	15	2158	65	87.11
C2					35			63 30
C3					55			50.24
C4					75			41.93
D1			50	25	15	2158	65	106 00
D2					35			76 06
D3					55			59 80
D4					75			49.56

Table 3 3 (Contd) Results of parametric studies (ELASTIC F model)

File Name	E_b (MPa)	E_{sb} (MPa)	E_s (MPa)	d_b (cm)	d_{sb} (cm)	I_r (cm^4)	Tie spacing (cm)	σ_v on top of subgrade (kPa)
B2T1	150	80	20	25	35	2158	50	54 74
B2T3							76	54 50
D2T1			50		35		50	75 22
D2T3							76	78.39
D1T1					15		50	99 61
D1T3							76	113.95
D4T3					75		76	49 69
D1I1	150	80	50	25	15	1600	65	110.50
D1I3						3055		100.70
D1B1	180	80	50	25	15	2158	65	102 00
D2B1s	180	00	50	60	00	2158	65	64 72
D2B2s	150	00	50	60	00	2158	65	68 40
D1SB1	150	60	50	25	15	2158	65	109 00
D1SB3		100						103 00
D2SB1s	000	60	50	00	60	2158	65	90.40
D2SB3s	000	100	50	00	60	2158	65	77.34

le 3 3 (Contd) Results of parametric studies (ELASTIC F model)

File Name	E_b (MPa)	E_{sb} (MPa)	E_s (MPa)	d_b (cm)	d_{sb} (cm)	I_r (cm^4)	Tie spacing (cm)	σ_v on top of subgrade (kPa)
34BD1s	150	80	20	100	00	2158	65	32 06
34BD3s				00	100			38 29

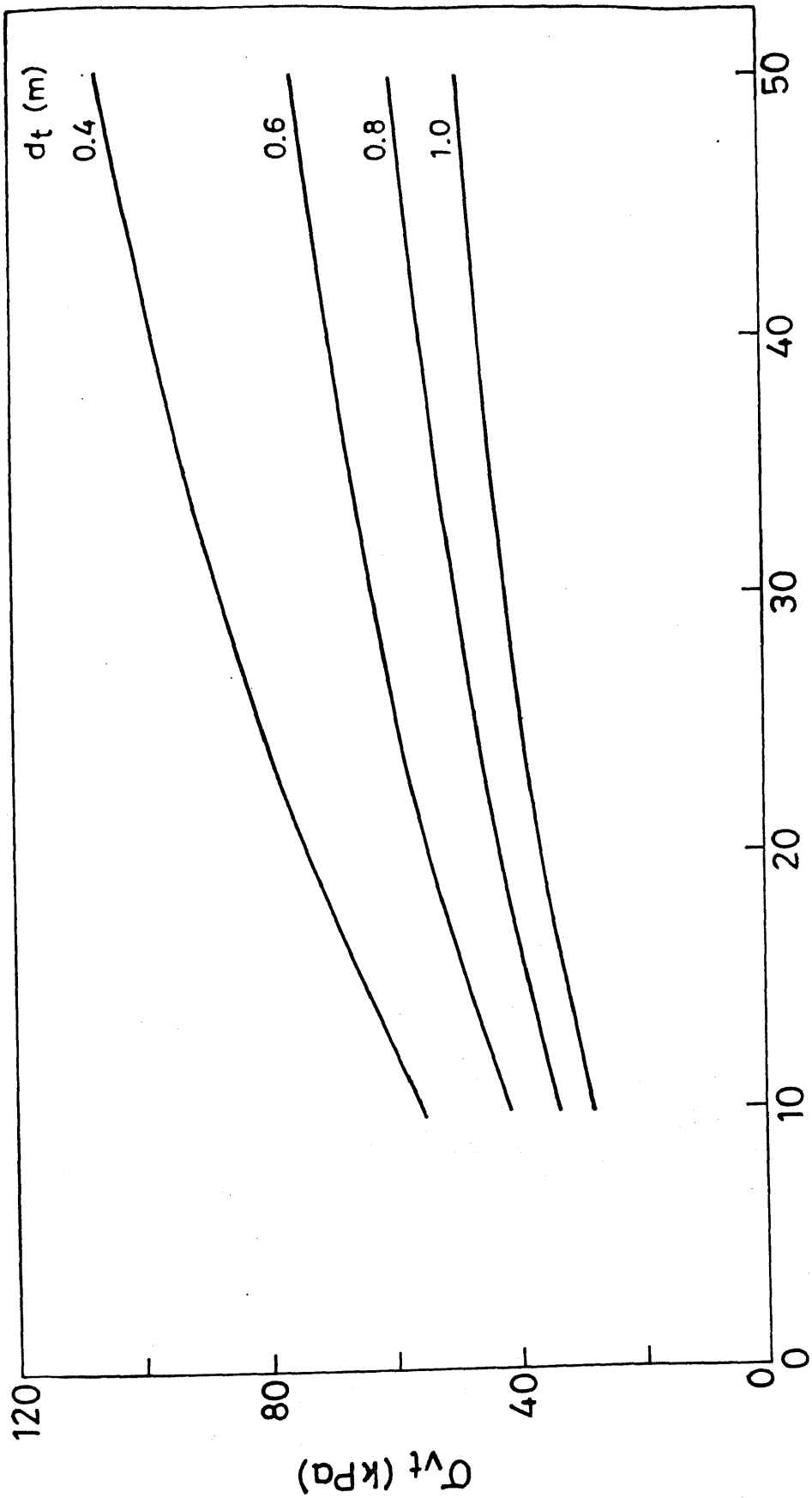

Fig. 3.5 Variation of σ_{vt} with E_s for Track 1 (ELASTIC·F model).

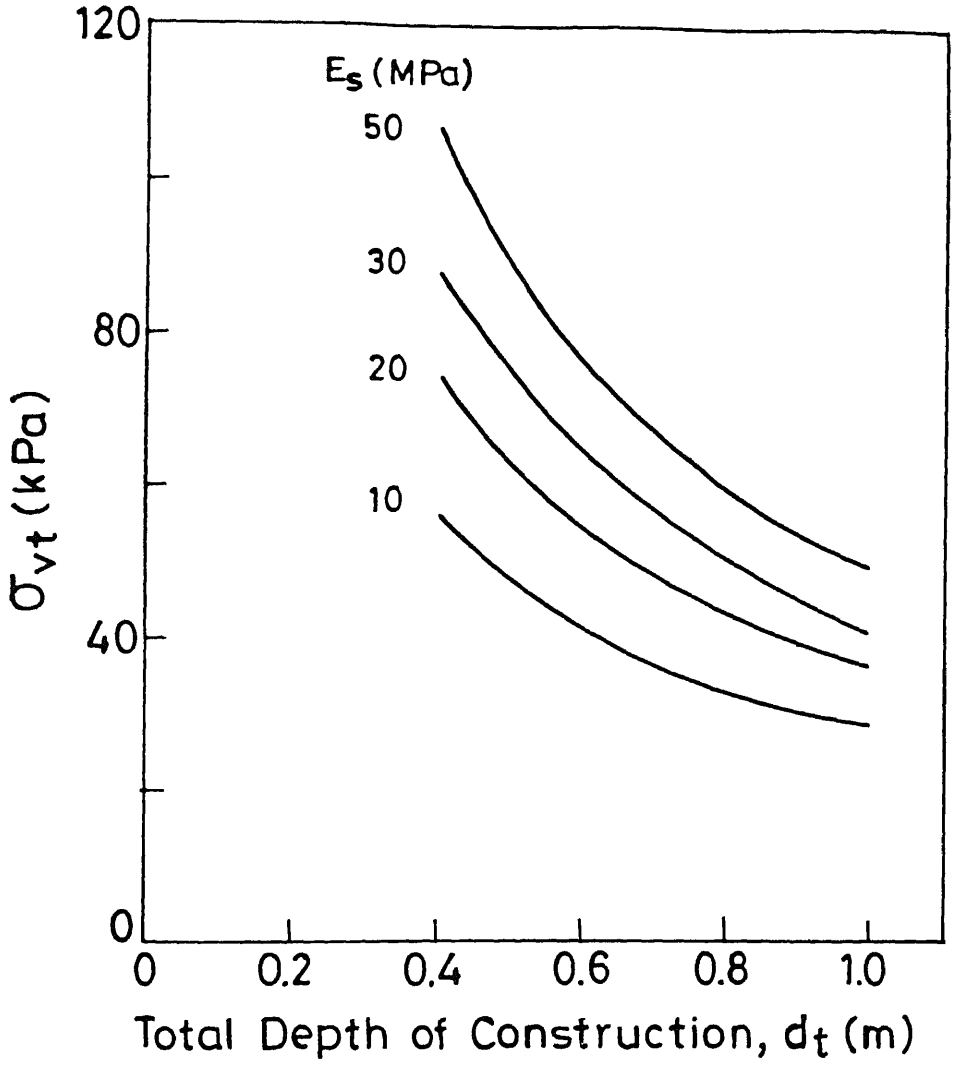

Fig. 3.6 Variation of σ_{vt} with total depth of construction for TRACK 1 (ELASTIC·F model)

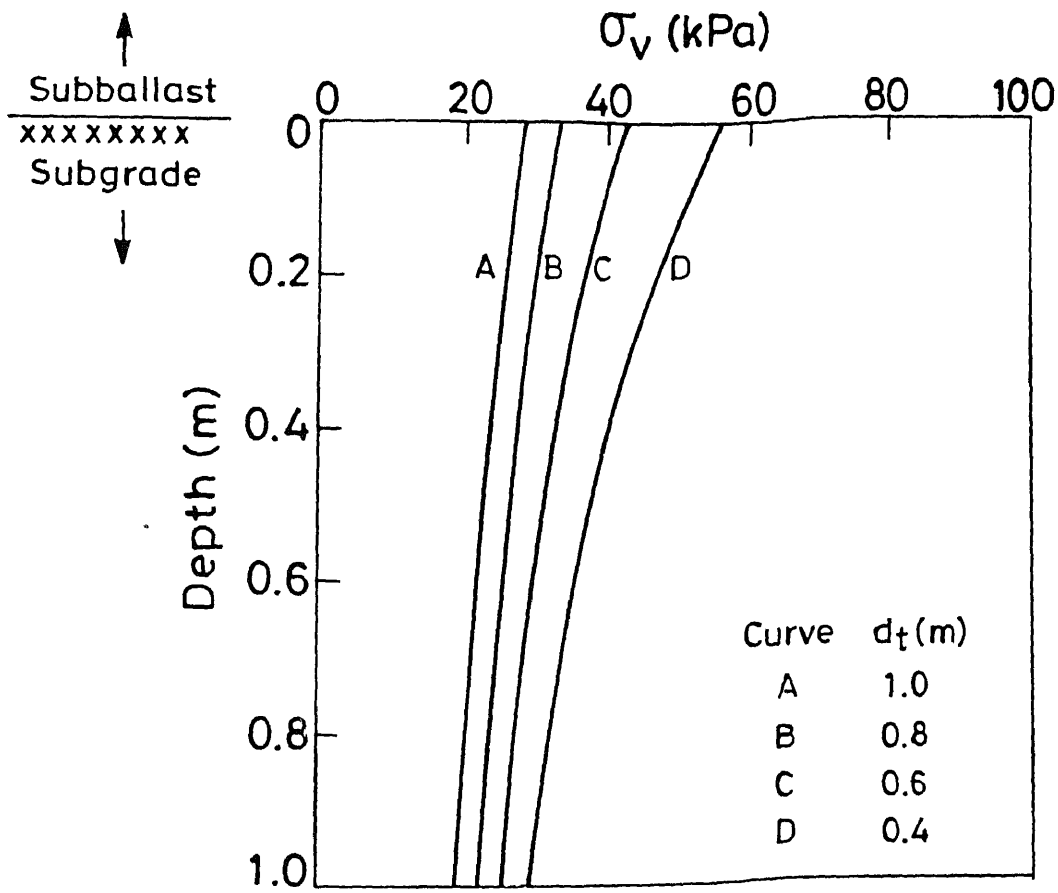

Fig. 3.7 Variation of σv inside the subgrade for E_s = 10 MPa for different dt (ELASTIC·F model)

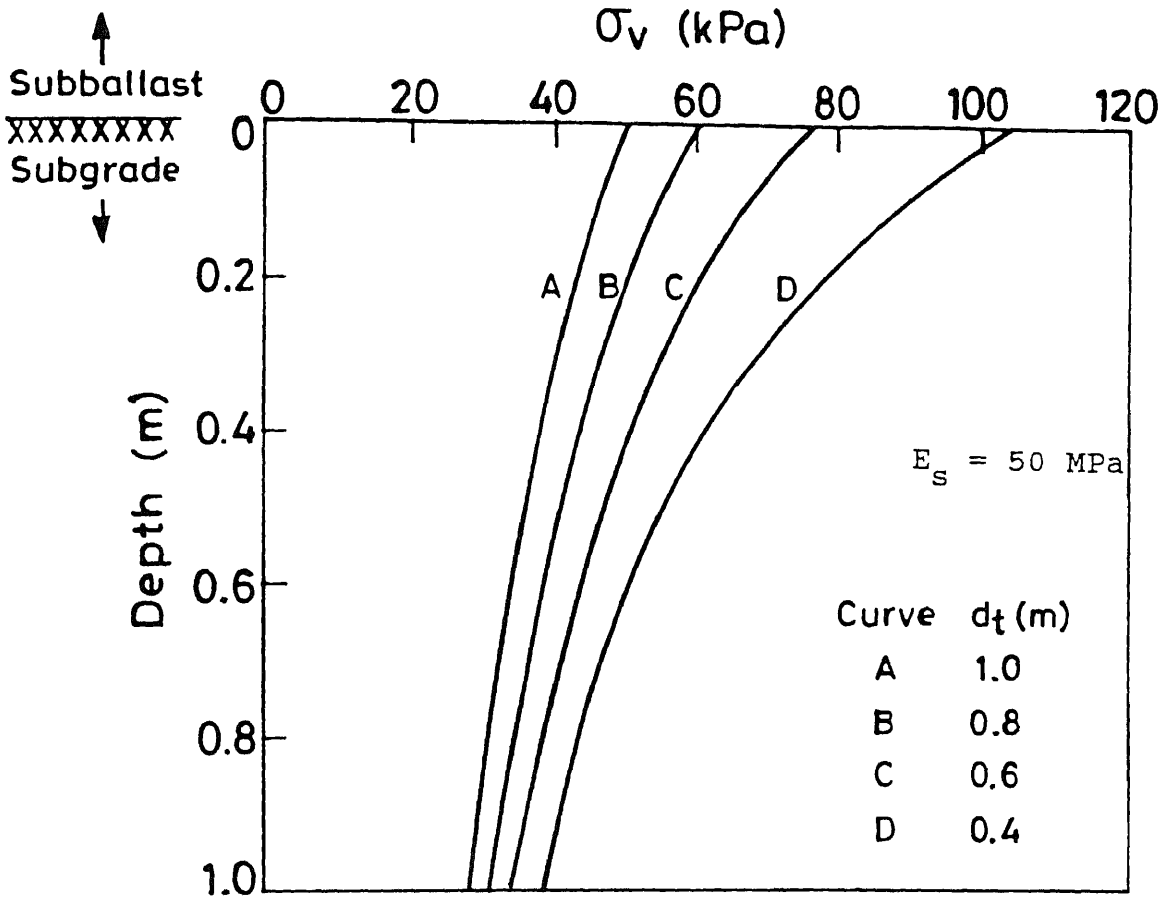

Fig. 3.8 Variation of σ_v with depth for different d_t (ELASTIC-F model)

the corresponding decrease is 50 % (E_s = 10 MPa). Thus, it can be seen that from point of view of stress dispersion, subgrade soil is more important if depth of formation is less.

Figures 3.9 and 3.10 show the variation of σ_v with depth under the wheel load for different soil types for d_t equal to 0.4 m and 1.0 m respectively.

From Figs. 3.7 to 3.10 it can be seen that for a given soil type, provision of more total depth of formation than a certain limit does not reduce the vertical stress on top of subgrade under the rail seat by significant amount.

Figure 3.11 shows the variation of maximum vertical stress on top of subgrade for different proportions of ballast and subballast depths but keeping the total depth of formation equal to 1.0 m.

From Fig. 3.11 , it is clear that increase in depth of ballast layer but keeping total depth of ballast and subballast layer constant does not reduce σ_{vt} significantly.

It is to be noted that while using ELASTIC.F model, empirical correlations of 'C' and 'E_s' values for similar types of formation and soil have been used (Sec. 3.2.4) . Hence, it is useful to check the variation of σ_{vt} values with formation coefficient 'C'. For d_t = 0.4 m and E_s = 10 MPa, 'C' was changed from 25 MN/m^3 (recommended value) to 250 MN/m^3 (extreme value in all categories). The change in maximum vertical stress on top of subgrade is only from 55 KPa to 66 KPa (Fig. 3.12). Next, 'C' was changed from 25 MN/m^3 to 75 MN/m^3 (recommended value for second category). The change in maximum vertical

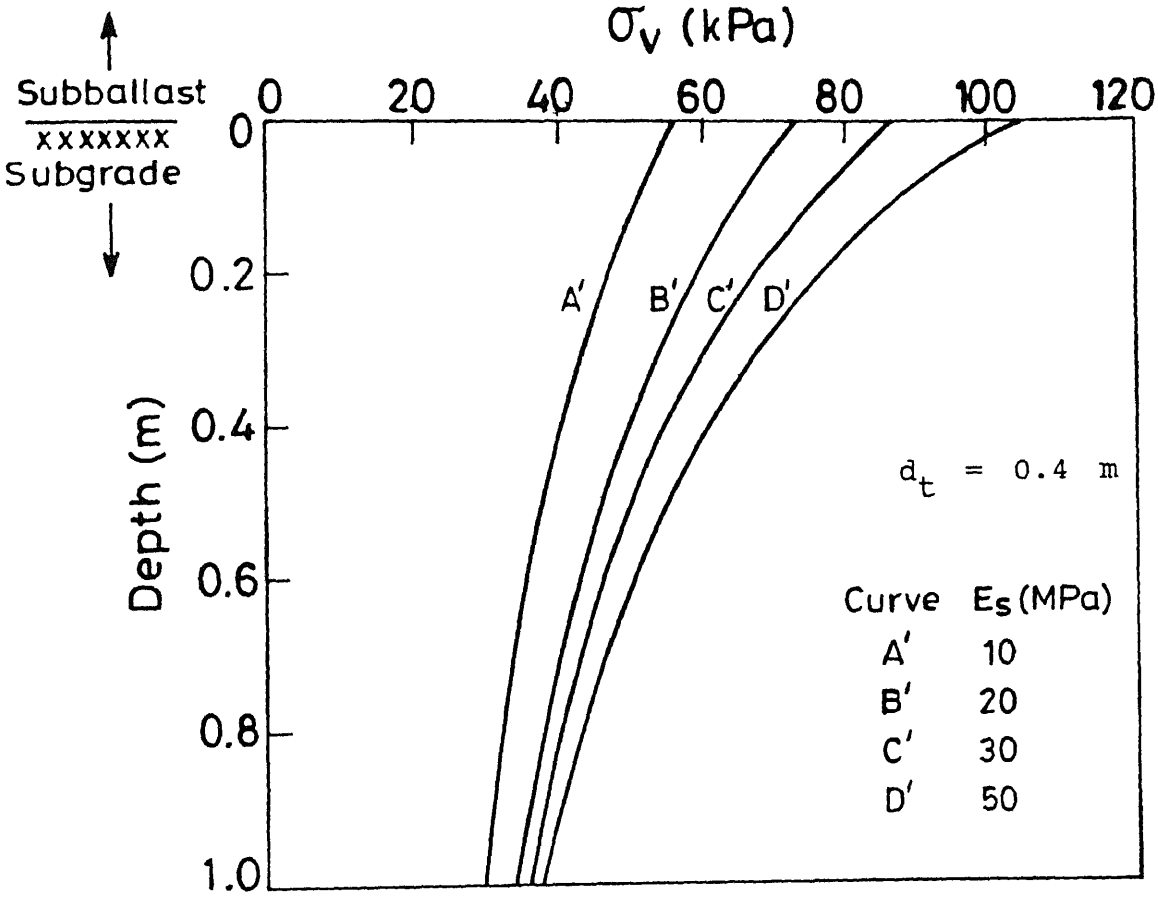

Fig. 3.9 Variation of σ_v with depth for different E_s (ELASTIC·F model)

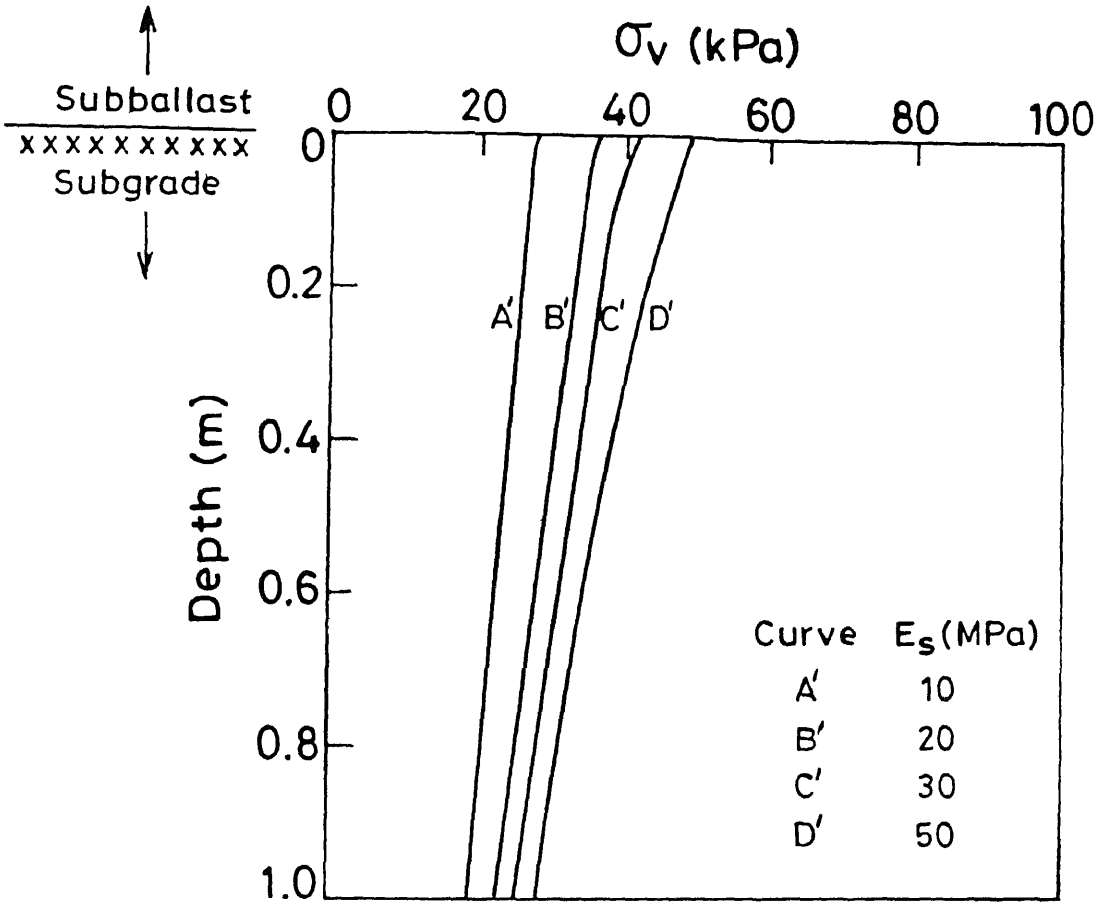

Fig. 3.10 Variation of σ_v inside the subgrade for $d_t = 1.0$m for different E_s (ELASTIC·F model)

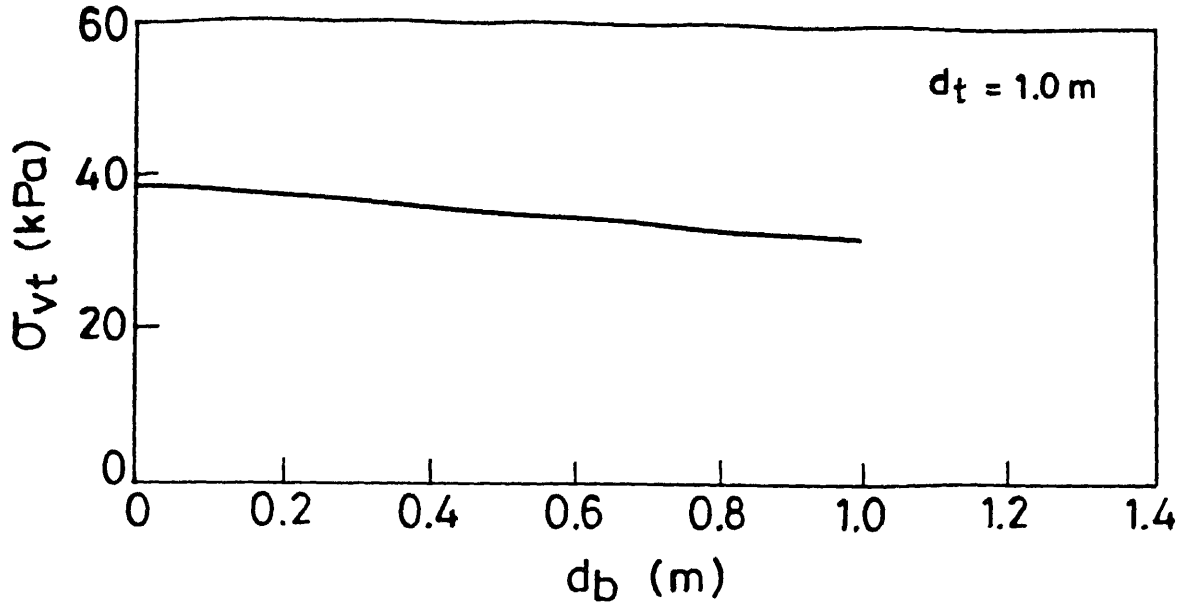

Fig. 3.11 Variation of σ_{vt} for different proportioning of ballast and subballast depth for d_t = 1.0m (ELASTIC·F model)

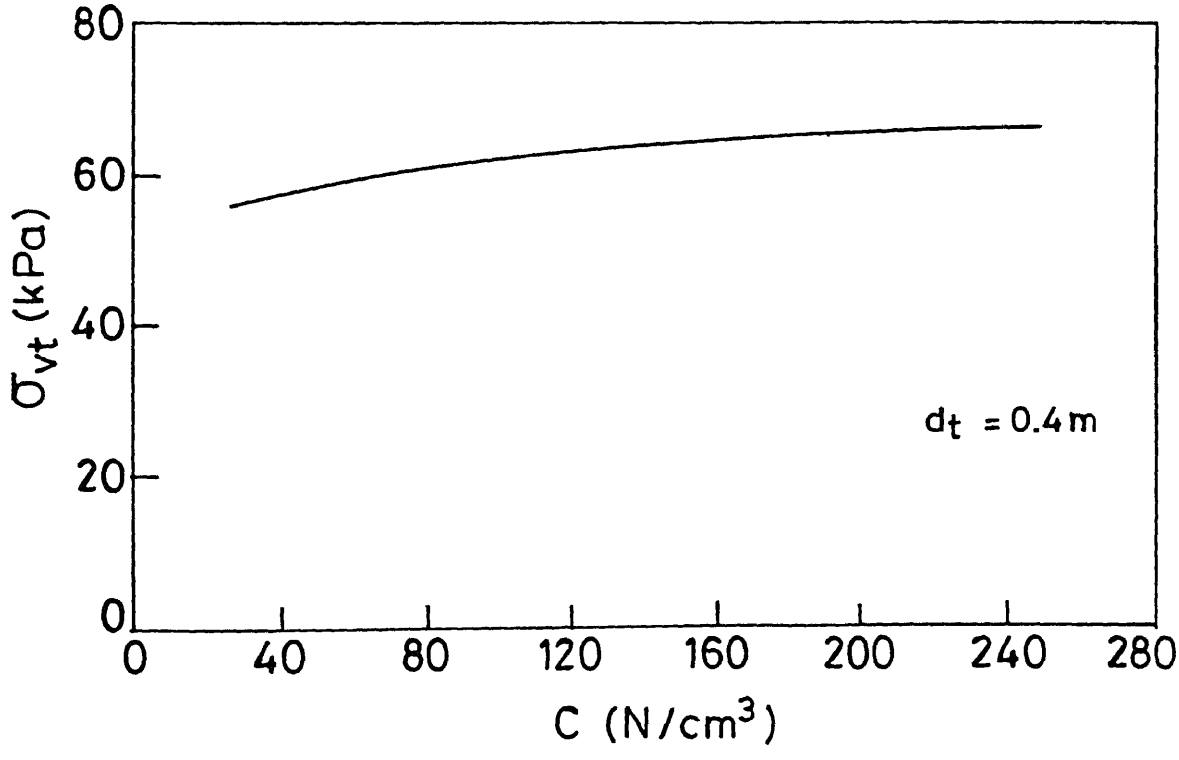

Fig. 3.12 Variation of σ_{vt} with formation coefficient 'C' for d_t = 0.4 m (ELASTIC·F model)

stress on top of subgrade is only of the order of 4 KPa (7 %). Also it will be shown in Fig. 3.41 that δ (or C) vary significantly only with E_s while other track parameters and depth of formation has negligible effect on δ (or C). Thus, the correlation between 'C' and 'E_s' (Table 3.1) is fairly good.

Figure 3.13 shows the effect of tie spacing on maximum vertical stress on top of subgrade. As the tie spacing increases, σ_{vt} increases as also noted by Stewart and Selig (1982). Two extreme values of tie-spacing have been used (0.50 m and 0.76 m). It may be seen that tie spacing has small effect on σ_{vt} for higher d_t (for d_t = 0.60 m, effect is 5 % while for d_t = 0.40 m, it is 15 %), in general , but this effect is even less for soft soil as compared to stiff soil (negligible for E_s = 20 KPa ; 6 % for E_s= 50 KPa).

Figure 3.14 shows the effect of moment of inertia of rail on vertical stress on top of subgrade under the rail seat for depth equal to 0.40 m. It may be noted that rail type has insignificant effect on σ_{vt}.

Figures 3.15 and 3.16 show the effect of Young's modulus of ballast (E_b) and subballast (E_{sb}) on σ_{vt} respectively. The Young's modulus values for both ballast and subballast layers within their given range have insignificant effect on σ_{vt}.

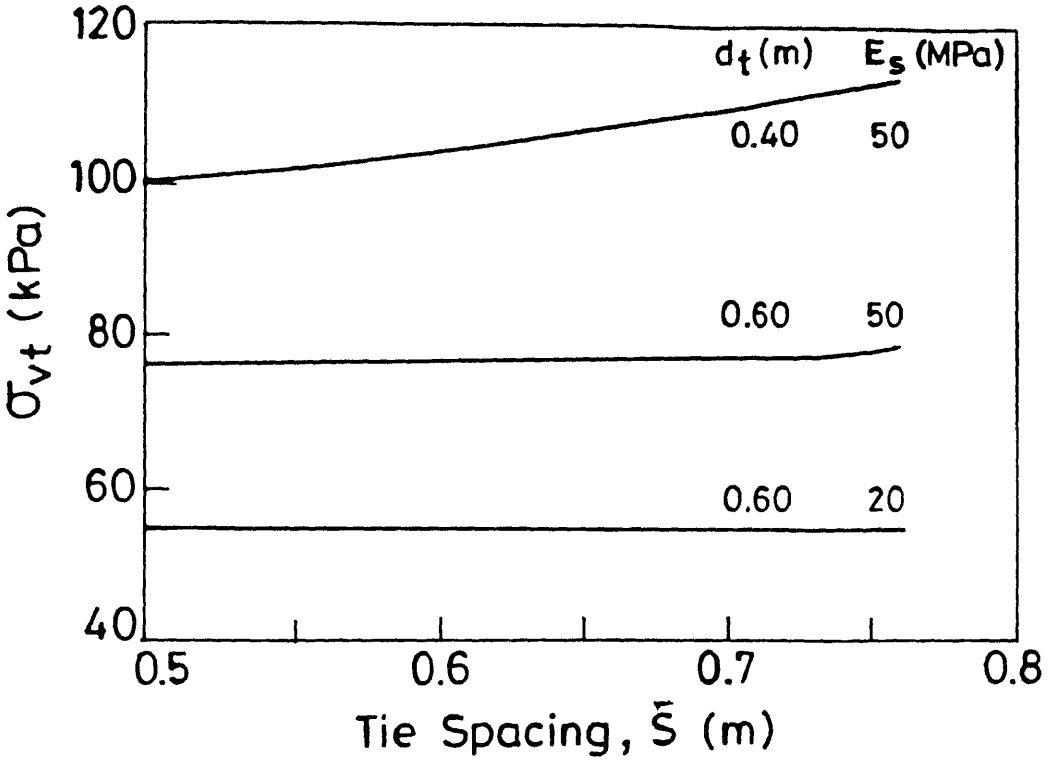

Fig. 3.13 Variation of σ_{vt} with tie spacing for different track conditions (ELASTIC-F model)

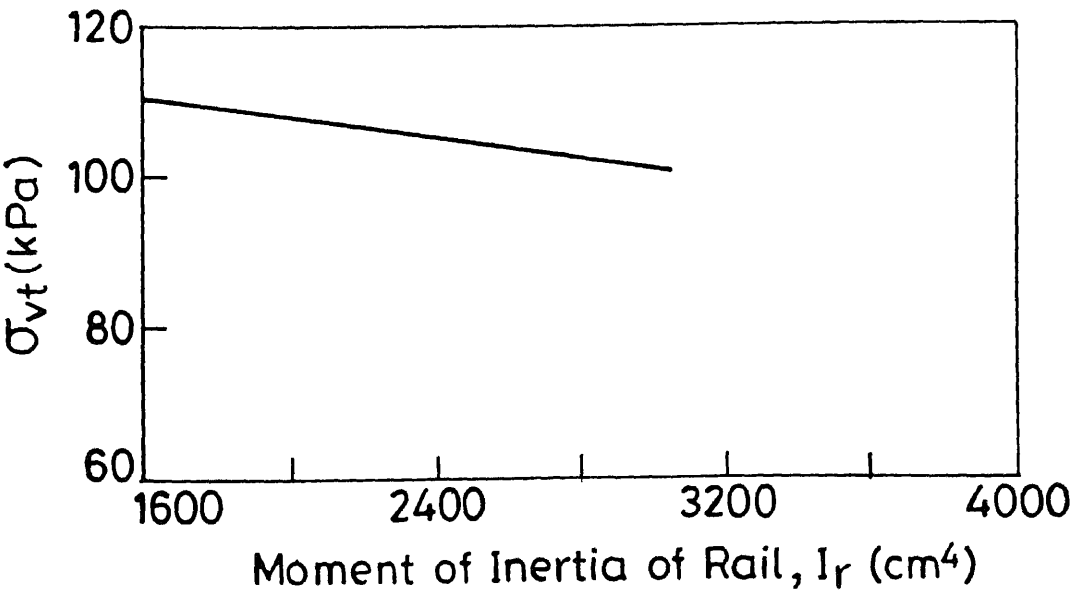

Fig. 3.14 Variation of σ_{vt} with moment of inertia of rail, I_r

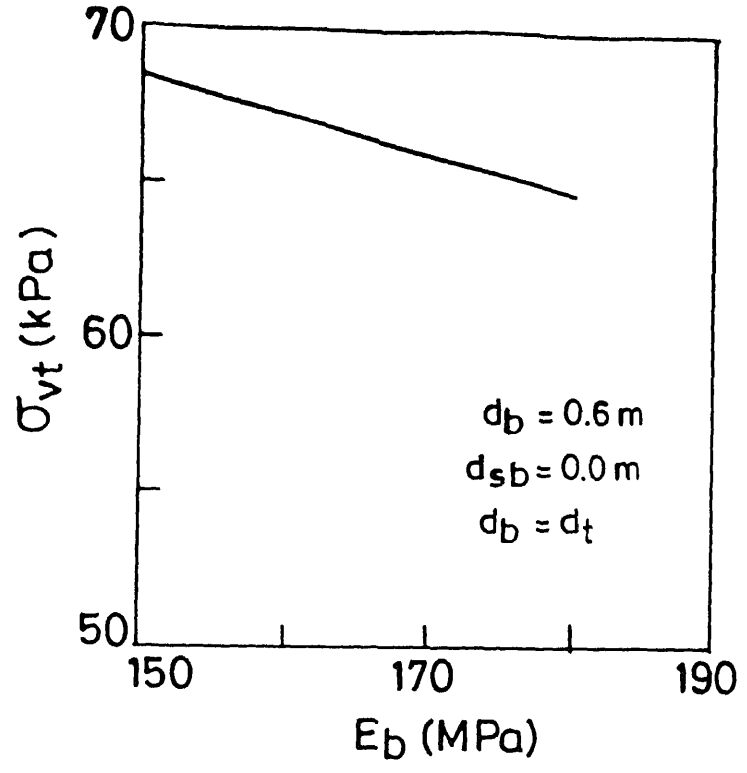

Fig. 3.15 Variation of σ_{vt} with Young's modulus of ballast (ELASTIC·F model)

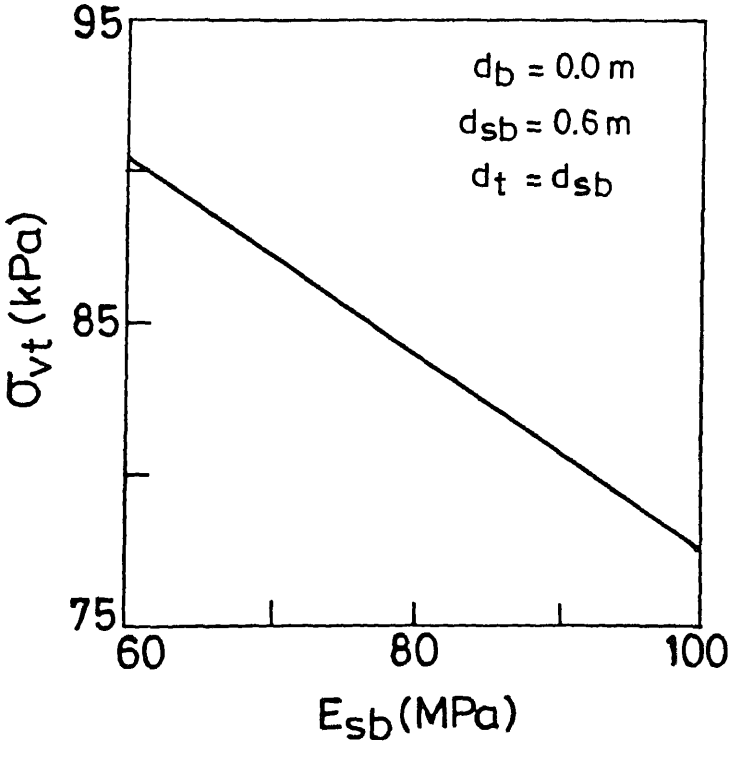

Fig. 3.16 Variation of σ_{vt} with Young's modulus of subballast (ELASTIC·F model)

3.3 TWO DIMENSIONAL FINITE ELEMENT ANALYSIS

3.3.1 INTRODUCTION

Finite element method is a well established technique and has been described in a number of books [e.g. Zienkiewicz and Taylor (1989); Cook et al. (1989); Rao (1989); Reddy (1986)]. Hence only the highlights of the routines developed have been described here.

All the finite element routines are based on displacement formulation of elasticity equations. All routines use linear, elastic material properties. Two dimensional finite element analysis of track has been carried out in order to calculate deflections and stresses inside the subgrade. Two dimensional finite element model for railway track has been described below in detail. Stress distributions and displacements for a typical track have been presented and a parametric study was carried out using two dimensional finite element analysis with reference to this track.

3.3.2 DESCRIPTION OF TWO DIMENSIONAL FINITE ELEMENT ROUTINES

Two finite element routines are developed , each of which has capabilities to solve both plane stress and plane strain problems. Names given to these routines are :

1. 2D4N

2. 2D8N

2D4N is a finite element routine which uses 4-noded linear isoparametric rectangular elements. 2D8N is a finite element routine which uses 8-noded parabolic isoparametric rectangular elements. Both these programs use similar formulations, techniques, inputs and outputs. Vertical and lateral deflections and stresses, and shear stresses at all nodes can be calculated. 2D4N routine is equipped with semi-automatic mesh generation facility while 2D8N routine is equipped with both semi-automatic and automatic mesh generation modules.

Both routines were tested for standard cantilever beam problem [Fenner (1986)] and Boussinesq's line load problem [Harr (1966)]. It was observed that 2D8N module gives better results with fewer number of elements as expected and hence, further analysis was done with 2D8N only for two dimensional finite element analysis. Comparison for Boussinesq's line load problem has been given in Appendix B1.

2D8N routine can handle layering of different materials and all types of boundary conditions. The routine has facility to simulate joint between different layers by 6-noded linear joint elements of zero thickness [(Goodman et al. (1968); Burgohain and Shah (1977)]. The results obtained from this routine have been checked with the standard matrix given by Vijayan (1981) for interface element .

This routine has the facility to simulate elastic

continuum by static infinite elements [Curnier (1983)]. However, use of infinite elements needs special kind of mesh discretization. Mesh should spread out in radial direction from the load element [Zienkiewicz et al. (1983)]. It has been noted that infinite elements with rectangular mesh discretization do not give better results. As the track problems do not allow this special kind of radial mesh discretization due to the presence of layering, infinite elements were not used for track problems.

Input in the automatic mesh generation module consists of basic parameters (e.g. total number of nodal points, material types, elements etc.), material properties, total number of compartments in x and z direction and length of each compartment, boundary conditions at four faces etc. Mesh generated will have rectangular lay out.

For generation of meshes of any shape, semiautomatic mesh generation facility can be invoked which requires input as basic parameters, material properties, nodal point data, element connectivity data, boundary conditions, etc.

Output from the routine consists of both horizontal and vertical stresses, shear stresses and principal stresses at all Gaussian points and extrapolated stresses at all nodal points along with displacements at all nodal points. Stress extrapolation is carried out using linear shape function [Cook et al. (1989)]. However, to cope with the enormous amount of data, a post processor facility has been provided using which important output can be obtained in the required form. Thus,

for e.g., output related to deflection and stresses at nodal points along depth below the load or in any horizontal compartment at given depth can be obtained.

As already mentioned, routines were checked for plane strain Boussinesq's problem with line load [see Appendix B1 ; Yudhbir, Kameswara Rao and Shahu (1991)]. An interesting feature was noted at this time. For mesh with 250 elements, and bottom and lateral boundaries at 6.0 m from the load, it was observed that computed vertical stresses and displacements were as good as exact but lateral stresses did not match with exact results throughout length and depth of mesh. Moreover, lateral stresses were found to vary with Poisson's ratio. Mesh refinement and change in boundary conditions were not much helpful. However, it was found that when lateral and bottom boundaries were fixed at 130 m, lateral stresses match with exact results and do not vary with Poisson's ratio anymore.

The notations used in program are shown in Fig. 3.17.

3.3.3 TWO DIMENSIONAL FINITE ELEMENT MODEL FOR RAILWAY TRACK (2D8N MODEL)

Reference axes chosen for finite element models are shown in Fig. 3.18.

Initially, both plane stress and plane strain cases were tried. For plane stress case, longitudinal section of track was analyzed in the similar way as for Illitrack model [Selig et al. (1979)]. Longitudinal section of track is a section which

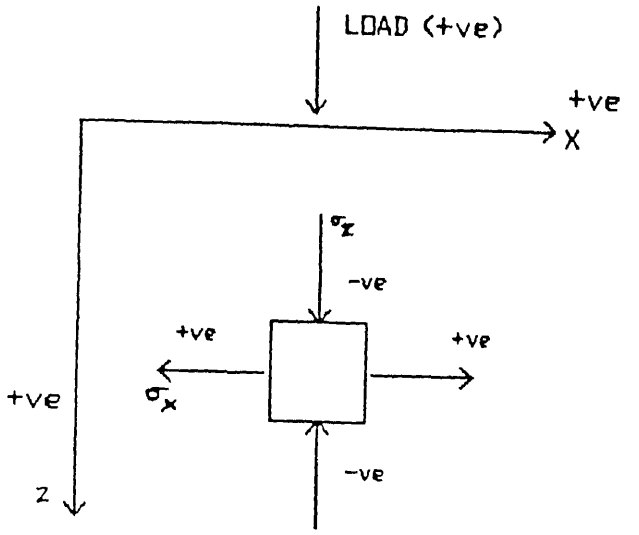

Fig. 3.17 NOTATIONS USED (2D8N MODEL)

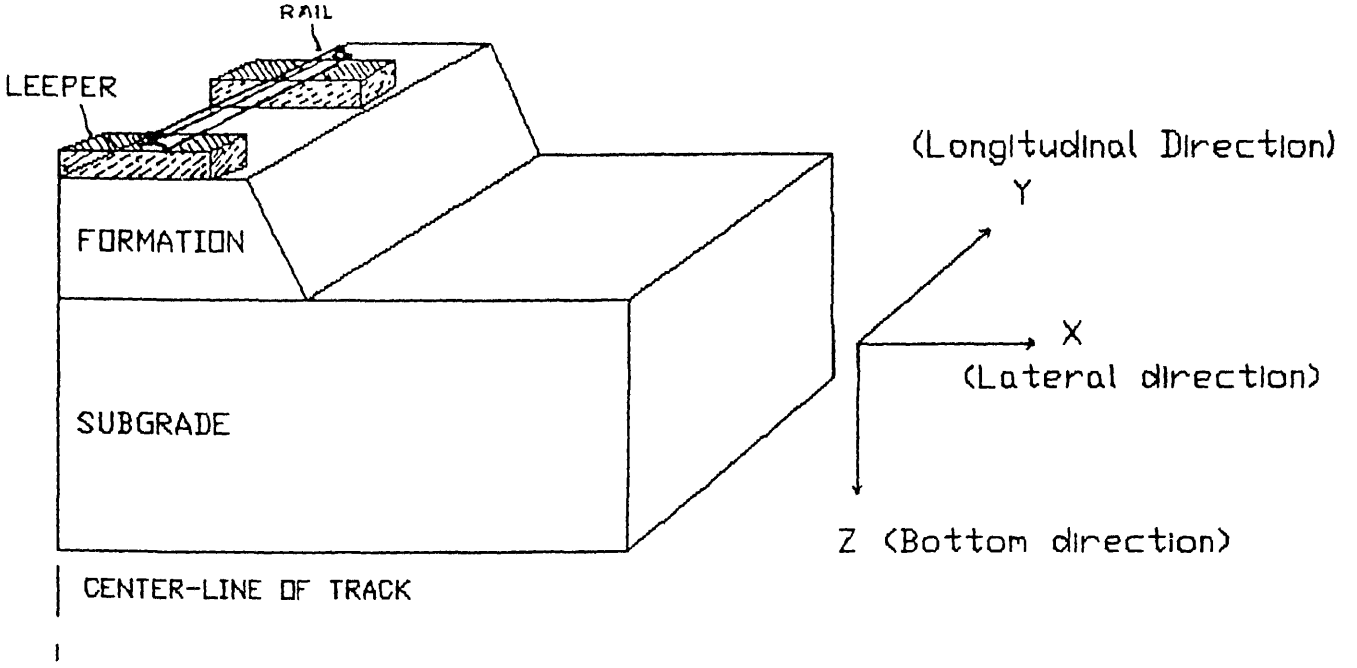

Fig. 3.18 TRACK STRUCTURE AND THE REFERRED DIRECTIONS

runs along the rails while transverse section is one which runs across the rails i.e. along the sleeper (Fig. 3.19).

Stresses calculated from plane stress case for a particular point at a given depth in longitudinal section, would be the average uniform stress at that depth in the transverse section. For example, if stress at the point A (at depth z) was found out as 6.5 KPa by plane stress analysis then uniform stress distribution at depth z in transverse direction will be 6.5 KPa. But it is well known that stresses in transverse section at any depth are non uniform [for e.g., see Selig et al. (1979)]. Also, the thickness of longitudinal section is varying from top to bottom and there is no rational way to decide which thickness is to be taken for analysis and if the thickness is to be varied from top to bottom then at what rate with the depth it should vary. Hence the plane stress case was subsequently discarded.

For plane strain case, transverse section of railway track is considered. For this case, all the sections in y-direction (Fig. 3.18) must be the same in loading and geometry everywhere for a very long distance so that strain in y-direction is zero i.e. $\varepsilon_y = 0$ and need not enter the analysis. For railway track, there are two difficulties in meeting with this requirement. First, the sleepers are not continuous but are discrete in y-direction. Second, due to the presence of concentrated wheel load, loading symmetry is not fulfilled.

Though sleepers are discrete in y-direction, they are assumed to be continuous in that direction but the overall

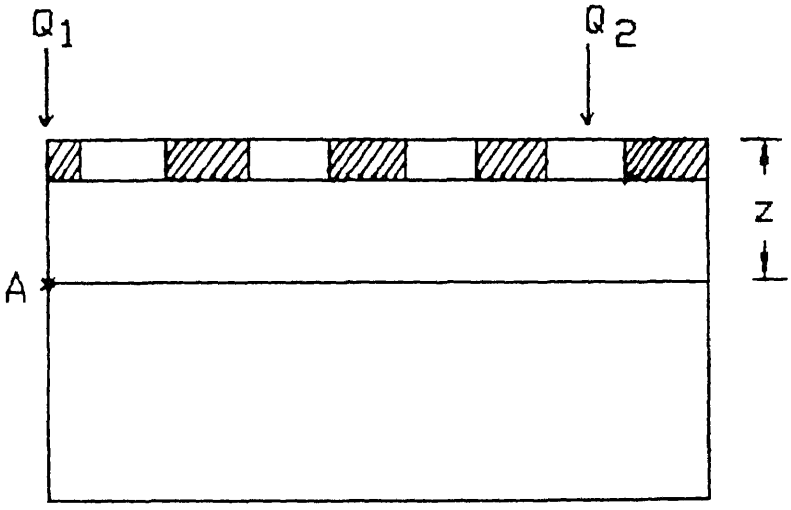

Longitudinal section

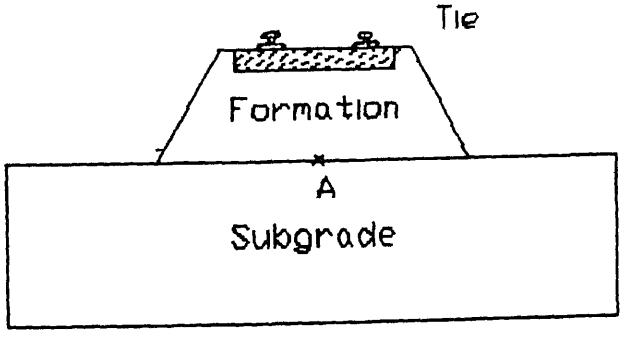

Transverse section

Fig. 3.19 TRACK SECTIONS

flexural stiffness EI of the continuous sleepers was made equal to that of the discrete sleepers.

For example - Considering the sleeper section as shown in Fig. 3.20, moment of inertia of discrete sleeper is given as

$$I_{t1} = b\ t^3 / 12 \tag{3.16}$$

where I_{t1} = moment of inertia of discrete sleeper.

Keeping the same sleeper thickness 't' and width 'b' for an equivalent continuous system,

$$E_{t1} I_{t1} = E_{t2} I_{t2} \tag{3.17}$$

$$b\ t^3\ E_{t1} / 12 = S\ t^3\ E_{t2} / 12 \tag{3.18}$$

$$E_{t2} = b\ E_{t1} / \bar{S} \tag{3.19}$$

where

E_{t1} = modulus of elasticity for discrete sleeper,

E_{t2} = modulus of elasticity for continuous sleeper, and

I_{t2} = moment of inertia for continuous sleeper.

In order to satisfy loading symmetry for plane strain case, wheel load is converted into equivalent line load. The magnitude of the line load can be decided by the following two empirical ways :

1. Figure 3.21 shows the wheel configuration for a typical

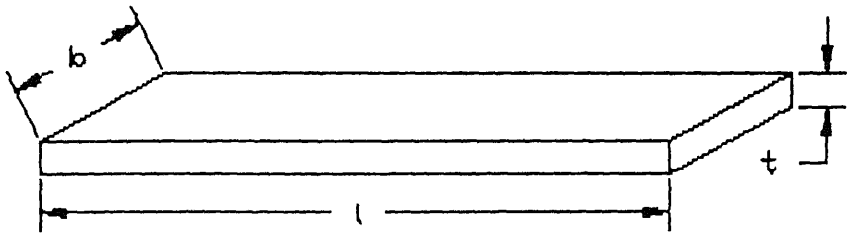

Fig. 3.20 SLEEPER SECTION

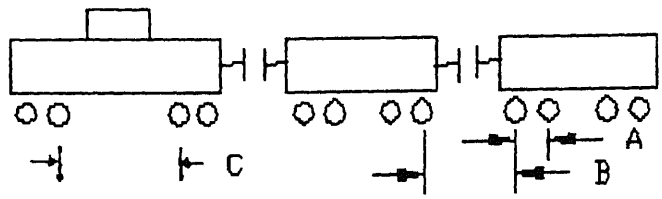

A = 1.7 m

B = 2.0 m

C = 11.0 m

Fig. 3.21 WHEEL CONFIGURATION

train [Selig et al. (1979)]. The spacing between different wheels of rail car is shown there. To be on the safer side, taking the spacing between two wheel loads equal to 1.70 m for the purpose of converting the wheel load into line load, average line load intensity can be obtained as :

For TRACK 2, load of one wheel = 144.657 kN

Then, equivalent line load on sleeper = 144.657/1.7 kN/m

= 85.092 kN/m

This method gives the average line load.

2. Load distribution given by Talbot et al. (1923) for wheel placed in the middle of two sleepers is shown in Fig. 3.22 and the load distribution given by Japanese railways for wheel on top of sleeper [Tadatoshi et al. (A)] is shown in Fig. 3.23.

Superposition of the above two cases gives required load distribution as shown in Fig. 3.24. Maximum line load intensity can be calculated as below (Fig. 3.24) :

Maximum load is taken by sleeper beneath the load (i.e. load sleeper) = 0.43 Q

Width of sleeper = b

= 0.254 m

Hence, line load intensity for load sleeper

= 0.43 × 144.657/ b

= 244.9 kN/m

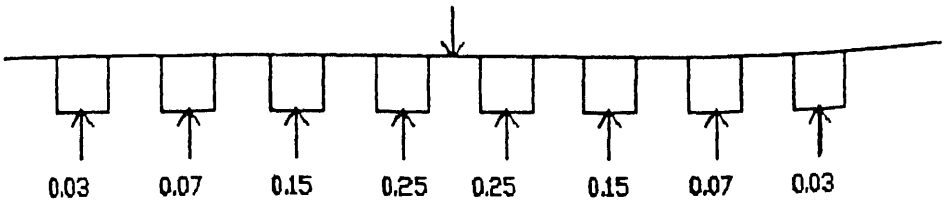

Fig. 3.22 LOAD DISTRIBUTION -- WHEN LOAD IS BETWEEN THE SLEEPERS.

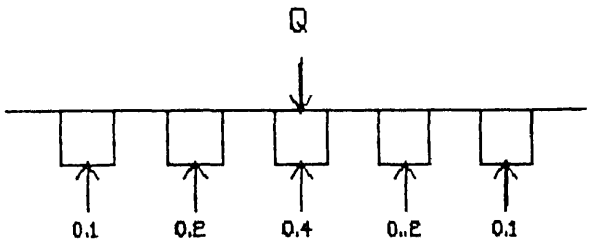

Fig. 3.23 LOAD DISTRIBUTION -- WHEN LOAD IS ON THE SLEEPER.

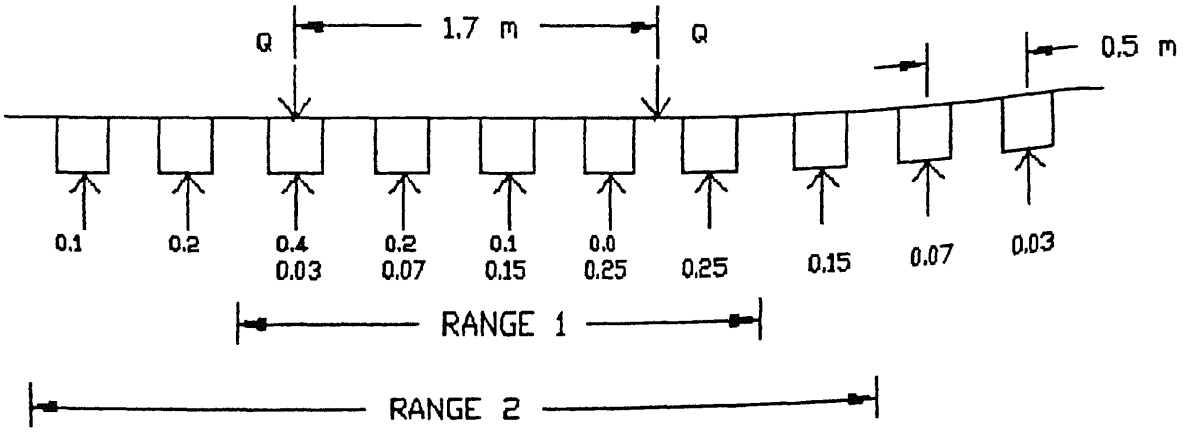

Fig. 3.24 LOAD DISTRIBUTION -- PRESENT PROBLEM

Thus, maximum line load intensity

$$= 244.9 \text{ kN/m}$$

Average line load intensity can be calculated as follows :

Considering range 1 [(the major load areas), Fig. 3.24] :

$$\text{Average line load intensity} = \frac{(0.43+0.27+0.25+0.25+0.25)Q}{5 \times 0.495}$$

$$= 84.75 \text{ kN/m}$$

Another difficulty in modelling occurs due to the presence of rail section. It is due to many reasons. Firstly, for two dimensional analysis, sleepers are assumed to be continuous in longitudinal direction. Thus, if rail element is modelled as two dimensional (2-D) linear element, flexural action of rail will be prevented and load distribution will be through direct shear action. This will induce error in results.

Secondly, while actual contact area between discrete sleeper and curvilinear rail is known, contact area between assumed continuous sleeper and rectangular rail section will have to be assumed without any rational basis.

Thirdly, the determination of magnitude of equivalent line load in place of concentrated wheel load on top of rail head will be very difficult.

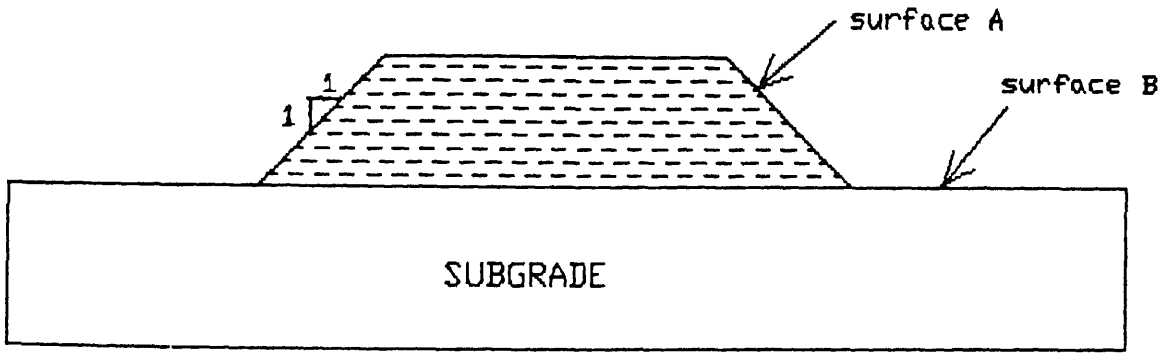

Fig. 3.25 Track formation originally used for calculations

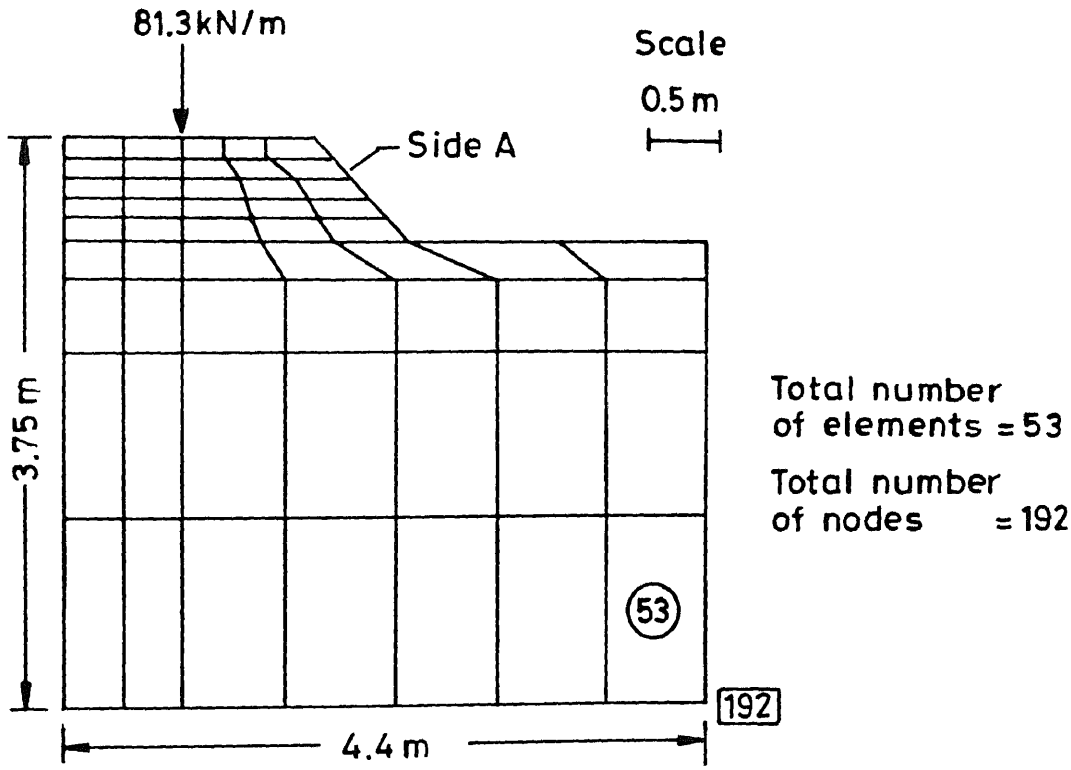

Fig. 3.26 Discretization for mesh A (2D8N model)

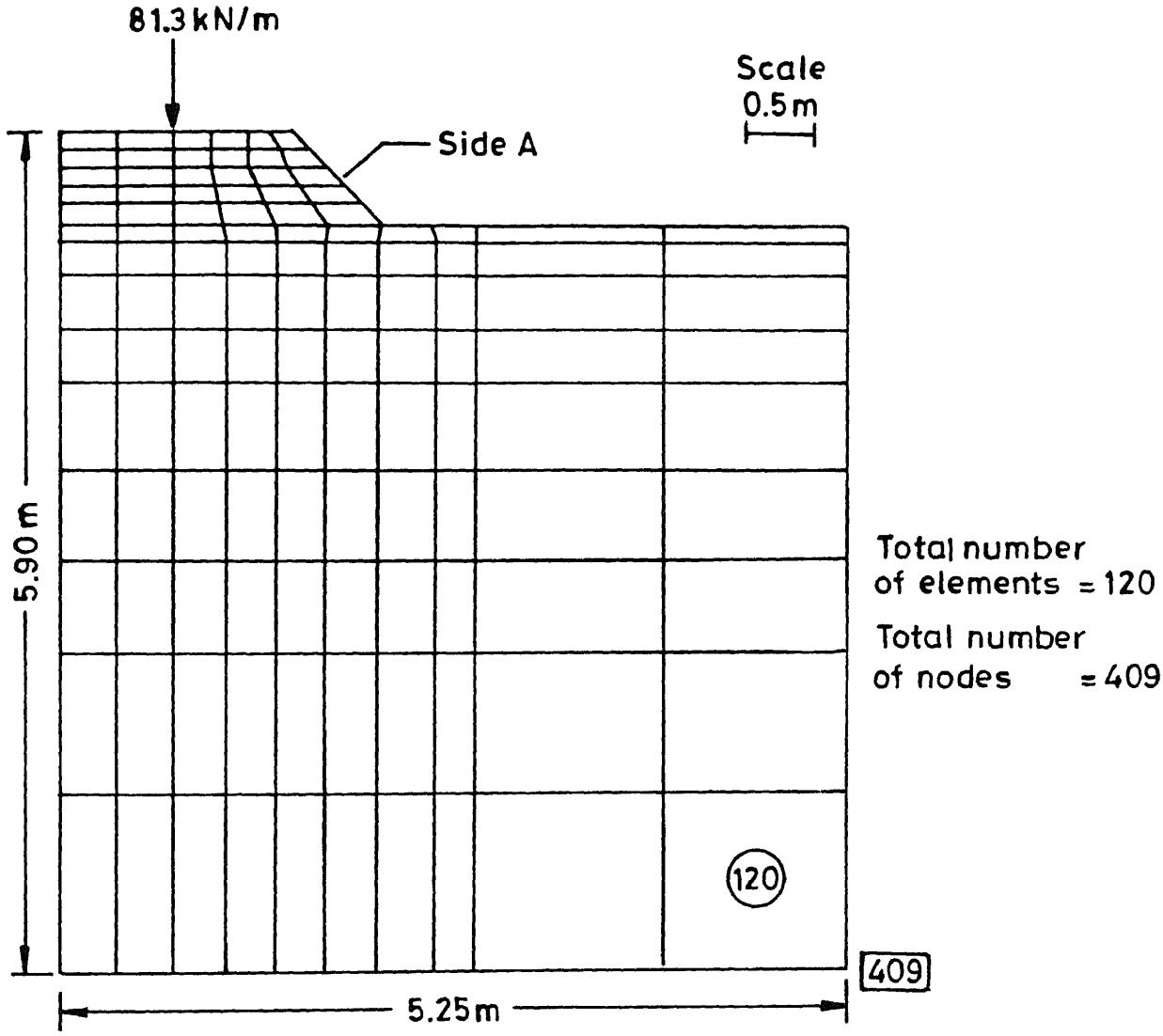

Fig. 3.27 Discretization for mesh B (2D 8N model)

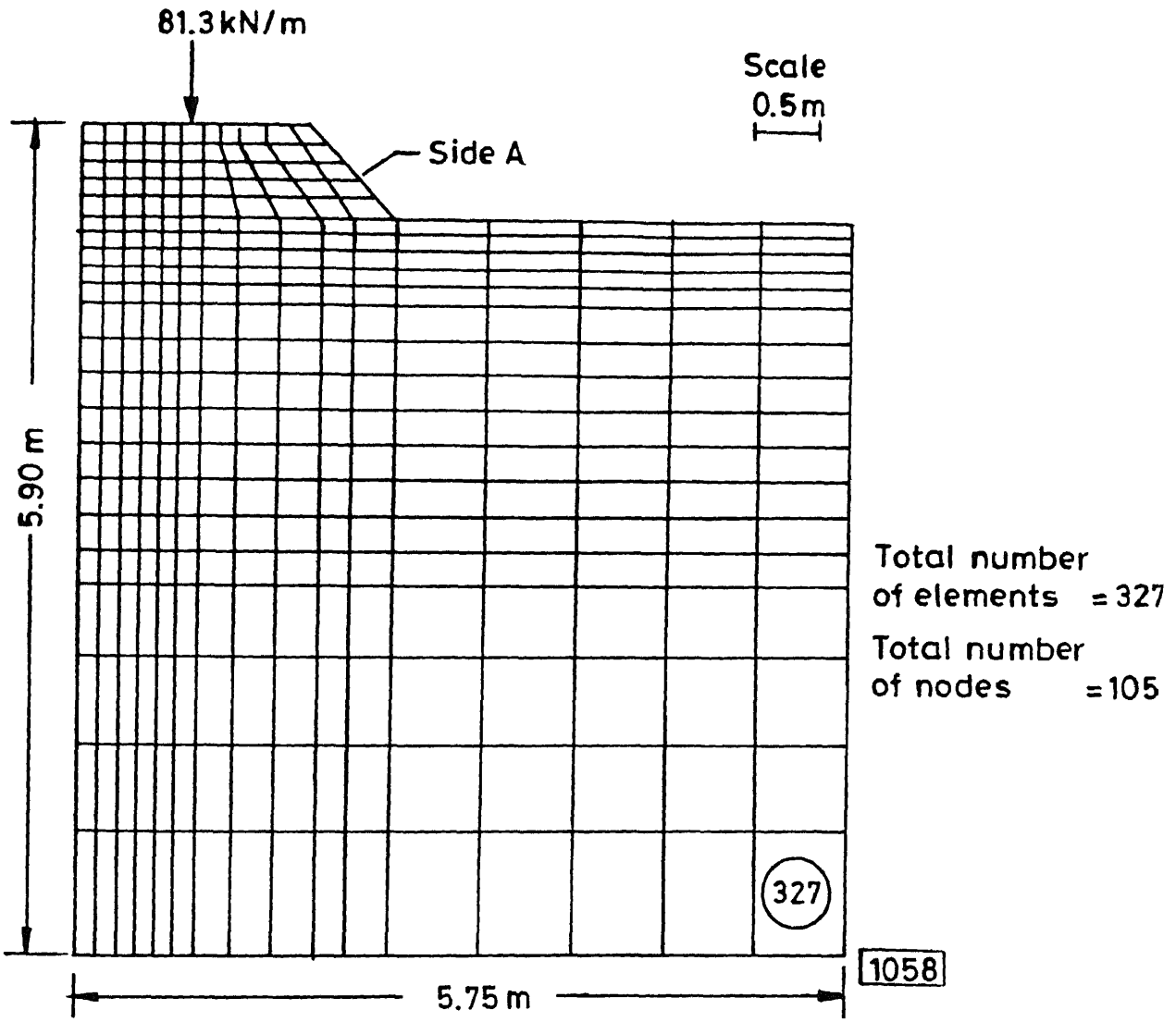

Fig. 3.28 Discretization for mesh C (2D8N model)

mesh B and mesh C , data for TRACK 2 [(same as FAST track section, Selig et al. (1979)] was used. Data for this track is given in Appendix A2.

For 2D8N modelling, E_t was modified to 5310 MPa and average line load intensity is taken as 84.75 kN/m while maximum line load intensity is taken as 244.9 kN/m .

Figures 3.29 to 3.31 show the results of finite element analysis using 2D8N routine with the above track parameters for Mesh A, Mesh B and Mesh C. Minor principal stress (σ_3) shows discontinuity at the interface of two layers (Fig. 3.30) because σ_3 depends on characteristics of the medium [Burmister (1945)].

From these figures, it is clear that major (σ_1) and minor principal stresses have converged for all meshes but displacements have converged for mesh B and mesh C only. Hence Mesh B may be adopted.

Mesh A to mesh C were generated by semi automatic mesh generation facility. But, even then, it took one to six hours to prepare and feed the input data. Hence, it is felt that it would be very helpful, if in place of sloping mesh, a rectangular mesh which could be generated by automatic mesh generation facility can be used.

In literature, it was found that Selig et al. (1979), and Desai and Siriwardane (1982) had used rectangular mesh to model the sloping track embankment. Hence, a trial with five rectangular mesh types [details are given in Tables 3.4(a) to 3.4(c) and Fig. 3.32] was carried out with a view to see

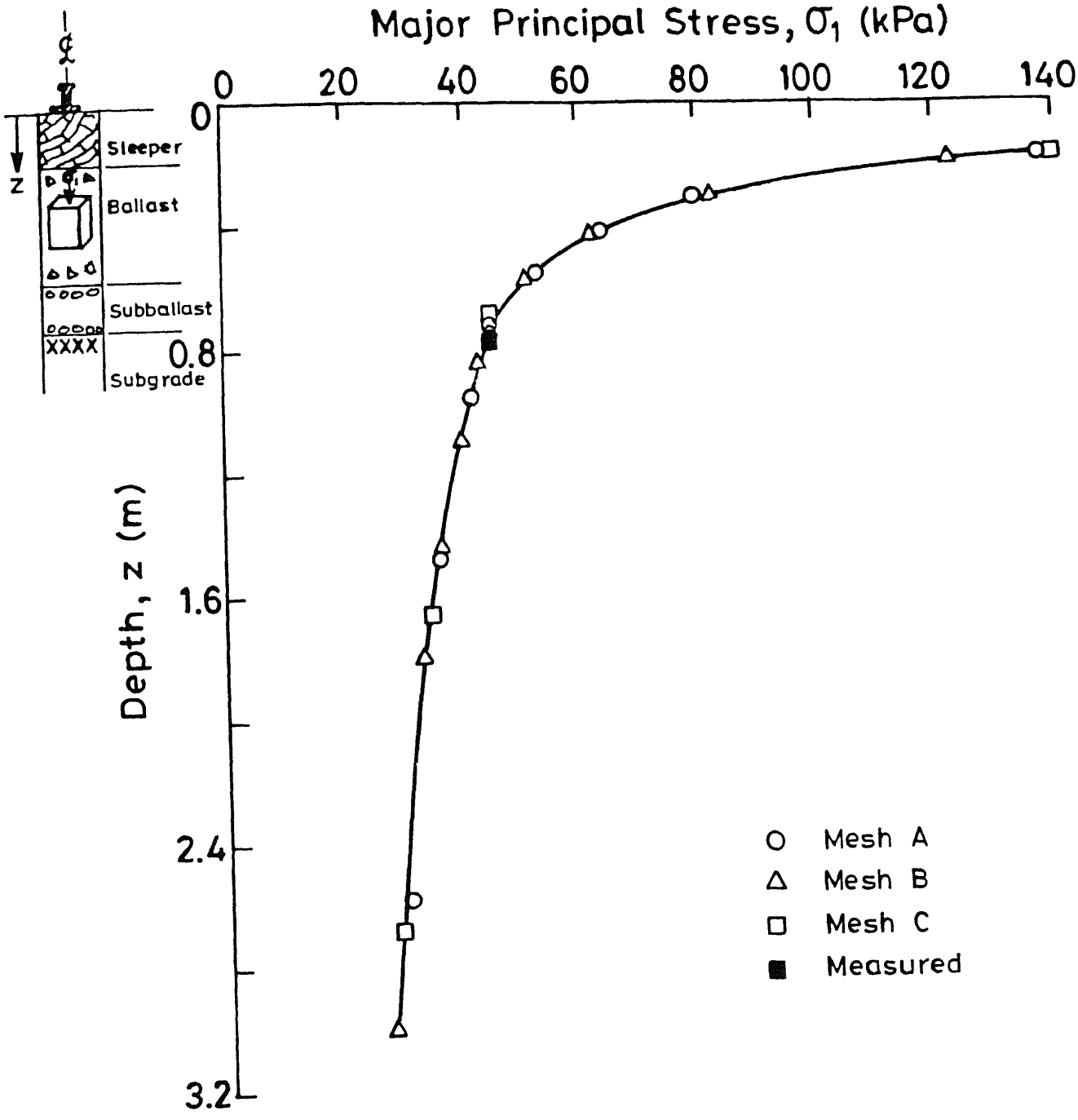

Fig. 3.29 Variation of σ_1 with depth for TRACK 2 (2D8N model)

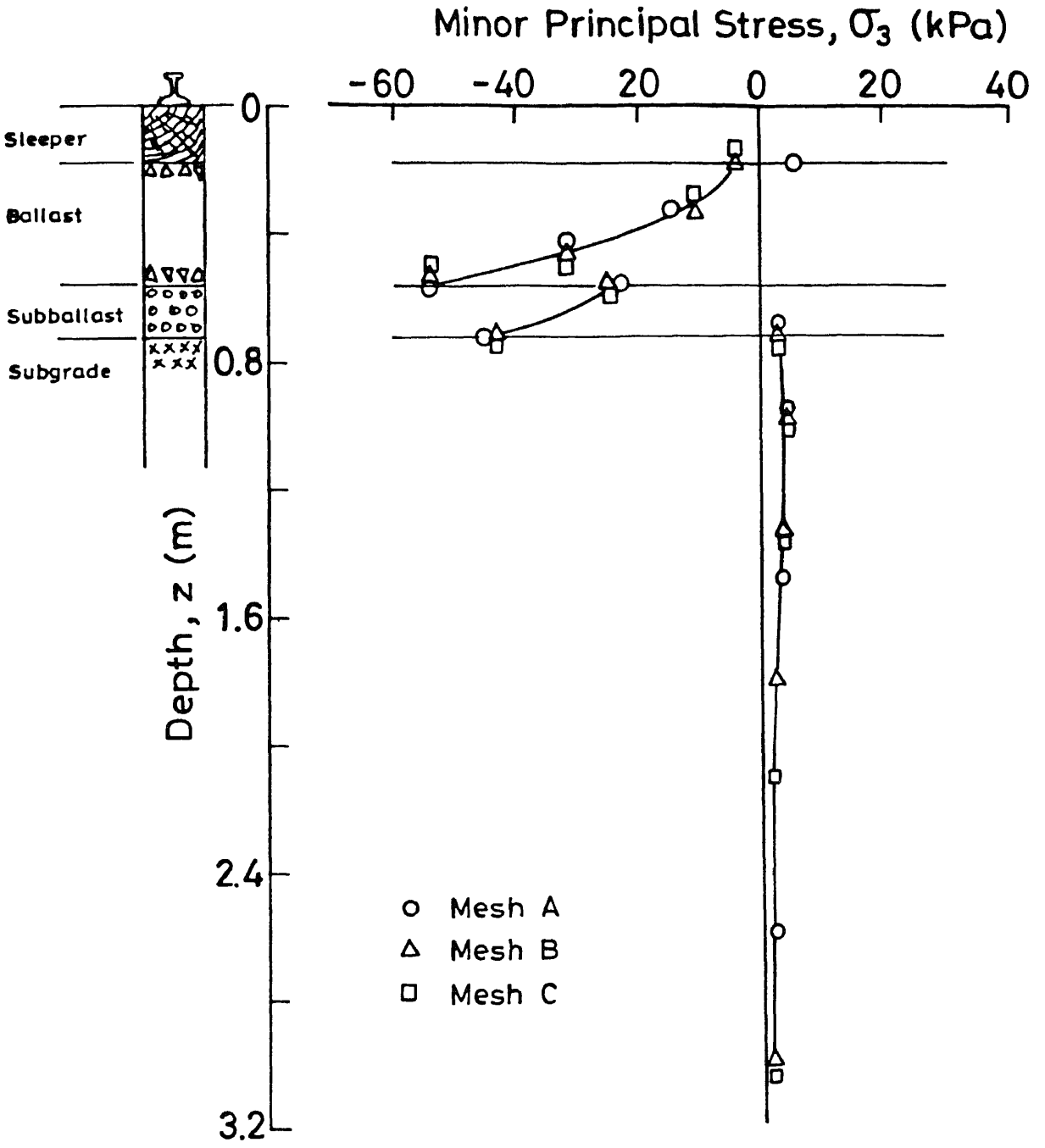

Fig. 3.30 Variation of σ_3 with depth for TRACK 2 (2D8N model)

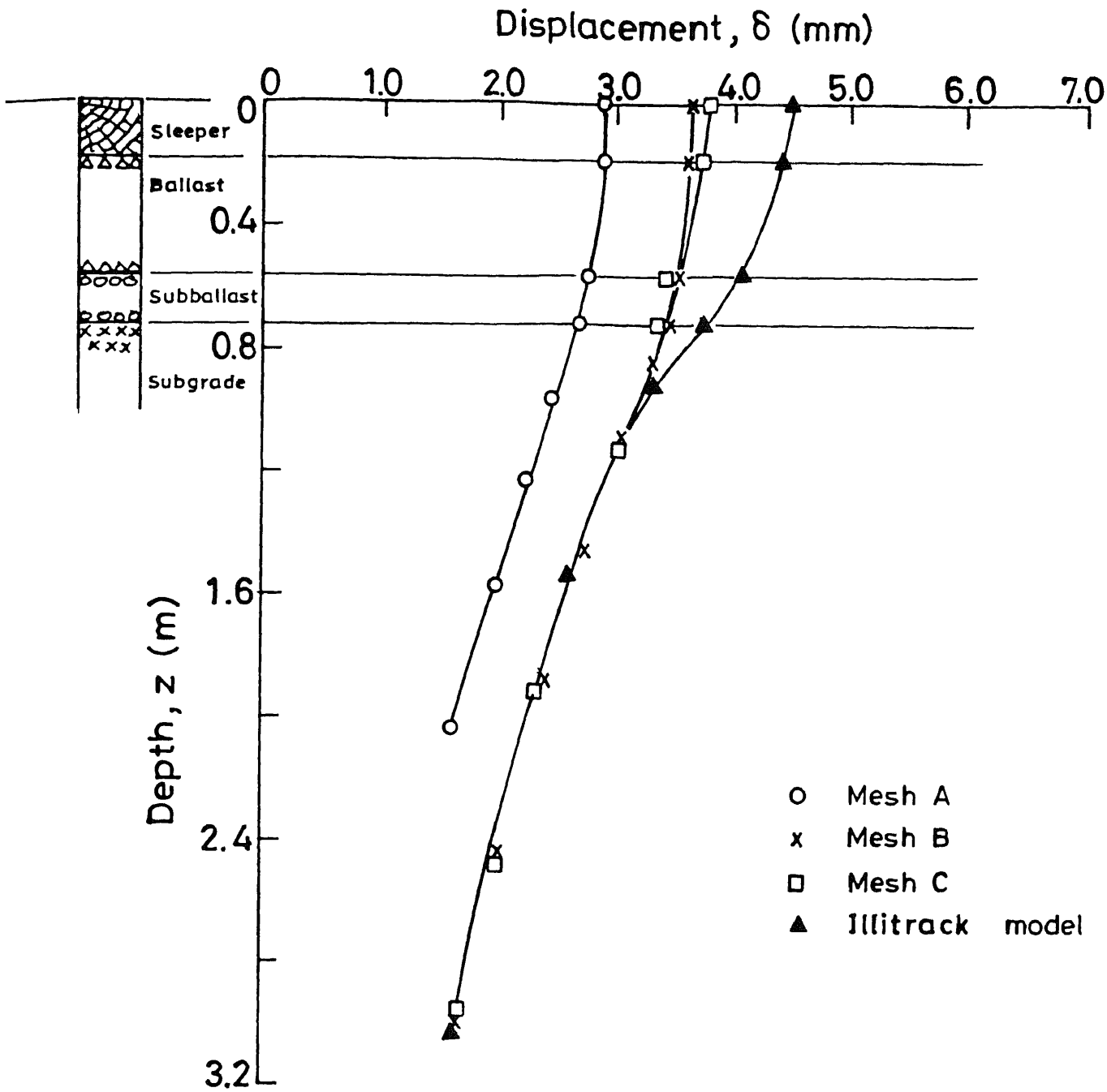

Fig. 3.31 Variation of δ with depth for TRACK 2 (2D8N model)

Table 3.4(a) Meshes used in trials for rectangular mesh selection

Mesh type	Length of Bottom Boundary (cm)	Length of Lateral Boundary (cm)	Total compartments*		Total number of elements
			Lateral	Vertical	
D	455	400	7	8	56
E	665	585	9	10	90
F	665	585	11	14	154
G	1425	1340	11	12	132
H	13700	13000	40	32	1280
B	595	525	SLOPING		120

* refer Fig. 3.32

Table 3.4(b) Compartment dimensions of meshes used in trials for rectangular mesh selection.

Mesh type	compartment dimensions in cm	
D	WLC	50.7, 31.7, 31.7, 22.8, 40.6, 76.2, 146
	WVC	12.7, 12.7, 12.7, 12.7, 15.2, 35.5, 101, 252
E	WLC	50.7, 31.7, 31.7, 22.8, 40.6, 63.5, 63.5, 127, 153
	WVC	12.7, 12.7, 12.7, 12.7, 15.2, 22.8, 38.1, 76.0, 152, 310.0
F	WLC	50.7, 16.5, 15.2, 16.5, 15.2, 22.8, 40.6, 63.5, 63.5, 127, 153
	WVC	12.7, 12.7, 12.7, 12.7, 15.2, 12.7, 22.8, 38.1, 38.1, 63.5, 63.5, 76.0, 101, 183
G	WLC	50.7, 31.7, 31.7, 22.8, 40.6, 63.5, 63.5, 127, 152, 254, 502
	WVC	12.7, 12.7, 12.7, 12.7, 15.2, 22.8, 38.1, 76, 152, 152, 305, 606
H	WLC WVC	FINE TO COARSE

* WLC = width of lateral compartment (cm) from left to right
* WVC = depth of vertical compartment (cm) from top to bottom.

Table 3.4 (c) Result of trials for rectangular mesh selection

Mesh type	σ_{1t} (kPa)	σ_{3t} (kPa)	displacement of top of sleeper (cm)
D	48.23	3.07	3.05
E	47.95	1.82	3.91
F	51.88	1.65	4.17
G	47.50	1.46	5.87
H	50.50	1.37	10.57
B	49.03	1.77	3.78

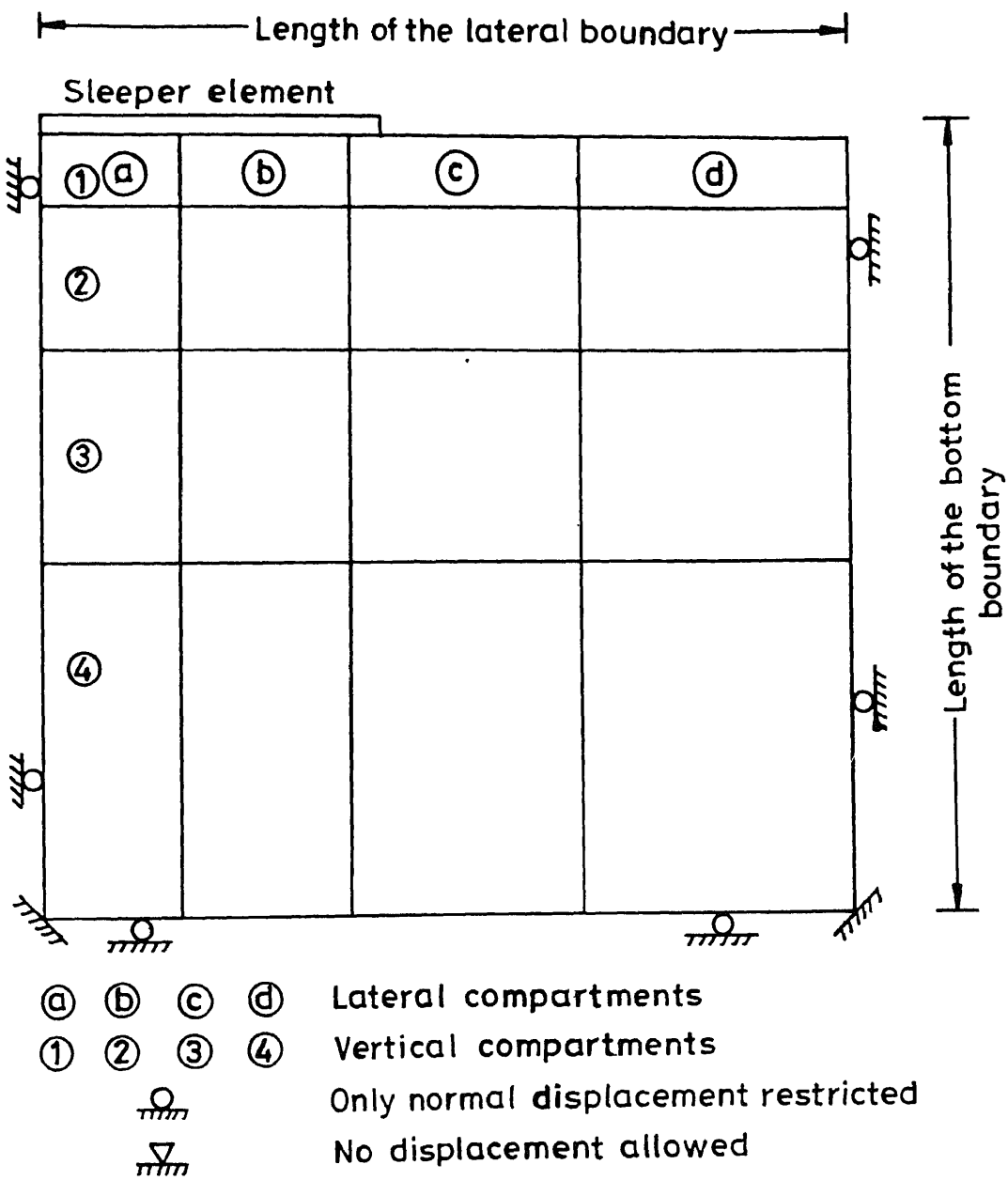

Fig. 3.32 Scheme for rectangular mesh discretization.

whether the same results can be obtained for rectangular formation as was obtained for sloping formation and to choose optimum rectangular mesh size if it gives good results.

Figure 3.33 shows the displacement variation for TRACK 2. It seems that as bottom and lateral boundary distances increase, displacements also increase. However, mesh E, mesh F and mesh B (sloping formation) give same results. Thus , fixing bottom and lateral boundary for rectangular mesh around 6.50 and 6.00 m from center line respectively gives results similar to that of sloping formation.

Figures 3.34 and 3.35 show that results have converged for all the meshes including mesh D. Mesh H shows less major principal stresses at all depths (Fig. 3.34) as compared to other meshes. It is due to the increase of stiffness of ballast and subballast layers due to the increase in width of these layers for mesh H.

Thus it can be seen that sloping track geometry can be modelled by rectangular mesh without loss of accuracy. Mesh E has been chosen as reference mesh for further 2D8N studies because, though stresses have converged for mesh D displacements are not satisfactory for mesh D. It is shown that further refinement does not give better answers and further increase in boundaries will give unsatisfactory displacement values. The optimum mesh boundaries (mesh E) will give the best results. Mesh H (Appendix B1) which gives most accurate results for elastic continuum has been shown to be less accurate for track problem.

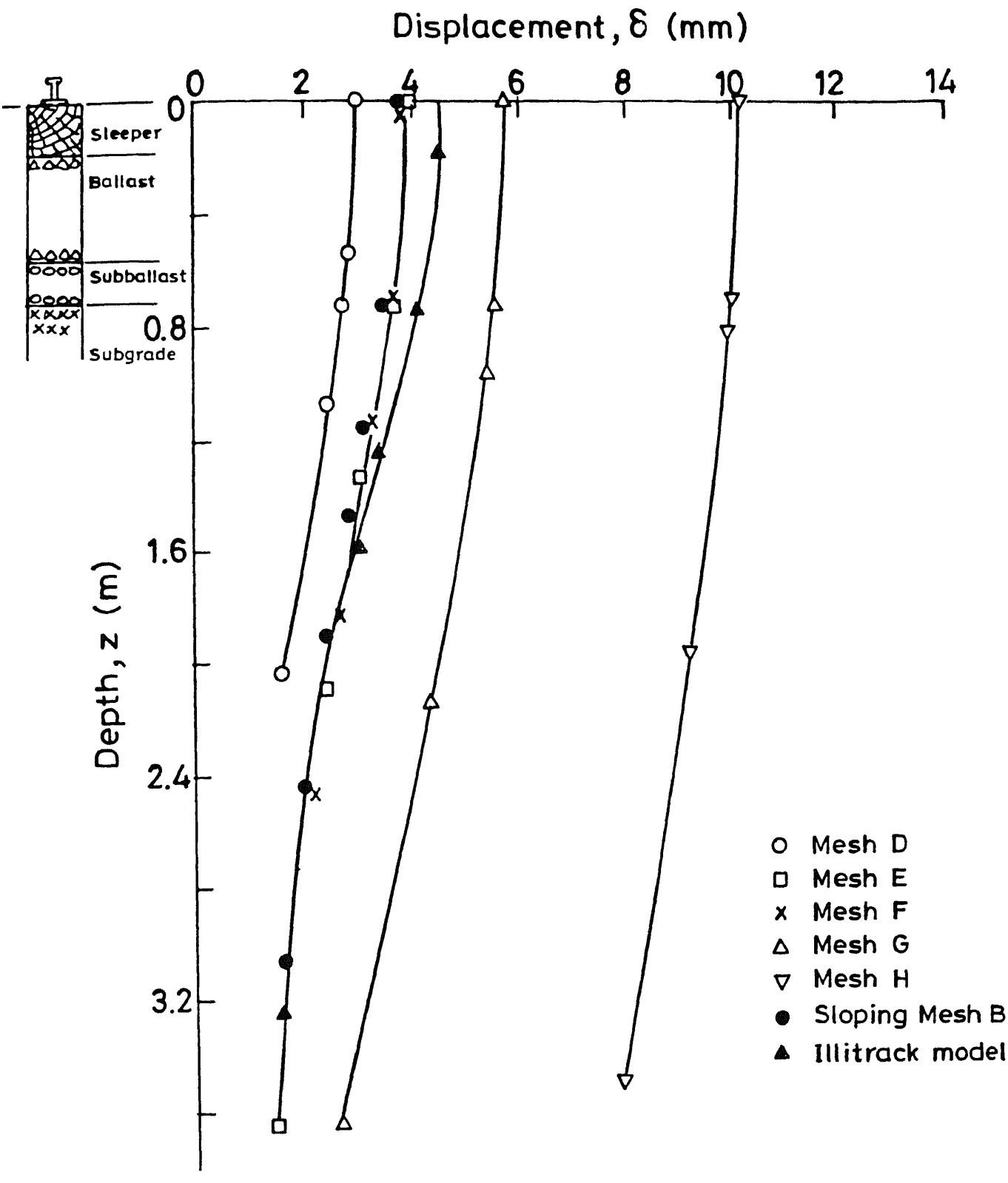

Fig. 3.33 Variation of δ with depth for TRACK 2 by different rectangular mesh discretizations (2D8N model)

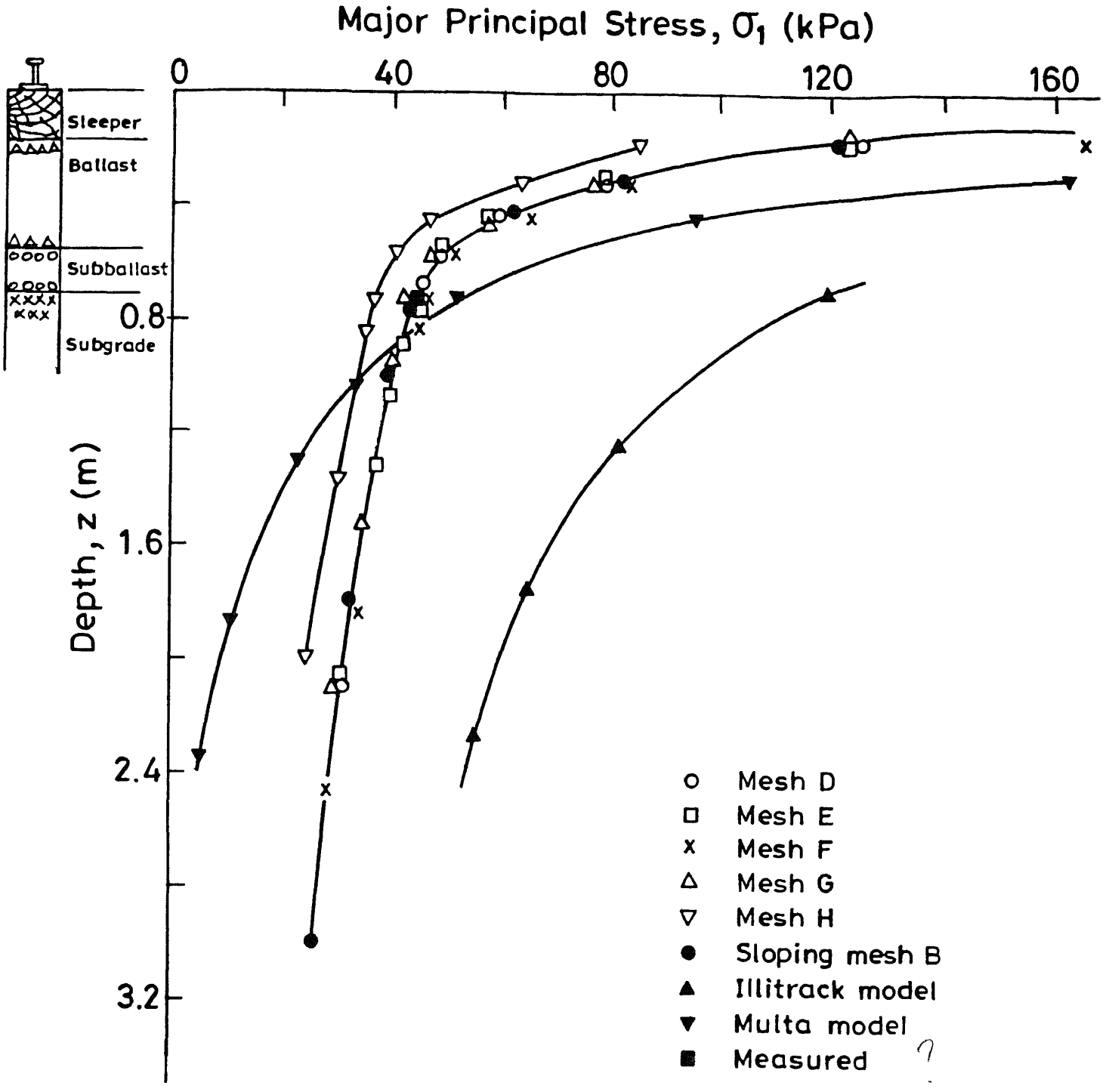

Fig. 3.34 Variation of σ_1 with depth computed by using different rectangular mesh discretizations for TRACK 2 (2D 8N model)

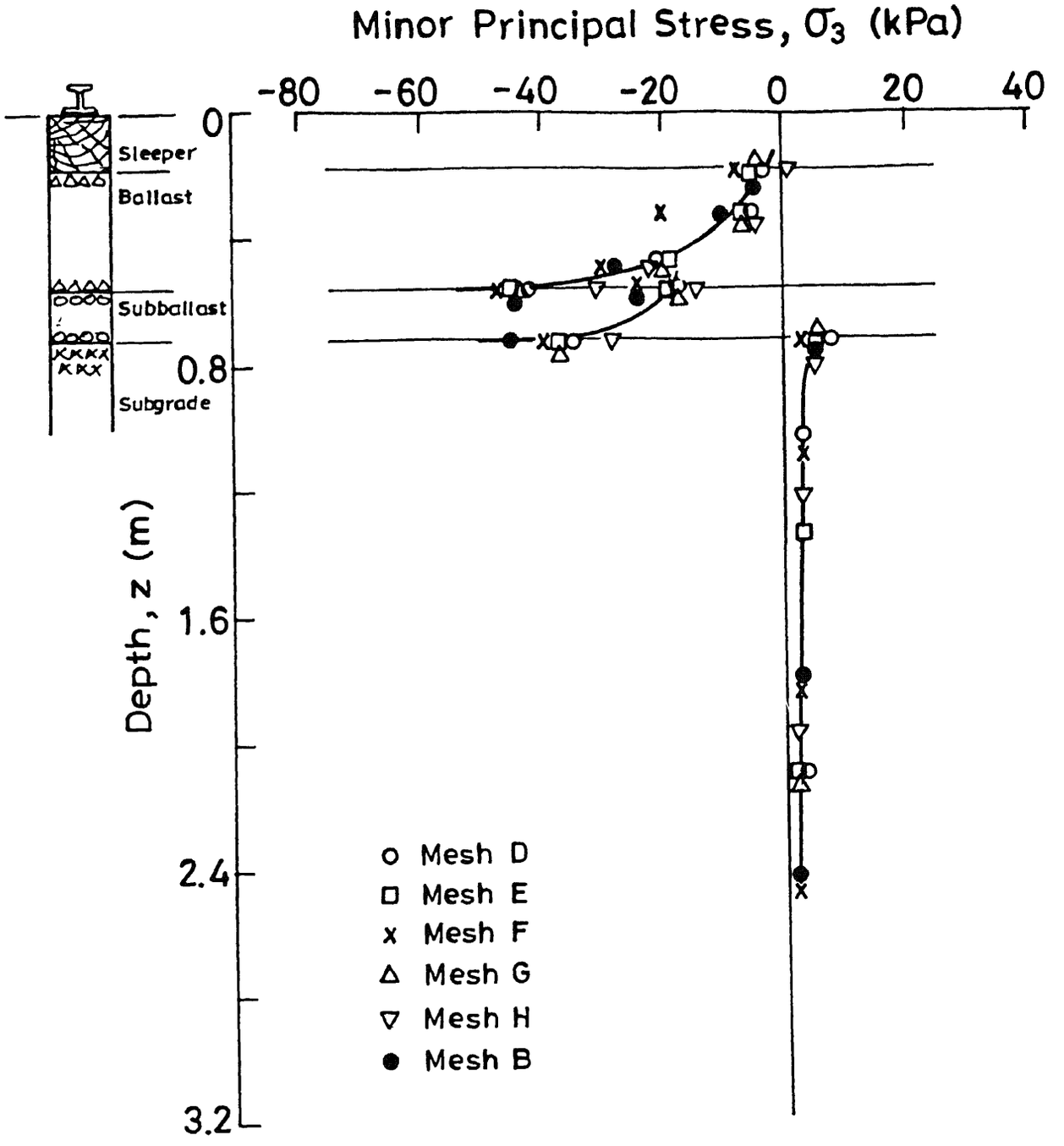

Fig. 3.35 Variation of σ_3 with depth computed by using different rectangular mesh discretizations for TRACK 2 (2D8N model)

Results obtained by Selig et al. (1979) for FAST TRACK section have been reproduced. Measured value of vertical stress at top of the subgrade is also shown.

3.3.5 LIMITATIONS

2D8N model has following limitations which restrict its general purpose use and reduce its versatility :

1. Effect of rail type on track structure can not be evaluated as rail element is absent in the analysis.

2. In 2D8N modelling, concentrated wheel load has been replaced by equivalent line load and the plane strain finite element analysis was carried out. Hence the stress distribution essentially shows the characteristics of line load. Thus, the rapid stress dispersion expected for the concentrated wheel is absent for equivalent line load and a very little stress dissipation with depth is obtained in this case. This can be seen by comparing MULTA results with 2D8N results in Fig. 3.34 inside the subgrade. It can be seen that 2D8N predicts conservative results in terms of vertical stress at deeper depths and compares well with measured vertical stresses at the top of subgrade in this case.

This also indicates the necessity of 3 dimensional analysis for track problem. However it is obvious that 3-D analysis takes more time as compared to 2-D analysis

[Zienkiewicz and Taylor (1989)] for same problem. Hence an attempt has been made to extract 3-D analysis results from 2-D analysis.

At shallower depths, concentrated wheel load gives rise to very high stress intensity which cannot be reproduced by average line load intensity. Hence, as a modification to 2D8N model, following guidelines have been suggested to reasonably predict stresses inside the track :

Major principal stress variation inside the track structure due to both average and maximum pressure intensity will essentially consist of two parts -- upper sharp curvilinear part and lower straight vertical part. The modification essentially consists of joining roughly the lower straight vertical part of average pressure intensity with sharp curvilinear part of maximum pressure intensity curve by a smooth transition which should be as small as possible (Fig. 3.36). It is to be noted that average pressure intensity is calculated as in Sec. 3.3.3 and can be taken as equal to wheel load/spacing between two axles (1.70 m) while the maximum pressure is equal to wheel load $\times$ 0.43 / width of sleeper. 0.43 indicates the percentage of total wheel load taken by the sleeper below the wheel load.

However, this modification applies to vertical stress only.

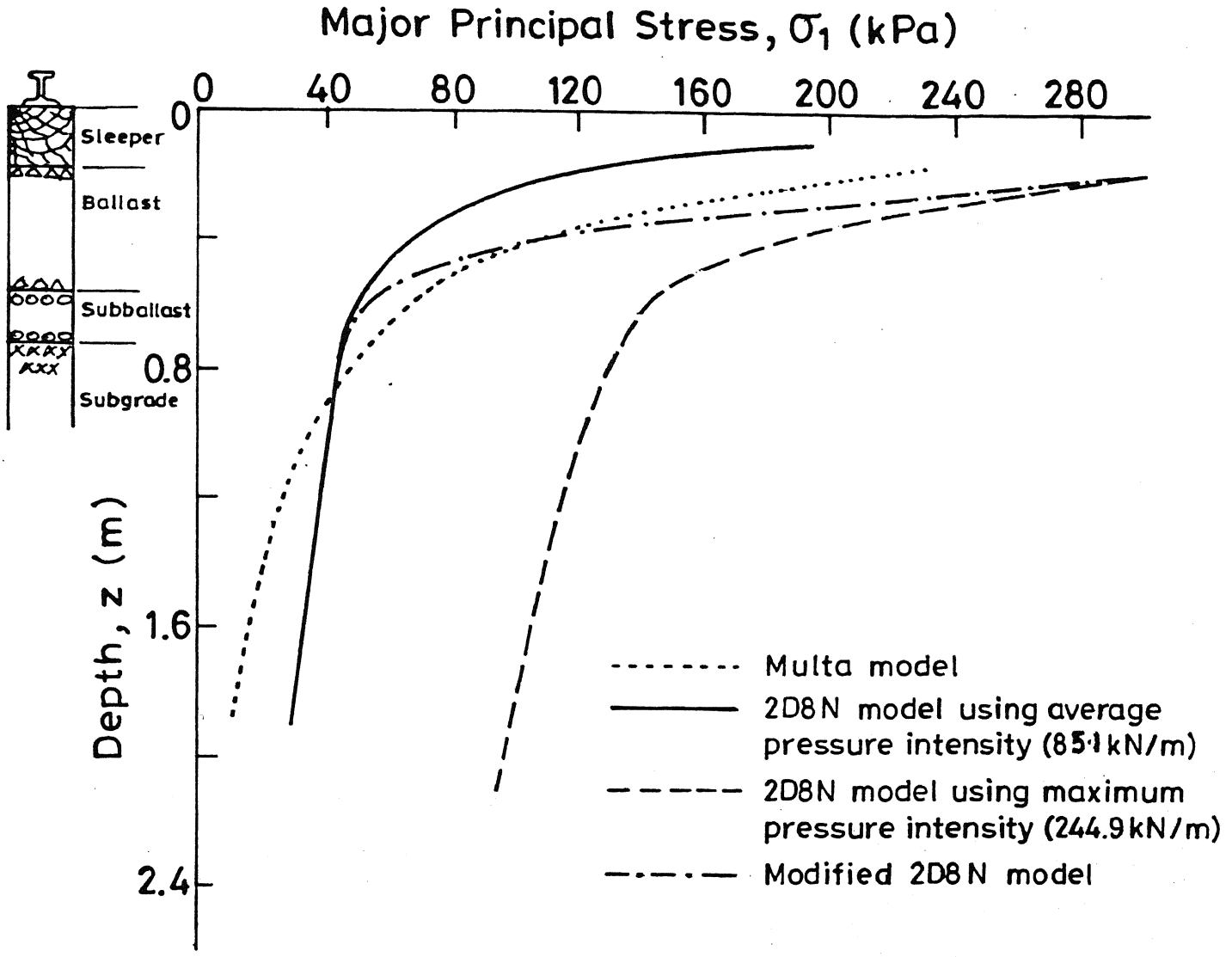

Fig. 3.36 Proposed modification to 2D8N model.

3.3.6 COMPARISON OF RESULTS

Comparison of predicted results using 2D8N model with other models and field test results is presented in Sec. 3.5.

3.3.7 RESULTS AND DISCUSSION

Parametric studies have been carried out with reference to TRACK 1. TRACK 1 is the representation of typical Indian track. Data for this track is given in Appendix A1. Results in terms of stresses and displacements at important locations are presented below for reference track along with the results of parametric studies. Analysis has been carried out both with and without joint element between different layers. The range of parameters used is as follows :

E_b = 150, 165, 180 MPa

E_{sb} = 60, 80, 100 MPa

E_s = 10, 20, 50 MPa

d_{sb} = 0.15, 0.35, 0.55 m

Joint element properties used are as given below (also see Sec. 3.4.6) :

Joint element property for tie and ballast interface :

k_n = 415200 MN/m^3

k_s = 4150 MN/m^3

Joint element properties for ballast and subballast layers :

$k_n = 4150 \text{ MN/m}^3$

$k_s = 550 \text{ MN/m}^3$

Joint element properties for subballast and subgrade interface :

$k_n = 550 \text{ MN/m}^3$

$k_s = 165 \text{ MN/m}^3$

E_{t1} for discrete real system was changed to E_{t2} for an equivalent continuous system as given below (Sec. 3.3.3)

$$E_{t2} = 0.249 \times 10550 / 0.65$$
$$= 4041.5 \text{ MPa}$$

Wheel load was converted into equivalent line load as follows :

$$\text{Average line load} = 159.4/1.7$$
$$= 93.77 \text{ KN/m}$$
$$\text{Maximum line load} = 0.43 \times 159.4 / 0.249$$
$$= 275.27 \text{ KN/m}$$

Normal displacement was restricted on sides and bottom while top edge was kept free. Two bottom corners were assumed as fixed.

Mesh E was used for discretization, in general.

Results of parametric studies have been tabulated in Table 3.5.

Table 3 5 Results of parametric studies (2D8N model)

File Name	E_b (MPa)	E_{sb} (MPa)	E_s (MPa)	d_{sb} (cm)	Analysis without joint element			Analysis with joint element		
					σ_{1t} (kPa)	σ_{3t} (kPa)	δ_{top} (cm)	σ_{1t} (kPa)	σ_{3t} (kPa)	δ_{top} (cm)
A1	150	80	10	15	46 73	8 45	0 966	46 12	8.37	0 999
A2				35	42.03	6.78	0 906	41 40	6 76	0 937
A3				55	37 88	6.00	0 847	37.44	5 94	0.876
B1			20	15	52 46	6 39	0.526	50.84	5 95	0.563
B2				35	47.52	4 89	0 506	46 12	4.51	0.540
B3				55	43.26	4 21	0 487	42 20	3.91	0 519
D1			50	15	60 83	4 60	0 240	56 03	2 51	0.279
D2				35	54 93	3 48	0 240	51 42	1.89	0 278
D3				55	50 36	2.73	0.240	47 77	1 38	0.276
B2SB1	150	60	20	35	48 36	4 61	0 518			
B2SB3		100			46 78	5 27	0 498			
B2B1	180	80	20	35	47 17	4 85	0 503			
B2BD1s	150	80	20	00	48 71	5 45	0 520			
B2BD2s				60	45 30	6 26	0 483			

Figure 3.37 shows displacement under the load with depth for the reference track by 2D8N with and without joint elements. Displacement remains fairly constant till top of subgrade as the tie, ballast and subballast layers have very low compressibility.

It has been noted that vertical and horizontal stress values at the top of subgrade remain same as that of major and minor principal stress values respectively. Hence, for 2D8N and 3D20N model, only variation of major and minor principal stress values has been presented.

Figures 3.38(a) to 3.38(c) show distribution of major and minor principal stresses and maximum shear stress with depth for reference track for 2D8N model with and without joint elements. Major principal stress predicted by modified 2D8N model is also shown. Major principal stress distribution is a smooth curve through all the layers. However, minor principal stress depends on media characteristics while major principal stress does not [Burmister (1945)]. Within one layer, minor principal stress decreases from top to bottom. Minor principal stress is tensile in ballast and subballast layers. While, in subballast layer, small tension (up to 50 KPa) may be allowed but ballast layer being fully granular cannot sustain any tension. This is the disadvantage of elastic analysis. This also calls for elasto-plastic analysis. However, later in Sec. 3.5, it is shown that results predicted from elastic analysis compare well with results from elasto-plastic analysis inside the subgrade. As the maximum shear stress depends on minor and

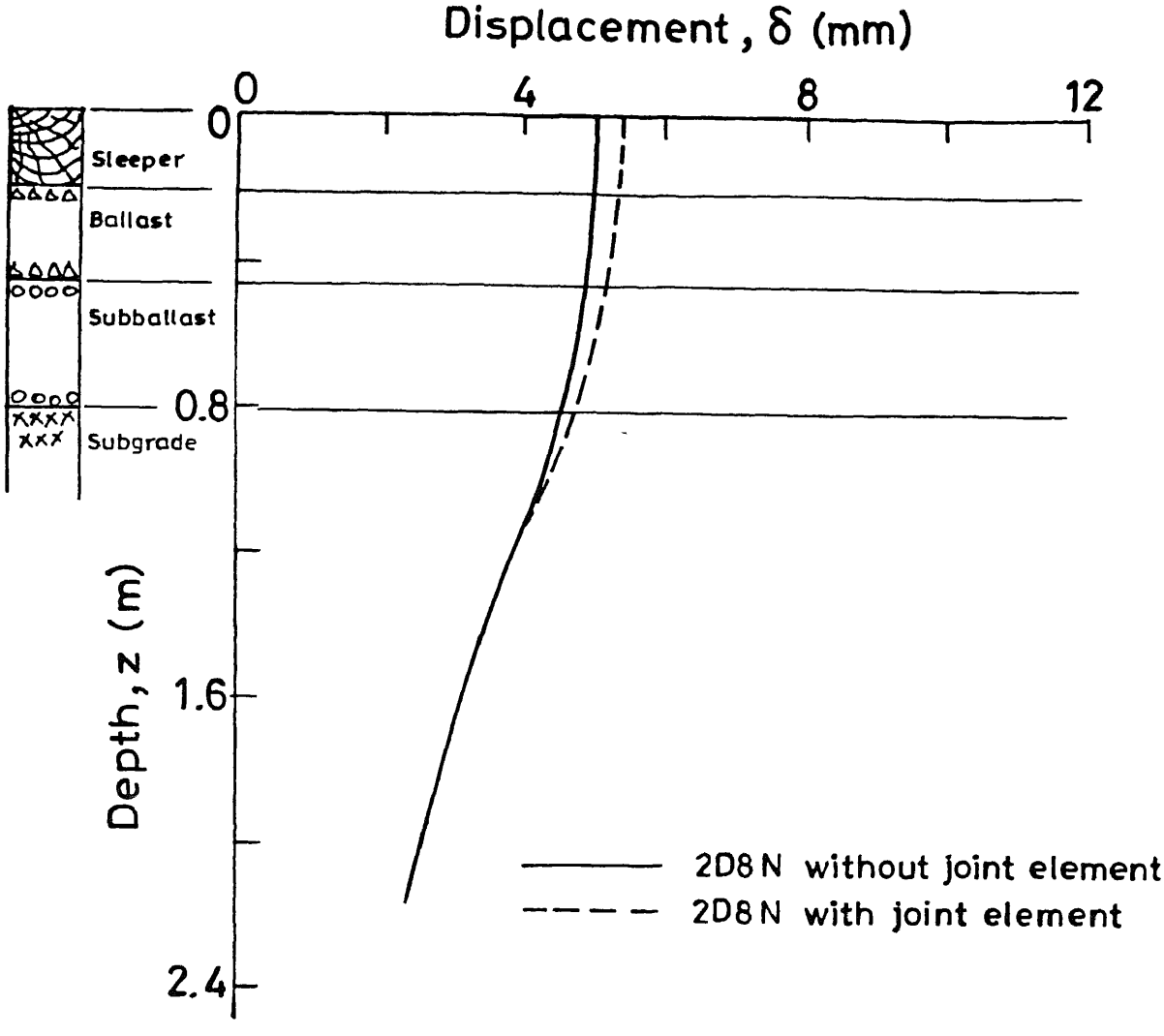

Fig. 3.37 Variation of displacement with depth for TRACK 1 (2D8N model)

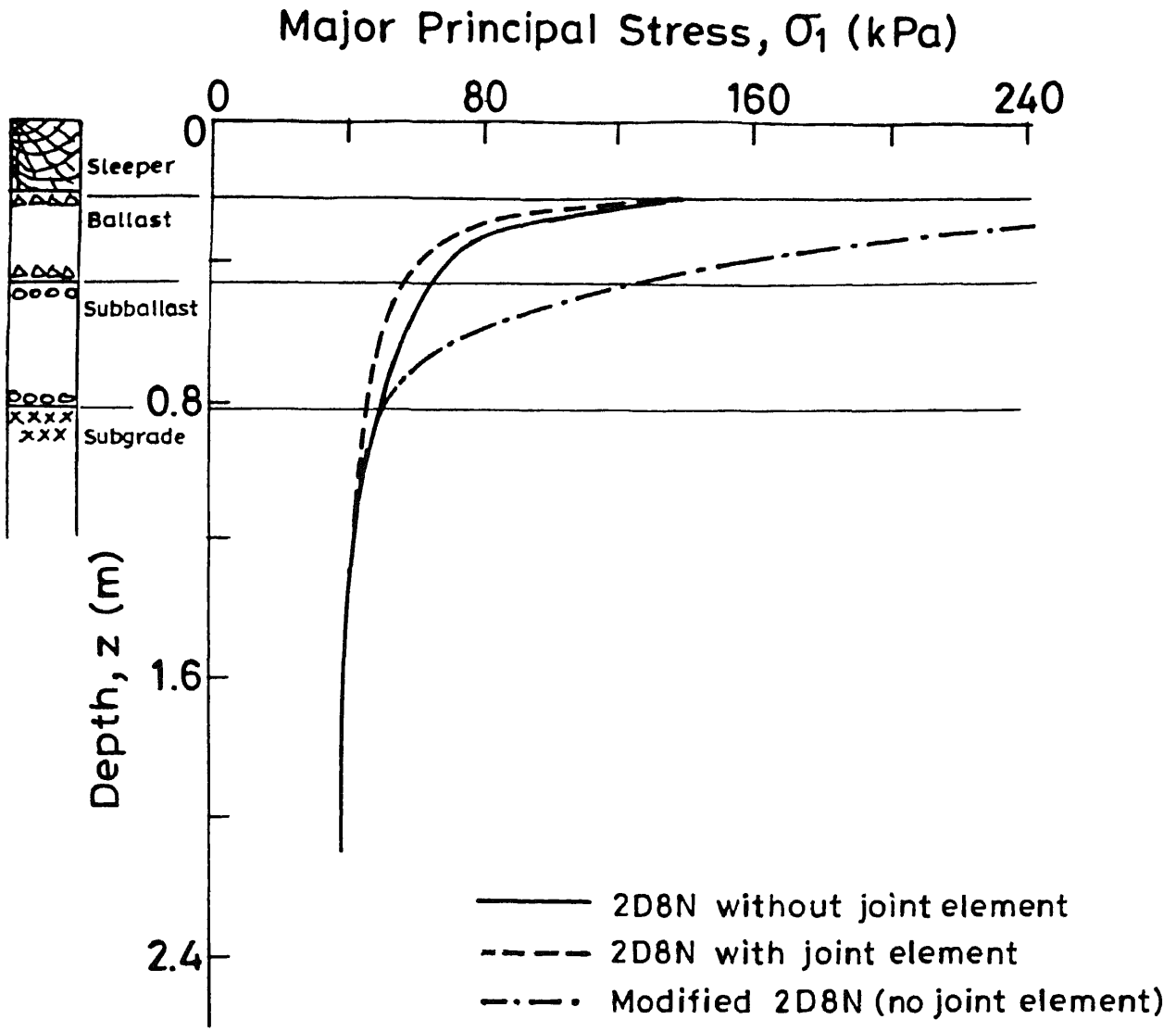

Fig. 3.38 (a) Variation of σ_1 with depth for TRACK 1 (2D8N and modified 2D8N model)

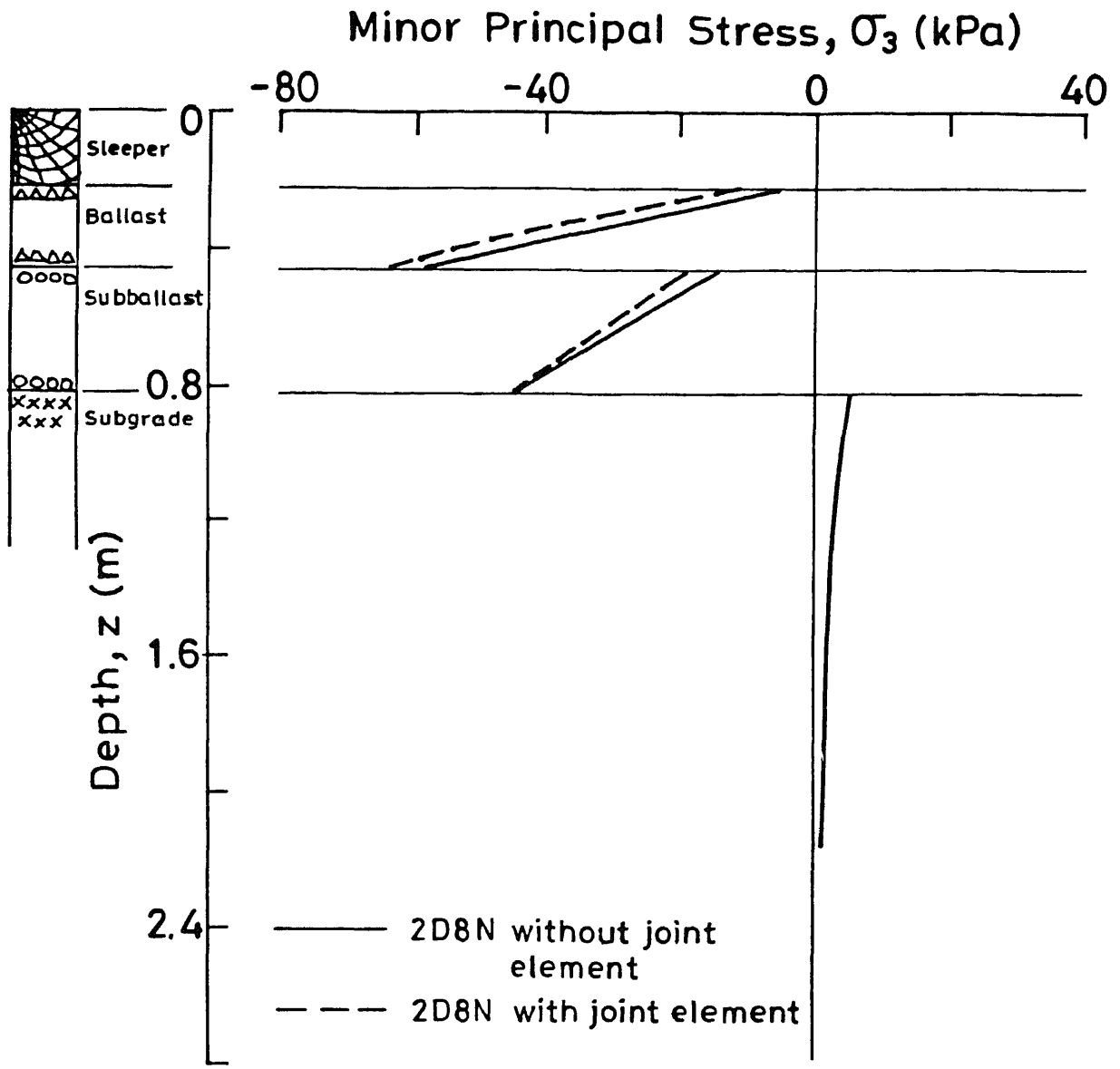

Fig. 3.38(b) Variation of σ_3 with depth for TRACK 1 (2D8N model)

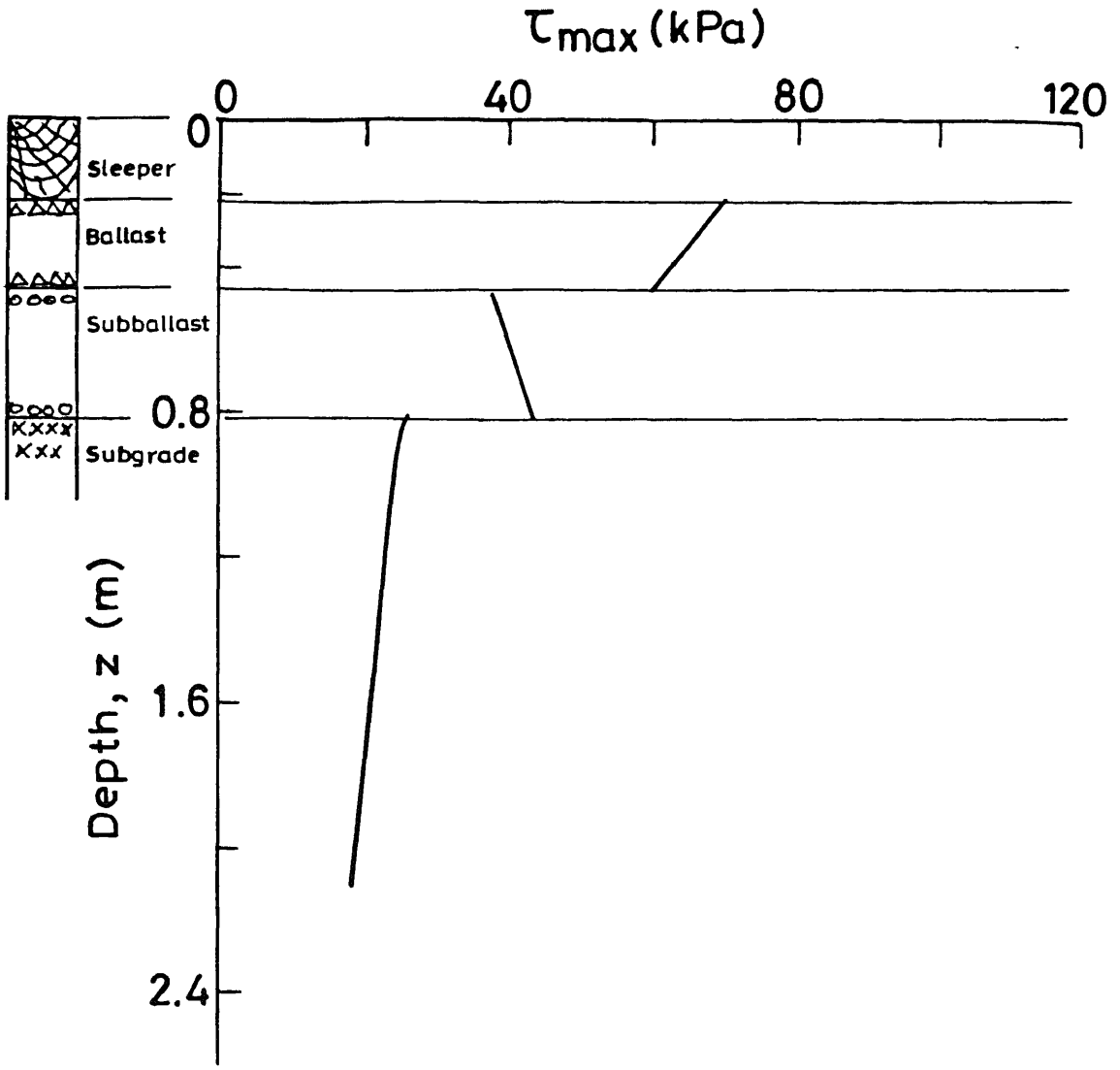

Fig. 3.38 (c) Variation of τ_{max} with depth for TRACK 1 (2D8N model)

major principal stresses, maximum shear stress curve also has discontinuity at the interfaces.

From Figures 3.38(a), it may be seen that the dispersion of major principal stress with the depth is poor. Stresses decrease by only 20 percent for 1 m depth inside the subgrade. This is because of the assumption of line load in this model.

Figure 3.39 shows major and minor principal stresses and Shear stress distribution on top of the subgrade with the length in x-direction (but inside the subgrade). It may be seen that maximum major principal stress occurs under the rail seat. As major principal stress is equal to vertical pressure on top of subgrade, maximum vertical pressure on top of subgrade is also located under the rail seat.

Figure 3.40 shows major and minor principal stress on top of subgrade under the rail seat (σ_{1t} and σ_{3t} respectively) for different soil types, for three different values of thickness of subballast layer. Thickness of ballast layer is kept constant (0.25 m) in all three cases. It can be seen that σ_{1t} increases with increase in Young's modulus of subgrade. σ_{3t} decreases with increase in Young's modulus of subgrade. However, both stresses decrease with increase in subballast depth. Results have been plotted with and without joint elements. The effect of joint elements is to reduce both types of stresses.

Figure 3.41 shows the displacement of top of sleeper for different soil types and for different depths of construction with and without joint elements. It can be seen that depth of

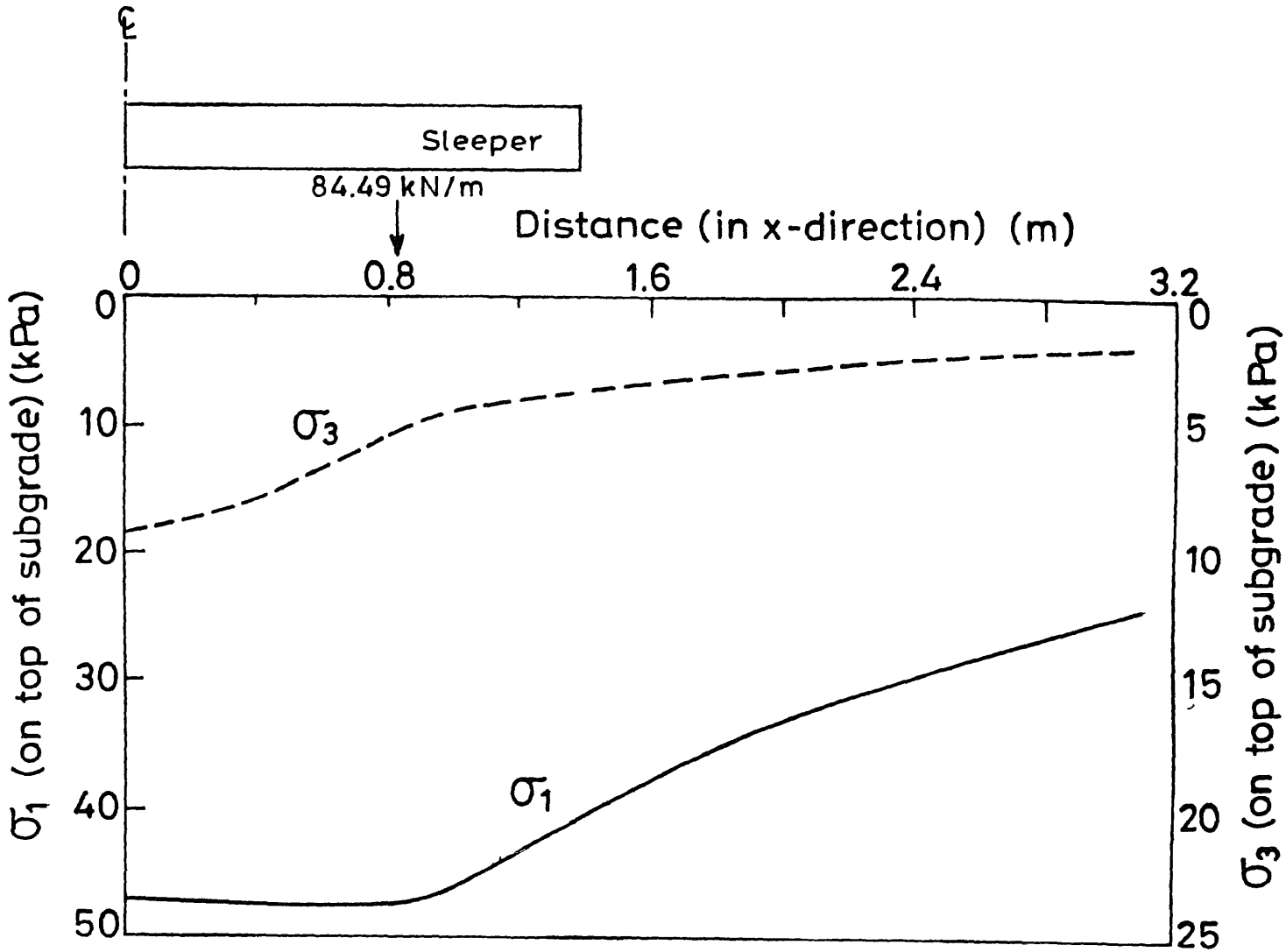

Fig. 3.39 Variation of major and minor principal stress along the sleeper on top of subgrade for TRACK 1 (2D8N model)

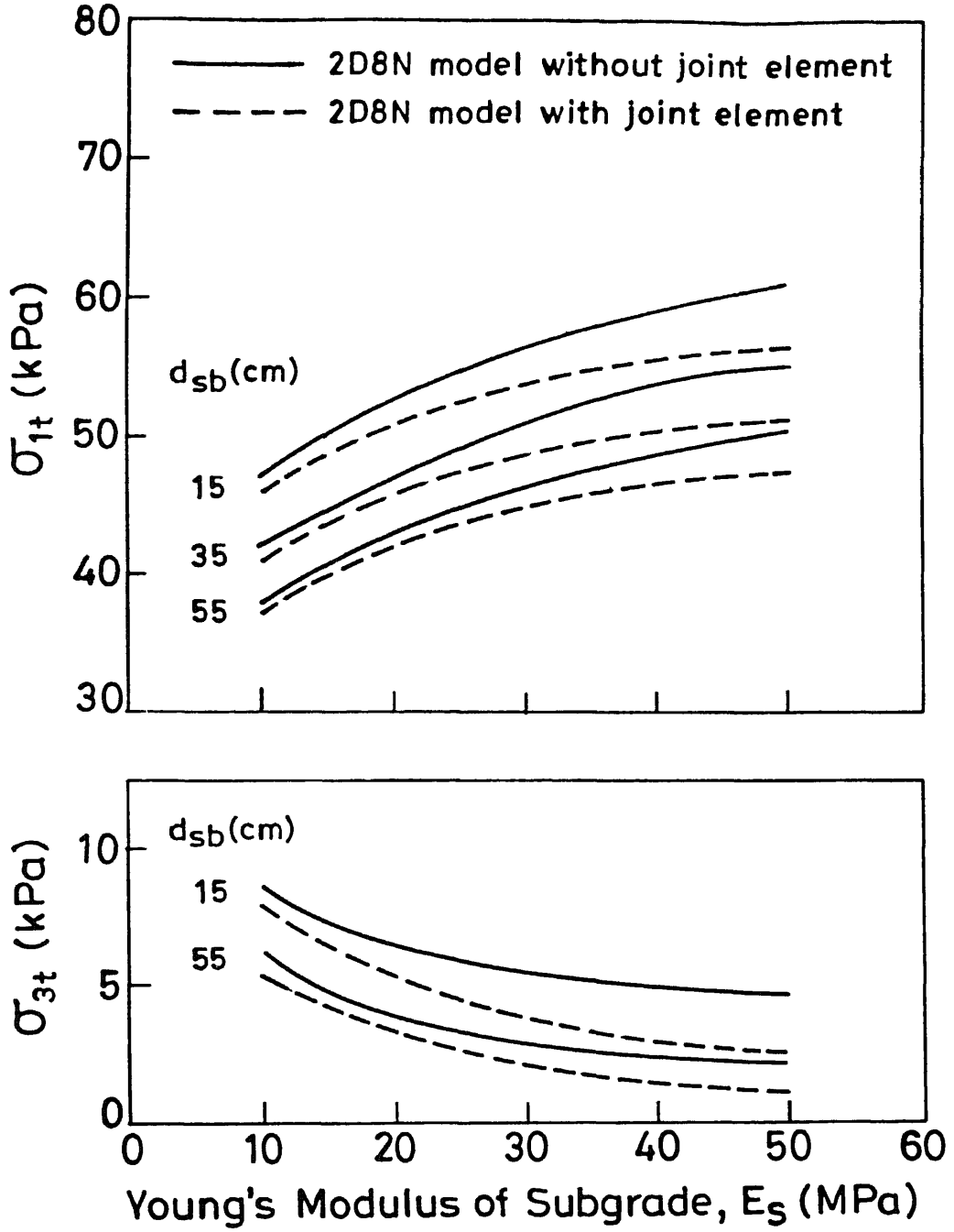

Fig. 3.40 Variation of σ_{1t} and σ_{3t} with E_s for different depths of subballast (2D8N model)

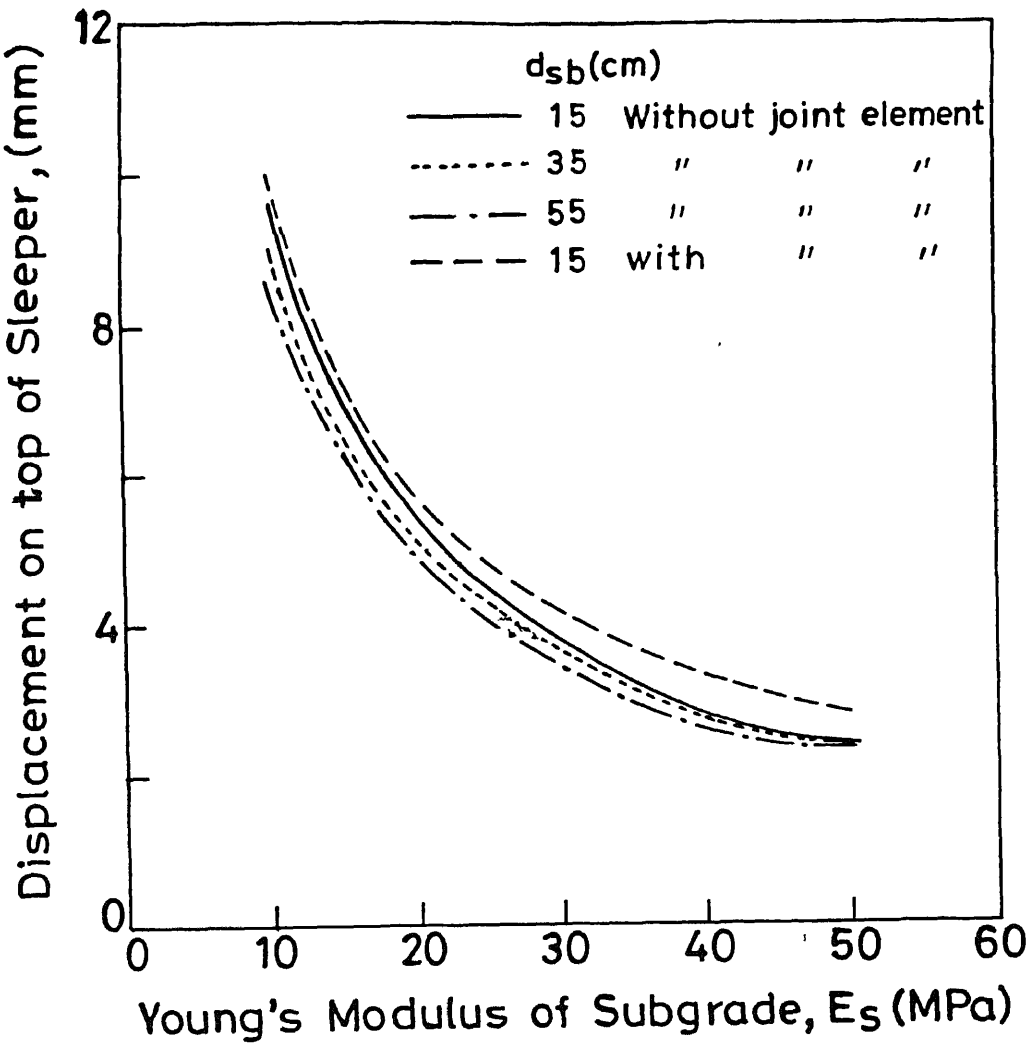

Fig.3.41 Variation of displacement on top of sleeper with E_s for different depths of subballast (2D8N model)

construction has very little effect on displacement whereas type of soil has very significant effect on displacement of top of sleeper. Effect of joint elements is to increase the displacement.

Figure 3.42 shows that the gain achieved by increasing the depth of ballast layer but keeping total depth of formation constant, in terms of reduction of settlement or major principal stress on top of subgrade is not significant.

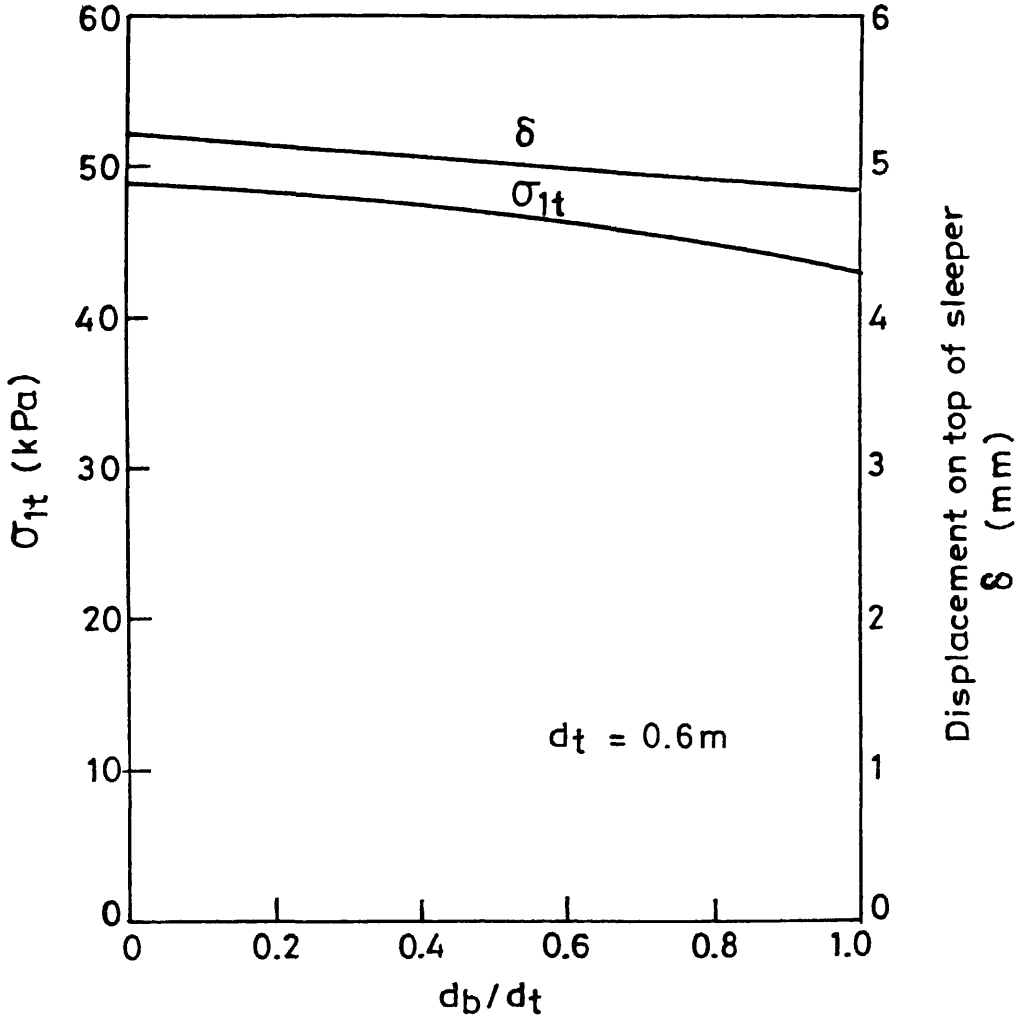

Fig. 3.42 Variation of σ_{1t} with d_b/d_t (2D8N model).

3.4 THREE DIMENSIONAL FINITE ELEMENT ANALYSIS

3.4.1 INTRODUCTION

Three dimensional finite element analysis of track has been carried out in order to calculate deflections and stresses inside the subgrade. Railway track model for three dimensional finite element analysis has been described below in detail. Stress distribution and displacements for a typical track have been presented and the parametric studies are carried out using three dimensional finite element analysis with reference to this track.

3.4.2 DESCRIPTION OF THE THREE DIMENSIONAL FINITE ELEMENT ROUTINES

Following 3-D finite element routines have been developed

1. 3D8N
2. 3D20N

Both routines are based on displacement formulation of elasticity equations. Both routines use linear, elastic material properties. 3D8N routine uses 8 noded linear isoparametric brick elements. 3D20N routine uses 20 noded isoparametric brick elements.

Both routines were tested successfully for standard

Boussinesq's problem and standard cantilever beam problem. Comparison of results from 3D20N routine (which has been used in this analysis) for Boussinesq's problem is given in Appendix B2 and comparison with exact solution of cantilever beam problem is given below. Comparison of results with exact solution has shown that 3D20N gives good results with quite less number of elements while 3D8N gives unsatisfactory results even with very high number of elements.

For example, consider the following standard cantilever beam problem [Fenner (1986)] :

Input data :

Cantilever beam

Deflection calculated at outer tip of beam

$\nu_{bm} = 0.3$

$E_{bm} = 1000000$

Table 3.6 shows the comparison of results from 3D8N vis - a - vis 3D20N model for this problem.

It is clear from Table 3.6 that even with 32 elements, 3D8N is not able to give good results because it has linear shape functions which cannot model bending satisfactorily while 3D20N routine gives nearly exact answer with only 2 elements. Also, same observations were noted for standard Boussinesq's problem [Yudhbir et al. (1991)]. Hence, 3D20N routine has been used for further finite element analysis.

3D20N routine can handle layering of different materials

Table 3.6 Beam problem --- 3D8N vis-a-vis 3D20N

Program used	Mesh refinement	FEM answer	Exact answer
3D8N	2 elements	0.00190	0.00864
	4 elements	0.00435	
	(ν_{bm}= 0.15)	(0.00439)	
	8 elements	0.00651	
	16 elements	0.00745	
	32 elements	0.00772	
3D20N	2 elements	0.00860	

* Above calculations are independent of unit system.

and all types of boundary conditions. The routine has facility to simulate joint between different layers by use of joint element of zero thickness [Goodman et al. (1968)]. 16 noded surface joint element based on relative displacement formulation has been used [Burgohain and Shah (1978)]. Joint element subroutine was checked for the algorithm given by Burgohain and Shah (1978).

3D20N routine has capability to analyze the soil structure interaction problems. It has facility to combine beam element with soil element. This routine has been checked by comparing results with MULTA model [Selig et al. (1979)] which also considers beam as 1-D element (Figs. 3.61 and 3.62).

Stress extrapolation from Gauss points to nodal points has been carried out by bilinear extrapolation.

Three types of data input facilities are available. In fully manual data type, data related to nodal point coordinates, element connectivity, etc. has to be fed for each and every point. But, main advantage of this routine is that one can prepare data for virtually any type of mesh discretization. In semiautomatic data input, data related to some nodal points and elements is needed. This can generate only linear geometric mesh patterns. Fully automatic data input facility can only be used to generate rectangular meshes. Data input consists of basic parameters (e.g. total number of nodal points, material types, elements etc.), material properties, total number of compartments in x, y and z direction and length of each compartment, boundary conditions on six faces and 8

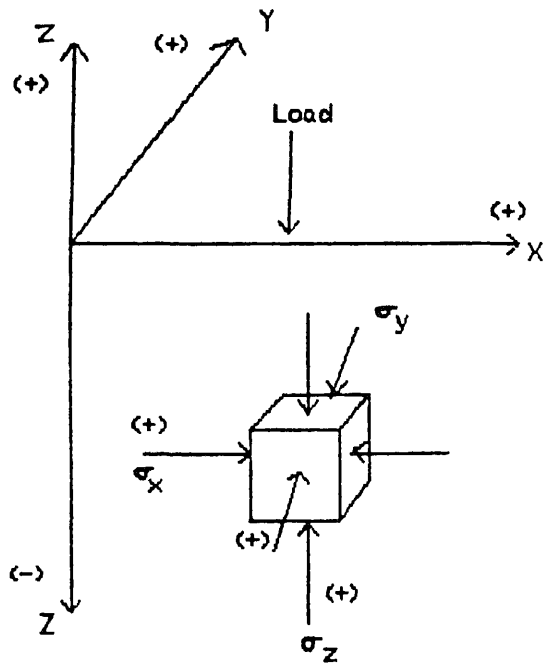

Fig. 3.43 NOTATIONS USED (3D20N MODEL)

3.4.3.2 Boundary conditions

The boundary conditions adopted for 3-D analysis were similar to that of 2-D analysis and are given below :

At all faces, displacements in the normal direction were restricted.

At all corner lines, displacements across the line were restricted. However, displacements in the direction of line were allowed.

At all corner nodes (except for top center node), all displacements were restricted.

On top center node, only vertical displacement was allowed.

3.4.3.3 Rail element

Rail has been replaced by one dimensional beam element having two degrees of freedom (displacement in vertical direction and rotation) at each node for finite element analysis. 1-D beam element has advantage over 3-D rail section of equivalent EI [Desai and Siriwardane (1982)] because if rail is modelled by 3-D element of equivalent EI then assumption will have to be made regarding contact area between rail and sleeper. As rail is supported directly over the sleeper for considerable distance, this area presumably, may have important bearing on stresses transferred. Thus, ratio of height to width of rectangular rail section chosen will be empirical and may affect direct stresses transferred to the sleepers. It can lead to underprediction of stresses and displacements at the top of

subgrade (Figs. 3.44 and 3.45).

In Figs. 3.44 and 3.45, displacement and stress distribution under the rail seat along the depth are shown. Two cases as given below are considered and in each case, EI of rail section is made equal to actual EI :

1. 1-D rail section
2. 3-D square rail section.

Also shown are the results predicted by MULTA and 3-dimensional finite element analysis by Desai and Siriwardane (1982). Desai and Siriwardane (1982) results and 1-D rail results are different due to the assumptions about rail section. However, 1-D rail gives best results compared to MULTA model which is like a closed form solution.

1-D rail also reduces computational time by reducing the total number of nodal points and the band width of global stiffness matrix.

Tie and rail connection for 1-D rail has been arrived at as follows :

Two cases have been considered regarding assumption of tie and 1-D rail connection :

a. Node where tie is connected with rail is not restrained in any direction.

b. Node where tie is connected with rail is restrained in lateral direction.

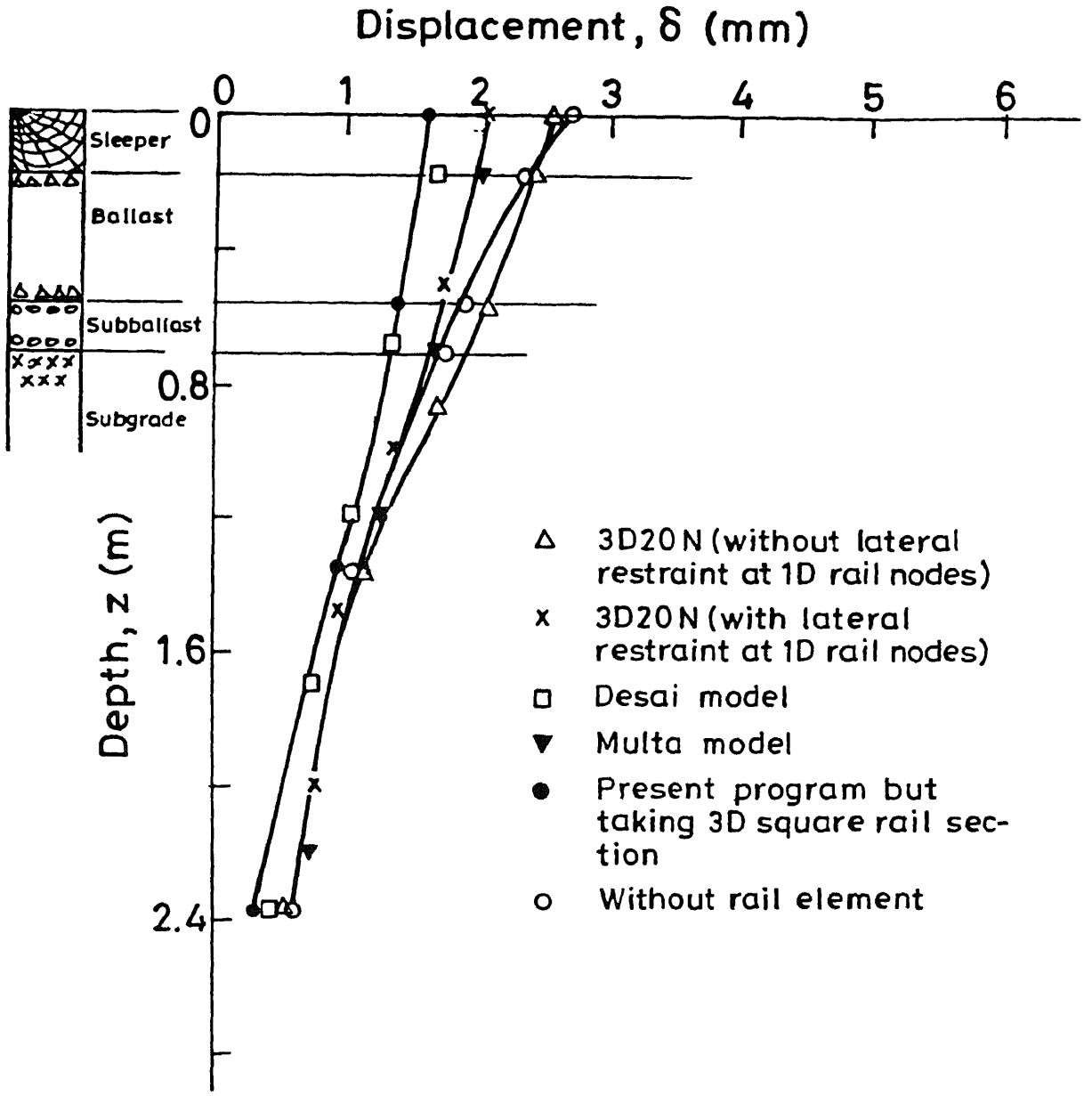

Fig. 3.44 Displacement under the rail seat versus depth for different rail conditions for TRACK 2

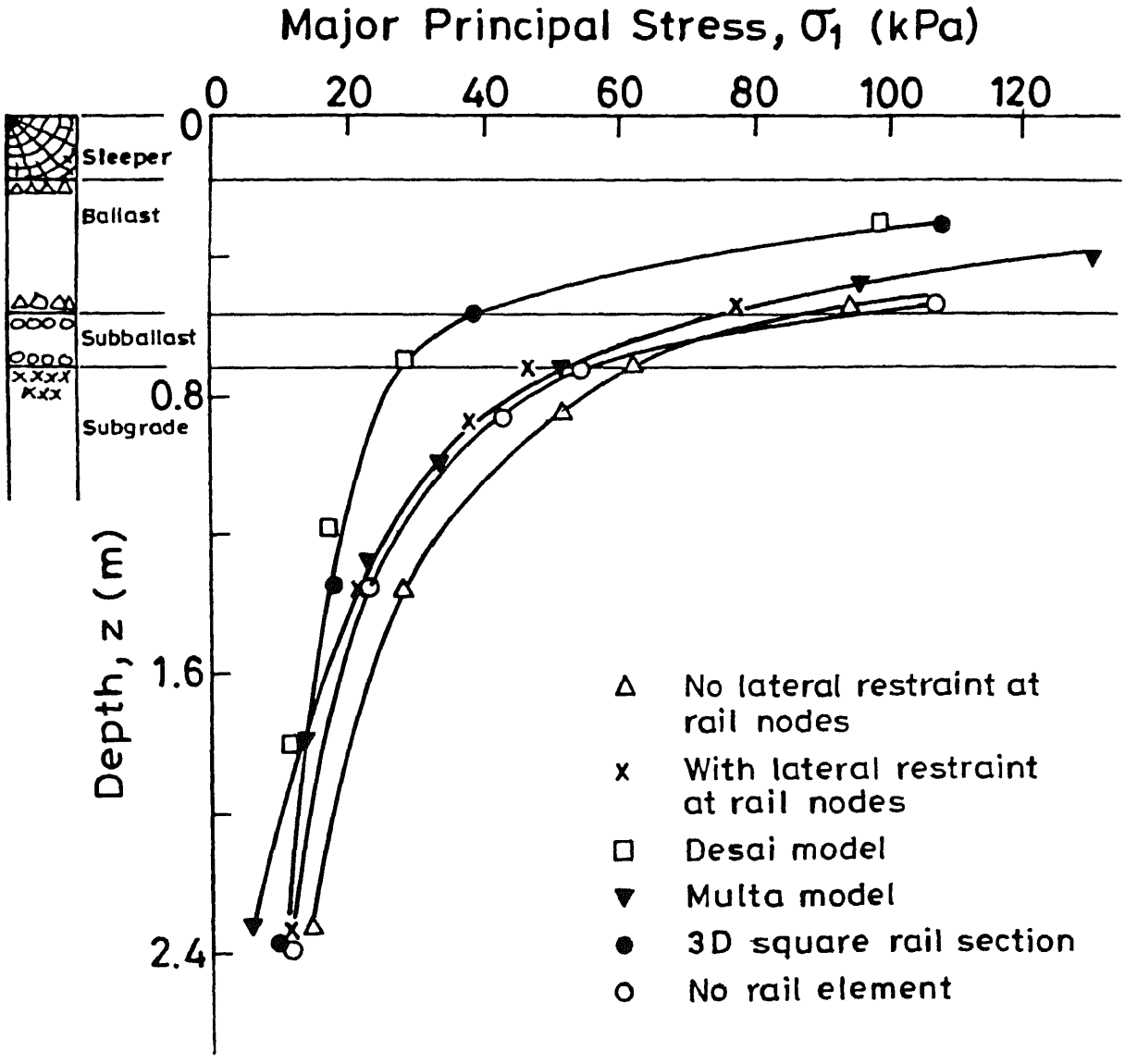

Fig. 3.45 σ_1 versus depth for different rail conditions for TRACK 2

It has been assumed that rail is free to rotate and displace vertically at the connection between rail and tie in both cases. Results for both these cases are shown in Figs. 3.44 and 3.45. Results also show stress distribution without rail element. Thus, the effect of presence of rail element can be seen. For further analysis, it is assumed that the rail is restrained in lateral direction.

3.4.3.4 Sleepers

Sleepers have been modelled by 3-D rectangular elements. Discontinuous nature of sleeper could be maintained here. However, to maintain the rectangular geometry, interspaces between adjacent sleepers (cess) and spaces on side of sleepers (crib) were filled with material of very low compressibility (E_f= 0.7 MPa).

A detailed parametric study was carried out to calculate E_f. The effect of filling cess and crib will obviously increase the stiffness of track and hence stresses on top of subgrade will reduce. Hence, a parametric study (using TRACK 2, single wheel load ; no joint element) was carried out with E_f= 0.007, 0.7, 210 MPa. The corresponding values of σ_{1t} were obtained as 44.57, 44.92 and 41.62 kPa. E_f = 0.7 MPa gave slightly higher results as compared to E_f = 0.007 MPa due to rounding off errors during calculations. Thus, E_f = 0.7 MPa was adopted as the Young's modulus of filling material.

3.4.4 SELECTION OF FINITE ELEMENT MESH

Rectangular track outline is adopted for 3-D analysis. The symmetry in x and y directions is made use of and hence only one quarter of track section need to be considered.

For choosing optimum mesh size, five types of mesh discretizations were studied. Tables 3.7(a) to 3.7(c) show the properties of five meshes used and the results obtained. Table 3.7(c) also shows the CPU time taken by these meshes to analyze TRACK 2 with single wheel load. Joint elements are not used. Mesh B' is recommended for finite element analysis. However, this mesh does not give sufficient points after 1 m depth to give clear picture of stress distribution. For this, mesh C' is recommended. Mesh C' is shown in Fig. 3.46.

It can be seen that results approach towards MULTA results which is a type of closed form solution but never underpredicts the stresses as in the case of Desai's 3DFEM model [Desai and Siriwardane (1982)]. In assuming 1-D rail , stresses dissipated by rail element by direct shear mechanism have been neglected and only bending resistance of rail element is considered. This gives safer and better results as compared to substituting rail by rectangular element of equivalent EI [Desai and Siriwardane (1982)] with some assumption about contact area between sleeper and rail and thickness of rail element.

Table 3.7(a) Meshes used in trials for 3-D mesh selection

Mesh type	x × y × z	x-boundary (cm)	y-boundary (cm)	z-boundary (cm)
A′	3 × 4 × 5	442	320	381
B′	4 × 6 × 6	442	320	381
C′	5 × 6 × 8	442	320	381
D′	7 × 8 × 10	660	420	650
E′	4 × 6 × 6	240	190	275

* x × y × z = x, y, and z denote total number of compartments in x- , y- and z- direction respectively.

Table 3.7(b) Compartment dimensions for meshes used in trials for 3-D mesh selection.

Mesh type	Compartment name	Compartment dimensions in cm
A′	X-COMPARTMENT	82.5, 54.5, 305.0
	Y-COMPARTMENT	12.7, 25.4, 25.4, 254
	Z-COMPARTMENT	17.8, 38.1, 15.2, 50.8, 254
B′	X-COMPARTMENT	41.9, 40.6, 54.5, 305,0
	Y-COMPARTMENT	12.7, 25.4, 25.4, 25.4, 25.4, 203.0
	Z-COMPARTMENT	17.8, 17.8, 20.3, 15.2, 50.8, 254.0
C′	X-COMPARTMENT	66.0, 16.5, 16.5, 38.0, 304.8
	Y-COMPARTMENT	12.7, 25.4, 25.4, 25.4, 25.4, 203.0
	Z-COMPARTMENT	17.8, 17.8, 20.3, 15.2, 15.2, 50.8, 101, 152
D′	X-COMPARTMENT	33.0, 33.0, 16.5, 16.5, 38.0, 114.0, 406.0
	Y-COMPARTMENT	12.7, 25.4, 25.4, 25.4, 25.4, 25.4, 25.4, 254
	Z-COMPARTMENT	5.08, 12.7, 17.8, 20.3, 15.3, 15.3, 30.5, 76, 152, 306
E′	X-COMPARTMENT	41.9, 40.6, 54.5, 101
	Y-COMPARTMENT	12.7, 25.4, 25.4, 25.4, 25.4, 76.2
	Z-COMPARTMENT	17.8, 17.8, 20.3, 15.2, 50.8, 152

Table 3.7(c) Result of trials for 3-D mesh selection.

Mesh type	CPU time taken on convex 220 (sec)	σ_{1t} (kPa)	Rail displacement (cm)
A′	74.6	56.0	0.240
B′	437.0	46.5	0.225
C′	1774.5	46.0	0.220
D′	12192.0	45.0	0.250
E′	433.0	48.0	0.195

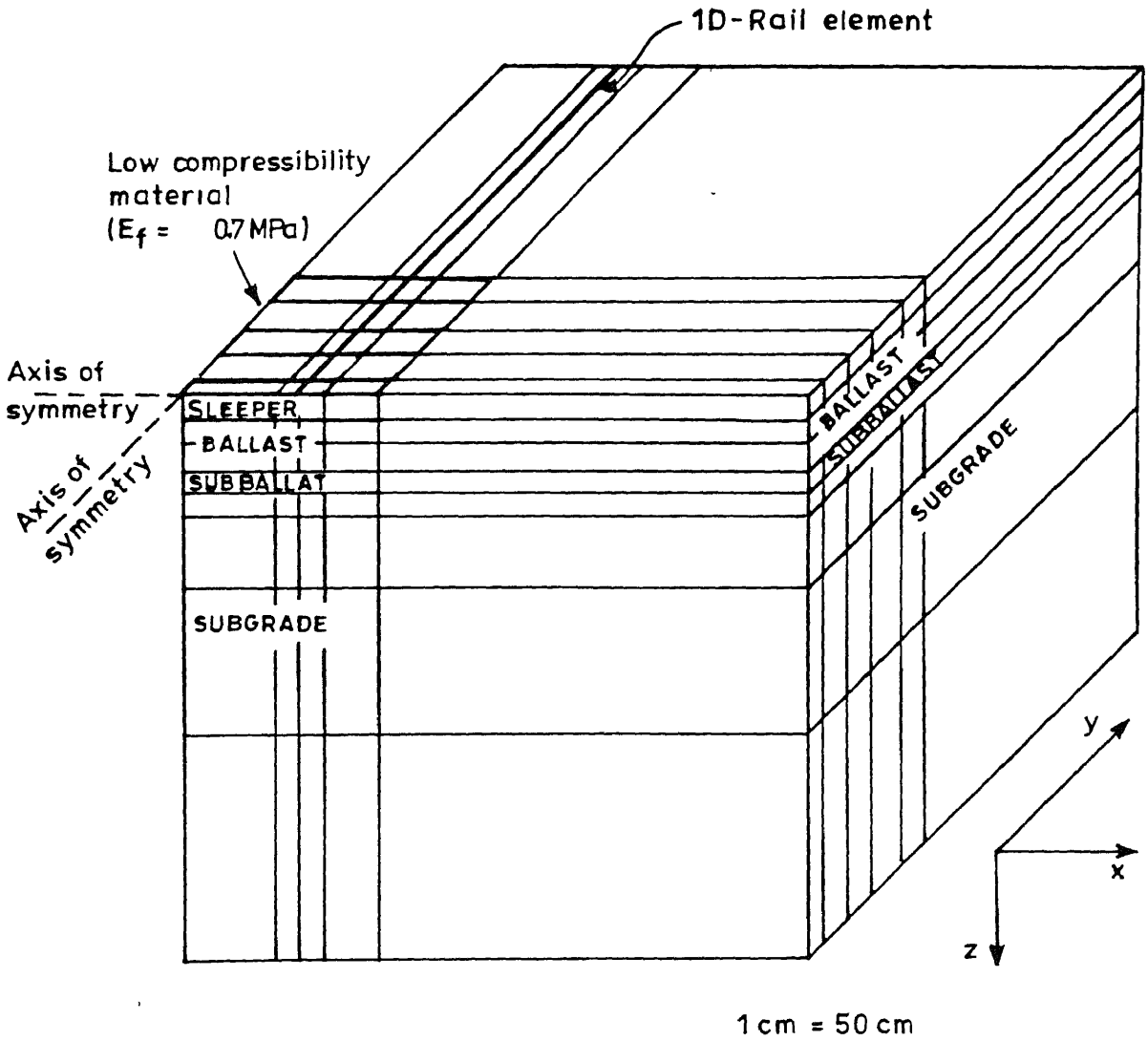

Fig. 3.46 Mesh C' discretization.

3.4.5 LIMITATIONS

Limitations of 3D20N model are discussed below :

1. 3D20N model is a linear, elastic 3-D finite element model and predicts stresses and displacements inside the subgrade.

Selig et al. (1979) have carried out the dynamic testing of track and found that one of the significant features shown by dynamic records is recoverable deformations of the track system under instantaneous loads and recommended the use of elastic models for predicting the dynamic response of the track system. They have also noted that the response of the track system is approximately linear. Hence assumption of linear elastic model may not be the limitation.

2. However, Janin et al. (1983b) pointed out that for railway track where a material of high modulus overlies one with a lower modulus, tensile horizontal stresses develop in the bottom of the top layers. One of the limitations of the elastic analysis is that the materials considered can support tension as well as compression. Thus, elastic analysis predicts tensile horizontal stresses in the granular layer which is clearly unrealistic. Hence, simple elastic analysis is unsuitable for predicting horizontal stresses in top layers.

However, Janin et al. (1983b) also conclude that elastic analysis is satisfactory for predicting vertical stresses acting on the subgrade. In Sec 3.5, it is shown that the

horizontal stresses predicted by elastic and elasto-plastic analysis inside the subgrade are in the same range. Moreover, it is to be noted that elasto-plastic analysis takes 10 times more time than elastic analysis.

Hence, unless the real mechanism of subgrade failure is understood (after close monitoring of track operation on subgrade for few years), elastic analysis may be the better and practical choice.

3.4.6 EVALUATION OF PARAMETERS USED IN CONSTITUTIVE RELATIONSHIP

3D20N analysis uses linear elastic material properties and hence Young's modulus and Poisson's ratio are the parameters to be evaluated for different materials.

In this study, two tracks have been considered. For TRACK 2, parameters suggested by Selig et al. (1979) have been used.

TRACK 1 is a typical Indian track. The best procedure for input parameters would have been to study constitutive modelling for media in track support structures as done by Janardhanam [Desai and Siriwardane (1982)]. However, in the absence of such data, ranges of parameters suggested by RDSO through personal discussion have been used.

To determine the Young's modulus of subgrade, cyclic plate load tests and cross hole wave propagation tests were carried out by RDSO. The detailed results are reported in Kumar et al. (1990), Kumar et al. (1991a) and Kumar et al. (1991b). Figure

3.47 shows the results of cross hole wave propagation tests on the running track for Sandilla-Rahimabad section near Lucknow at five different locations. However, it was noted that at short depths below formation level, soil might be mixed with ballast and moorum and hence, at these depths, Young's modulus of subgrade measured is higher. Cyclic plate load test was carried out on top of formation and hence reflects the same trend (Table 3.8). Hence, Young's modulus of subgrade was taken as 20 MPa for the reference track.

Joint elements have been used between tie-ballast, ballast-subballast and subballast-subgrade interfaces. The values of joint stiffness have been determined as follows : The following guidelines can be noted in literature.

1. A high joint stiffness is a value which yields negligible joint displacements when compared to the elastic displacements of the layers; a low stiffness is a value which leads to joint displacements that dwarf the elastic displacements of the blocks; a moderate joint stiffness corresponds to displacements of joints of the same order of magnitude as the elastic displacements of the layers [Goodman et al. (1968)].

2. Value of k_n is normally 10^5 times the maximum value of Young's modulus of the bodies in contact to avoid significant overlapping. For 'no slip' condition, k_{s1} and k_{s2} are given high values similar to k_n and for perfectly smooth contact with

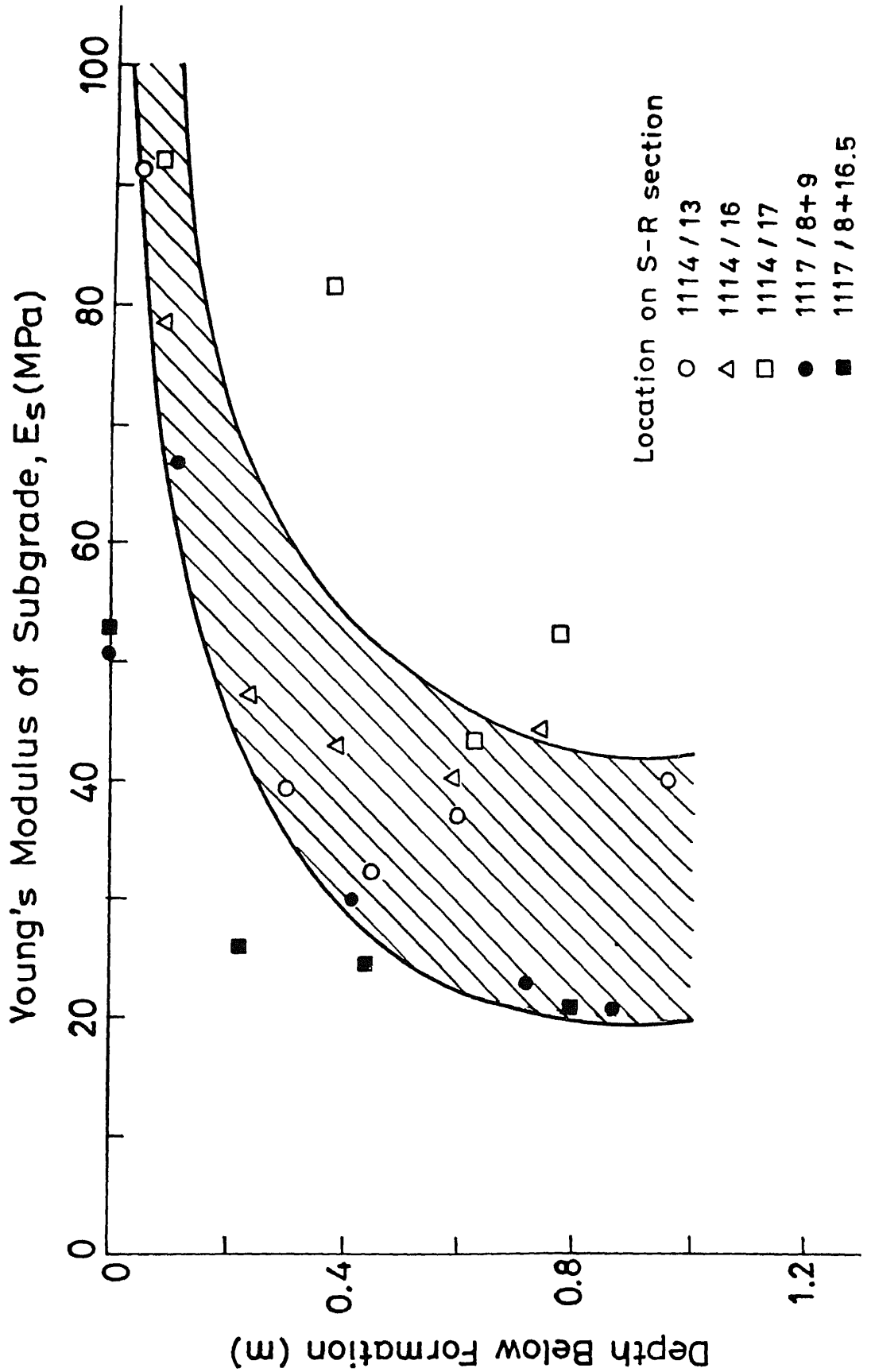

Fig. 3.47 Es versus depth below formation level - wave propagation test results on Sandila - Rahimabad section.

Table 3.8 Summary of cyclic plate load test results (Tests carried out on Sandila-Rahimabad section near Lucknow)

Location*	E_s (MPa)
1114/3	53.5
1114/16+2	38.5
1114/17	55.2
1116/8+9	62.0

* Location indicates section on the operating track.

no resistance to slip, $k_{s1} = k_{s2} = 0$. In case of separation, $k_n = k_{s1} = k_{s2} = 0$ [Burgohain and shah (1978)].

3. It has been observed from the examples given in literature that moderate values of k_n are of the order of E/l where E is Young's modulus of adjoining layer and l is the thickness of the block while low values of k_{s1} and k_{s2} are of the order of 1/10 th of k_n (moderate) [Goodman et al. (1968)].

From personal discussion with RDSO, the following range of joint stiffnesses has been recommended :

Interface	k_n	k_{s1}	k_{s2}
tie-ballast interface(1)	high	small	small
ballast-subballast interface (2)	moderate	moderate	moderate
subballast-subgrade interface (3)	moderate	moderate	moderate

Next, a detailed parametric study was carried out to evaluate the effect of each joint stiffness. Following procedure was adopted for parametric study :

With reference to TRACK 2, according to guidelines given above the following track parameters were taken as reference values :

Interface	k_n(MN/m^3)	k_{s1}(MN/m^3)
1	415000	4150
2	8300	900
3	1400	550

$$k_{s1} = k_{s2}$$

The range of values varied is as follows :

Interface 1

k_n (MN/m^3) 41500000., 415000., 8300., no joint element

k_{s1}(MN/m^3) 4150., 550.

Interface 2

k_n(MN/m^3) 8300., 550.

k_{s1}(MN/m^3) 900., 280., 55.

Interface 3

k_n (MN/m^3) 1400., 550., 140.

k_{s1}(MN/m^3) 1400., 550., 55.

The above ranges are chosen because for very high values, results become constant and for very low values instability occurs (i.e. change in displacement becomes significant).

Keeping in mind that displacement of tie, ballast and subballast layers is of the order of 0.2 to 0.4 mm and that of subgrade is 1.55 mm and following the guidelines given by RDSO

and using results of parametric study, the following values of joint stiffnesses were arrived at :

	$k_n (MN/m^3)$	$k_{s1} (MN/m^3)$	$k_{s2} (MN/m^3)$
Interface 1	415000.	4150.	4150.
Interface 2	4150.	550.	550.
Interface 3	550.	165.	165.

3.4.7 COMPARISON OF RESULTS

Comparison of predicted results using 3D20N model with other models and field test results is presented in Sec. 3.5.

3.4.8 PARAMETRIC STUDIES

Parametric studies have been carried out for a range of parameters with reference to TRACK 1. TRACK 1 is a representation of the typical Indian track. Details of this track given in Appendix A1 have been arrived at after personal discussion with RDSO and from published RDSO reports.

Parametric study has been carried out with reference to this track by changing the following track parameters.

Young's modulus of ballast = 150, 180 MPa

Young's modulus of subballast = 60, 80, 100 MPa

Depth of subballast = 0.15, 0.35, 0.55, 0.75 m

Young's modulus of soil = 10, 20, 30, 50 MPa

Moment of inertia of rail = 1600, 2158, 3055 cm^4

Tie spacing = 0.50, 0.65, 0.76 m

Making use of symmetry, only one-fourth of the track section has been discretized. Mesh C' shown in Fig. 3.46 has been used to model the reference track. For various sub-ballast thicknesses, mesh division in z-direction was varied. Rail element has been modelled as one dimensional beam with equivalent EI as that of rail section. Joint elements were used at all the three interfaces viz. tie-ballast, ballast-subballast and subballast-subgrade. The properties of joint elements used are :

	k_n	k_{s1}	k_{s2}	(all in
Tie ballast interface	415000.	4150.	415.	MN/m^3)
Ballast subballast interface	4150.	550.	55.	
Subballast subgrade interface	550.	165.	165.	

Boundary conditions used are same as mentioned in Sec. 3.4.3.2.

Double wheel load has been considered throughout this analysis.

3.4.9 RESULTS AND DISCUSSION

In this section, first the trends observed for reference track are presented and then the results of parametric studies

have been discussed.

Figures 3.48 to 3.52 show the typical results in terms of stresses and displacements for reference track, TRACK 1. Figures 3.48 to 3.51 show results for three cases viz. double wheel load with joint elements, double wheel load without joint elements and single wheel load without joint elements. This brings out the effect of double wheel load and joint elements.

It was found that due to the vertical nature of wheel load, vertical stresses and major principal stresses as well as lateral stresses and minor principal stresses are same for single wheel load case. Hence, in this study, only principal stresses are considered.

Figure 3.48 shows the displacement under the load. Figures 3.49(a) and 3.49(b) show the major and minor principal stresses inside the subgrade. Minor principal stress distribution has been shown inside the formation and subgrade. As granular material cannot sustain tension, minor principal stress in granular material has no meaning. It has been shown in Sec. 3.5 that stresses inside the subgrade calculated by elastic analysis match well with the stresses calculated by elasto-plastic analysis which takes into consideration 'no tension ' condition in granular material.

It may be seen (Fig. 3.49a) that for single wheel load case, σ_1 decreases from 53 kPa on top of subgrade to 17 kPa at 1.0 m inside the subgrade. This shows that 68 % stress dispersion takes place within 1 m inside the subgrade while for double wheel load, it is only 14 % (from 42 kPa to 36 kPa).

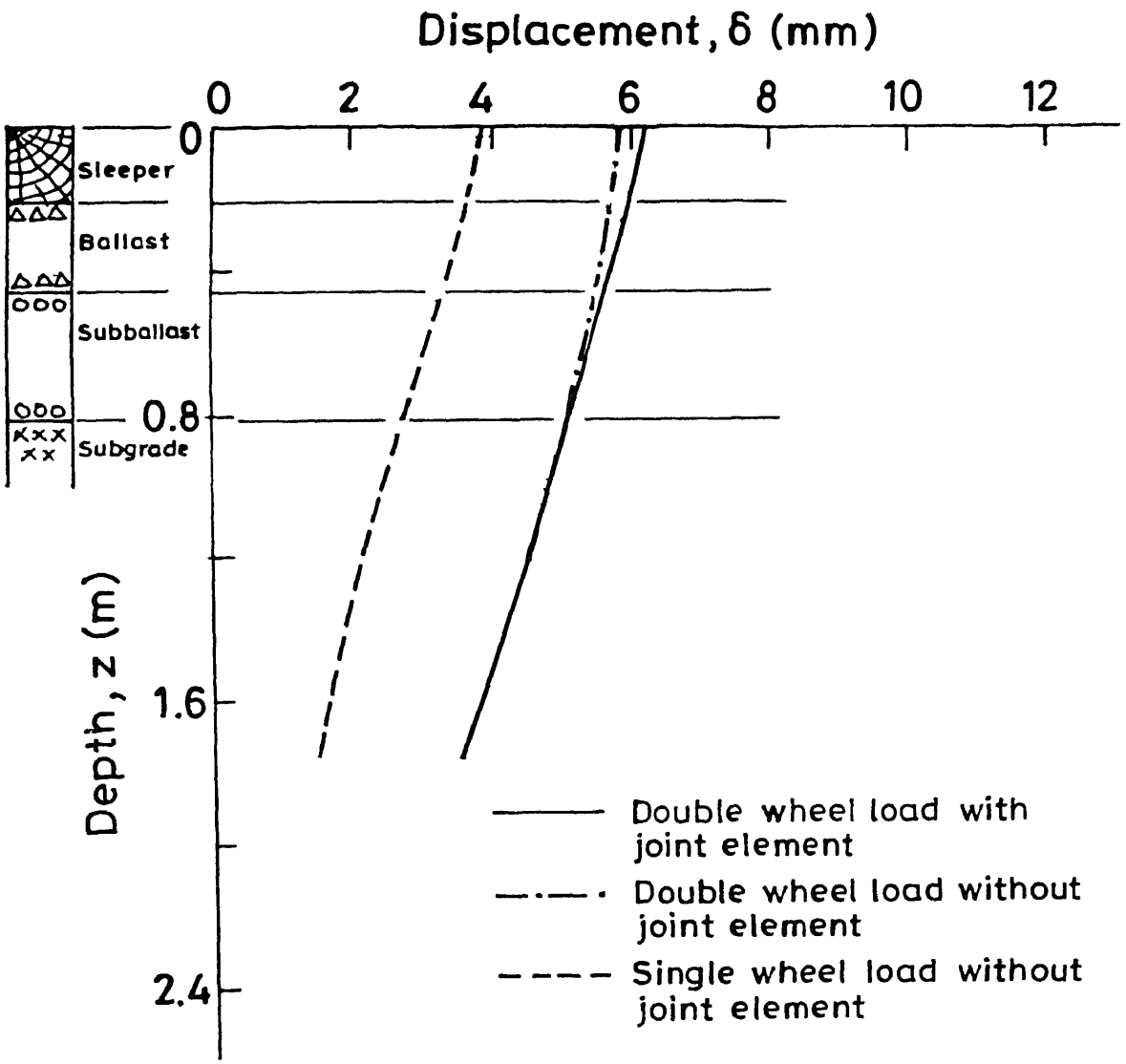

Fig. 3.48 Variation of displacement under the rail seat with depth for TRACK 1 (3D20N model)

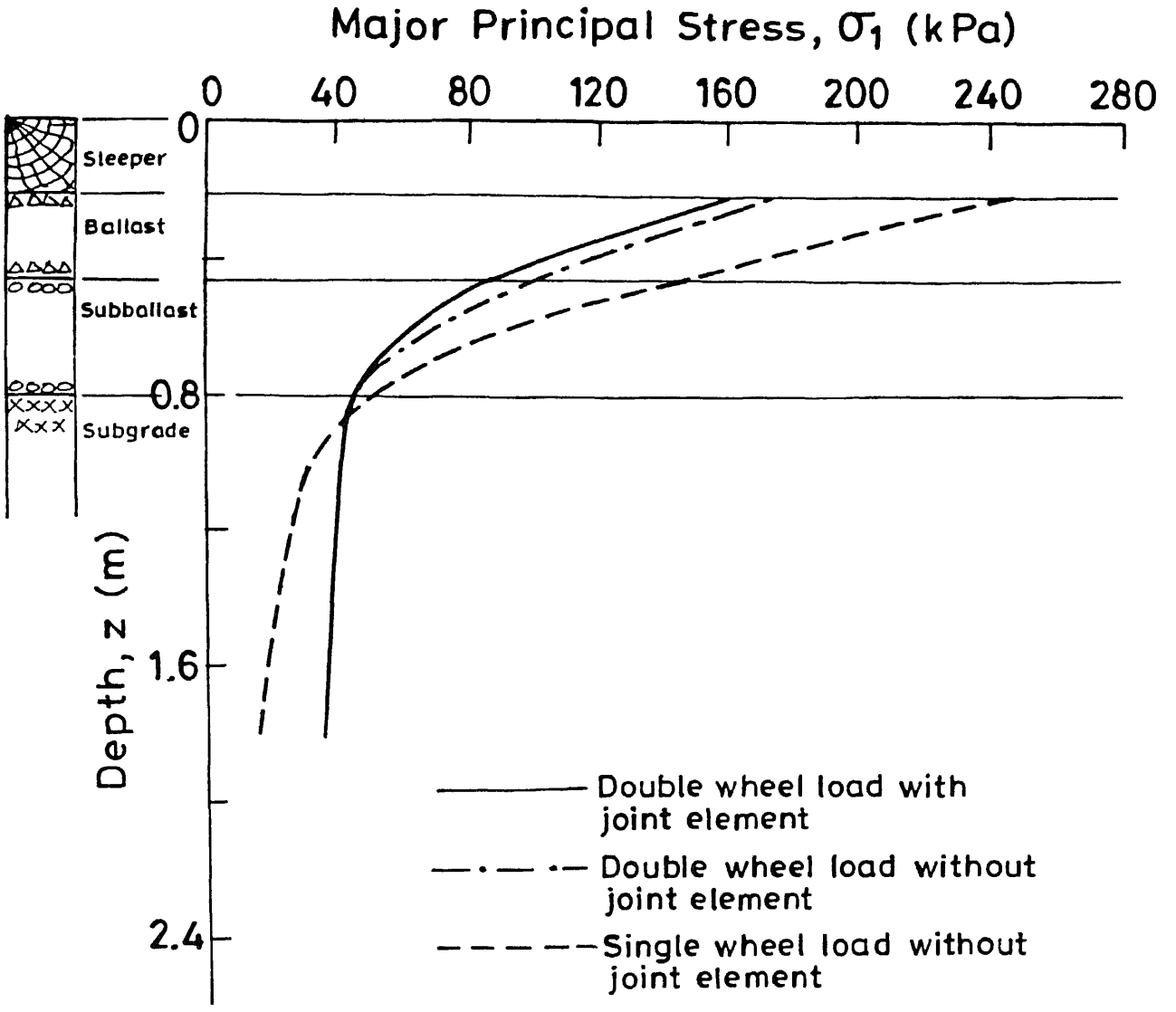

Fig. 3.49(a) Variation of σ_1 with depth for TRACK 1 (3D20N model)

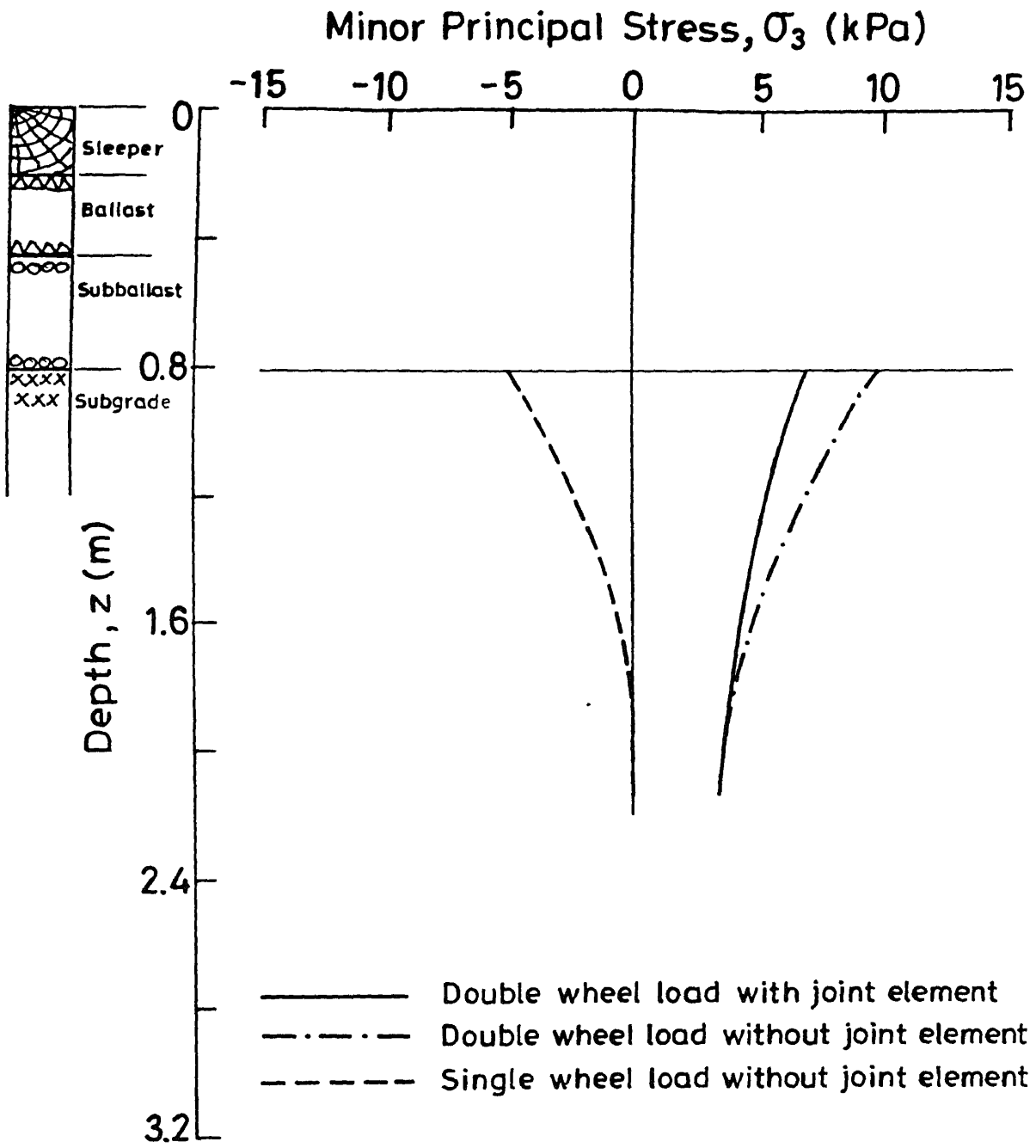

Fig. 3.49(b) Variation of σ_3 with depth for TRACK 1 (3D20N model)

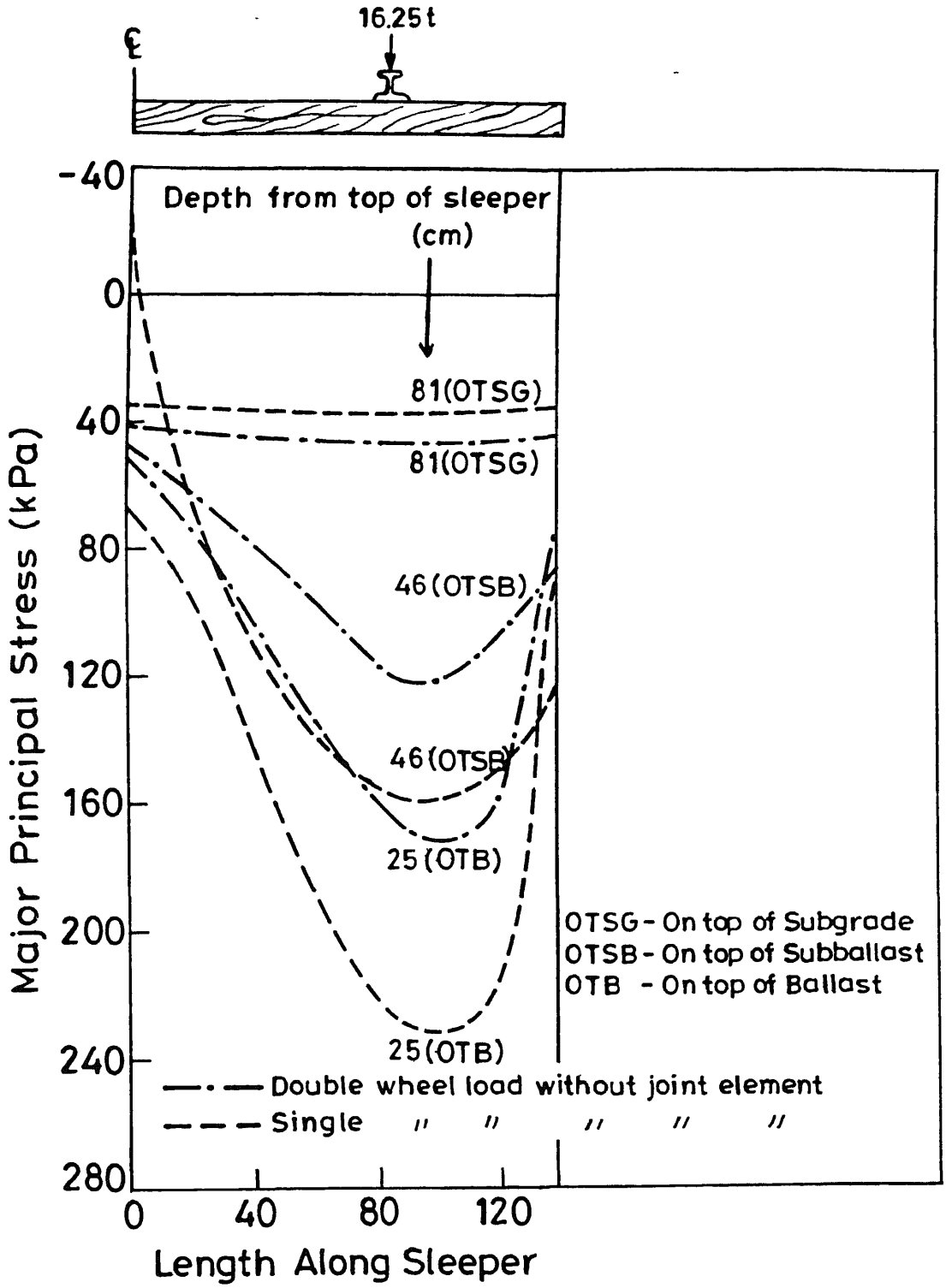

Fig. 3.50 Variation of major principal stress along the sleeper at different depths for TRACK 1 (3D20N model)

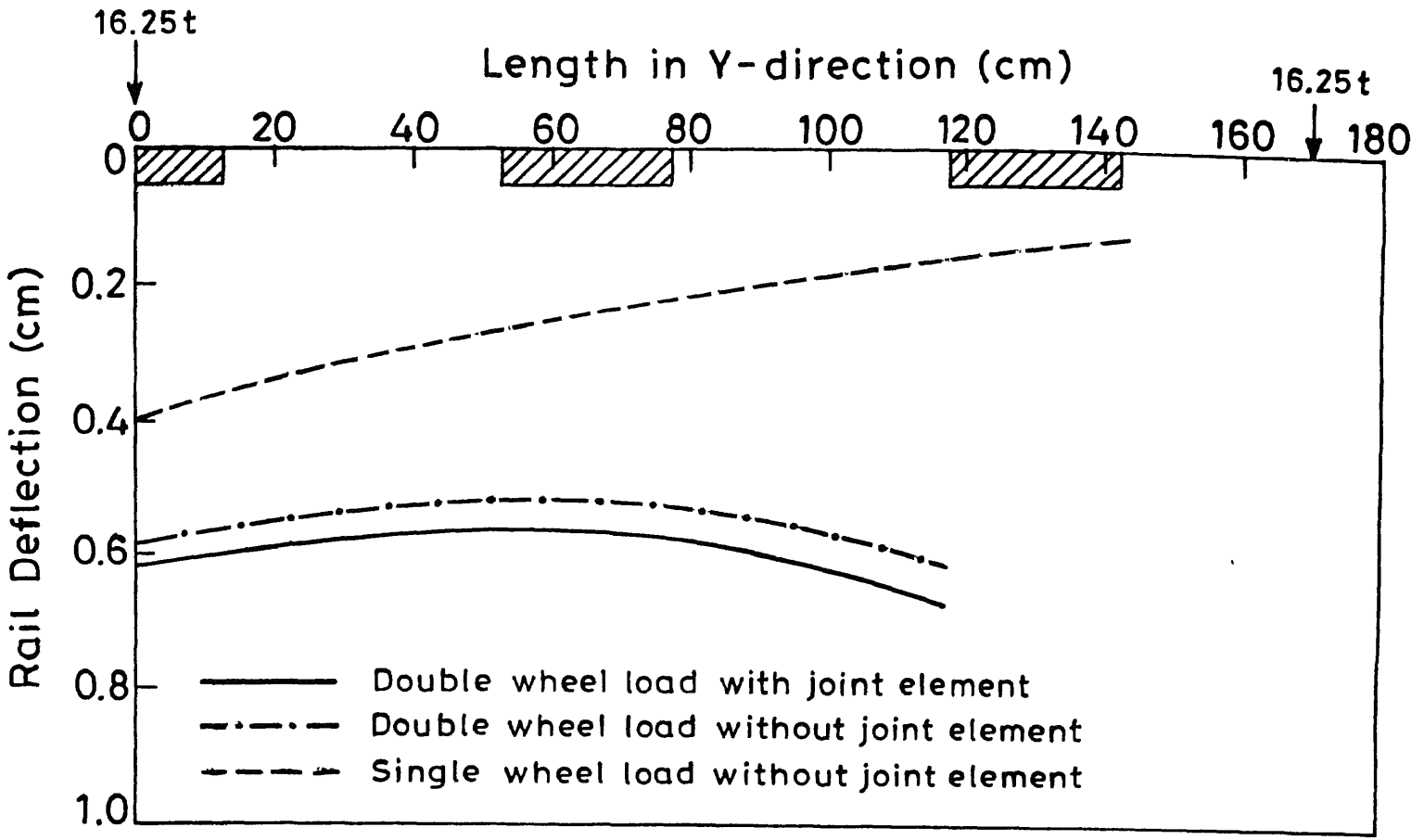

Fig. 3.51 Variation of rail deflection along the rail direction for TRACK 1 (3D20N model)

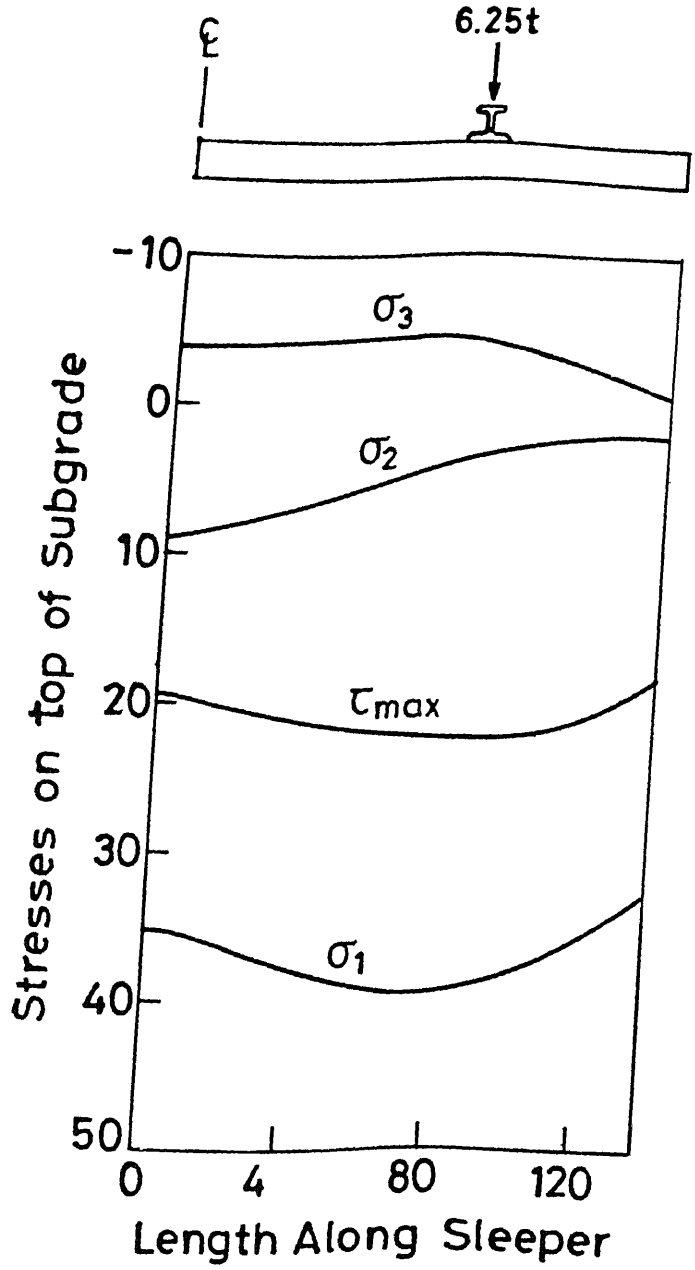

Fig. 3.52 Stresses on top of subgrade along the sleeper for single wheel load with joint element (3D20N model)

It may be seen (Figs. 3.48 and 3.49) that effect of joint element is to reduce stresses and to increase displacements in top layers. Joint element reduces σ_1 by 8 % on top of subgrade. Joint element reduces σ_3 from 10 kPa to 7 kPa on top of subgrade while δ on top of sleeper increases from 5.8 mm to 6.2 mm (increase by 7 %). Desai and Siriwardane (1982) have also observed increase in δ on top of sleeper of similar magnitude (for 147.15 kN load, δ increases by 6 %).

Effect of double wheel load is to reduce the stresses at shallow depths and increase the stresses at deeper depths (below 0.80 m in this case). Double wheel load increases δ on top of sleeper from 3.9 to 5.8 mm (i.e. by 8 %) while σ_3 increases from 5 to 10 kPa on top of subgrade. σ_1 decreases from 248 kPa to 178 kPa on top of ballast for double wheel load case but the changes are negligible on top of subgrade.

Figure 3.50 shows major principal stress distribution along the sleeper at depth equal to 0.46 m and 0.81 m. Maximum stress on top of subballast and ballast is found to be slightly on the right side of the rail seat. However, on top of subgrade, maximum major principal stress occurs below the rail seat. These findings are similar to those observed by Selig et al. (1979).

Figure 3.51 shows the rail deflection along the rail (in the y-direction). Figure 3.52 shows the distribution of major, intermediate (σ_2), minor principal stresses and maximum shear stress (τ_{max}) on top of subgrade for single wheel load case with joint elements. It may be noted that maximum major

principal stress occurs below the rail seat but τ_{max} on top of subgrade is maximum slightly to the right of the rail seat. However, the difference between maximum τ_{max} and τ_{max} below the rail seat is insignificant and for all practical purposes, τ_{max} below the rail seat may be taken as maximum τ_{max} on top of subgrade.

As already mentioned above, four types of track structure and four types of subgrade were selected for parametric studies. Each track structure was put on each type of subgrade and 3-D finite element analysis was carried out. Track structure 2 with subgrade 2 (TRACK 1) has been used as reference track for parametric studies. These studies were carried out to see the effect of tie spacing, moment of inertia of rail, quality of ballast and quality of subballast on the major principal stress on top of subgrade. Results of parametric studies are given in Table 3.9.

A non-dimensional parameter 'm ' has been introduced as a measure of ballast , subballast and subgrade characteristics as

$$m = \frac{E_{equ}}{E_s} \qquad (3.20)$$

where

E_{equ} = equivalent Young's modulus of ballast and subballast layer and is expressed as

Table 3 9 Results of parametric studies (3D2ON model)

File Name	E_b (MPa)	E_{sb} (MPa)	E_s (MPa)	d_b (cm)	d_{sb} (cm)	I_{r_4} (cm^4)	Tie spacing (cm)	E_{equ} (MPa)	m	Stresses on top of subgrade		
										σ_1 (kPa)	σ_2 (kPa)	σ_3 (kPa)
A1	150	80	10	25	15	2158	65	123 75	12.375	44 03	19.40	11.04
A2					35			109 17	10 917	39 46	16 10	8.40
A3					55			101 87	10 188	35 34	13 60	6 70
A4					75			97 50	9.750	31.90	11.65	5.72
B1			20	25	15	2158	65	123 75	6 188	49.32	22 68	9.50
B2					35			109 17	5 460	45 04	19.80	7.40
B3					55			101 87	5 094	41.39	16.65	5.85
B4					75			97 50	4.875	38 38	14.12	4.91
C1			30	25	15	2158	65	123 75	4 125	52.24	24.90	8.55
C2					35			109 17	3 640	47 69	22 20	6.71
C3					55			101 87	3 400	44.57	18 88	5 28
C4					75			97 50	3 250	41.88	15 90	4 41
D1			50	25	15	2158	65	123.75	2.475	55.52	27.86	7.50
D2					35			109.17	2 183	50 51	25 50	6.00
D3					55			101 87	2.037	47 89	21 99	4.73
D4					75			97 50	1.950	45 90	18 54	3.92

Table 3 9 (Contd) Results of parametric studies (3D20N model)

File Name	E_b (MPa)	E_{sb} (MPa)	E_s (MPa)	d_b (cm)	d_{sb} (cm)	I_r (cm^4)	Tie spacing (cm)	E_{equ} (MPa)	m	Stresses on top of subgrade		
										σ_1 (kPa)	σ_2 (kPa)	σ_3 (kPa)
			FOR	DOUBLE	WHEEL	LOAD						
B2SB1	150	60	20	25	35	2158	65	97 5	4 875	45.43	20.47	7 15
B2SB2		100						120 83	6 042	44 49	19.23	7 76
B2B1	180	80	20	25	35	2158	65	121 67	6 083	44 624	19 03	7 21
B2B2	165							115 42	5 771	44 626	19 31	7.28
B2I1	150	80	20	25	35	1600	65	109 17	5 460	46 186	19.38	7 43
B2I3						3055		109 17	5 460	44 200	20 10	7.46
A1I3			10		15	3055		123.75	12 375	43.06	19 90	11.11
D4I3			50		75	3055		97 50	1 950	45 34	31 92	18 33
			FOR	SINGLE	WHEEL	LOAD						
B2T1si	150	80	20	25	35	2158	50	109 17	5 460	36 77	3 60	-3.40 (tension)
B2T2si							65			39.28	3 67	-4 49
B2T3si							76			41 22	3 70	-5 01
A1T1si			10	25	15	2158	50	123 75	12 375	37.55	6 10	-3 30
D4T1si			50		75		50	97 50	1 950	32 03	1 76	-2 30
A1T3si			10		15		76	123 75	12 375	44 06	6 40	-5 40
D4T3si			50		75		76	97 50	1 950	33 90	1 70	-3.10

$$E_{equ} = \frac{E_b d_b + E_{sb} d_{sb}}{d_b + d_{sb}} \qquad (3.21)$$

with

E_b = Young's modulus of ballast,

E_{sb} = Young's modulus of subballast,

d_b = thickness of ballast layer, and

d_{sb} = thickness of subballast layer.

E_{equ} can be derived on basis of stress distribution in the track system as follows :

Figures 3.53 and 3.54 show the assumed stress distribution in the track system for actual and equivalent system. Therefore,

$$(d_b + d_{sb}) \tan \theta = d_b \tan \theta_1 + d_{sb} \tan \theta_2 \qquad (3.22)$$

Let us assume,

$$d_b E_b + d_{sb} E_{sb} = (d_b + d_{sb}) E \qquad (3.23)$$

i.e.
$$E = \frac{E_b d_b + E_{sb} d_{sb}}{d_b + d_{sb}} \qquad (3.24)$$

From Eqs. (3.22) and (3.24),

$$E / \tan \theta = \frac{E_b d_b + E_{sb} d_{sb}}{d_b \tan \theta_1 + d_{sb} \tan \theta_2}$$

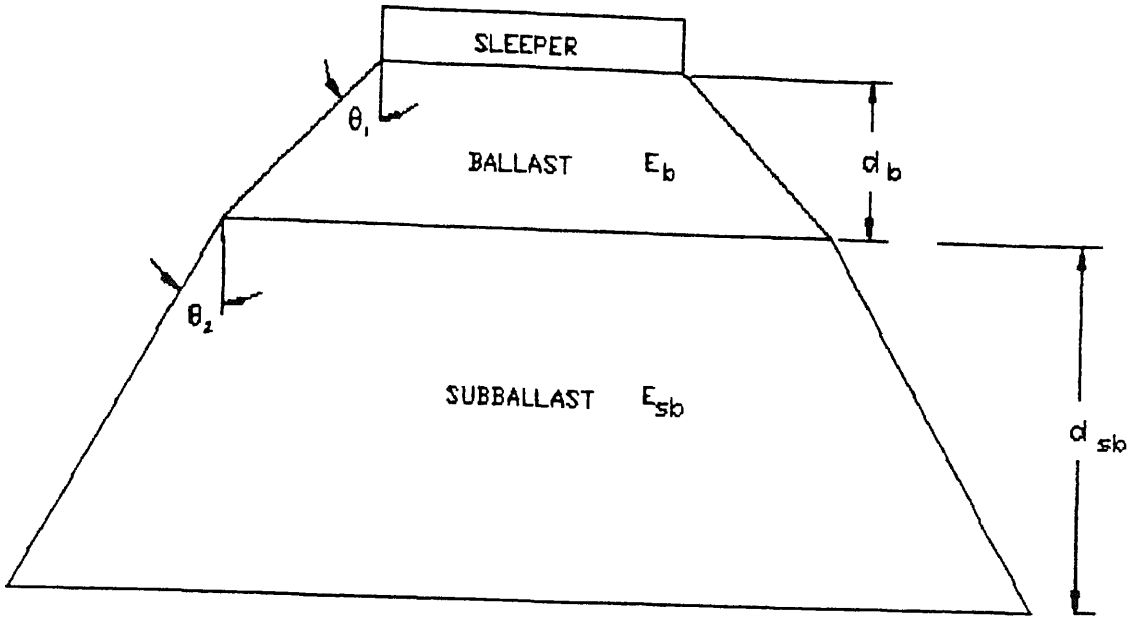

Fig. 3.53 STRESS DISTRIBUTION IN ACTUAL TRACK SYSTEM (TADATOSHI ET AL., A)

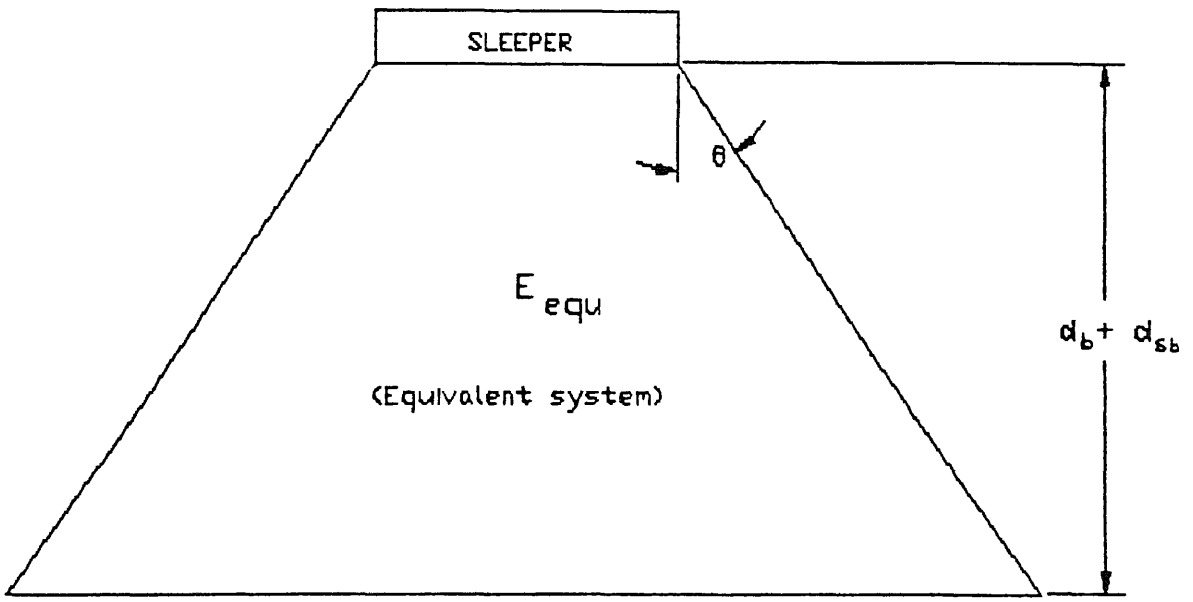

Fig. 3.54 Assumed stress distribution in equivalent track system.

$$= \frac{(d_b E_b / d_{sb} E_{sb} + 1) E_{sb}}{(d_b \tan \theta_1 / d_{sb} \tan \theta_2 + 1) \tan \theta_2}$$

(3.25)

For a given track structure, θ_1 and θ_2 are constant,

Hence $E \propto \tan \theta$ (3.26)

E_{equ} can also be obtained by assuming track consisting of composite elastic plates as shown below :

For composite plates, neutral surface is located by (Fig. 3.55)

$$y_n = \frac{E_1 \bar{y}_1 A_1 + E_2 \bar{y}_2 A_2}{E_1 A_1 + E_2 A_2} \quad (3.27)$$

$$\therefore (E_1 A_1 + E_2 A_2) y_n = E_1 \bar{y}_1 A_1 + E_2 \bar{y}_2 A_2 \quad (3.28)$$

Thus $E_{equ} A_{equ} = E_1 A_1 + E_2 A_2$ (3.29)

If b is constant,

and $d_{equ} = d_1 + d_2$,

$$E_1 d_1 b + E_2 d_2 b = E d b$$

$$\therefore E_1 d_1 + E_2 d_2 = E d$$

Plate 1 -- Ballast
Plate 2 -- Subballast

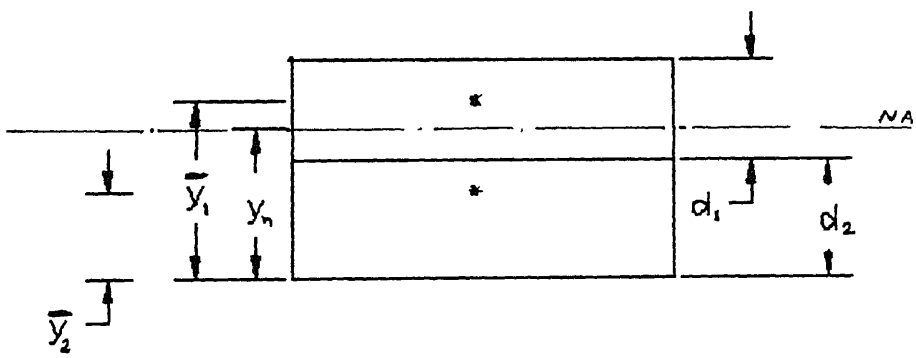

Fig. 3.55 ELASTIC PLATES

$$\therefore \quad E_{equ} = \frac{E_1 \, d_1 + E_2 \, d_2}{d_1 + d_2} \tag{3.30}$$

This is same as Eq. (3.21). However this assumption is good for elastic analysis only because it enables the plate to take tension.

Results of parametric studies are shown in Figs. 3.56 to 3.60. Figures 3.56 and 3.57 show the effect of Young's modulus of subballast layer on top subgrade stresses. Figure 3.57 shows the effect of Young's modulus of ballast layer on stresses at the top of subgrade. Increase in E_{sb} from 60 MPa to 100 MPa decreases σ_{1t} by 2 % while increase in E_b from 150 MPa to 180 MPa decreases σ_{1t} by only 1 %.

Figure 3.58 shows variation of top subgrade stresses with moment of inertia of rail. Increase in moment of inertia of rail from 1600 to 3055 cm^4 decreases σ_{1t} by 5 %. This finding is same as reported by So (1978). Figure 3.59 shows the variation of top subgrade stresses with tie spacing. Tie spacing has moderate effect on stresses on top of subgrade (about 6 to 17 percent for change in tie spacing from 0.50 to 0.76 m).

Figure 3.60 shows the variation of stresses on top of subgrade with m for four depths of construction. As m increases, major principal stress on top of subgrade decreases. Also, as depth of construction increases, major principal stress on top of subgrade decreases as expected. As noted in Sec. 2.4, there are two aspects in track stability namely the

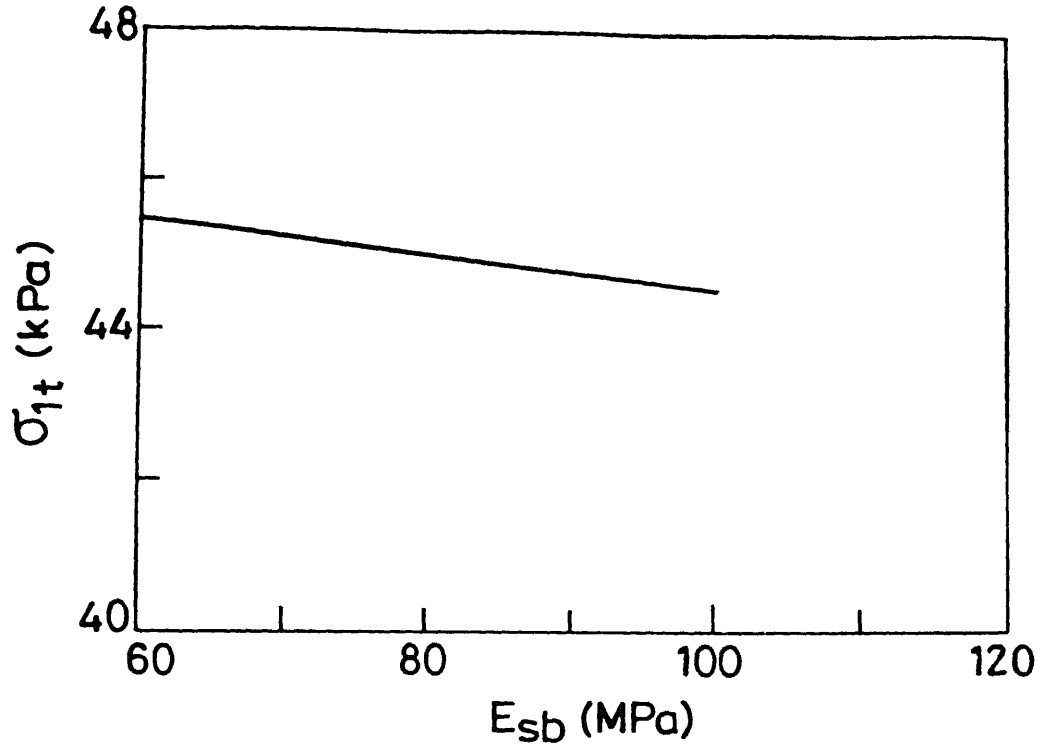

Fig. 3.56 Variation of σ_{1t} with Young's modulus of subballast, E_{sb} for reference Track (3D20N)

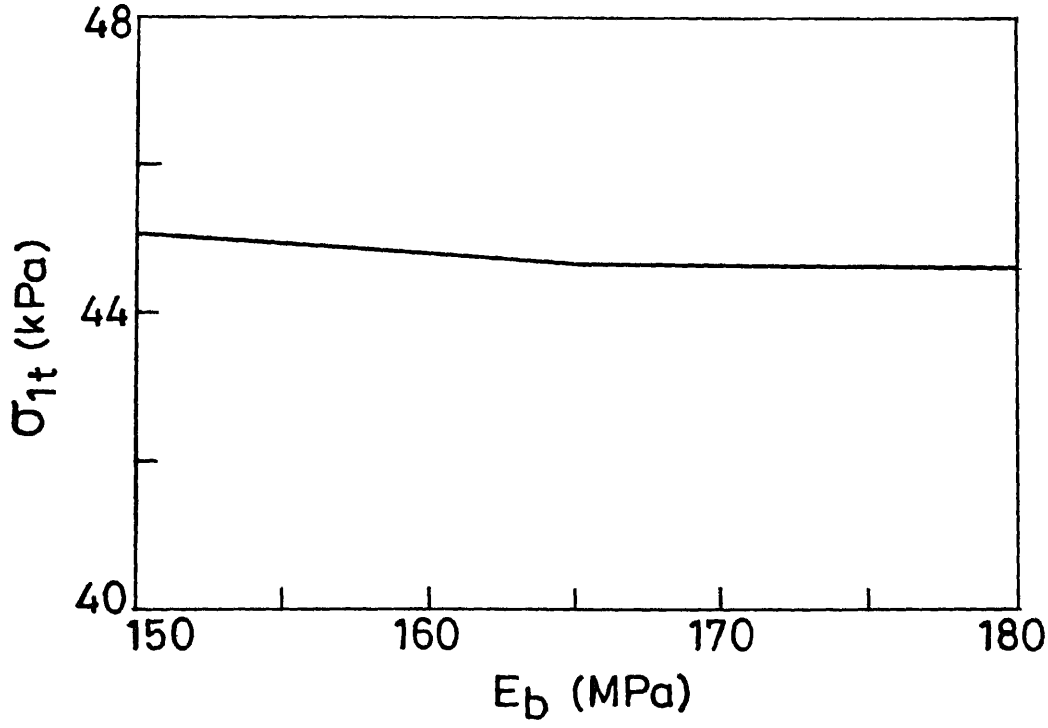

Fig. 3.57 Variation of σ_{1t} with Young's modulus of Ballast, E_b for reference Track (3D20N)

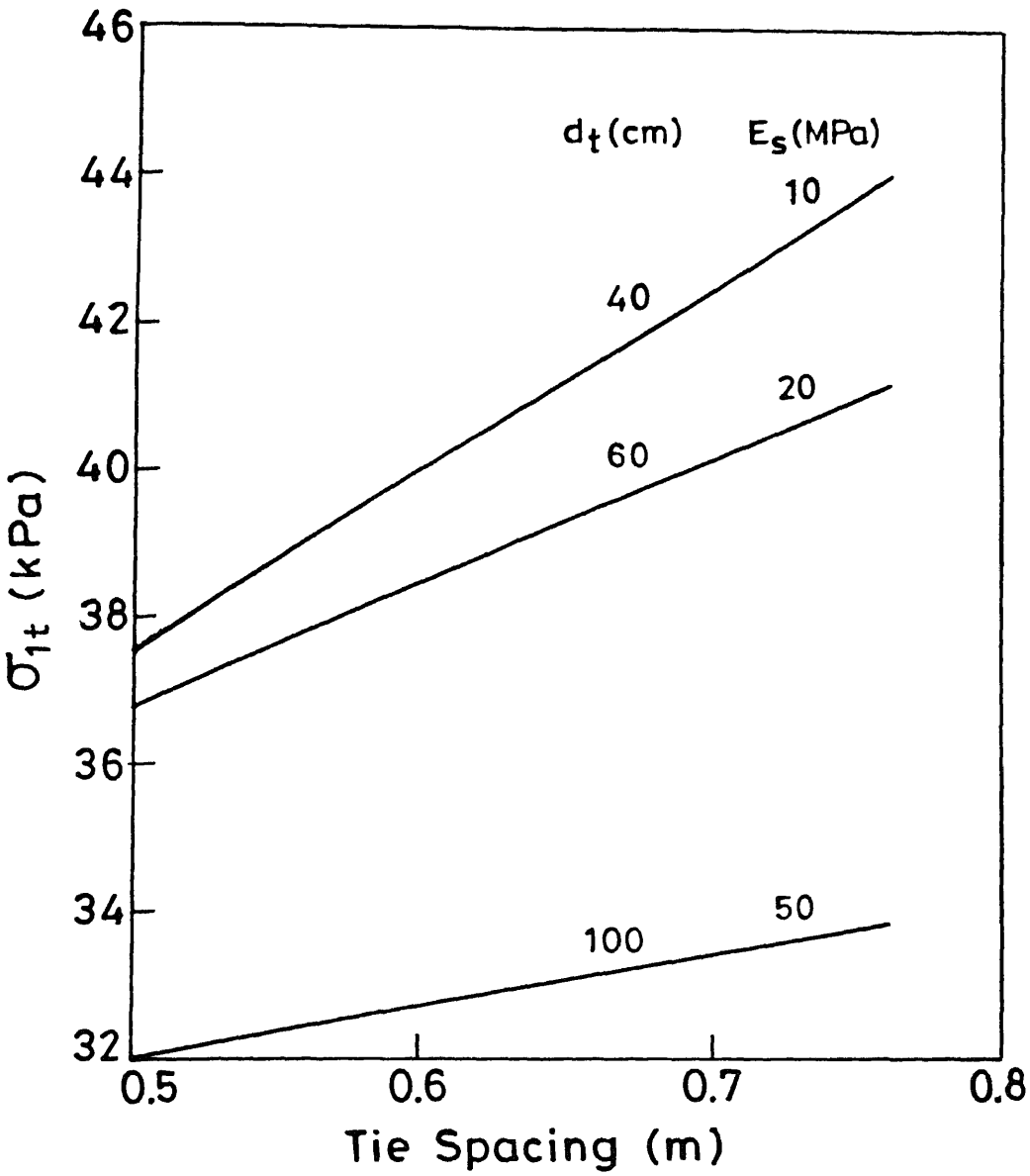

Fig. 3.59 Variation of σ_{1t} with tie spacing for TRACK 1 (3D20N)

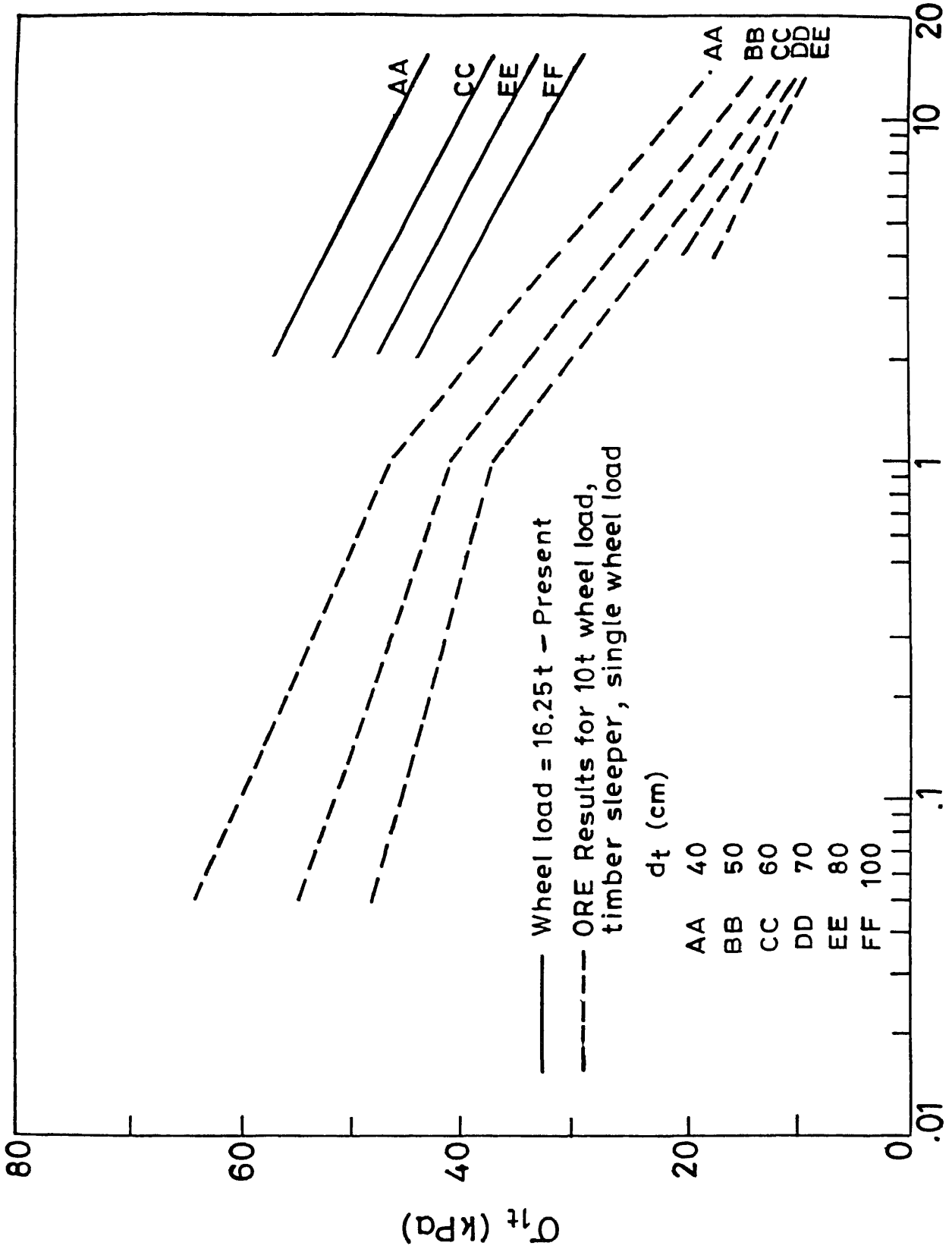

Fig. 3.60 Variation of σ_{1t} with m.

track equipment which consists of rail and tie spacing and the formation quality which is related to quality and thickness of better materials and the quality of subgrade. It can be observed that if m is changed by changing the formation quality either by changing quality or thickness of formation or quality of subgrade, it will follow the trend shown in Fig. 3.60 for a particular track equipment. However, if track equipment is changed, stresses will not follow the trend shown there. Thus, in Fig. 3.60, change in major principal stress on top of subgrade due to the change in Young's modulus of subballast layers will follow the curve for that particular depth. However, if tie spacing is changed, then major principal stress observed, will not follow the trend in Fig. 3.60. Thus formation quality is represented by m.

Figure 3.60 also shows the results from Janin et al. (1983c) predicted by elasto-plastic analysis by Rosalie model. These results also show straight line relations. Two sets of results can be compared by making following corrections.

a. Magnitude of load : Janin et al. (1983c) presented results for wheel load = 10 t.

b. Janin et al. (1983c) carried out calculations for single wheel load.

However, discrepancy in results occurs which may be due to the following reasons :

1. For results given by Janin et al. (1983c), subgrade depth has been taken as only 0.15 m thick and bottom is assumed to be restrained.

2. Janin et al. (1983c) presented results for track consisting of four different layers with an additional gravel layer. However, in the absence of sufficient data about thickness of different layers, an average value of E_{equ} = 150 MPa has been assumed. In reality, E_{equ} will be changing with the structure type.

3.5 COMPARISON OF RESULTS

The three models described above viz. ELASTIC.F, 2D8N (also modified form) and 3D20N have been compared with published results predicted by other models and measured in the field. Results of four track studies viz. FAST TRACK (TRACK 2), So (1978) track, Vienna Arsenal single sleeper and Derby panel full scale model tests and field measurements carried out by Research, design and specifications organization, Indian railways (RDSO) have been compared. As far as possible, comparison of results has been made for displacements, major and minor principal stresses. For TRACK 1, results predicted by using the three models have been compared with results obtained by published empirical formulae. For comparison, $4 \times 6 \times 6$, $4 \times 6 \times 8$ and $4 \times 6 \times 10$ mesh discretizations have been used.

3.5.1 FAST TRACK

Selig et al. (1979), and Desai and Siriwardane (1982) have reported stresses and displacements using elastic model based on Burmister's multilayer theory and finite element analysis respectively on FAST TRACK. The track description for FAST TRACK is same as for TRACK 2 and is given in Appendix A2.

Figures 3.61 and 3.62 show vertical displacement and vertical stress distribution below the wheel load along the depth for FAST TRACK using various models mentioned therein. Using the same track parameters, results were predicted for

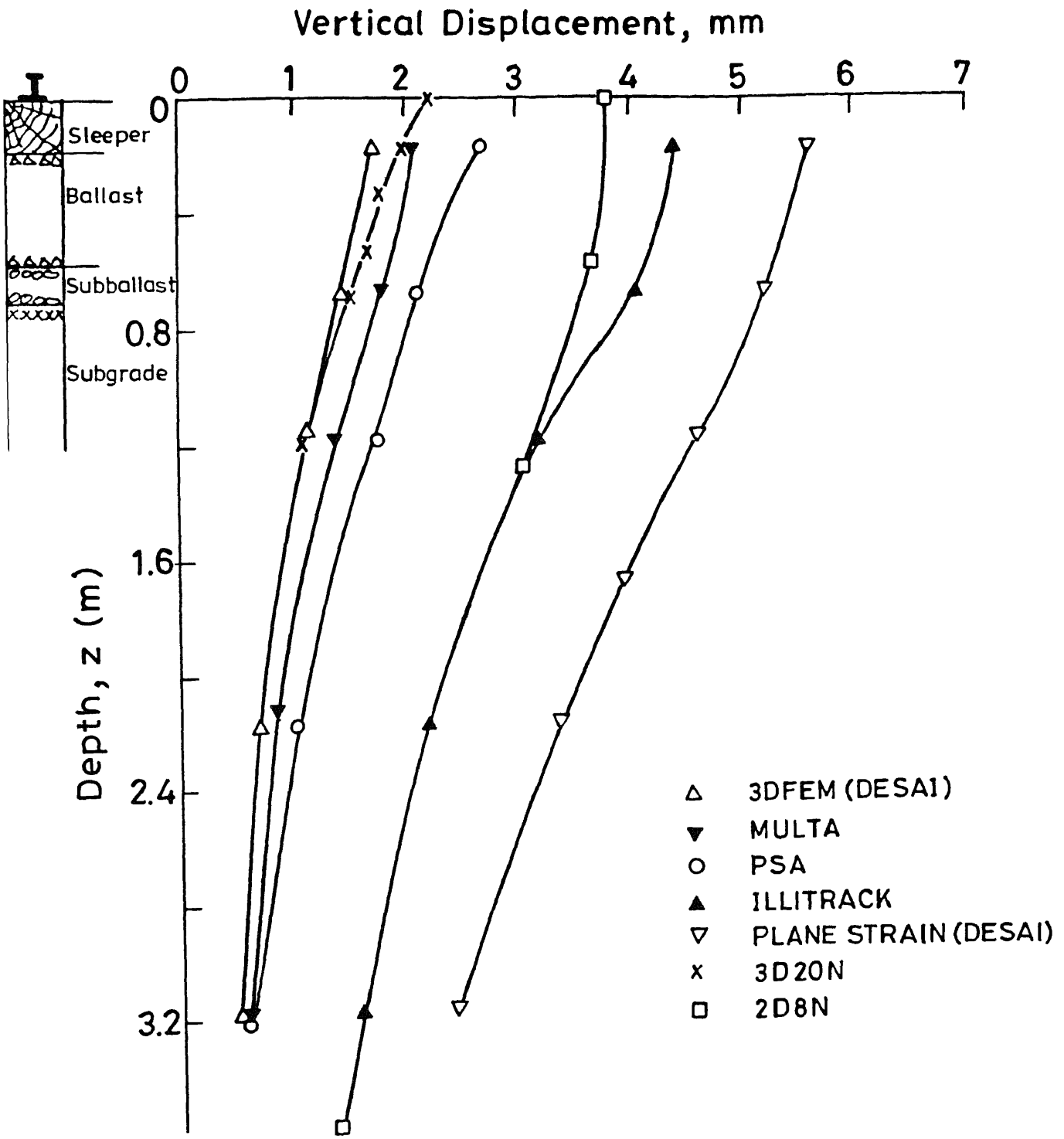

ig. 3.61 Comparison of results-vertical displacement with depth for FAST Track.

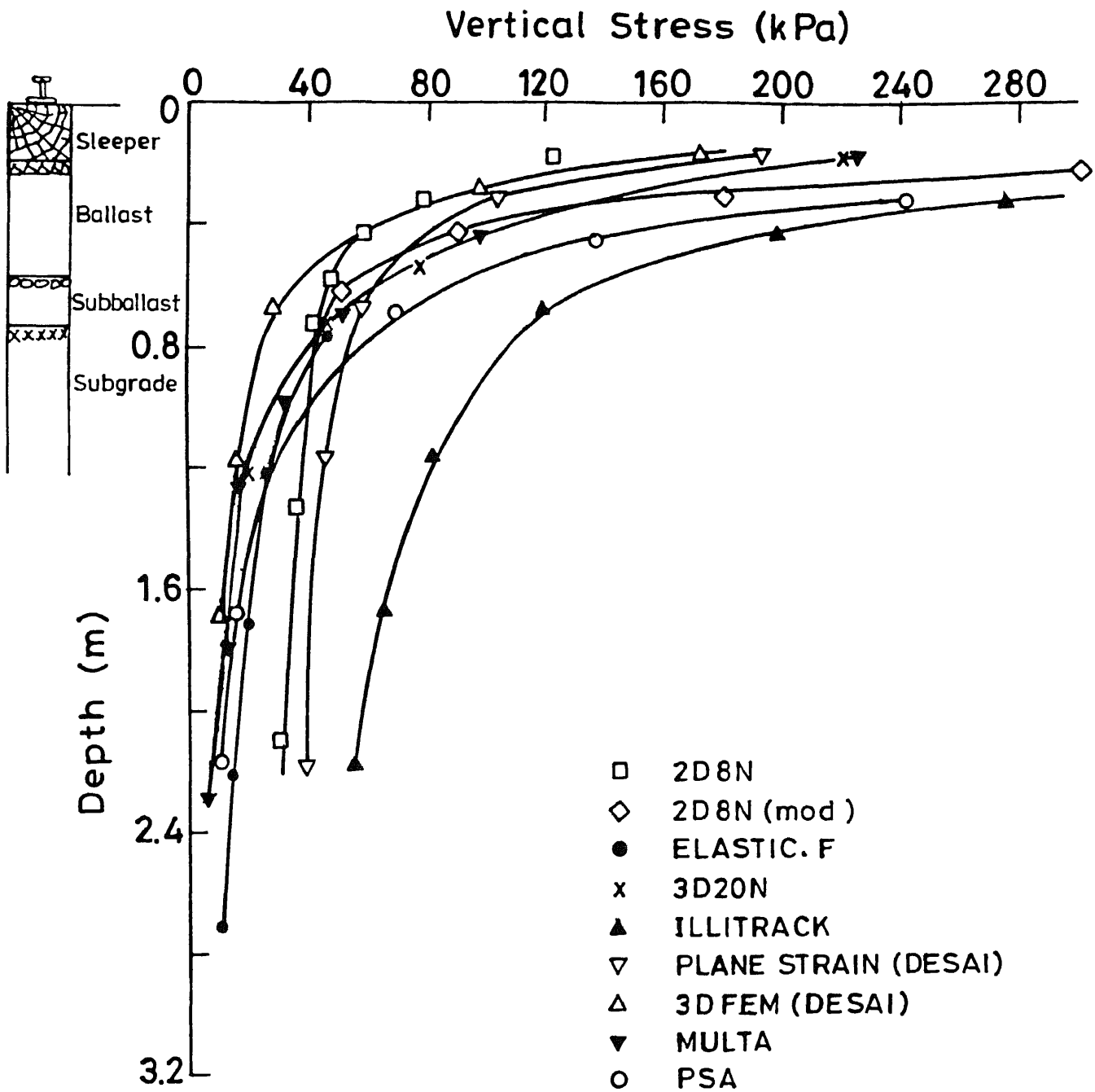

Fig. 3.62 Comparison of results for vertical stress with depth for FAST Track.

single wheel load using ELASTIC.F, 2D8N and 3D20N models. Joint elements were not used. It is clear that 3D20N predicts results similar to MULTA model which is like a closed form solution. Stress prediction by using ELASTIC.F model is also very close to MULTA model. However, it can be seen that 2D8N model predicts lower stresses at shallower depths. Modified 2D8N gives results that are quite satisfactory.

Figure 3.63 shows the stress distribution along the sleeper by using the various models. At subgrade top (71 cm depth), both 2D8N and 3D20N give results close to MULTA model. However, at shallower depths (0.18 m), 2D8N predicts lower stresses. 3D20N gives results similar to MULTA for all depths. Figure 3.64 compares displacement along the rail predicted by 3D20N model with MULTA, PSA and ILLITRACK models.

3.5.2 SO (1978) TRACK

So (1978) has carried out finite element studies and has predicted results in terms of variation of maximum vertical stress on subgrade for change in tie spacing, ballast depth and Young's modulus of subgrade with reference to the typical track.

The properties of reference track along with the ranges of parameters used by So (1978) are given in Appendix A3.
For the present comparison, in addition to above properties for this track, following parameter has been assumed :

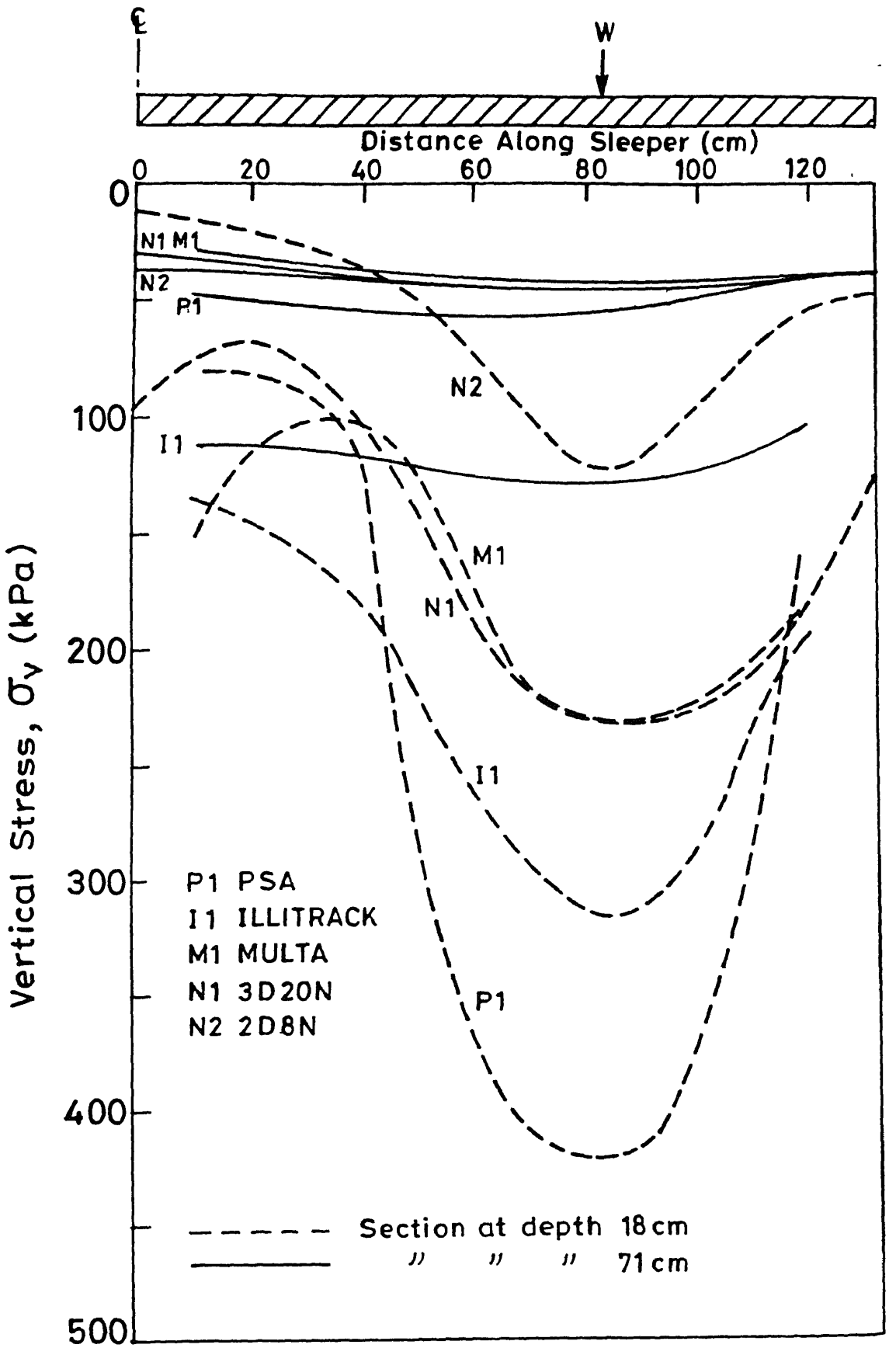

Fig. 3.63 Comparison of results for vertical stress along sleeper at 18 cm depth for FAST Track.

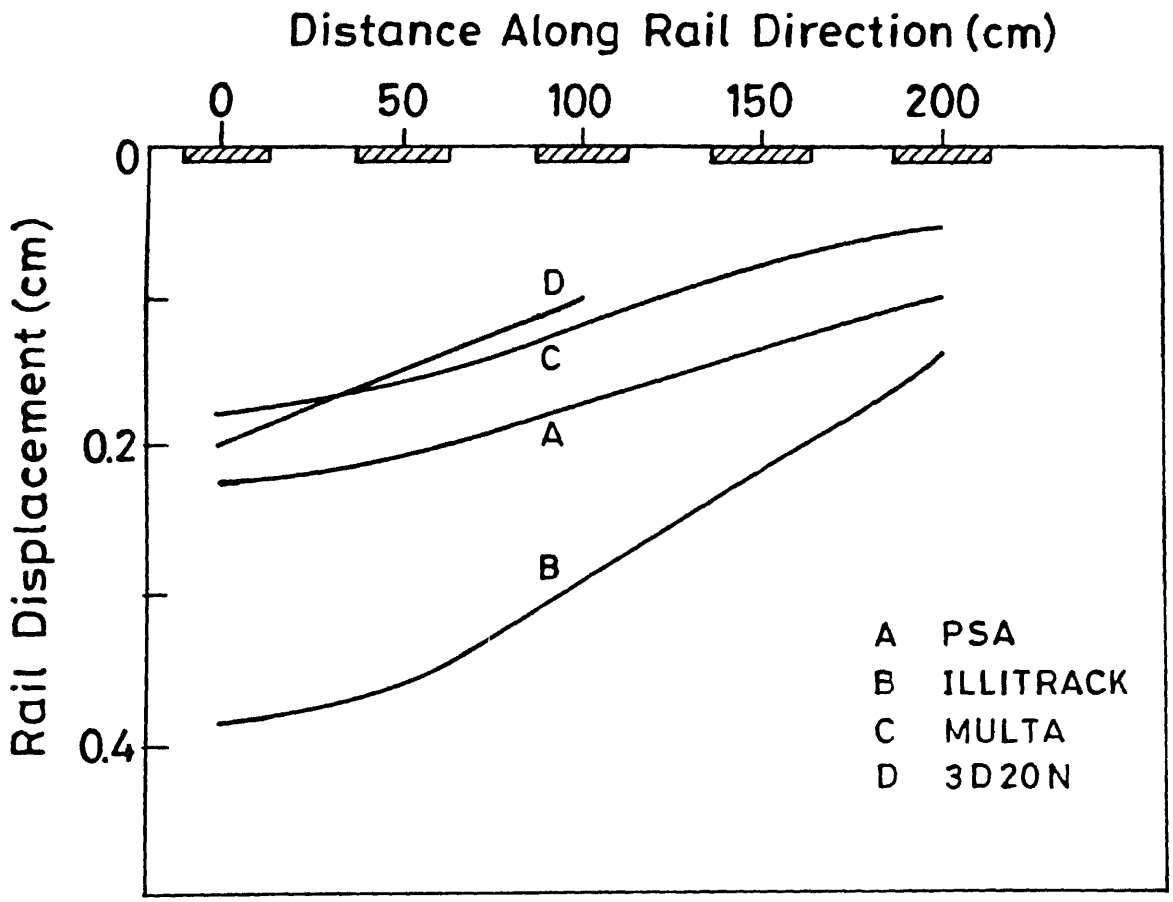

Fig. 3.64 Comparison of results for rail displacement alon rail direction for FAST Track.

$$E_b = 100 \text{ MPa}$$

The range of parameters used for ELASTIC.F and 2D8N models is as given below :

Tie Spacing = 0.508, 0.610, 0.711 m

Ballast depth = 0.152, 0.305, 0.610 m

Young's modulus of subgrade = 13.79, 27.85, 55.16 MPa

The parameters used for 3D20N program are given as below :

Tie Spacing = 0.508, 0.711 m

Ballast depth = 0.305, 0.610 m

Young's modulus of subgrade = 27.85, 55.16 MPa

Figures 3.65 to 3.67 show the variation of maximum vertical subgrade pressure with tie spacing, ballast depth and Young's modulus of subgrade for all 4 models viz. So (1978), ELASTIC.F, 2D8N and 3D20N models.

Results predicted by 3D20N and ELASTIC.F model compare well with So (1978) model.

3.5.3 VIENNA ARSENAL SINGLE SLEEPER AND DERBY PANEL FULL SCALE MODEL TESTS

Janin et al. (1982), Janin et al. (1983a), Janin et al. (1983b) and Janin et al. (1983c) report the results of tests carried out at Vienna Arsenal and Derby. They also report the

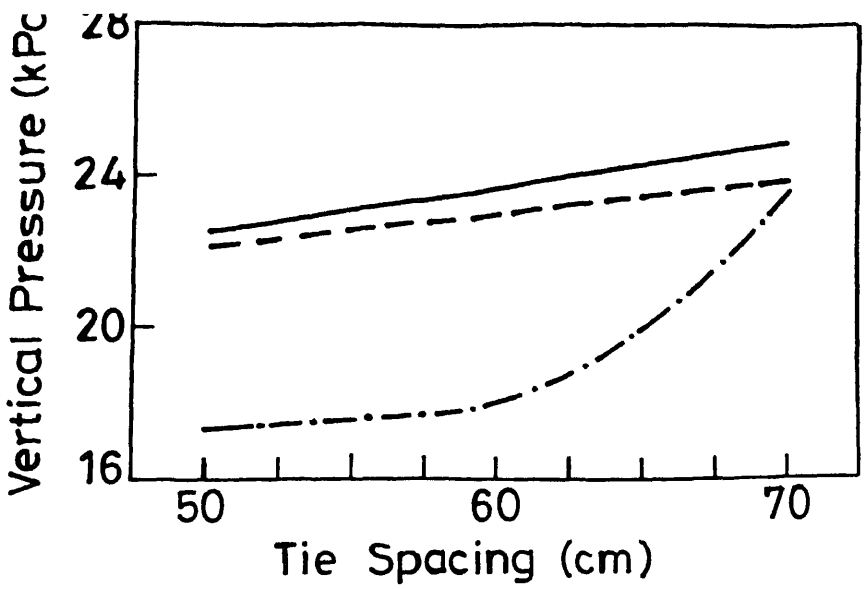

Fig. 3.65

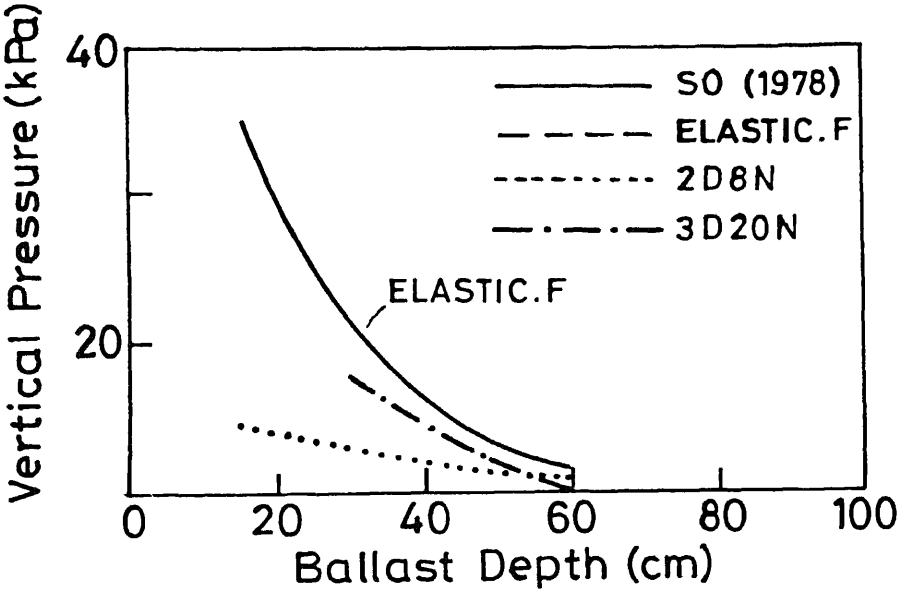

Fig. 3.66

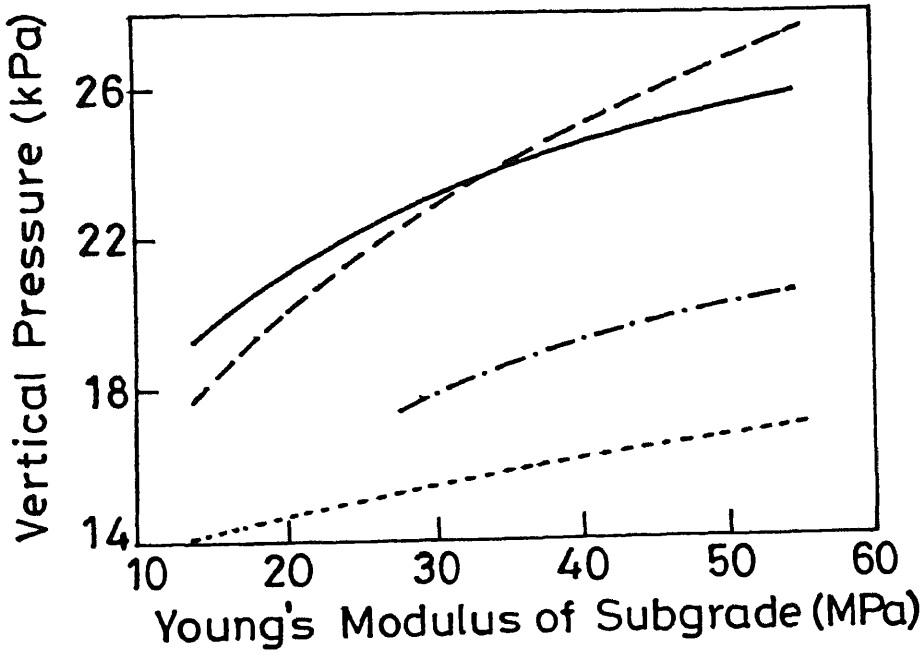

Fig. 3.67

Fig. 3.65-3.67 Comparison of results with SO (1978)

prediction of results by using elastic and elasto-plastic finite element model 'ROSALIE ' and a model based on layered elastic theory 'BISTRO '.

Tests at Vienna Arsenal were carried out on five structures. For structures 1 to 4 , a soil type with E_s= 20 MPa and for structure 5 , a soil type with E_s= 50 MPa were used. These tests were carried out in box type model and load was put on a single sleeper.

Tests at Derby were carried out on four other different structures. All structures were tested for two different soil types viz. Boulder clay (E_s= 11 MPa) and Keuper Marl (E_s= 30 MPa). These tests were carried out on full scale panel with proper wheel loading. Structures 1 to 5 and structures 1 to 4 tested at Vienna and Derby have been shown in Fig. 3.68 respectively. Details of tracks used for Derby and Vienna tests are given in Appendix A4.

Results from Vienna and Derby tests and their model predictions viz. elastic layered model 'BISTRO ' and finite element elastic and elasto-plastic 'ROSALIE ' models have been compared with predictions by models ELASTIC.F, 2D8N and 3D20N. For ELASTIC.F model, for Derby track, sand layer has been assumed to have same Young's modulus as subgrade. Vienna single sleeper test could not be predicted by ELASTIC.F. Also Vienna tracks showing stiff layer over soft layer could not be predicted by this method.

Figures 3.69 and 3.70 show theoretical and test results for vertical stresses and total resilient displacement for

A STRUCTURES TESTED AT VIENNA

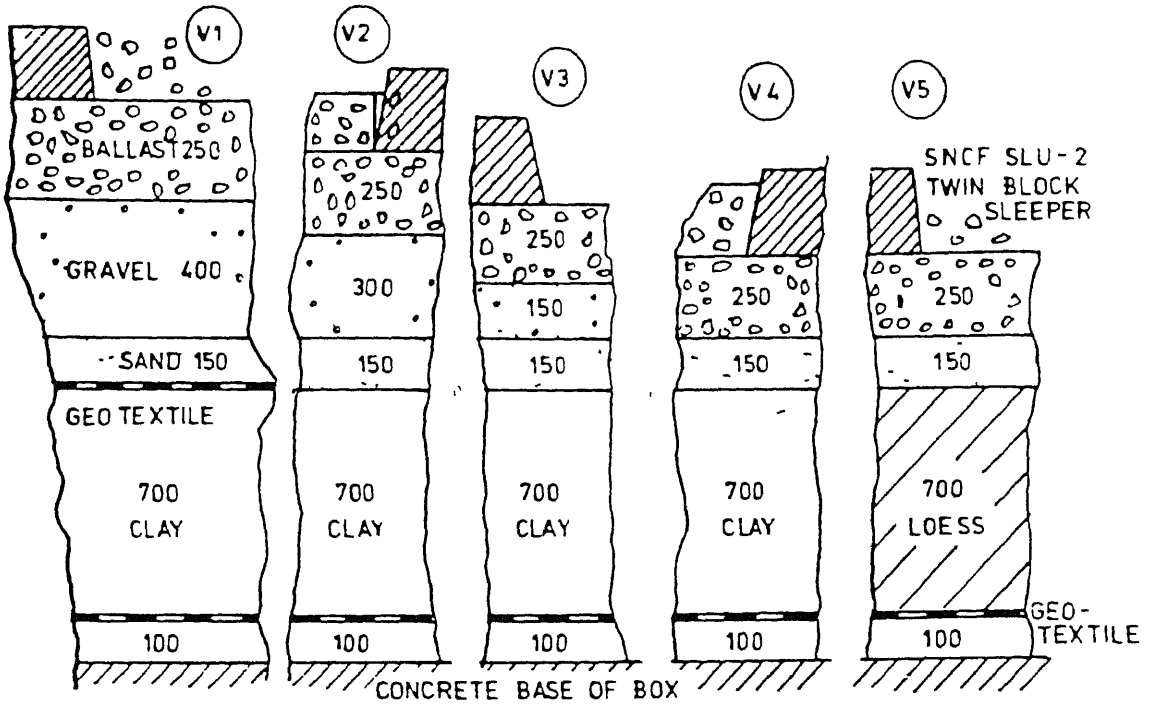

B STRUCTURES TESTED AT DERBY

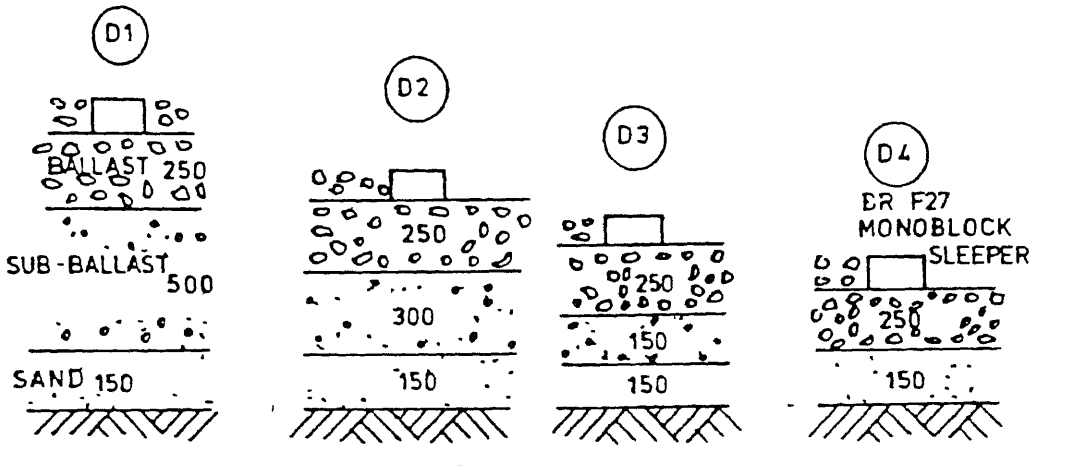

SUB-GRADE (1) KEUPER MARL AND (2) 1000mm BOULDER CLAY OVER KEUPER MARL

Fig. 3.68 Structures tested at Vienna and Derby (Janin et al., 1983B).

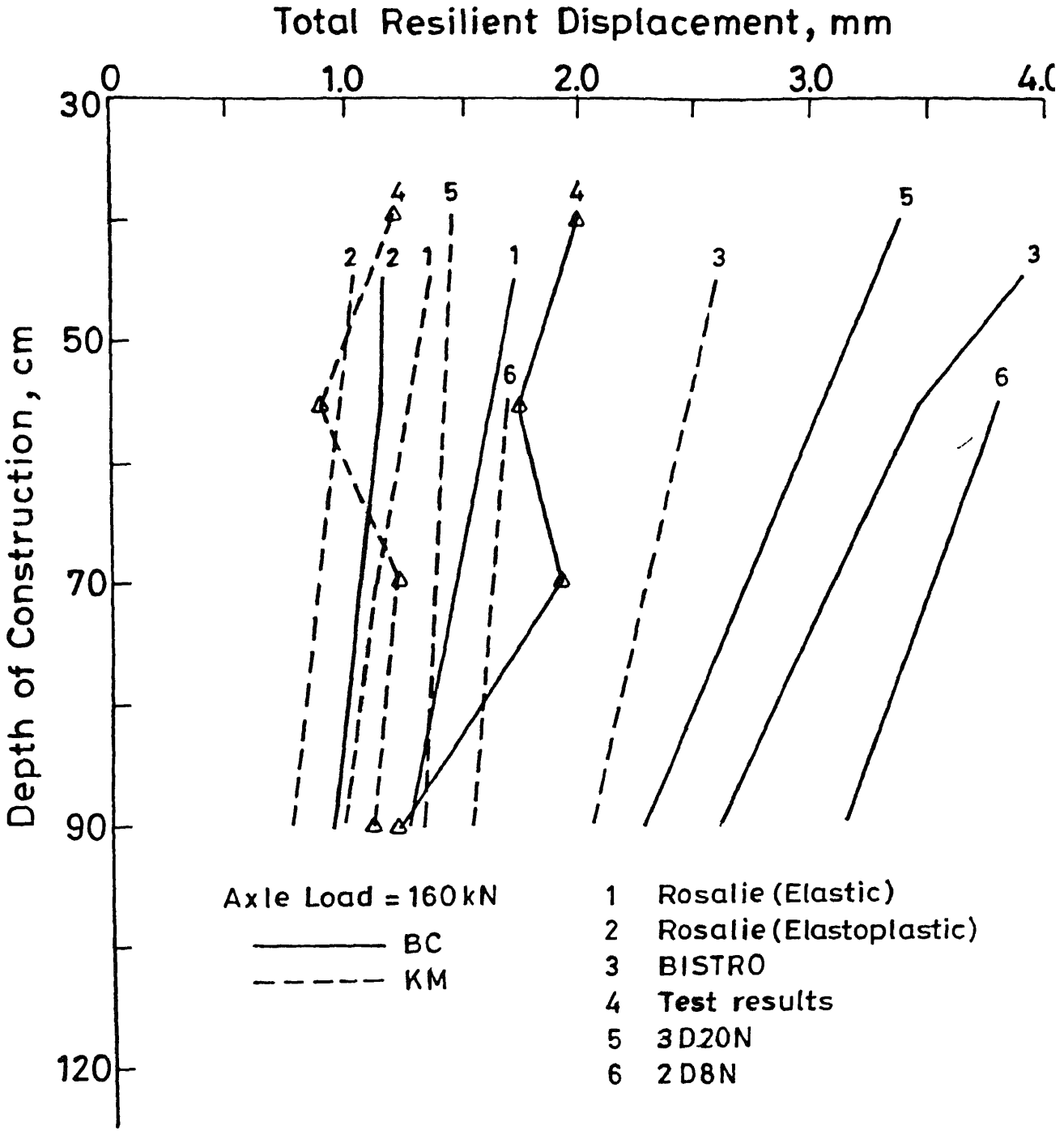

g. 3.69 Comparison of results for total resilient displacement for Derby Panel tests

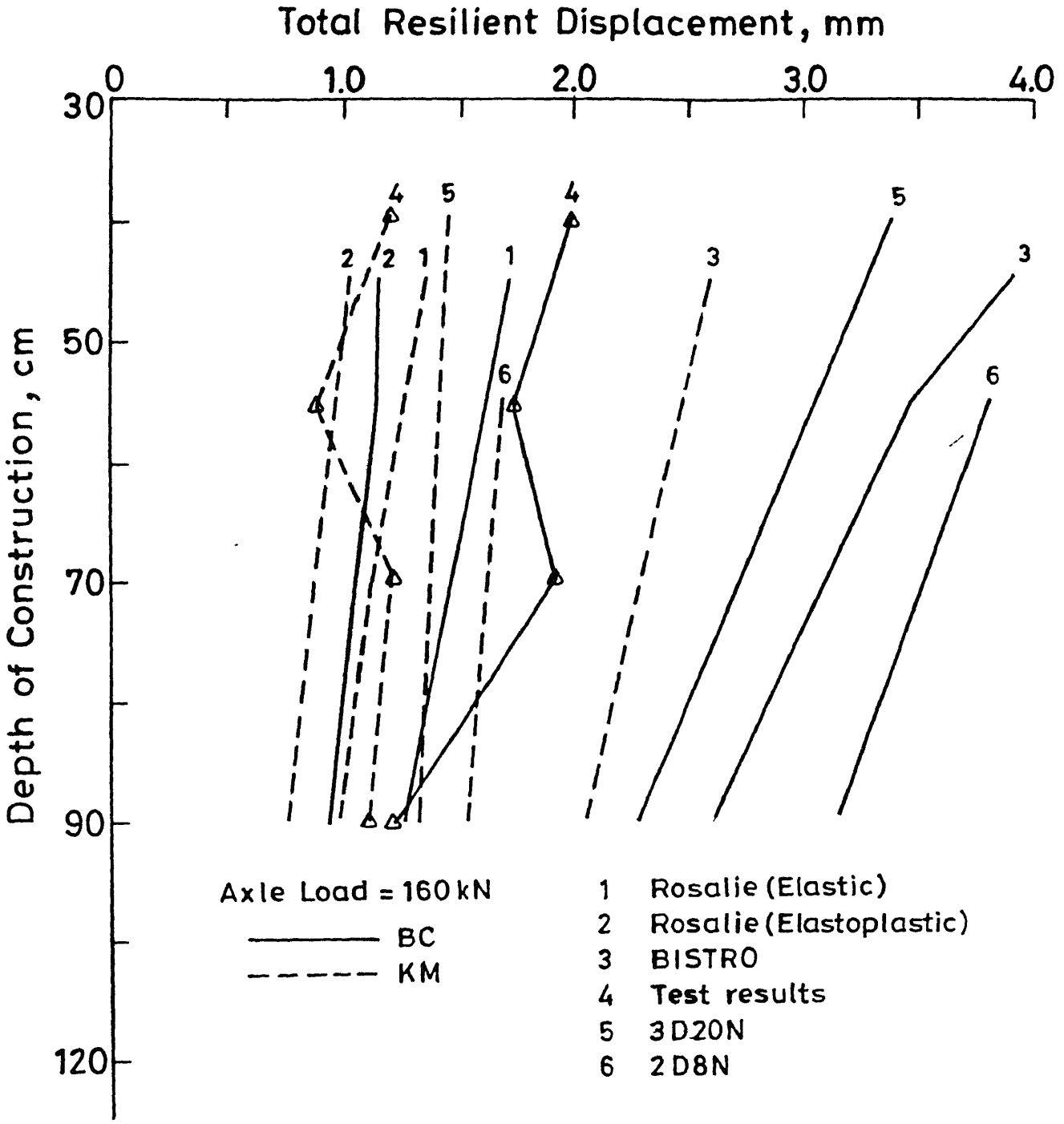

ig. 3.69 Comparison of results for total resilient displacement for Derby Panel tests

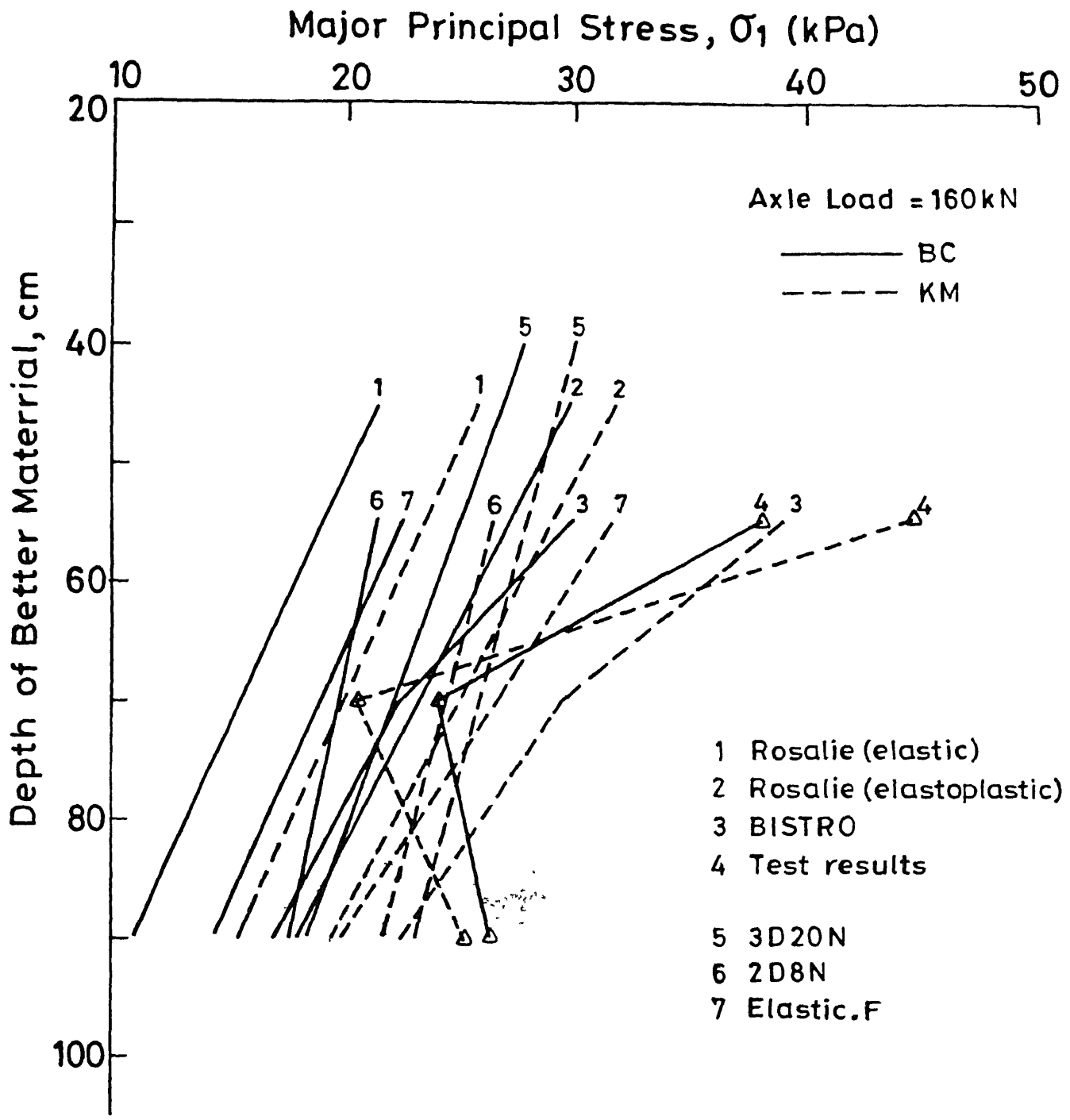

Fig. 3.70 comparison of Results for Major principal stress for Derby Panel tests

track panel tests at Derby with ELASTIC.F, 2D8N and 3D20N models. The results compare reasonably well.

Figure 3.71 summarizes the test results in terms of vertical stress carried out by using single sleeper at Vienna and panel tests at Derby. Predictions, in general, fall within the data scatter except for Derby structure 1.

Figure 3.72 compares horizontal stress distribution as measured for Vienna structure No. 2 and the same predicted inside the subgrade using 3D20N model. Figure 3.73 compares horizontal stresses on top of subgrade for Derby structures predicted by elasto-plastic 'ROSALIE ' analysis with 3D20N elastic analysis.

Figure 3.74 shows the results obtained using elasto-plastic model 'ROSALIE ' for the purpose of preparation of design charts for Vienna type structures. However, due to insufficient data reported by Janin et al. (1983c) regarding proportion of depths of different layers, it has been decided to compare these results with the results of 3D20N for Vienna structures with full panel.

From this comparison, it is clear that 3D20N model predicts vertical stresses throughout the track and horizontal stresses inside the subgrade well within the range with test results and with the analysis carried out by elasto-plastic analysis. Also, it is relevant to mention here that Desai and Siriwardane (1982) have recommended the use of two dimensional and three dimensional linear elastic finite element model for general use and have suggested that elasto-plastic 3-D finite

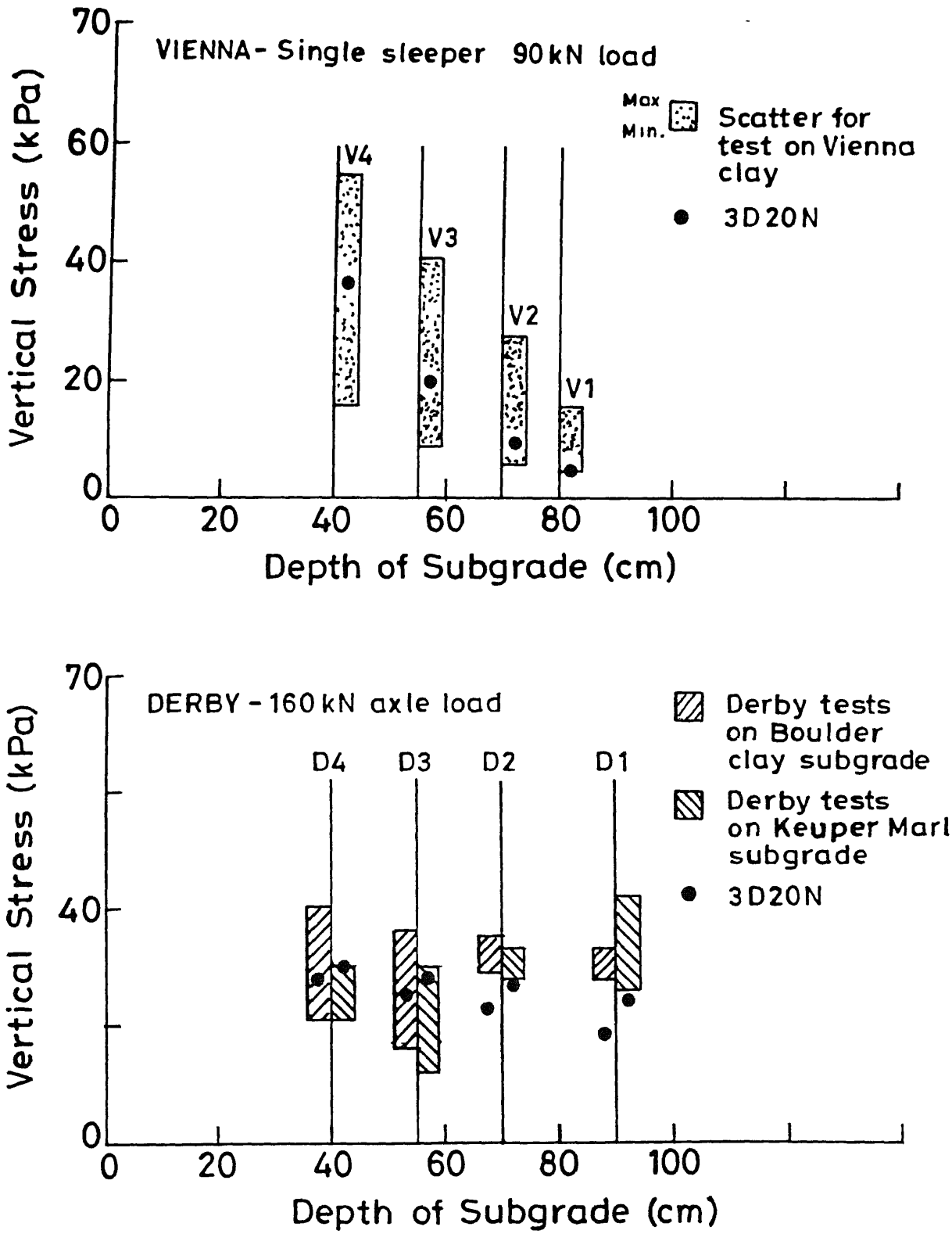

Fig. 3.71 Comparison of results in terms of vertical stresses for Vienna and Derby Tests.

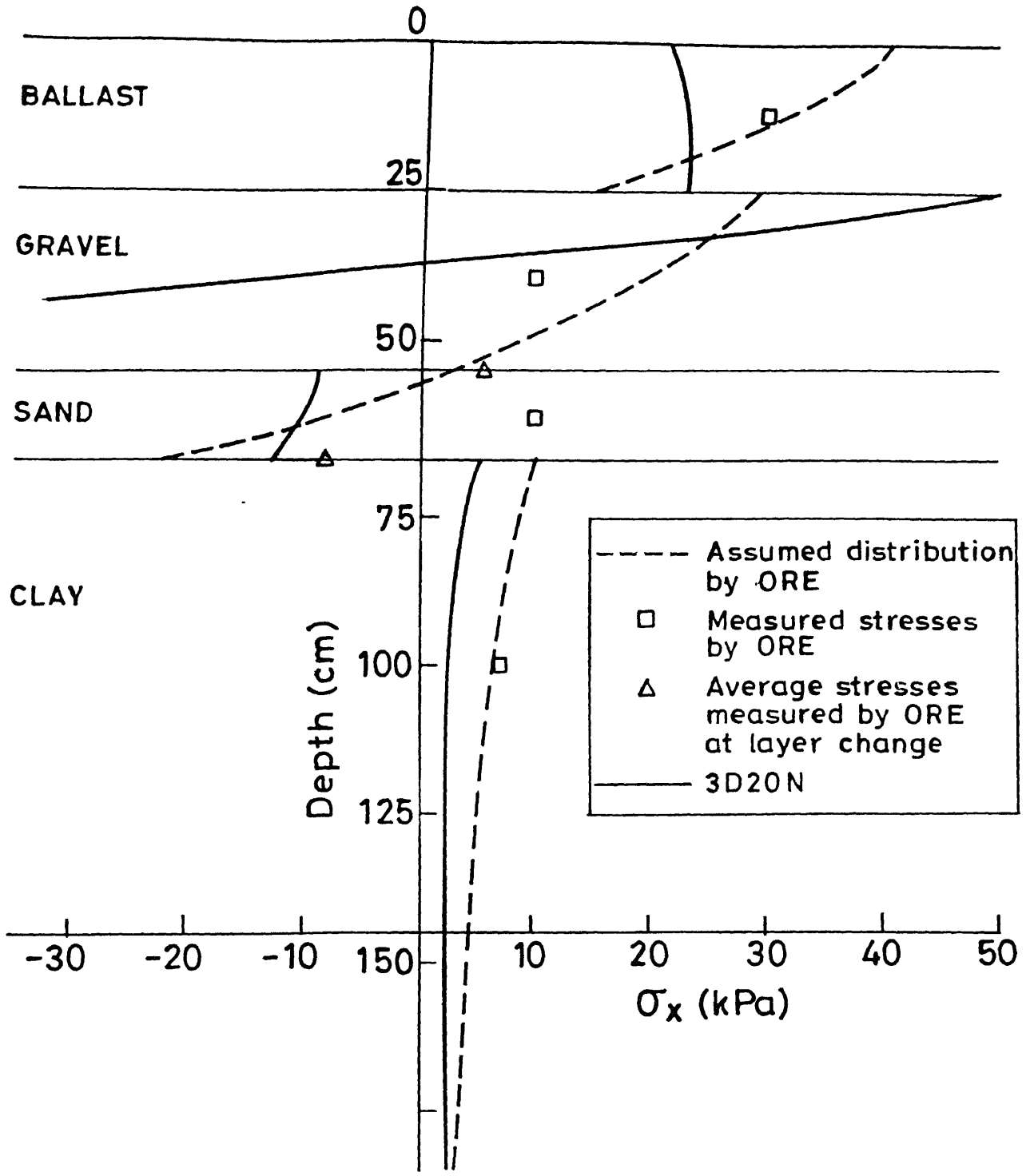

Fig. 3.72 Comparison of results for horizontal stresses for Vienna structure NO. 2

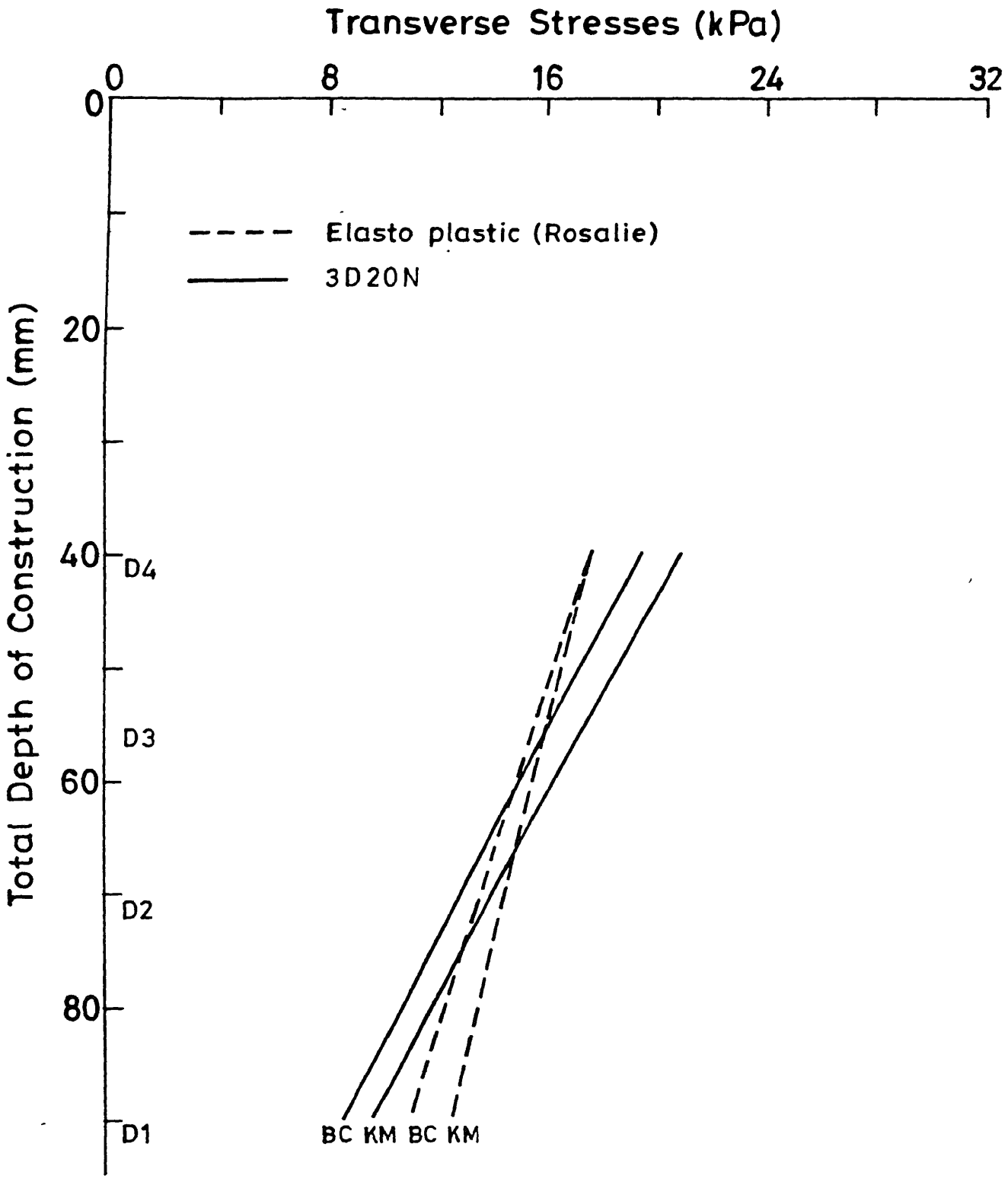

ig. 3.73 Comparison of results for transverse stresses for Derby structures.

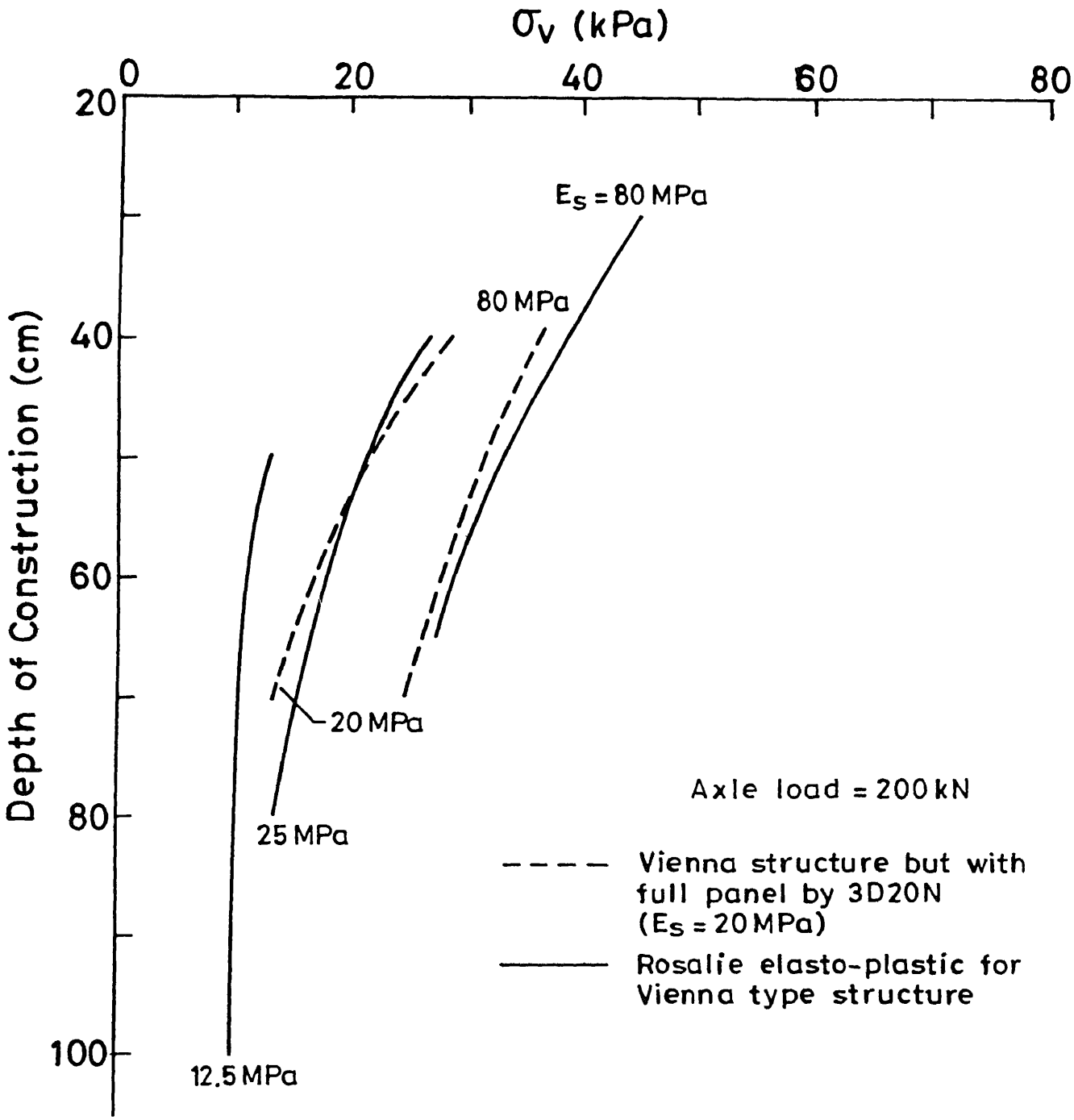

Fig. 3.74 Comparison of results with Rosalie elasto plastic model.

element analysis may be used in special circumstances such as evaluation of stresses on curves, loss of ties, higher axle loads etc.

3.5.4. FIELD MEASUREMENTS BY RDSO ON INDIAN RAILWAYS

Field measurements carried out by RDSO have been reported by Kapoor et al. (1967a), Kapoor et al. (1967b) and Mukerji and Yog (1974). Measured results have been compared with the analytical results obtained by ELASTIC.F, 2D8N and 3D20N models in terms of deflection of sleeper, top formation pressure and the effect of double wheel load. In addition, field measurement of formation pressure due to the long haul train trials at Mandah road station, Allahabad division, 1986 have also been compared [RDSO (C)].

Details of track used for tests carried out by RDSO along with the data assumed for purpose of modelling are given in Appendix A5. The results of these tests are also mentioned therein.

3.5.4.1 Tests conducted on section No. 2 on Ambala - Ludhiana section (1964-1967)

Comparison of results for section no. 2 on Ambala - Ludhiana section has been tabulated in Table 3.10. Pressure has been calculated at midheight in sand layer.

Table 3.10 Comparison of results for section no. 2, Ambala-Ludhiana section.

Result in terms of	Observed		Prediction by			
	Range	Average	elastic.f	2D8N	mod. 2D8N	3D20N
Formation Pressure (kPa)	64.0 to 225.0	86.32	69.75	29.43	79.46	69.75
Displacement (cm)	1.5 to 2.75	2.08	----	1.240	----	0.163

3.5.4.2 Tests conducted at section No. 6 on Ambala Ludhiana section (1964-67)

Comparison of results for section no. 6 on Ambala - Ludhiana section has been shown in Table 3.11. The predicted results seemingly do not compare well with the test results for this section. However, it is noted that range of scatter observed in this field study is very high and average value does not have much significance.

3.5.4.3 Tests conducted on a dead-end siding near canal bed site at RDSO, Lucknow

Details of track structure for tests conducted at this site is also given in Table 3.12 in addition to Appendix A5. Comparison of results is shown in Table 3.13.

3.5.4.4 Field measurement of formation pressure due to long haul train trials at Mandah road station, Allahabad division

Comparison of Results in terms of top formation pressure is given in Table 3.14.

3.5.5 EMPIRICAL FORMULAE AVAILABLE IN LITERATURE

Results in terms of top subgrade pressure from three model viz. ELASTIC.F, modified 2D8N and 3D20N models have been compared with the results obtained from empirical formulae available in literature [Kapoor et al. (1967a)] in Table 3.15 for the track tested by RDSO with 0.20 m depth of formation for

Table 3.11 Comparison of results for section no. 6, Ambala-Ludhiana section.

Result in terms of	Observed		Prediction by			
	Range	Average	elastic.f	2D8N	mod. 2D8N	3D20N
Formation Pressure (kPa)	52.97 to 105.0	84.37	47.58	25.01	60.82	31.49
Displacement (cm)	0.736 to 0.152	0.1016	----	0.073	----	0.010

Table 3.12 Track properties for canal bed site, Lucknow

Track structure type	Ballast depth (cm)	Blanket depth (cm)
1	15.0	22.7
2	15.0	45.4
3	20.0	22.7
4	20.0	45.4
5	25.4	22.7
6	25.4	45.4

Table 3.13 Comparison of results for canal bed site, Lucknow. (All pressure values are in kPa)

Track structure type	Average value of formation pressure observed	Predicted by		
		elastic.f	mod. 2D8N	3D20N
1	131.45	109.87	152.06	114.80
2	63.76	68.70	58.86	73.60
3	99.08	95.16	137.34	101.00
4	55.92	61.80	56.90	65.70
5	87.31	82.40	127.53	87.31
6	49.05	55.92	55.92	59.84

Table 3.14 Comparison of results for Mandah Road Station, Allahaba division . (All pressure values are in kPa).

Speed (kmph)	Average value of formation pressure observed	Predicted by		
		elastic.f	mod. 2D8N	3D20N
65	193.26	137.34	206.0	116.7

* Predicted for axle load = 22.8 t (for Box wagon) + 44.5 % dynamic augment for 66 kmph speed [RDSO (D)].

Table 3.15 Comparison of results with empirical formulae

Serial No.	Empirical Method	σ_{vt} (kPa)
1	Observed	86.32
2	Formula T.P. No. 245	198.16
3	Formula Monograph no. 12 (average)	53.96
4	Formula Monograph no. 12 (maximum)	313.92
5	Talbot's Formula	214.84
6	JNR formula (Japanese)	149.11
7	German Formula	206.01
8	Elastic.f	69.65
9	Mod. 2D8N	29.43
10	D20N	69.65

section no. 2 on Ambala - Ludhiana section. The wheel load and track modulus used were 70 kN and 28.2 MPa respectively.

From Table 3.15, it may be seen that results obtained by using empirical methods are 2 to 4 times greater than the measured results for this Indian track. While for the same track, ELASTIC.F and 3D20N model predict stresses within 20 % of the measured stresses which is the range of measurement for these results.

3.6 COMPARISON OF THE THREE MODELS

In this section, results obtained from 3 models viz. ELASTIC.F, 2D8N and 3D20N model for TRACK 1 have been discussed.

It may be seen from Figs. 3.40 and 3.60 that results obtained from 2D8N lie within 10 % of results obtained by 3D20N model. But it may be noted that 2D8N will underpredict stresses on top of subgrade for smaller depth of formation and will overpredict it for large depths due to 2-D nature of this model. Also from Figs. 3.5 and 3.60, it may be noted that results obtained from ELASTIC.F lie from 5-20 % of results obtained by 3D20N in general and can vary up to 90 % for high values of E_s and low values of d_t.

The percentage variation in results predicted by each of the 3 models for same variation of different parameters has been compared in Table 3.16. Comparison of results for variation of different parameters viz., tie spacing, ballast

Table 3 16 Comparison of results predicted by three models

Change in parameter	% change in vertical stress on top of subgrade predicted by			Reference
	ELASTIC F	2D8N	3D20N	
E_s increases from 10 to 50 MPa	75 - 100 (I*)	30 (I)	25 - 44 (I)	Refer Figs 3.5, 3.40 and 3.60
d_t increases from 0.4 to 1.0 m	50 - 54 (D*)	23 (D)	18 - 29 (D)	Refer Figs. 3.5, 3.40 and 3.60
Stress dispersion in 1 m from top of subgrade	30 - 35	20	14 - 68	Refer Figs. 3.8, 3.38a, 3.49
Increase in tie-spacing from 0 50 m to 0 765 m	5 - 15 (I)	----	6 - 17 (I)	Refer Figs. 3.13 and 3 59
Increase in I_r from 1600 to 3200 cm^4	9 (D)		5 (D)	Refer Figs. 3.14 and 3.58
Increase in E_{sb} from 60 to 100 MPa	14 (D)		2 (D)	Refer Figs. 3.16 and 3.56
Increase in E_b from 150 to 180 MPa	5 (D)		1 (D)	Refer Figs. 3 15 and 3.57

*(D) -- Decrease
(I) -- Increase

depth and E_s with results of So (1978) has already been shown in Figs. 3.65 to 3.67.

CPU time for the 3 models is compared in Table 3.17.

Table 3.17 Comparison of CPU time on Convex 220 computer systems for three models

Model type	Elastic.f	Mod. 2D8N	3D20N
CPU (secs)	0.04	1.6	1774